Improvement of the Thermodynamic Description of Polar Molecules and Their Mixtures in the SAFT Framework
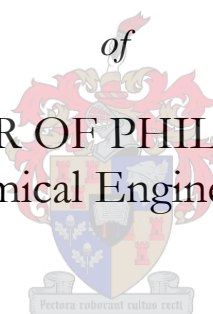
by

Jamie Theo Cripwell

Dissertation presented for the Degree

of

DOCTOR OF PHILOSOPHY
(Chemical Engineering)

in the Faculty of Engineering
at Stellenbosch University

Supervisor
Prof. A.J. Burger

Co-Supervisor
Prof. C.E. Schwarz

March 2017

Declaration

By submitting this dissertation electronically, I declare that the entirety of the work contained therein is my own, original work, that I am the sole author thereof (save to the extent explicitly otherwise stated), that reproduction and publication thereof by Stellenbosch University will not infringe any third party rights and that I have not previously in its entirety or in part submitted it for obtaining any qualification.

From the research presented in this thesis, *two* original papers have already been published in peer-reviewed journals and another *two* papers are in preparation for publication. The development and writing of these papers (published and unpublished) were the principal responsibility of myself and, for each of the cases where this was not entirely true, a declaration is included in the dissertation indicating the nature and extent of the contributions of co-authors.

Date: …March 2017……

"Do or do not, there is no try…"

For Rosie

ABSTRACT

Chemical processes are designed around the manipulation of thermodynamic properties of chemical species and their mixtures. The ability to predict these properties accurately has driven the development of thermodynamic models from the humble beginnings of the van der Waals equation to the fundamental statistical mechanical theories we have today. Despite the successes of recent years resulting from improved fundamental understanding and availability of increased computational power, the accurate representation of certain chemical species and some thermodynamic properties remain elusive. This is particularly true of the holistic properties of polar components and their mixtures, which is the focus of the work presented here.

Arguably the most successful product of the more fundamental approach to thermodynamic modelling is the Statistical Associating Fluid Theory (SAFT). This equation of state has allowed for the accurate representation of molecular geometries, molecular association and the accurate representation of polar interactions. The resulting model framework produces highly accurate predictions of mixture phase equilibria of many systems, which has been the focus of the model's development. Exceptions still remain however, with one such systematic fault providing specific context for model improvement in this work.

A central aim of this work was to establish whether there is deterioration in the predictive capacity of polar sPC-SAFT when applied to the phase equilibrium of different polar isomers. This follows from previous work, where such systematic deterioration was found for ketones, and is extended to ethers and esters here. A lack of previously measured data for isomers of these polar functional groups necessitated generation of such experimental data. Thus, new isobaric vapour-liquid equilibrium data were generated for two C_6 ether isomers with n-heptane, and five C_6 ester isomers with n-octane at *60* kPa. The experimental data showed that significant differences in mixture phase behaviour and resulting phase envelopes are present for each isomer considered, consistent with the experimental trend seen for ketones.

Modelling of the experimental data using sPC-SAFT with the Jog & Chapman (JC) and Gross & Vrabec (GV) polar terms showed that similar trends to that witnessed for ketones previously are apparent for ethers and esters. Using pure component data alone, sPC-SAFT$_{GV}$ parameters were determined for all but one considered isomer, displaying a consistent level of accuracy in the prediction of mixture VLE. Significant parameter degeneracy was apparent for sPC-SAFT$_{JC}$ however, resulting in an inability to regress unique parameter sets for less polar isomers. The results constitute the first case of systematic superiority of the Gross & Vrabec polar term over that of Jog & Chapman.

The modelling results served to clarify the relationship between isomer identity and predictability of the component properties. The predictive capacity of polar sPC-SAFT decreases as the behaviour of the isomer approaches that of an equivalent size/mass nonpolar component. In the case of ketones previously and esters here, this behaviour is linked to the shifting of the polar group centrally, while a

Abstract

more terminally located functional group produces this result in ethers. The incorporation of VLE data in the parameter regression, or fixing the value of the polar parameter, were shown to be excellent mitigation strategies for regressing accurate parameter sets.

The systematic difficulties in modelling isomer phase behaviour raises questions over the overall predictive capacity of the sPC-SAFT$_{JC}$ and sPC-SAFT$_{GV}$ models. Combined with the previously demonstrated inability of these models to simultaneously model phase equilibria and derivative properties using a single parameter set lead to the decision to consider a new polar SAFT framework. To this end, the recently developed SAFT-VR Mie equation of state provided an ideal foundation, and the new SAFT-VR Mie^{JC} and SAFT-VR Mie^{GV} variants, using the same JC and GV polar terms, were proposed.

An extensive regression exercise demonstrated the difficulty with which polar SAFT-VR Mie parameters are determined. This comes as a result of the more complex regression space, being a function of five regressed parameters (σ, m, ε/k, λ_r and x_p/n_p). For SAFT-VR Mie^{JC} in particular, the problem of broad minima in the objective function was more widespread, resulting in an inability to generate parameter sets with nonzero polar contributions. This was true for all components when considering pure component data alone, but also for the ketone functional group when mixture data were considered. This finding supports similar conclusions drawn for sPC-SAFT and points to an inferiority of this variant. SAFT-VR Mie^{GV} proved a more robust model and, applied to the same phase behaviour of isomeric systems, demonstrated that the model performs at least as well as its sPC-SAFT counterpart when a unique parameter set was determined.

As with polar sPC-SAFT before it, accurate parameter sets were shown to be determinable for SAFT-VR Mie^{GV} when VLE data were incorporated in the regression procedure. These optimum *VLE* parameter sets were demonstrated to produce highly accurate predictions, not only for the traditional application to mixture phase equilibria, but to derivative properties such as speed of sound in mixtures as well. This signifies a significant improvement over the polar sPC-SAFT framework, achieving the elusive simultaneous prediction of VLE and derivative properties using a single parameter set. Novel application to mixture excess properties further demonstrates that, while the new polar SAFT-VR Mie models yield similar predictions to their sPC-SAFT counterparts, room for improvement still exists. This is particularly true for representation of the temperature dependence of A^r in SAFT type models.

The prediction results of the *Correlation* parameter sets represent the most significant contribution of this work - the reliance of generating an accurate parameter set on the availability of mixture VLE data is simply not an acceptable caveat in promoting a new predictive model. Here, the value of the polar parameter is fixed to physically meaningful values while the remaining parameters are regressed using pure component data alone. In particular, the pure component speed of sound is incorporated to produce a more well-balanced parameter set. Using these parameters improves the prediction of mixture speed of sound, while incurring only a small deterioration of the mixture VLE prediction. However, the ability to yield such accurate, holistic predictions for polar components by regression using pure component data alone is a characteristic of a truly predictive model.

OPSOMMING

Chemiese prosesse word rondom die manipulering van die termodinamiese eienskappe van chemiese spesies en hul mengsels ontwerp. Die vermoë om hierdie eienskappe akkuraat te voorspel, het die ontwikkeling van termodinamiese modelle aangespoor; van die eenvoudige Van der Waals-vergelyking, tot die hedendaagse fundamentele statistiese meganika-modelle. Ten spyte van die sukses wat, as gevolg van 'n verbeterde fundamentele insig en die beskikbaarheid van toenemende rekenaarvermoë, in die laaste jare behaal is, is die akkurate voorstelling van sekere chemiese spesies en sommige termodinamiese eienskappe nog ontwykend. Dit is veral die geval vir die holistiese eienskappe van polêre komponente en hul mengsels, wat die fokus van hierdie ondersoek is.

Die *Statistical Associating Fluid Theory* (SAFT) is stellig die mees suksesvolle produk van die soeke na 'n meer fundamentele benadering tot termodinamiese modellering. Hierdie toestandsvergelyking het die akkurate voorstelling van molekulêre geometrie, molekulêre assosiasie, en van polêre interaksies teweeggebring. Die modelraamwerk lewer hoogs akkurate voorspellings van die mengsel-fase-ewewig van baie sisteme, wat die fokus van die model se ontwikkeling was. Daar is egter nog steeds uitsonderings. Een van hierdie sistematiese foute bied die spesifieke konteks vir modelverbeterings in hierdie ondersoek.

Een van die sentrale doelwitte van hierdie ondersoek was om te bepaal of die voorspellingsvermoë van polêre-sPC-SAFT verswak wanneer dit op die fase-ewewig van verskillende polêre isomere toegepas word. Dit volg uit 'n vorige ondersoek, waar sistematiese verswakking vir ketone gevind is. Hierdie ondersoek word na eters en esters uitgebrei. 'n Tekort aan literatuurdata vir isomere van hierdie funksionele groepe het die meet van sulke eksperimentele data genoodsaak. Nuwe data vir isobariese damp-vloeistof-ewewig (VLE) is vir twee C_6-eterisomere met n-heptaan, en vyf C_6-esterisomere met n-oktaan by 60 kPa gegenereer. Die eksperimentele data wys dat merkbare verskille in die mengsel-fasegedrag en gepaardgaande fasediagramme vir elke isomeer aanwesig is, wat in ooreenstemming is met die tendens wat vir ketone waargeneem is.

Modellering van die eksperimentele data, deur gebruik te maak van sPC-SAFT, met die Jog & Chapman (JC) en Gross & Vrabec (GV) polêre terme, wys dat soortgelyke tendense, wat voorheen vir die ketone waargeneem is, ook vir die eters en esters sigbaar is. Deur slegs suiwer-komponentdata in die regressieprosedure in te sluit, is sPC-SAFT$_{GV}$ parameters vir alle isomere, behalwe een, bepaal. Hierdie parameters vertoon deurgaans dieselfde akkuraatheid wanneer mengsel-VLE voorspel word. Beduidende parameter-ontaarding is egter duidelik vir sPC-SAFT$_{JC}$, wat daartoe gelei het dat geen parameters vir minder-polêre isomere bepaal kon word nie. Hierdie resultate vorm die eerste geval van sistematiese superioriteit van die Gross & Vrabec-polêre term teenoor dié van Jog & Chapman.

Die modelleringsresultate verduidelik die verhouding tussen die identiteit van die isomeer en die voorspellingsvermoë van die komponent se eienskappe. Die voorspellingsvermoë van polêre-sPC-SAFT

neem af soos die isomeergedrag streef na dié van 'n ekwivalente grootte/massa nie-polêre komponent. Vir ketone en esters gaan hierdie gedrag gepaard met die skuif van die polêre groep na die sentrale koolstofatoom, terwyl die eter met die polêre groep op die buitenste koolstofatoom dieselfde gedrag voortbring. Twee verskillende strategieë het akkurate parameterstelle gelewer: deur VLE-data in die regressieprosedure in te sluit, of die waarde van die polêre parameter vas te maak.

Die sistematiese struikelblokke in die modellering van isomeergedrag, bring vrae oor die voorspellingsvermoë van sPC-SAFT$_{JC}$ en sPC-SAFT$_{GV}$ na vore. Hierdie vraagstuk, tesame met die onvermoë van die modelle om met dieselfde parameterstel tegelykertyd fase-ewewig en ander termodinamiese eienskappe te voorspel, het daartoe gelei dat 'n nuwe polêre-SAFT-raamwerk oorweeg is. Die onlangs ontwikkelde SAFT-VR Mie toestandsvergelyking het die ideale grondslag hiervoor gebied, en, deur gebruik te maak van dieselfde JC- en GV-polêre terme, is die nuwe SAFT-VR Mie^{JC}- en SAFT-VR Mie^{GV}-variante voorgestel.

'n Omvattende regressie-oefening het getoon dat dit moeilik is om parameters vir die polêre-SAFT-VR Mie modelle te bepaal. Dit is as gevolg van die meer komplekse regressieruimte wat nou uit vyf regressieparameters (σ, m, ε/k, λ_r, en x_p/n_p) bestaan. Breë minima in die doelfunksie was vir veral SAFT-VR Mie^{JC} problematies, en het daartoe gelei dat unieke parameterstelle nie gegenereer kon word nie. Dit was die geval vir alle komponente wanneer slegs suiwer-komponentdata in die regressieprosedure oorweeg is, maar ook vir ketone, selfs met die toevoeging van mengseldata. Hierdie bevinding staaf soortgelyke gevolgtrekkings wat vir sPC-SAFT gemaak is, en dui op 'n ondergeskiktheid van hierdie modelvariant. SAFT-VR Mie^{GV} is die meer robuuste model, en wanneer dit op dieselfde fasegedrag van isomeersisteme toegepas word, presteer die model ten minste so goed soos sPC-SAFT$_{GV}$ met 'n unieke parameterstel.

Soos vir die polêre-sPC-SAFT modelle, kon akkurate parameterstelle vir SAFT-VR Mie^{GV} bepaal word wanneer VLE-data by die regressieprosedure gevoeg is. Die optimum *VLE*-parameterstelle kon hoogs akkurate voorspellings lewer, nie net vir die tradisionele toepassing op mengsel-fase-ewewig nie, maar ook van ander termodinamiese eienskappe soos die spoed-van-klank in mengsels. Dit dui op 'n noemenswaardige verbetering teenoor die polêre-sPC-SAFT-raamwerk: 'n enkele parameterstel kan nou gebruik word om VLE en ander termodinamiese eienskappe tegelyk te beskryf. Die polêre-SAFT-VR Mie modelle lewer voorspellings vir mengsel-oormaateienskappe wat soortgelyk aan dié van hul sPC-SAFT eweknieë is, en dui daarop dat die modelle nog kan verbeter. Dit is veral die geval vir 'n akkurate voorstelling van die temperatuurafhanklikheid van A^r in SAFT-tipe modelle.

Die resultate wat met die *Korrelasie*-parameterstelle verkry is, verteenwoordig die mees noemenswaardige bydra van hierdie werkstuk – dat die generering van akkurate parameterstelle op die beskikbaarheid van mengsel-VLE-data afhanklik is, is nie 'n aanvaarbare voorbehoud vir 'n model wat op voorspellings gerig is nie. Daarteenoor lewer die *Korrelasie*-metode polêre parameters wat tot fisies-betekenisvolle waardes vasgemaak is, terwyl die oorblywende parameters deur regressie met insluiting van slegs suiwer-komponentdata bepaal word. Suiwer-komponent spoed-van-klankdata word gebruik om 'n

meer gebalanseerde parameterstel te lewer. Hierdie parameters lewer verbeterde voorspellings van mengsel-spoed-van-klank, terwyl mengsel-VLE voorspellings slegs 'n klein bietjie verswak. Die vermoë om sulke akkurate, holistiese voorspellings vir polêre komponente te lewer, deur regressieprosedures wat slegs suiwer-komponentdata insluit, is 'n eienskap van 'n model wat werklik voorspellend is.

ACKNOWLEDGEMENTS

I would also like to extend personal thanks to the following people.

- Prof's A. J. Burger and C. E. Schwarz for your guiding hands, while still giving me the freedom to choose my own direction.
- Dr A. J. de Villiers for providing the basis and model framework from which this project would grow.
- Mrs H. Botha and Mrs. L. Simmers for your assistance with all of my analytical work.
- The Separations Technology research group, for providing a sounding board and group support when things get tough (as they do) during any research undertaking.
- Ms Sonja Smith, my "Padawan" apprentice. Having someone who *understood* the journey was invaluable – thank you for the innumerable ways you helped make this possible, and for sharing my quirky humour.
- My parents, Jonathan and Lesley, for their continuous support and unquestionable faith in me – you always made me feel like the outcome was never in doubt.
- Finally, my wife Rose, for whom this is dedicated. None of this would have been possible without your love, support and empathy. You are my tether in rough seas, and my inspiration every day – my love and gratitude always.

NOMENCLATURE

Symbol	Description
A/NkT	Helmholtz free energy
A	Homolgous group specific constant for fixing polar parameter n_p/x_p
a	van der Waalsian energy parameter
$BIPs$	Binary Interaction Parameters
b	van der Waalsian co-volume parameter
C_P	Isobaric heat capacity
C_V	Isochoric heat capacity
F	State function, or dimensionless residual Helmholtz energy
f_i	Fugacity of component i
$\underline{G}^{ex}$	Excess Gibbs free energy
$g_i(r)$	Radial distribution function of component i over an intermolecular distance r
$\underline{H}^{ex}$	Excess enthalpy
H_i^{vap}	Enthalpy of vaporisation for component i
k	Boltzmann constant
L	Parameter in Wisniak's L/W consistency test
M_w	Molecular weight
m	Number of segments in the reference chain
N	Avogadro's number
n	Number of moles
n_p	Number of polar segments in the chain
OF	Regression objective function
P	Absolute pressure
P_i^{vap}	Vapour pressure of component i
ΔS_i^{vap}	Entropy of vaporisation for component i
T	Absolute temperature
T_i^{sat}	Boiling temperature of component i
T_r	Reduced temperature
u^{liq}	Speed of sound in compressed liquid
$u(r)$	Intermolecular/pair potential function as a function of intermolecular distance r
$\underline{V}$	Molar volume
$\underline{V}^{ex}$	Excess molar volume
W	Parameter in Wisniak's L/W consistency test
x_i	Mole fraction of component i in liquid phase
x_p	Fraction of polar segments in the chain
y_i	Mole fraction of component i in vapour phase
z_i	Mole fraction of component i in feed
γ_i	Activity coefficient of component i
ε	Dispersion energy parameter
ε^{AB}	Energy of association between sites A & B
θ	Generic thermodynamic property
κ^{AB}	Volume of association between sites A & B

Nomenclature

λ	Intermolecular potential range
λ_a	Attractive potential range
λ_r	Repulsive potential range
μ	Dipole moment
ρ_i	Compressed liquid density
ρ_i^{sat}	Saturated liquid density
σ	Segment diameter

Super/ Subscript	Description
r	Residual property
assoc	Contribution due to association
calc	Calculated value
chain	Contribution due to chain formation
disp	Contribution due to dispersion forces
ex	Experimental value/Excess property (as appropriate)
ideal	Ideal gas contribution
polar	Contribution due to polar forces
seg/mon	Contribution inherent in monomeric segments
sat	Saturation property
c,d	Experimental points *c* and *d*
i	Property of component *i*

Abbreviation	Description
AAD	Average Absolute Deviation: $$AAD = \frac{1}{np}\sum_{i}^{np}\frac{\left|x^{calc} - x^{\exp}\right|}{x^{\exp}} \times 100$$
EoS	Equation of State
SAFT	Statistical Associating Fluid Theory
SAFT-0	Statistical Associating Fluid Theory as developed by the research group of Chapman
SAFT$_{HR}$	Statistical Associating Fluid Theory as developed by Huang & Radosz
PC-SAFT	Perturbed Chain Statistical Associating Fluid Theory
sPC-SAFT	Simplified Perturbed Chain Statistical Associating Fluid Theory
sPC-SAFT$_{GV}$	Simplified Perturbed Chain Statistical Associating Fluid Theory with Gross & Vrabec Polar Term
sPC-SAFT$_{JC}$	Simplified Perturbed Chain Statistical Associating Fluid Theory with Jog & Chapman Polar Term
SAFT-VR	Statistical Associating Fluid Theory for Potentials of Variable Range
SAFT-VR+D	Statistical Associating Fluid Theory for Potentials of Variable Range Accounting for Dipolar Interactions
SAFT-VR Mie	Statistical Associating Fluid Theory for Mie Potentials of Variable Range
SAFT-VR Mie^{GV}	Statistical Associating Fluid Theory for Mie Potentials of Variable Range with Gross & Vrabec Polar Term
SAFT-VR Mie^{JC}	Statistical Associating Fluid Theory for Mie Potentials of Variable Range with Jog & Chapman Polar Term
TPT-1	Thermodynamic Perturbation Theory of First Order

TABLE OF CONTENTS

Chapter 1:   INTRODUCTION

While the long term solution to the world's looming energy crisis may be the development and implementation of cutting-edge technologies, a more accessible medium term solution may be the optimisation of energy usage in existing equipment. Thermodynamics provides a means of studying and quantifying this kind of energy transfer, while defining the limits of what is physically achievable in the process. Thus, by employing a highly accurate thermodynamic model to describe the process, wastage of energy can be minimised.

Distillation is still the most extensively used and one of the most energy intensive separation technologies in process industries today. Distillation manipulates the principles of thermal and chemical equilibrium to achieve separation of chemical mixtures into the desired pure component species. As a result, many of the thermodynamic models developed in recent years have been geared towards the accurate representation of phase equilibria, often exclusively so. Such developments have come at the expense of accurate representation of other, less widely used thermodynamic properties. This focus has made these models correlative at best and somewhat limited in their application.

A highly accurate thermodynamic model, which is the goal of the work proposed here, would require not just correlation of thermodynamic properties, but accurate prediction of these properties. Achieving this level of accuracy requires a fundamental approach to the development of such models. This necessitates looking at the microscopic effects that are responsible for the macroscopic properties of these components. Over the past three decades, the focus of thermodynamic modelling research has shifted to explicitly account for the different intermolecular interactions of different species by incorporating size, shape and energetic effects at the molecular level. Arguably the most successful product of this research has been the Statistical Associating Fluid Theory (SAFT), and it is this family of equations of state (EoSs) that forms the basis of the work proposed here.

1.1   The Thermodynamic Description of Mixtures

The driving force behind the development of thermodynamic models has historically been the desire to accurately describe phase equilibrium. Indeed it is this focus which gives the van der Waals EoS (van der Waals, 1873) such fundamental status:

$$P = \frac{RT}{\underline{V} - b} - \frac{a}{\underline{V}^2}$$

1.1

Introduction

Equation 1.1 was the first pressure explicit EoS capable of predicting two phase equilibria and was the foundation upon which the development of such models as the Soave-Redlich-Kwong (Soave, 1972) and Peng-Robinson (Peng & Robinson, 1976) equations of state were based. These semi-empirical EoSs still enjoy widespread industrial application today due to their relative simplicity and robustness in application to petrochemical mixtures in particular (Wei & Sadus, 2000).

The limited theoretical basis of these cubic EoSs however restricts the applicability and performance of these models. This is demonstrated by their well-documented inability to accurately model the complex and strongly non-ideal interactions present in polar and associating components (Wei & Sadus, 2000). Furthermore, the semi-empirical nature of the Soave-Redlich-Kwong and Peng-Robinson EoSs means that their performance is subject to the availability of experimental equilibrium data to which model constants can be regressed (Cotterman *et al.*, 1986). This last point highlights both the importance of accurate experimental phase equilibrium data, as well as the need to develop more predictive models for application to complex system where no such data are available or indeed measurable. This premise, combined with the exponential growth in available processing power in the past twenty years, lead to the development of more fundamental fluid theories and EoSs in recent years (Economou & Donohue, 1991).

The Statistical Associating Fluid Theory is one such fundamentally based model framework, originally developed from the seminal first order thermodynamic perturbation theory (TPT-1) of Wertheim in a series of four papers (Wertheim, 1984a & b, 1986a & b). The theory proposes that chemical species are represented by a reference fluid comprising chains of component-specific, spherical segments containing an inherent and unique energy contribution. The contributions of intermolecular dispersion forces, molecular association and polar interactions to this inherent chemical energy are accounted for by distinct mathematical functions using a sound theoretical basis. The result, and ensuing model framework, is a summation of these contributions in the residual Helmholtz energy of the system:

$$\frac{A^r}{NkT} = \frac{A^{seg}}{NkT} + \frac{A^{chain}}{NkT} + \frac{A^{disp}}{NkT} + \frac{A^{assoc}}{NkT} + \frac{A^{polar}}{NkT} \qquad \text{1.2}$$

Modelling of phase equilibria requires an accurate description of the component fugacities in order to address the equilibrium criterion of equal fugacities for each component in each phase. In the SAFT framework, this requires an accurate description of the compositional derivative of the residual Helmholtz energy of equation 1.2 (Kontogeorgis & Folas, 2010):

$$\ln \frac{f_i}{z_i P} = \left(\frac{\partial {A^r}/{NkT}}{\partial n_i} \right)_{T,V,n_{j \neq i}} - \ln \frac{PV}{NkT} \qquad \text{1.3}$$

While the prediction of phase equilibrium has driven the development of thermodynamic models to date, the field of thermodynamics is not limited to this single application. Indeed, using the residual Helmholtz energy of equation 1.2 as a starting point and employing appropriate Maxwell relations, the interconnectivity of thermodynamic properties can be demonstrated.
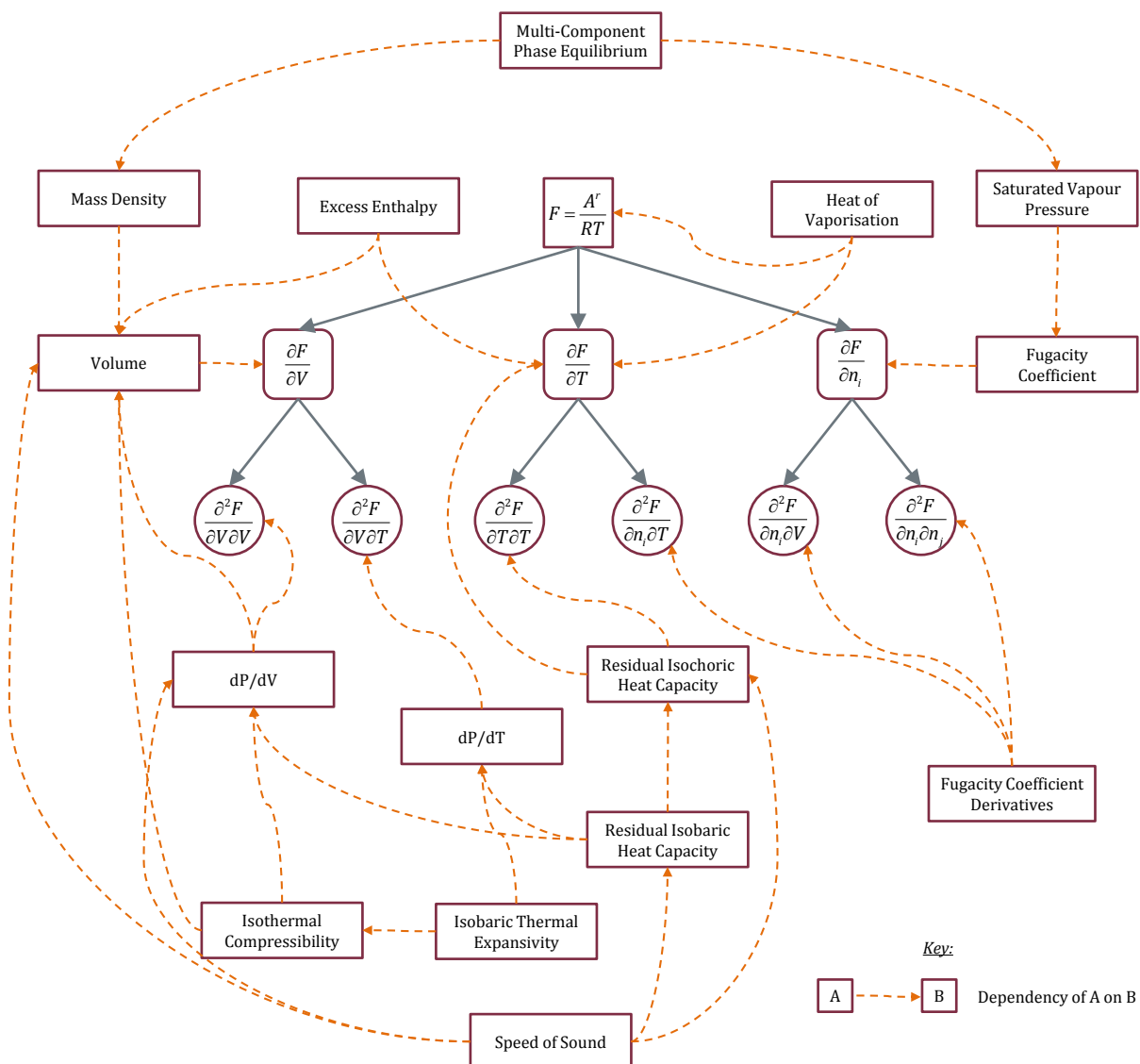
Figure 1.1: Schematic representation of the interconnectivity of thermodynamic properties using the residual Helmholtz energy as a reference point. Figure redrawn and adapted from de Villiers (2011)

Figure 1.1 shows the plethora of potential applications of thermodynamic models to properties of industrial and practical importance. To date, the description of these properties has taken a backseat to the accurate representation of phase equilibria resulting in separate correlative model development specific to these properties. As the predictability of phase equilibria plateaus however, with ever increasing accuracy in ever more complex systems, a more holistic approach to model development is beginning to emerge. This approach takes into account the very nature of thermodynamic properties.

1.2   Problem Identification

While much progress has been made to date to account for the different types of intermolecular interactions that influence the macroscopic properties of pure fluids and their mixtures, room for improvement still exists. One such consideration is the role of strong dipolar interactions of chemical families such as ketones, esters and ethers, and the role that these strong intermolecular forces play in defining the thermodynamic behaviour of such components. Two recent studies (de Villiers, 2011 & Cripwell, 2014) have suggested that subtle yet physically important contributors to these physical properties are, as yet, unaccounted for within the existing SAFT framework.

The work of Cripwell (2014) compared the predictions of the sPC-SAFT EoS with two different polar terms, *viz.* that of Jog & Chapman (sPC-SAFT$_{JC}$) and of Gross & Vrabec (sPC-SAFT$_{GV}$), in predicting the phase behaviour of ketone structural isomers with a common second component. The comparative study identified a previously undocumented superiority of sPC-SAFT$_{GV}$ over sPC-SAFT$_{JC}$. The former provided consistently good pure predictions for the mixture VLE of each of the structural isomers while the latter exhibited marked deterioration in predictive capacity. Specifically, the pure predictions systematically worsened from the most to the least polar structural isomer. This study raised two questions that still need to be addressed: the first is whether these trends extend to other polar functional groups; the second is whether the deficiency is inherent to the parent framework or simply the superiority of one polar term over another.

De Villiers (2011) adopted a holistic approach to addressing the thermodynamic description of mixtures and assessed the predictive capacity of sPC-SAFT in describing the derivative and excess properties of mixtures. For polar components in particular, it was shown that neither sPC-SAFT$_{JC}$ nor sPC-SAFT$_{GV}$ could accurately predict both equilibrium and derivative/excess properties for mixtures using a single parameter set. While no other SAFT variants were considered, it was concluded that this deficiency was inherent to the sPC-SAFT framework.

The success of the SAFT family of EoSs in the prediction of phase equilibria has been extensively reported in recent years, for ever more complex and nuanced systems (Tan *et al.*, 2008). The holistic predictive strength of these models is still largely unaddressed however, and is gaining more attention in the literature. The identification of bias afforded to the phase behaviour of specific functional isomers, as well as addressing the all-round predictive strength of SAFT-type models, represent opportunities for investigation and further improvement of this fundamental model family.

1.3   Study Objectives & Thesis Structure

The overarching aim of this study is to identify a superior polar SAFT variant, with emphasis on assessing the effects of structural isomerism on binary phase behaviour and the predictability of

thermodynamic properties beyond phase equilibria. To this end, the study objectives are outlined and detailed in the subsections below, with the expected original contributions highlighted.

1.3.1   Generation of Low Pressure Phase Equilibrium Data

The experimental phase of the study, presented in Chapters 3 & 4, involves the generation of isobaric phase equilibrium data for the structural isomers of medium length esters and ethers with a normal alkane exhibiting a similar boiling point. Specifically, the following systems will be measured:

- C_6 ethers with n-heptane
    - butyl ethyl ether/n-heptane
    - di-n-propyl ether/n-heptane
- C_6 esters with n-octane:
    - pentyl formate/n-octane
    - butyl acetate/n- octane
    - propyl propanoate/n- octane
    - ethyl butanoate/n- octane
    - methyl valerate/n- octane

The generation of mixture data for these systems fill the gap in the literature, to be highlighted in the literature review, regarding VLE data for structural isomers with a common second component at the same physical conditions.

The following original contributions arise from this phase of the study:

i.   New isobaric VLE data for binary systems comprising one aliphatic C6 ether structural isomer with n-heptane

ii.   New isobaric VLE data for binary systems comprising one aliphatic C6 ester structural isomer with n-octane

1.3.2   Polar sPC-SAFT: Structural Isomers & Phase Equilibrium

The focus of Chapter 5 is to extend the assessment of the predictive capacity of sPC-SAFT$_{JC}$ and sPC-SAFT$_{GV}$, initiated by Cripwell (2014), to the ester and ether functional groups using the experimentally measured data of Chapter 4. To this end, the following objectives are specified:

- Thermodynamic modelling, using sPC-SAFT$_{JC}$ and sPC-SAFT$_{GV}$, of the experimentally measured binary phase behaviour of:
    - the five C_6 esters with n-octane
    - the two C_6 ethers with n-heptane
- Assessment of the performance of each model, for the phase behaviour of each structural isomer, in each homologous group:

o   Identify trends in predictive capacity of each model

o   Do both models give equally good pure predictions of the mixture phase behaviour of each isomer?

The following original contribution is made from the initial modelling phase:

i.   Accounting for the effect of functional group location on mixture phase behaviour of the structural isomers of polar, non-associating molecules with a common second component with polar sPC-SAFT.

1.3.3   Accounting for Dipolar Interactions in a SAFT-VR Mie Framework

As is demonstrated in Chapter 6, the SAFT-VR Mie EoS looks to be a promising variant of the SAFT moving forward, with good all-round predictive capacity in the published work based on this model variant so far. This work has however, been restricted in scope with limited application to real fluid mixtures and no attempt has been made to explicitly account for the anisotropic dipolar forces present in some of these molecules. Therefore, the goal of Chapters 7 & 8 is thus to extend the SAFT-VR Mie EoS to the study of polar molecules by explicitly accounting for dipolar interactions using two widely accepted dipolar terms in the SAFT formalism:

- Extension of the SAFT-VR Mie EoS with the dipolar terms of Jog & Chapman and of Gross & Vrabec
- Determine pure component parameters for a range of polar, non-associating molecules
- Assess the model predictions for pure component and binary mixture phase equilibria
- Compare these predictions to those of the nonpolar SAFT-VR Mie variant so as to answer the question:

"Is it necessary to explicitly account for dipolar interactions in the SAFT-VR Mie EoS?"

Given that a central aim of the study is to determine whether the properties of the structural isomers of polar molecules and their mixtures can be accurately predicted in all cases using the SAFT family of EoSs, it is of particular interest to:

- Assess the performance of both the original, nonpolar as well as the proposed polar SAFT-VR Mie EoS to accurately predict the binary phase behaviour of each polar structural isomer with a common second component. This assessment is be carried out for all functional groups under consideration.

Finally, given the demonstrated superiority of SAFT-VR Mie over its more established PC-SAFT counterpart in accurately predicting thermodynamic derivative properties, a further objective was to:

- Assess the prediction of thermodynamic derivative and excess properties of polar, non-associating compounds using the proposed polar SAFT-VR Mie EoS.

The following novel contributions are made from this final phase of the work:

i.   Accounting for dipolar interactions in the SAFT-VR Mie framework: extension with two established dipolar terms.
ii. Understanding the effect of polar functional group location on binary mixture equilibria: a comparative study using polar sPC-SAFT and SAFT-VR Mie.
iii. Prediction of thermodynamic derivative and excess properties of polar molecules and their mixtures using polar SAFT-VR Mie.

Chapter 2: LITERATURE REVIEW

2.1 SAFT Family of Equations of State

The Statistical Associating Fluid Theory has its roots in the fields of statistical thermodynamics and perturbation theory, fields that came to prominence in the 1970's and 1980's. Like their contemporary cubic equation of state counterparts, these theories account for the hard-sphere repulsive and dispersive forces between molecules. However, they further consider the energy associated with, and the structural influence of, chain formation and allow for the consideration of molecular association, previously unaccounted for by the popularised cubic EoSs (Wei & Sadus 2000). The origin of the SAFT EoS will be presented in the following section, before the variants and extensions of interest to this work are highlighted.

2.1.1   History of SAFT

The origin of the consideration of molecular association in EoSs was the work of Wertheim (Wertheim, 1984 a, b, 1986 a, b), whose seminal papers provided an analytical means of describing the energetic contribution of association between spherical particles. Molecular association, or hydrogen bonding, is a major source of nonideality in pure fluids and mixtures, and so the ability to explicitly account for these interactions enhances the predictive capacity of an EoS. Further, if one considers association between two such spherical segments, and takes the limit of infinitely strong association at infinitely small bonding sites, the result is an approximation of a covalent bond. Algebraically, this yields an analytically simple means for correlating the polymerisation of monomers to form chains (Müller & Gubbins, 2001). Thus, the major contribution of Wertheim's work was a means of explicitly accounting for hydrogen bonding and molecular association, forces which have a major influence on intermolecular interactions.

It was the research group of Chapman (Chapman *et al.*, 1989, 1990) who first incorporated Wertheim's theory into the development of an EoS, proposing the Statistical Associating Fluid Theory. This original SAFT, often referred to as SAFT-0 (Tan *et al.* 2008), proposed an EoS in the form of a summation of contributions to the Helmholtz free energy.

$$\frac{A}{NkT} = \frac{A^{ideal}}{NkT} + \frac{A^{seg}}{NkT} + \frac{A^{disp}}{NkT} + \frac{A^{chain}}{NkT} + \frac{A^{assoc}}{NkT} \qquad 2.1$$

The Helmholtz free energy serves as an ideal foundation for the development of a molecular EoS as all other equilibrium thermodynamic properties are readily calculable by appropriate differentiation (von Solms *et al.*, 2003).

The physical picture of Wertheim's TPT-1, and thus of the SAFT reference fluid, is a chain of homonuclear, tangentially bonded spherical segments. Accounting for chain formation allows for the effect of non-spherical molecular structure on bulk fluid properties to be quantified. Compared to the hard-sphere representation of van der Waalsian EoSs, this physical picture is much more representative of our understanding of molecular structure, as depicted in Figure 2.1.
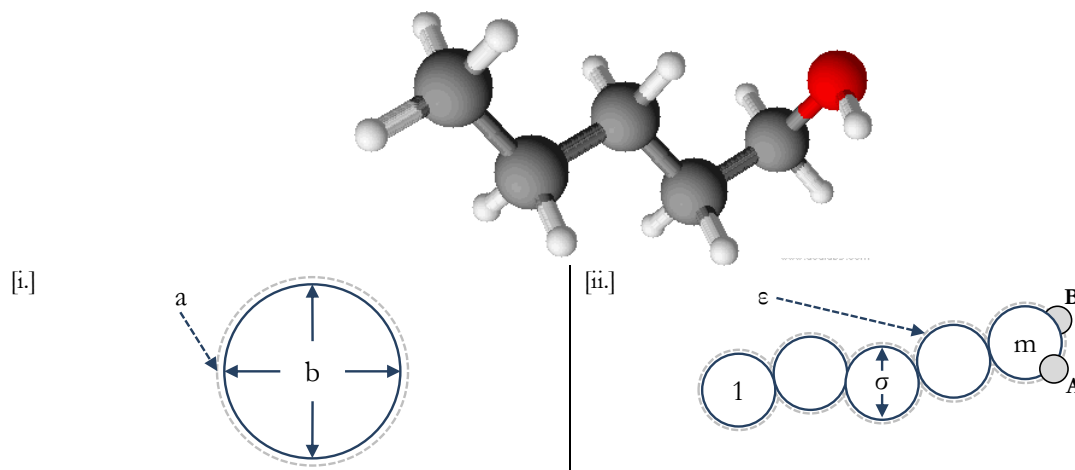
Figure 2.1: Representation of 1-pentanol using [i.] van der Waalsian reference fluid with energetic (a), and co-volume (b) parameters & [ii.] SAFT type reference with segment size (σ), segment number (m) and segment energy (ε) parameters. Two further parameters characterise association at sites A & B on the chain

The reference fluid comprises spherical segments of a characteristic diameter, σ, which interact via an intermolecular potential characterised by the depth of the potential well, ε. These monomers are then covalently bonded, using Wertheim's TPT-1, to form chains of m segments, where m is representative of the chain length. Finally, hydrogen bonding between the segments of different chains is characterised by the association strength and volume between the association sites A on segment i and B on segment j (ε^{AB} and κ^{AB} respectively). The SAFT component parameters provided in Figure 2.1 [ii.] are the same parameters proposed by Chapman *et al.* (1989, 1990) and have been retained in this form in most subsequent variations of the theory.

Although Chapman *et al.*'s papers are the historical roots of the SAFT EoS, the variant most widely referenced as the fundamental basis of subsequent modifications is that of Huang & Radosz (1990, 1991), often referred to as SAFT$_{HR}$. The differences between SAFT-0 and SAFT$_{HR}$ are subtle, incorporating the same overall framework but different intermolecular potentials and expressions for the dispersion energy (Economou, 2002). This point deserves explanation, particularly in the context of this study, where the performance of two different SAFT variants is to be assessed and compared. The primary difference between different SAFT versions is the choice of a reference fluid and thus, the description of the intermolecular dispersion forces (Kontogeorgis & Folas, 2010).

The reference fluid is fully described by the specification of monomer geometry and the choice of intermolecular potential. The choice of potential function further necessitates the selection of an algebraic function to quantify the intermolecular forces, typically in the form of a "dispersion term". This hierarchy

is summarised in Figure 2.2. For example, both SAFT-0 and SAFT$_{HR}$ make use of a hard sphere monomer, a characteristic of many of the early formulations of the SAFT, but the difference between them is the choice of pair potential function. SAFT-0 uses a Lennard-Jones potential, employing the dispersion term of Cotterman *et al.* (1986) developed for Lennard-Jones spheres in the Perturbed Hard Chain Theory framework. SAFT$_{HR}$ on the other hand, uses a simpler square-well potential, whose dispersion term is parameterised using molecular simulation data generated by Alder *et al.* (1972).
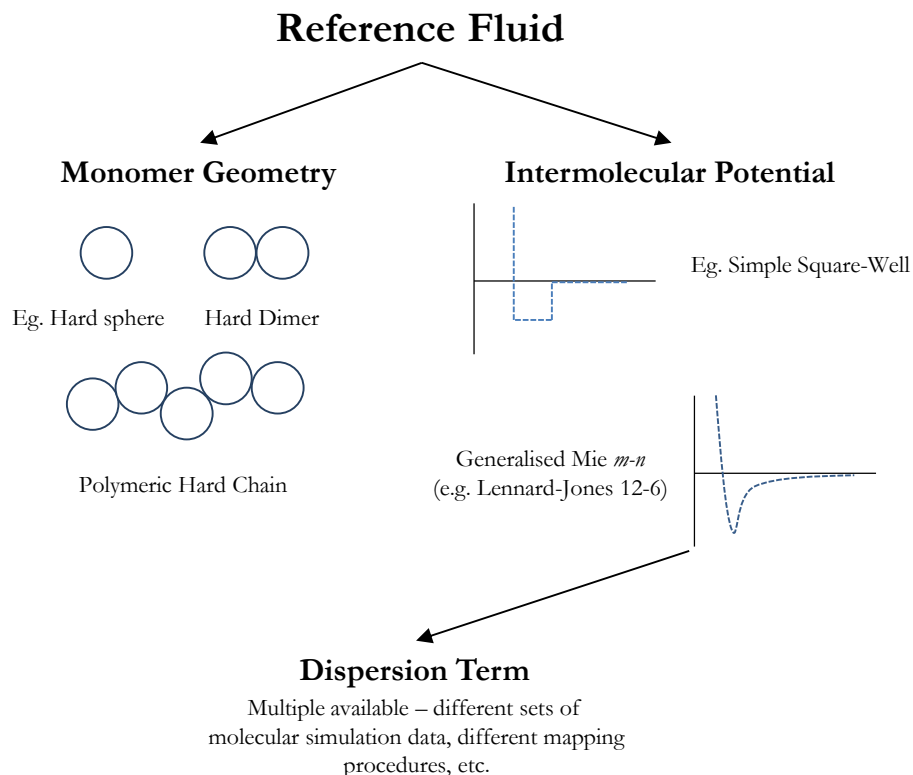
Figure 2.2: How the reference fluids of different SAFT variants are defined. The multiplicity of combinations explains the large number of SAFT variants published since SAFT-0.

The hierarchy depicted by Figure 2.2 explains the large number of SAFT variants available in the literature today, the subtle differences between these versions being their theoretical interpretation and approximation of physical reality. Of particular interest to this work are two such variants that consider particularly different reference fluids, both geometrically and in their description of intermolecular forces: the perturbed chain SAFT (PC-SAFT) and the SAFT with interactions of variable range (SAFT-VR). The former is the subject of the following section, while a discussion of the SAFT-VR framework is reserved for Chapter 6.

2.1.2   Perturbed Chain SAFT

The perturbed chain SAFT, developed by Joachim Gross and Gabriele Sadowski in a series of three papers (Gross & Sadowski, 2000, 2001, 2002), differs notably from SAFT-0 and SAFT$_{HR}$ in the descriptions of the geometry of the reference fluid. As suggested by its name, the reference fluid of PC-SAFT comprises hard *chain* monomers, as opposed to the hard *spheres* of its contemporaries. These

chain monomers are themselves made up of hard sphere segments, interacting with a modified square well potential proposed by Chen & Kreglewski (1977). This modified potential, detailed in Figure 2.3, is used to account for the phenomenon of soft repulsion exhibited by real fluids, while maintaining the mathematical convenience of the simple square well potential.
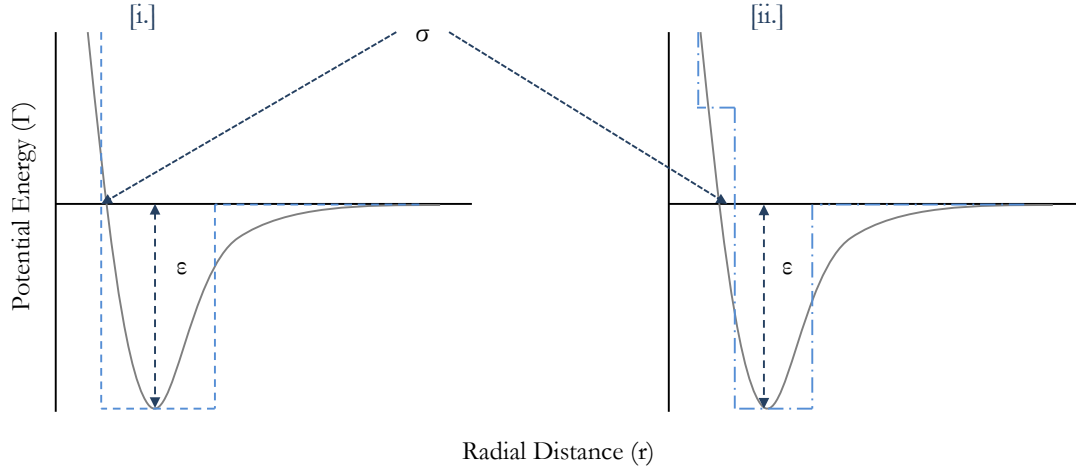
Figure 2.3: Simplified approximations for intermolecular potentials [i.] Square well in SAFT$_{HR}$, & [ii.] Modified square well PC-SAFT. The parameterisation of both models is identical, viz. σ, m & ε.

These hard sphere segments are then covalently bonded using the TPT-1 framework common to all SAFT variants to form the monomeric chain reference fluid. Algebraically, this is tantamount to rearranging the terms of equation 2.1 as:

$$\frac{A}{NkT} = \frac{A^{ideal}}{NkT} + \left(\frac{A^{seg}}{NkT} + \frac{A^{chain}}{NkT} \right) + \frac{A^{disp}}{NkT} + \frac{A^{assoc}}{NkT}$$

2.2

where: $$\frac{A^{mon}}{NkT} = \left(\frac{A^{seg}}{NkT} + \frac{A^{chain}}{NkT} \right)$$

This simple reformulation of the residual Helmholtz energy has important physical consequences for the EoS because in the SAFT framework, the pair potential is applied to the monomer fluid in the dispersion term. Thus, because the monomer fluid comprises chains in PC-SAFT, only after the chain monomers are formed is the dispersion term applied to the reference fluid. For SAFT variants where the monomer fluid comprises hard spheres, $A^{mon} = A^{seg}$ in equation 2.1, and the pair potential is applied to the hard sphere segments prior to chain formation. This results in an overlapping of the dispersion field of the segments, conceptually illustrated in Figure 2.4, resulting in overestimation of the dispersion forces between molecules.

This dispersion term takes the form of a second order perturbation expansion, according to the theory of Barker & Henderson (1967a, b). The integrals in the radial distribution function and intermolecular potential are approximated by power series, rather than analytically derived (Gross & Sadowski, 2001). The procedure for determining the constants of the power series involves fitting the

correlations to data for n-alkanes, using an intermediate assumption of hard chains interacting via a Lennard-Jones potential. The authors argue that this procedure is justified and indeed preferable given that, by "incorporating information of real substance behaviour," the error inherent in the approximations for the pair potential and the radial distribution function, "can be corrected to a certain extent" (Gross & Sadowski, 2001). Thus, the choice of a somewhat simple intermolecular potential in the EoS is compensated for by incorporating real fluid properties into the fitting procedure.

SAFT-0, SAFT$_{HR}$

$A^{seg}(=A^{mon})+A^{disp}$
$A^{seg}+A^{disp}+A^{chain}$

PC-SAFT

A^{seg}

$A^{mon}=(A^{seg}+A^{chain})$
$(A^{seg}+A^{chain})+A^{disp}$
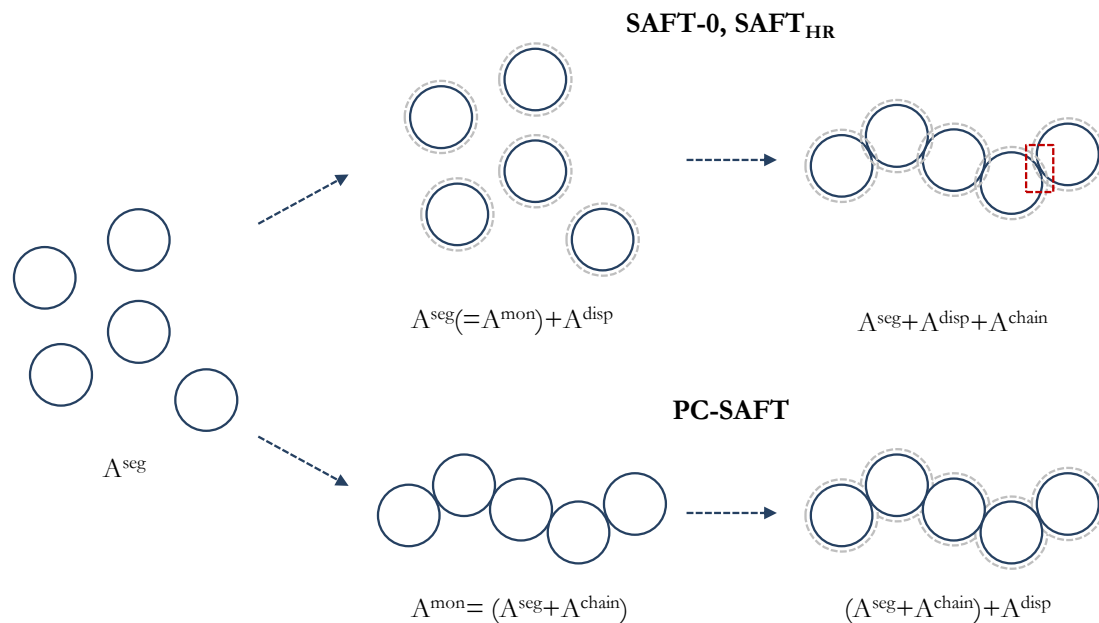
Figure 2.4: Hard sphere (SAFT-0, SAFT$_{HR}$) and hard chain (PC-SAFT) reference fluids. The overlapping of dispersion fields in hard-sphere monomer reference fluids is highlighted.

Therefore, the strength of PC-SAFT is that the dispersion term is more physically representative of real intermolecular forces because its reference fluid is geometrically representative of real molecules. The result of this realism is that the EoS consistently outperforms its hard-sphere monomer contemporaries in the prediction of pure fluid and mixture behaviour (Gross & Sadowski 2001, 2002). It has further been successful in such a variety of applications as modelling polydispersity, the description of biological systems and characterising solid-fluid boundaries in copolymer crystallisation (Tan *et al.,* 2008). The success of PC-SAFT is exemplified by the fact that, apart from the fundamental SAFT$_{HR}$, it is the only variant to be included into the widely used Aspen Plus® process simulation software.

2.1.3   sPC-SAFT: A Mathematical Simplification

In an effort to reduce its computational intensity, and thus make it a more accessible option for the engineering community at large, von Solms *et al.* (2003) proposed a modification of the PC-SAFT EoS. The modification came in the form of a uniformity assumption for the temperature dependent diameter of the reference fluid segments, which leads to two mathematically simplified expressions. The first is for the radial distribution function, the other for the segment contribution, A^{seg}, to the residual Helmholtz free

energy. Extensive testing of this modification found that the simplified expressions, "simplify the calculation of phase equilibrium properties… without loss of accuracy" (von Solms, 2003) and for this reason, this variant is employed in this work rather than PC-SAFT.

2.2   Dipolar Interactions: Unique Intermolecular Forces

Molecular polarity arises as a result of the presence of lone electron pairs on certain atoms within a molecule, resulting in a charge distribution and the generation of a permanent electric field surrounding the molecule (Assael *et al.,* 1998). These permanent fields result in strong electrostatic forces, the strength and nature (attractive/repulsive) of which are highly dependent upon the orientation of the molecule, as illustrated schematically in Figure 2.5.
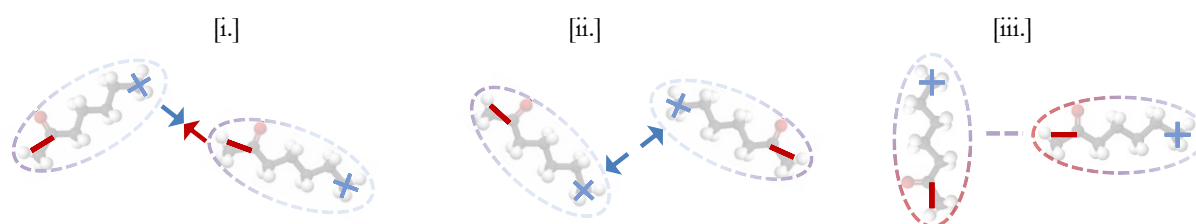
Figure 2.5: Schematic representation of anisotropic dipolar intermolecular forces. [i.] If molecules are favourably oriented, strong attractive electrostatic forces result. [ii.] If like-poles are aligned, strong repulsive forces result. [iii.] If poles are non-axially aligned, no significant electrostatic forces result.

When considering such polar molecules and their mixtures, earlier SAFT variants simply assumed that the dispersion term in equation 2.1 could be numerically adjusted to account for these dipolar interactions. The result is an artificially large value for the dispersion energy, which leads to poor predictions of the properties of polar fluid mixtures (de Villiers, 2011). However, the strength and anisotropic nature of the electrostatic forces between polar molecules distinguish them from the much weaker London dispersion interactions discussed in the previous section. For this reason, a number of authors have attempted to explicitly account for these dipolar interactions within the SAFT framework, resulting in a number of "polar" terms to add to the residual Helmholtz energy of the system, as per equation 2.3.

$$\frac{A}{NkT} = \frac{A^{ideal}}{NkT} + \frac{A^{seg}}{NkT} + \frac{A^{disp}}{NkT} + \frac{A^{chain}}{NkT} + \frac{A^{assoc}}{NkT} + \frac{A^{polar}}{NkT} \qquad \text{2.3}$$

2.2.1   Polar Term of Jog & Chapman

While dipolar terms had been previously developed for polar hard sphere fluids, a corresponding term for dipolar chains was first proposed by the research group of Jog & Chapman (Jog & Chapman, 1999; Jog *et al.,* 2001) in the framework of SAFT$_{HR}$. Considering the polar molecules to be dipolar hard

spheres introduces inherent limitations of the theory, similar to the case of a hard sphere reference fluid in van der Waalsian type EoSs (Jog *et al.,* 2001):

- the minimum distance between molecules is overestimated,
- the molecule as a whole is considered polar rather than specific functional groups, and
- the orientation of the dipole is unaccounted for.

All three inherent assumptions, schematically presented in Figure 2.6, limit the influence of the dipolar interactions on fluid behaviour. This is due to the dependence of these interactions on intermolecular distances and the position of the dipole within the chain. The success of the work of Jog & Chapman over previous attempts is thus the ability to explicitly account for the effects of molecular geometry and that specific functional groups (or segments) are polar, rather than the molecule as a whole.
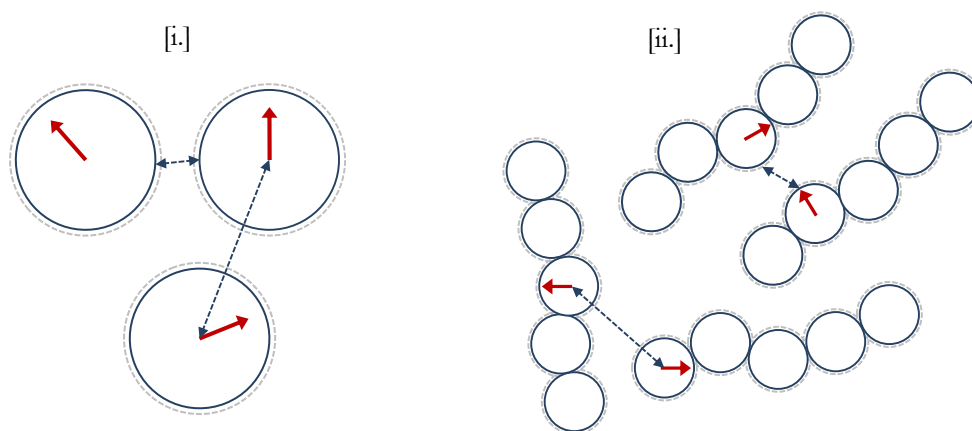
Figure 2.6: Difference between [i.] dipolar hard sphere and [ii.] dipolar segmented chain approaches. The overestimation of intermolecular, or inter-dipole distances are highlighted. Further, orientation and location of dipole are arbitrary in [i.], but explicitly accounted for in [ii.].

The polar contribution to the Helmholtz free energy in equation 2.3 is determined by means of a *u*-expansion. Here, the second and third order terms are given explicitly, with higher order terms approximated by a Padé approximant (Rushbrooke *et al.,* 1973), as per equation 2.4.

$$\frac{A^{polar}}{NkT} = \frac{A_2}{1 - \dfrac{A_3}{A_2}}$$

2.4

The second (A_2) and third (A_3) order terms are calculated as functions of the segment size and dispersion energy parameters as well as the functional group dipole moment (μ). These terms also contain complex integrals for the two- and three-body correlation functions, which themselves are functions of the radial distribution and angular functions. As with the dispersion term, highlighted in the hierarchy of Figure 2.2, there are a number of analytical expressions for these integrals which allow the second and third order terms of equation 2.4 to be explicitly calculated. Jog & Chapman (1999) used the result of

Rushbrooke *et al.* (1973), where the dipole is assumed to be aligned perpendicular to the molecular axis, to express the integrals as simple analytical functions of the segment diameter.

A similar approach had been taken for dipolar hard sphere models, but Jog *et al.* (2001) accounted for the different molecular geometry of chain molecules by introducing a new regressable parameter, x_p. This "fraction of dipolar segments" parameter has physical meaning when approximately equal to the inverse of the component segment number (viz. m^{-1}). This represents a single polar segment in the chain, or physically, a single polar functional group in the carbon backbone of the molecule. In this way, the polar term is only applied to the x_p fraction of polar segments in the reference fluid from which the chain molecules are built in the SAFT framework. Results with this new polar SAFT EoS were generally excellent, and it was emphasised that explicitly accounting for the fundamental difference between dipolar interactions and dispersion forces make the EoS more predictable (Jog *et al.,* 2001).

Jog & Chapman's polar term was later incorporated, without alteration, into the PC-SAFT (Tumakaka & Sadowski, 2004) and sPC-SAFT (de Villiers *et al.,* 2011) frameworks. Given that, as highlighted earlier, PC-SAFT is a more sophisticated and recent variant than its SAFT$_{HR}$ counterpart, this may at first appear a logical progression. However, this successful extension has subtle yet important consequences for the SAFT framework as a whole and this work in particular: it shows that the Jog & Chapman polar term is readily extendable to other SAFT variants, despite these variants having different reference fluids and dispersion terms.

2.2.2   Polar Term of Gross & Vrabec

The research group that developed the PC-SAFT EoS went on to develop their own polar term within the PC-SAFT framework. Gross & Vrabec (2006) drew on the success of Jog & Chapman before them, and used the same physical picture of a chain comprised of both polar and nonpolar segments, viz. Figure 2.6 [ii.]. They also employed the Padé approximant formulation for a third order *u*-expansion of the polar contribution to the residual Helmholtz energy (equation 2.4). However, the primary difference between the polar terms of Jog & Chapman and of Gross & Vrabec came in the way the integrals over the two- and three-body correlation functions were approximated.

Gross & Vrabec made use of molecular simulation data for dipolar point-dipole fluids interacting with a Lennard-Jones potential to fit correlations for the integrals over the two- and three-body correlations functions. The point-dipole reference fluid is different to the tangent-sphere fluid used by SAFT however. Thus a correlation between the properties of the two fluids was developed so that the molecular simulation results could be interpreted within a TPT-1 framework (Gross & Vrabec, 2006). A power series in the segment density, itself a function of the segment diameter, was then fitted to the simulation data to yield approximations for the required integrals.

In the same way that Jog & Chapman introduced the x_p parameter to account for the fraction of dipolar segments in the chain, Gross & Vrabec introduced the "number of dipolar segments", n_p. This

parameter was originally set equal to *1*, the authors arguing that this was physically representative of the influence of a single polar functional group in a carbon chain (Gross & Vrabec, 2006). By setting the value of n_p equal to unity meant that Gross & Vrabec's polar term did not introduce a further regressable parameter to the nonpolar PC-SAFT's existing parameter set. This also avoided the numerical problem of a broad minimum in the objective function when considering models with four or more parameters, as was found in some instances with the Jog & Chapman polar term (Al-Saifi *et al.,* 2008; de Villiers *et al.,* 2011).

Similar treatments of quadrupolar molecules (Gross, 2005) and ionisable dipoles (Kleiner & Gross, 2006) went further to demonstrate the success of this approach. In a comparative study, incorporating both the Jog & Chapman and Gross & Vrabec polar terms into the sPC-SAFT framework, de Villiers *et al.,* (2011) argued that the n_p parameter should be left regressable in the same fashion as x_p if the two terms are to be judged on an equal footing. The study showed no clear superiority on the part of either polar term, but the most important result was that the transferability of the polar terms between SAFT variants was demonstrated.

2.3 Structural Isomerism: Properties & Equilibria

Structural or constitutional isomers are compounds with the same molecular formula, but different arrangements of the atoms. As a result of the formulaic similarity between the molecules, the properties of structural isomers are only subtly different. The ability to differentiate between such subtle differences constitutes a stringent test for any model. Thus, the accurate prediction of, and distinction between, the properties of structural isomers represents an interesting test of the predictive capacity of the SAFT EoSs.

The effects of structural isomerism are more pronounced in organic molecules containing polar or associating functional groups. The strength of the dipolar interactions are directly related to the location of the functional group within the molecule, as schematically illustrated in Figure 2.7. When a polar functional group is located near a terminal methyl group, the charge distribution about the molecule is highly asymmetrical and the dipolar interactions are strongest, resulting in significant deviation from ideality. As the polar group shifts centrally however, the charge distribution becomes symmetric about the molecule. This culminates in a dampening of the dipolar interactions of the molecule, producing smaller deviations from ideal behaviour.
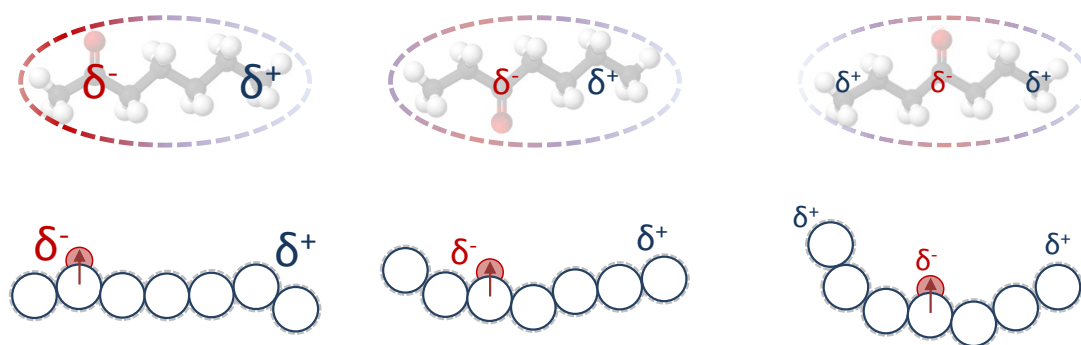
Figure 2.7: Schematic representation of the effect of polar functional group location on the charge distribution of the molecule (upper) and the structural impact of this charge distribution(lower). Font size indicative of the respective strength of dipolar interactions for the structural isomers.

The different intermolecular interactions of the different isomers manifest themselves on a macroscopic level in their associated phase behaviour. This is most readily seen in the unique vapour pressures of different structural isomers, as typified for the three structural isomers of heptanone in Figure 2.8. This is an important result for this study in particular, as trends in pure component vapour pressures are known to significantly influence the phase behaviour of mixtures containing these components.
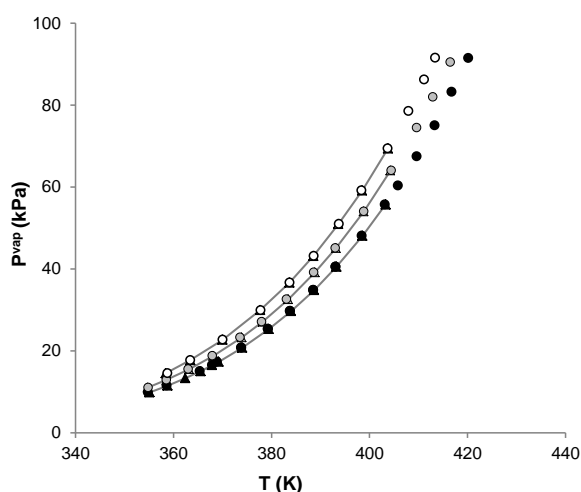
Figure 2.8: Vapour pressures of structural isomers of heptanone: ● 2-heptanone, ◐ 3-heptanone and ○ 4-heptanone. Key: ● Cripwell (2014) and ▲ Wu & Sandler (1988), with trend line through reference data.[1]

Literature Review

2.3.1   Mixture Phase Behaviour: Past Work

In a previous study (Cripwell, 2014), the effect of polar functional group location on the associated binary phase behaviour of polar structural isomers with a common second component was investigated. Using ketones as the homologous series of interest, the three constitutional isomers of heptanone were each paired with n-octane, n-nonane and n-decane and isobaric VLE data were generated for each of these nine systems (Cripwell *et al.,* 2015). It was found that the effect of the carbonyl group location within the chain was pronounced enough to generate distinct phase envelopes and azeotropic points for each isomer. This was particularly true for the case of mixtures where the second component exhibited a similar vapour pressure, as shown in Figure 2.9.
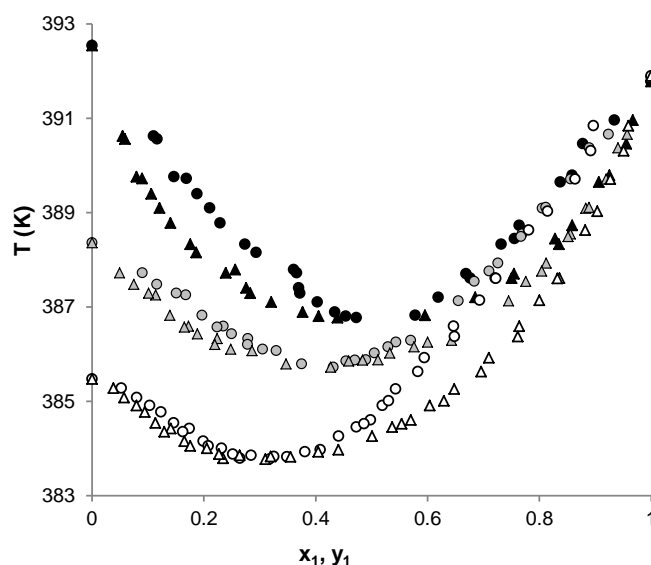
Figure 2.9: Isobaric VLE data for 2-heptanone (●& ▲), 3-heptanone (◐ & △) and 4-heptanone (○& △) with n-nonane at 40 kPa. The influence of carbonyl group location in ketone chain on the phase behaviour is highlighted.[2]

The ability of the sPC-SAFT$_{JC}$ and sPC-SAFT$_{GV}$ EoSs to accurately predict the witnessed phase behaviour of all nine binary systems, using parameters regressed from pure component properties alone, was assessed. Both models were found to give accurate predictions of the phase behaviour of the most polar isomer (2-heptanone) with all three n-alkanes, but the predictive capacity of sPC-SAFT$_{JC}$ was found to decrease rapidly as the functional group moved centrally. Specifically, the quality of the sPC-SAFT$_{JC}$ pure prediction worsened for the two less polar isomers (3- & 4-heptanone), to the extent that no prediction for the 4-heptanone case was possible as a unique parameter set could not be determined. As seen in Figure 2.10, the sPC-SAFT$_{GV}$ prediction did not suffer from the same shortcomings and the quality of the pure prediction remained high for all three isomers with each alkane.

---

[2] Reprinted (adapted) with permission from Cripwell et al., "Vapor–Liquid Equilibria Measurements for the Nine n-Alkane/Ketone Pairs Comprising 2-, 3-, and 4-Heptanone with n-Octane, n-Nonane, and n-Decane", J. Chem. Eng. Data, 2015, 60 (3), 602-611. Copyright (2015) American Chemical Society.
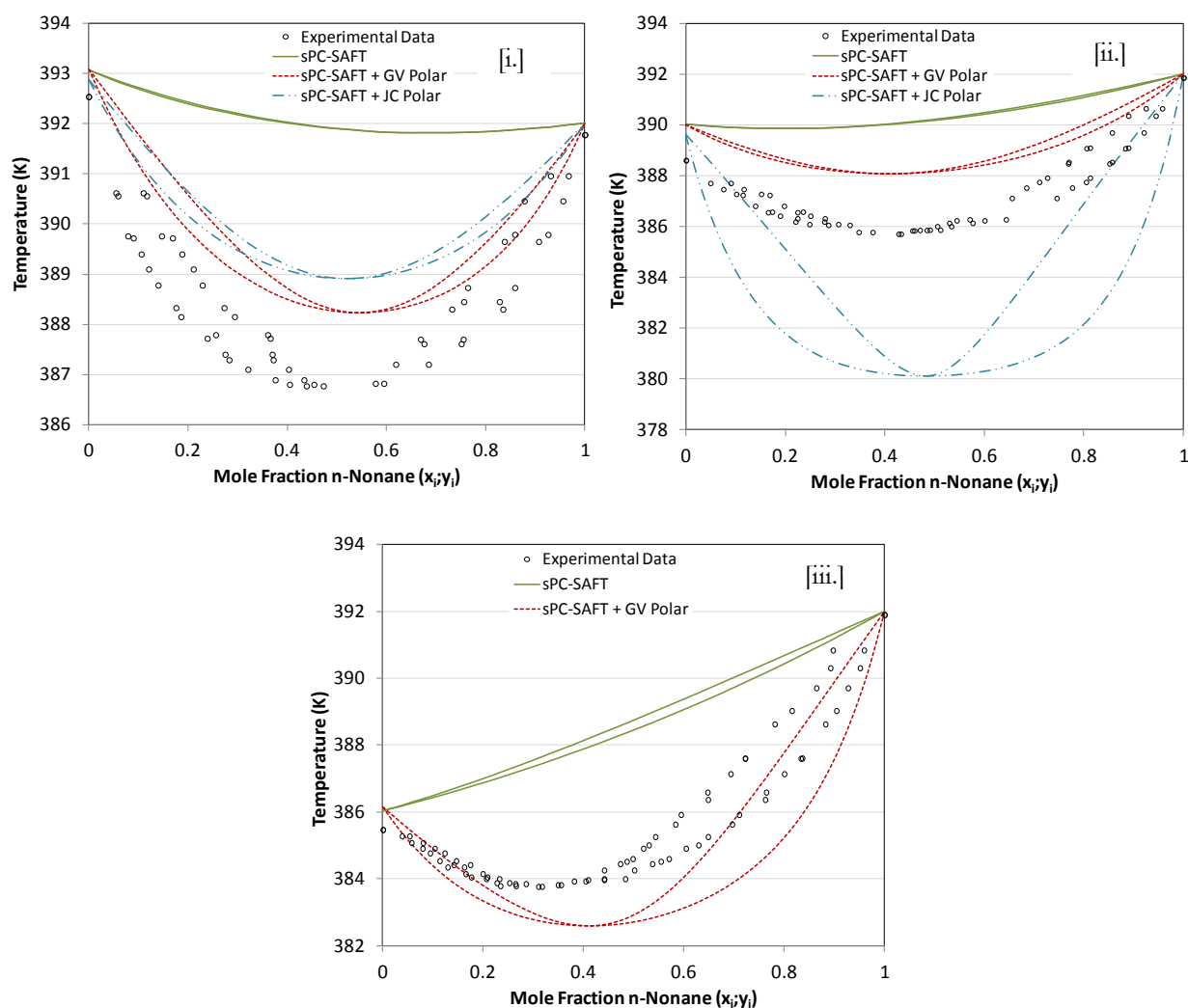
Figure 2.10: Pure predictions for isobaric VLE in [i.] n-nonane/2-heptanone, [ii.] n-nonane/3-heptanone & [iii.] n-nonane/4- heptanone systems at 40kPa. The worsening predictions of the sPC-SAFT$_{JC}$ parameter sets are highlighted in this progression. Figure reprinted from Cripwell (2014).

Given that this was the first demonstration of a clear superiority of one polar term over the other, a natural recommendation of the study was to establish whether the observed trends hold for other polar functional groups. For such an assessment to be made, reliable data with which to test these predictions are necessary.

2.3.2   Previously Measured Polar Isomer/n-Alkane VLE Data

The functional groups of interest to an extended investigation of the effect of structural isomerism on mixture phase behaviour are non-associating, unbranched, linear polar molecules. An extension of the previous study requires that the second component in the mixture be a normal alkane. This is to ensure that any observable difference between the phase behaviour of the different isomers are attributable to the shifting polar functional group alone, rather than any interaction of these groups with other polar and/or associating groups (Cripwell, 2014). The ester and ether functional groups satisfy this requirement, with the functional group structures schematically presented in Figure 2.11. Further, these

homologous groups omit the consideration of molecular association when considered in mixtures with n-alkanes.

[i.]	[ii.]	[iii.]
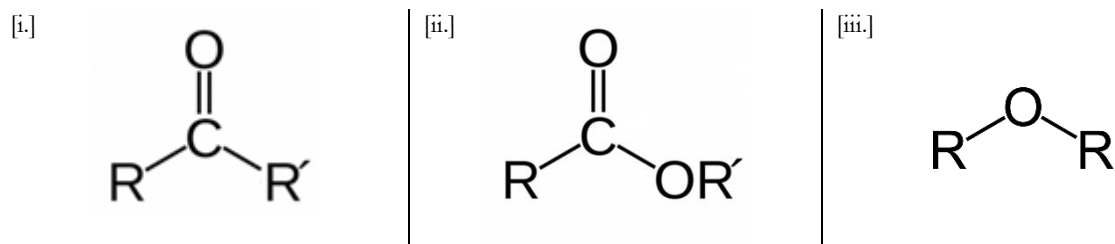
Figure 2.11: Schematic representation of [i.] ketone, [ii.] ester and [iii.] ether functional group structures

Table 2.1 summarises the availability of previously published VLE data for ether/n-alkane systems. Only ethers with the potential of three or more structural isomers are considered, limiting the summary to those ethers with a carbon number of *5* or greater. It is readily apparent that many more data sets are available for the phase behaviour of branched chain ethers than for their unbranched counterparts. This is due in large part, to the industrial relevance of branched ethers as fuel additives with good anti-knocking properties (Marsh *et al.,* 1999). Of significance to this study however, is that no published data sets are available for each linear isomer of a given length ether with a common n-alkane.

Table 2.1: Available VLE data in literature for aliphatic ethers (C₅ or heavier) with alkanes

Ether	Alkane	Reference
C₅ Ethers		
methyl butyl ether	heptane	Treszczanowicz*et al.*(1986)
ethyl propyl ether	*none*	
*methyl tert-butyl ether	hexane	Wisniak *et al.* (1997a)
	heptane	Segovia *et al.*(1998)
	octane	Wisniak *et al.* (1997b)
C₆ Ethers		
methyl pentyl ether	*none*	
ethyl butyl ether	*none*	
dipropyl ether	heptane	Gmehling *et al.* (1979)
	octane	Maripuri & Ratcliff (1972)
	nonane	
*methyl tert-amyl ether	hexane	Mejía *et al.* (2011)
	heptane	
*ethyl tert-butyl ether	hexane	Reich *et al.* (2000)
	heptane	
	octane	
	heptane	Gmehling & Onken (1999)

*Branched ethers

For esters, a plethora of data are available that systematically consider the effect of varied alkanolic or acidic chain lengths (while the other is kept constant) on the phase equilibria of these components in mixtures with a common second component. However, as the available data sets of

Table 2.2 attest, no individual studies or indeed collection of studies have systematically considered the phase equilibria of all linear isomers of a given ester with a common second component. Here, isomers of C_4 or larger are considered due to the greater degree of structural isomerism inherent in the ester homologous group.

Table 2.2: Available VLE data in literature for unbranched aliphatic esters (C_4 or heavier) with alkanes

Ester	Alkane	Reference
C₄ Esters		
propyl formate	heptane octane nonane	Galván *et al.* (1994)
ethyl acetate	hexane	Park *et al.* (2002) Gorbunova, *et al.*(1965)
	heptane octane	Shealy & Sandler (1985) Chen & Hu (1995)
Methyl Propionate	*none*	
C₅ Esters		
butyl formate	*none*	
propyl acetate	heptane nonane	Ortega *et al.* (2001)
ethyl propionate	*none*	
methyl butyrate	*none*	
C₆ Esters		
amyl formate	*none*	
butyl acetate	*none*	
propyl propanoate	heptane nonane	Ortega *et al.* (2001)
ethyl butyrate	*none*	
methyl valerate	*none*	
C₇ Esters		
hexyl formate	*none*	
amyl acetate	nonane	Kirss *et al.* (2001)
butyl propionate	*none*	
propyl butyrate	heptane nonane	Ortega *et al.* (2001)
ethyl valerate	*none*	
methyl caproate	*none*	

The lack of available data for ester and ether isomers to perform the same modelling exercise as was done for ketones necessitate and justify the generation of new phase equilibrium data for this purpose.

2.4 Thermodynamic Consistency

The accuracy and reliability of experimental phase equilibrium data are vital if those data are to be used to assess the predictive accuracy of thermodynamic models. As a thermodynamic property, equilibria data can be tested for their conformance to our understanding of the fundamental thermodynamic

Literature Review

principles at play. In the case of phase equilibrium, this is governed by the Gibbs-Duhem equation (Sandler, 2006):

$$0 = -\left(\frac{\partial \theta}{\partial T}\right)_{P,n_i} dT - \left(\frac{\partial \theta}{\partial P}\right)_{T,n_i} dP + \sum x_i d\bar{\theta} \qquad 2.5$$

This theoretical thermodynamic consistency correlation demonstrates the interconnectivity of partial properties in a solution and that these properties are not independent. The excess Gibbs energy is used as the hypothetical property Θ of equation 2.5, thus, application to a binary mixture in the special case of isothermal and isobaric conditions results in (Smith *et al.* 2005):

$$0 = x_1 \frac{d\ln\gamma_1}{dx_1} + x_2 \frac{d\ln\gamma_2}{dx_1} \qquad 2.6$$

The Gibbs-Duhem equation in this form is a theoretically derived relationship adhering to strict thermodynamic principles. However, the activity coefficient is determinable from experimental phase equilibrium data, with the compositions easily measured. The right hand side of equation 2.6 is therefore readily calculated for an experimental data set, but the data's adherence to the equation's equality criterion is a test of that data set's adherence to thermodynamic principles and thus its thermodynamic consistency. Equation 2.6 also serves as the basis for a number of thermodynamic consistency tests developed in the literature.

2.4.1   McDermott-Ellis Consistency Test

The McDermott-Ellis consistency test (McDermott & Ellis, 1965) is a point-to-point consistency test, which assesses the thermodynamic consistency of each successive pair of data points. In this way, inconsistent data can be identified and excluded as they arise. The test starts by numerically integrating equation 2.6 over the whole composition range using the trapezoidal rule to yield:

$$0 = \sum \left(x_{i,c} + x_{i,d}\right)\left(\ln\gamma_{i,d} - \ln\gamma_{i,c}\right) \qquad 2.7$$

The summation is over all components in the mixture for consecutive data points, *c* and *d*. Given the uncertainty inherent in experimental measurements, strict adherence to the need for equation 2.7 to equal zero was considered excessively limiting in the assessment of experimental data. McDermott and Ellis thus vaguely suggested that the criterion for judging between consistent and inconsistent data be dependent upon the accuracy of compositional measurement. The guideline provided was a maximum deviation of *0.01* for uncertainties of *±0.001* mole fraction. This indefinite criterion was refined by

Wisniak & Tamir (1977), who argued that this maximum should be considered a function of the respective uncertainties in the measurable physical properties according to:

$$0 = \sum \left(x_{i,c} + x_{i,d} \right) \left(\frac{1}{x_{i,c}} + \frac{1}{x_{i,d}} + \frac{1}{y_{i,c}} + \frac{1}{y_{i,d}} \right) \Delta x + 2 \sum \left| \ln \gamma_{i,d} - \ln \gamma_{i,c} \right| \Delta x$$
$$+ \sum \left(x_{i,c} + x_{i,d} \right) \frac{\Delta P}{P} + \sum \left(x_{i,c} + x_{i,d} \right) \beta_i \left(\frac{1}{\left| T^{sat}_{c} + \delta_i \right|^2} + \frac{1}{\left| T^{sat}_{d} + \delta_i \right|^2} \right) \Delta T \qquad 2.8$$

In equation 2.8, the Δ terms are the experimental uncertainties in the relevant measure quantity, while β_i and δ_i are the B_i and C_i constants respectively.

Point-to-point tests, such as the McDermott-Ellis consistency test, constitute one of two broad types of consistency tests. Unlike the point-to-point tests, area consistency tests consider the data set as a whole and define a tolerance with which the consistency of that data set can be judged. One such area consistency test is the L/W consistency test as described in the following section.

2.4.2   L/W Consistency Test.

The general description of the Gibbs free energy for equation 2.5 can be defined in terms of the excess enthalpy and excess volume of the system:

$$0 = \frac{H^{ex}}{NkT^2} dT - \frac{V^{ex}}{NkT} dP + \sum x_i d \ln \gamma_i \qquad 2.9$$

The starting point for such area consistency tests as the L/W test is the integration of equation 2.9 over the entire composition range. If the special case of isobaric and isothermal conditions is once again assumed, the result is an integral of the natural logarithm of the activity coefficient ratio over the composition range:

$$0 = \int_0^1 \ln \frac{\gamma_2}{\gamma_1} dx_1 \qquad 2.10$$

Thus, a plot of *ln(γ₂/γ₁)* against the composition, using any experimental data set, yields a plot crossing the *x*-axis along the binary composition range. For that data to be considered thermodynamically consistent, the areas above and below the curve need to be equal (Wisniak, 1994).

For a given experimental data set however, the equality criterion of equation 2.10 can never truly be met given that phase equilibria measurements are made at *either* constant temperature *or* constant pressure conditions. Starting instead with the full Gibbs free energy description of equation 2.9, in the

case of isothermal operation, the excess volume can be assumed approximately constant, yielding the same result as presented in equation 2.10 for data consistency testing (Wisniak, 1994). Excess enthalpy however, can never be assumed constant and thus the isobaric operation case does not simply reduce to the convenient representation of equation 2.10. The need to account for the effects of excess enthalpy is a significant hurdle as such data are rarely for the whole composition range, at the relevant temperature and pressure of interest.

In the development of the L/W consistency test, Wisniak (1993) sought to address this problem by considering the $\underline{G}^{ex}$-T relationship at equilibrium rather than the Gibbs-Duhem equation explicitly:

$$\underline{G}^{ex} = NkT\sum x_i \ln \gamma_i \qquad 2.11$$

By assuming that nonidealities are confined to the liquid phase, experimental activity coefficients can be calculated using Raoult's law. Similarly, assuming a constant heat of vaporisation and negligible liquid molar volume compared to that of the vapour, the Clausius-Clapeyron equation can be used to defined the ratio of the system pressure to the component vapour pressures, yielding the following description of $\underline{G}^{ex}$ (Wisniak, 1993):

$$\Delta S = \sum x_i \Delta S_i^{vap}$$

$$w = \sum x_i \ln\left(\frac{y_i}{x_i}\right) \qquad 2.12$$

$$\therefore \underline{G}^{ex} = \sum x_i \Delta S_i^{vap}\left(T_i^{sat} - T\right) + NkT\sum x_i \ln\left(\frac{y_i}{x_i}\right)$$

Wisniak (1993) used this result to derive an expression for the mixture bubble point in terms of the defined parameters:

$$\gamma_i = \frac{y_i P}{x_i P_i^{sat}}$$

$$\ln\frac{P}{P_i^{vap}} = \frac{\Delta H_i^{vap}\left(T_i^{sat} - T\right)}{NkT_i^{sat}T} = \frac{\Delta S_i^{vap}\left(T_i^{sat} - T\right)}{NkT} \qquad 2.13$$

$$T_b = \sum \frac{x_i \Delta S_i^{sat} T_i^{sat}}{\Delta S} - \frac{\underline{G}^{ex}}{\Delta S} + \frac{NkTw}{\Delta S}$$

This bubble point relation can be manipulated to yield an equality relationship which serves the basis for the L/W consistency test, where the index z refers to equilibrium pairs of VLE data:

$$L_z = \sum_z \frac{x_i \Delta S_i^{sat} T_i^{sat}}{\Delta S} - T_b = \frac{G^{ex}}{\Delta S} - \frac{NkTw}{\Delta S} = W_z \qquad 2.14$$

Integrating equation 2.14 over the composition range yields the equality criterion and area basis of the L/W test:

$$L = \int_0^1 L_z dx_1 = \int_0^1 W_z dx_1 = W \qquad 2.15$$

As with the McDermott-Ellis test previously, strict adherence to this equality constraint is excessively limiting for real experimental data. As a result, Wisniak defined an acceptable deviation to account for experimental uncertainty.

$$D = 100 \frac{|L-W|}{L+W} \qquad 2.16$$

Wisniak proposed that thermodynamic consistency of an experimental data set is indicated by a maximum value for *D* of *3* to *5*. The lower limit is based on similar limits for the Herrington area test while the upper limit accounts for errors resulting from potential uncertainty in heats of vaporisation (Wisniak, 1993). Data not adhering to these contraints may thus be declared thermodynamically inconsistent. The important caveat however, is that because this development was not derived from the Gibbs-Duhem equation, data cannot be considered thermodynamically *consistent* using this test alone. It is thus necessary to use a theoretically based test, such as the McDermott-Ellis test of the previous section, in conjunction with the L/W test to rigorously assess the thermodynamic consistency of experimental data.

2.5 Chapter Summary

This chapter provided background on the development of the SAFT family of EoSs up to and including the variants and polar terms of interest to this study. The role of the dipole moment in distinguishing the behaviour of polar molecules from their nonpolar counterparts was discussed, and the subtle but important role of its location in the carbon chain was highlighted. The effect of this functional group location on mixture phase behaviour for different isomers was shown to be the focus of previous work and the basis of the work presented here. However, the lack of available data in the literature to extend the modelling investigation to ethers and esters was highlighted and the need to generate new experimental VLE data for such systems was underlined. Addressing this deficiency defined the objectives of the experimental phase of this work and the means by which these data were generated is the subject of the following chapter.

Chapter 3: EXPERIMENTAL METHODOLOGY

The aim of this chapter is to describe the experimental approach adopted to generate isobaric phase equilibrium data. In the sections that follow, a description of the materials will be provided while the apparatus and methodology used will be described in detail.

3.1 Materials

Table 3.1 lists the chemicals used for both the phase equilibrium experiments, and the subsequent analysis of the equilibrium samples. The chemical assays on a mass basis are listed, with all components purchased from Sigma Aldrich.

Table 3.1: List of chemicals used for phase equilibrium experiments with purities on a mass basis

Component	CAS Number	Purity (mass%)
n-heptane	142-82-5	99%
n-octane	111-65-9	≥99.0%
2-butanone	78-93-3	≥99.7%
2-heptanone	110-43-0	98%
methyl valerate	624-24-8	99%
ethyl butanoate	105-54-4	99%
propyl propanoate	106-36-5	99%
butyl acetate	123-86-4	≥99.5%
pentyl formate	638-49-3	95%
butyl- ethyl-ether	628-81-9	99%
di-n-propyl ether	111-43-3	≥99.0%
2-ethyl-1-hexanol	104-76-7	≥99.6%

All components listed in Table 3.1 were analysed by gas chromatography prior to experimentation in order to verify the listed purities by looking for significant impurity peaks. The results of the analysis indicated that all components adhered to or exceed their listed assays. All but one (pentyl formate) of the components used during the phase equilibrium experiments were at least 99 mass% pure and were thus considered appropriate for use.

The results for the pentyl formate indicated that a significant impurity of approximately 5 mass% was indeed present. Subsequently, a sample of the ester was analysed by gas chromatography-mass spectrometry (GC-MS) where the impurity was identified as 1-pentanol (see Appendix A for the GC-MS results). The most convenient means of stripping the 1-pentanol from the pentyl formate was by means of pot distillation, but first it was necessary to determine whether the desired separation could be achieved via distillation. To this end, it was desirable to find existing experimental data for a binary mixture of

1-pentanol/pentyl formate to determine the phase behaviour for the system at atmospheric pressure, and whether an azeotrope is present in the systems at these conditions. However, no data for the system were available in the literature and in lieu of using an experimental data set, it was necessary to use a thermodynamic prediction of the system as a first approximation.

This system comprises an associating 1-alkanol and a polar ester and can thus be modelled within a polar sPC-SAFT framework with appropriate pure component parameters. As with the experimental data however, no parameters have been published for pentyl formate in any SAFT framework. On the other hand, parameters have been published for two of pentyl formate's structural isomers (de Villiers *et al.,* 2011a) as well as for 1-pentanol (de Villiers *et al.,* 2011b). While modelling these systems does not give an accurate representation of the phase behaviour of the 1-pentanol/pentyl formate system, the trends apparent for the azeotropic point in the systems containing the ester's isomers at least indicate whether purification of the ester by distillation is possible. To this end, the phase behaviour of the 1-pentanol/propyl propanoate and 1-pentanol/butyl ethanoate systems were modelled at atmospheric pressure (in Stellenbosch, ± 1 bar), and the results are presented in Figure 3.1.
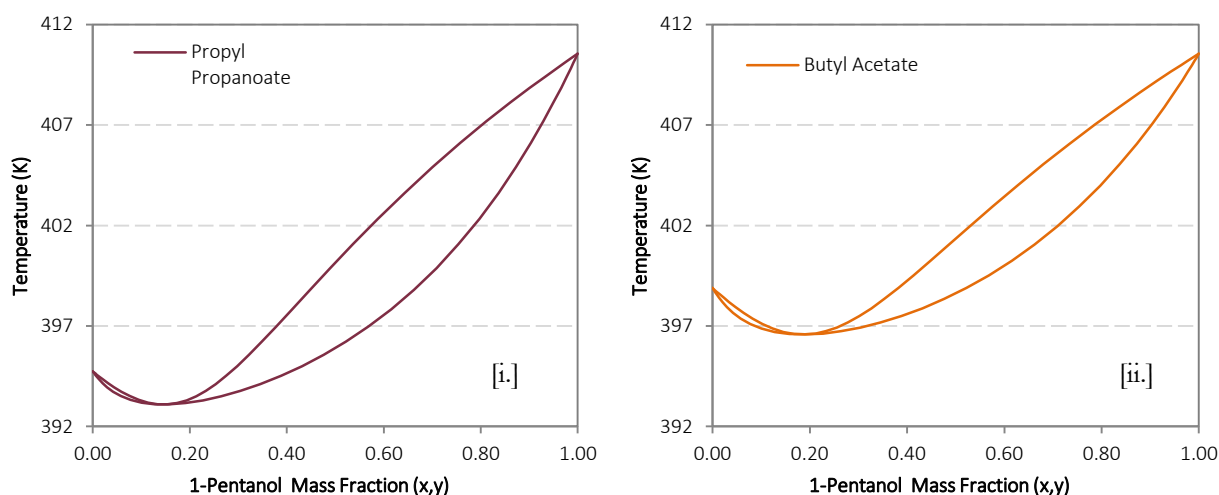
Figure 3.1: sPC-SAFT GV predictions for the phase behaviour of [i.] 1-pentanol/propyl propanoate and [ii.] 1-pentanol/butyl ethanoate systems at 1 bar

Given that the results in Figure 3.1 show azeotropic behaviour in the 1-pentanol/propyl propanoate and 1-pentanol/butyl ethanoate systems, it is reasonable to assume that similar positive deviations from ideality exist in the 1-pentanol/pentyl formate system. Furthermore, it is apparent from Figures 3.1 [i.] and [ii.] that the azeotropic point is getting richer in 1-pentanol as the *alkyl-* chain of the ester lengthens; specifically at ± 14 mass% for the propyl ester and ± 18 mass% for the butyl ester. Thus, it is reasonable to assume that this trend continues for the pentyl ester and that any azeotrope present in the system does not prevent purification of the pentyl formate by distillation. Furthermore, by analysing the form of the phase envelopes, we can intuit that distillation of the *95* mass% pure pentyl formate will produce a liquid phase richer in the ester, while the vapour phase will approach the azeotropic composition with successive runs in a batch still.

With the expectation of producing a bottoms product richer in pentyl formate, the stock material was batch distilled four times, with the liquid product of each successive run analysed by the GC-MS to determine the change in composition. After the fourth run, it was noted that no significant change in the concentration had taken place compared to the results of the third run, bearing in mind the minimum volume of purified pentyl formate required to run the VLE experiments. Thus, purification yielded a product of *98.2* mass% purity, according to the GC-MS analysis (results in Appendix A), which was considered acceptable for the purposes of the experimental work.

3.2 Apparatus

An all-glass dynamic recirculating still was used to measure the phase equilibrium data, schematically presented in Figure 3.2. The full figure legend is available in the works of Pienaar (2011) and Cripwell (2014), although appropriate descriptions are provided in Sections 3.2.1 and 3.3 that follow. The unit is a commercially produced still, model VLE 100D from Pilodist of Germany.

3.2.1   Unit Description

Primary operation of the still takes place in the boiling chamber (1.3), where an electrical immersion heater (10) is installed concentrically and supplies sufficient heat to partially vaporise the liquid mixture. At the top of the boiling chamber, the unit walls converge to the base of a spirally curled Cottrell tube (1.2) where slugs of liquid and vapour pass by a pressure differential into the separation chamber. During this time, concentrated mass transfer between the two phases takes place and it is here that phase equilibrium is attained. At the interface between the Cottrell pump and the separation chamber, the two phases pass over a Pt-100 temperature probe (7) where the equilibrium temperature is measured. The two phases split within the separation chamber; the denser liquid leaving at the base while the vapour rises to the top of the chamber. Construction of the chamber ensures that liquid drops do not become entrained in the rising vapour, and prevents partial condensation of the vapour phase within the chamber.

After the phases are split, the liquid flows down a graduated line to the liquid phase sampling point (11), where a condenser (1.7) is located above the sampling point to ensure the equilibrium liquid remains in the liquid phase for sampling. The vapour on the other hand passes through the first of two condensers (1.12) so as to produce a condensed equilibrium vapour to be taken from the vapour sampling point (12). As with the liquid arm of the unit, a second condenser (1.11) is present to make sure the condensed vapour remains in the liquid phase to ensure a representative sample. Provision is made however, at the top of the separation chamber (sampling point 1.5) to allow the extraction of an equilibrium vapour sample in the vapour phase prior to the condenser. The shallow wells at the liquid and condensed vapour sampling points ensure that the accumulating equilibrium phase is consistently renewed by the flow of new material from the separation chamber. From the wells, the condensed equilibrium phases are returned to the mixing chamber (1.1), where a magnetic stirrer serves the dual purpose of mechanically stirring the mixture and inducing flow of the mixture back into the boiling chamber. From here, the circulation procedure is repeated. The still was originally modified to house an ultrasonic

homogeniser (17) for the measurement of vapour-liquid-liquid equilibria. While the homogeniser was not used in this work, it does need to be secured in its housing to keep the unit sealed during operation.

The unit as illustrated in Figure 3.2 is installed within an extraction cabinet due to the flammable nature of the components used. Pressure is measured by means of a Wika UT-10 pressure transmitter with an operating range of *0-1.6* bar abs and a calibrated accuracy of *0.1* % of full scale output (thus in absolute quantities, *1.6* mbar). The maximum operating temperature of the still is rated at *250* °C, with temperature recorded using a four-wire Pt-100 probe connected to a digital Hart Scientific thermometer with an accuracy of *0.03* °C. The probe was calibrated by a SANAS approved laboratory prior to commencement of this study, with the certificate of calibration (provided in Appendix B) indicating an uncertainty in temperature measurement of *0.1* °C over the temperature range of interest to this study. This drift was accounted for in the recorded temperatures presented in this work.

Figure 3.2: Schematic representation of the Pilodist dynamic recirculating still used for VLE measurements. Figure reprinted with permission (Pienaar, 2011)

3.3   Experimental Procedure

A brief description of the experimental procedure is presented in this section, giving an overall summary of unit operation and analysis of the equilibrium samples. The numerical references in parentheses refer to the labels of Figure 3.2 as in Section 3.2 previously.

3.3.1   Preliminaries

As alluded to in Section 3.1, accurate measurement of phase equilibrium data is contingent on uncontaminated pure component species in the charged binary mixture. Thus, prior to operation of the still, it was important to ensure that the unit was both clean and dry to prevent contamination. To this end, the unit had to be washed beforehand with an appropriate volatile solvent to remove liquid residues from previous experiments (this procedure will be described in Section 3.3.4) followed by running compressed air through the unit to vaporise residues of the washing solvent.

Given the relatively volatile nature of some of the components used in this work, it was necessary to use chilled water as the cooling medium in the condensers. Thus it had to be ensured that the water in the bath had been left to cool by the chiller for an appropriate time before the pump was turned on to circulate the water through the unit's condenser lines. At this stage, the still could be turned on and the controlling software opened.

3.3.2   Unit Preparation

In order to run the still under vacuum, the appropriate selection needed to be made within the control software and using the three-way valve on the pneumatic box of the still. Before adding the mixture of interest to the unit, the homogeniser needed to be securely fitted in its housing and the discharge valve (1.4) closed. At this point, approximately *110* cm^3 of one of the pure components in the mixture could be charged to the feed burette, although this amount was somewhat variable and dependent on the volatility of the components in the mixture. The fed volume needed to least completely submerge the immersion heater (10) when the liquid was fed to the mixing chamber (1.1) from the feed burette. With the liquid loaded, the magnetic stirrer was turned on.

The reason experiments were always started with a pure component was twofold: firstly, the pure component boiling point could be used as a means of verification at the start of each run, ensuring no contamination at the start of the experiment and; secondly, the most systematic way of moving across the composition space would be to successively add small amounts of the second component to the first already charged to the still.

Within the controller software, the heater power had to be specified, along with the set points for the mantle temperature and the operating pressure. The heater power once again depended on the volatility of the components in the given mixture while the mantle temperature depended on the equilibrium temperature for the given feed composition. The heater power is set as a percentage of the

total output and needed to be correctly balanced to achieve equal circulation of both equilibrium phases for sampling. Too low a power setting and the mixture would be heated but not vaporised resulting in no vapour return, while too high a setting would vaporise too much of the mixture and result in no liquid circulation. The mantle heater maintained the temperature of the separation chamber wall so as to prevent unintentional condensation of the vapour phase before the condensers (1.11 & 1.12). However, due to the rudimentary on-off control of the mantle heater, large oscillations around its set point were evident during experiments and thus the set point had to be set some *15* °C lower than the equilibrium temperature to ensure the mantle temperature did not exceed the equilibrium value.

The installed pressure transmitter was a modification to the original unit and changed the means by which the pressure was regulated. The original setup employed a Pilodist M101 pressure control system to automatically control the system pressure under vacuum operation. This made use of simple on-off control of the vacuum pump, but resulted in fairly large pressure oscillations (±*5* mbar) around the operating set point which, at system pressures of *600* mbar, were considered too large. Thus, the set point on the controller was fixed at a value *50* mbar lower than the operating pressure to ensure the vacuum pump stayed on, while the amount of vacuum drawn from the unit was manually throttled to maintain the desired operating pressure. This produced much smaller oscillations (max ±*2* mbar), resulting in a more stable equilibrium within the unit.

3.3.3   Experimental Runs

A given experimental run was commenced once the set points had been fixed. Using appropriate power settings, the liquid began circulating within *5* minutes while condensed vapour return was evident within *20* minutes. Due to the concave nature of the sample collection ports beneath the sampling wells (11 & 12), periodic flushing of the ports was necessary to clear the liquid film accumulated from previous runs to prevent contamination. These ports were flushed after *20* and then *40* minutes in the following manner:

- The solenoid valves for both the liquid and vapour arms of the still (8 & 9) were opened using the remote control within the unit casing. The valves were only opened to allow a small amount of each phase to wash the walls of the ports before being closed again.
- The liquid accumulated as a result of flushing was then drained into the respective glass receiver vials (5 & 5.1) by opening the respective stop valves (1.8 & 1.16). These valves were then immediately closed again.
- After the second flushing at *40* minutes, the flushed liquid needed to be removed. To this end, the isolation valves (1.10) for both phases needed to be closed before the vacuum could be broken, so as to isolate the respective arms of the still. In this way, the vials could be removed while vacuum operation of the still was maintained. To do so required subsequently opening the aeration valves (1.18) before removing the vials and discarding the flushed liquid.

- The sample vials were then swapped for clean ones for taking the equilibrium samples. Upon replacing the vials and refitting them to the still, the aeration valves could be closed and the isolation valves opened to bring the pressure in the arms back down to the operating pressure.

Replacing the vials after the flushed liquid was discarded resulted in a small surge in the system pressure (and the coupled equilibrium temperature) as the arms were brought back down to the operating pressure. This inevitably affected the equilibrium and thus the still was left to run for a further *20* minutes to allow for the micro-fluctuations caused by the flushing procedure to level out and for the equilibrium to be reobtained. In this way, equilibrium was attained after *60* minutes of run time and was indicated by a stable vapour temperature and steady return of both phases. A vapour circulation rate of *30* drops per minute at the vapour return point (left of 12) was considered sufficient to produce a large enough equilibrium sample to prepare analytical samples.

While a liquid phase equilibrium liquid sample was taken (11), the equilibrium vapour phase could be taken as either a vapour (1.5) or a condensed liquid (12). Due to the complete miscibility of all binary ester/alkane and ether/alkane mixtures considered in this study, combined with the technical difficulties in manually extracting a large enough vapour sample, it was decided that condensed vapour samples would be taken in this study. Samples were taken as per the procedure for flushing detailed above, with the obvious exception that the samples were kept for preparing analytical samples rather than being discarded. The vapour temperature was monitored while the solenoid valves were opened to ensure that no temperature changes occurred during sampling – this constant temperature was recorded as the equilibrium temperature for that run.

Once the equilibrium samples had been taken, the given experimental run came to an end and the still was stopped and the aeration valves opened to bring the unit back up to ambient pressure. In the case where additional runs were being performed on that day, more of the second component could be introduced to the unit via the feed burette at this point. The amount of the component to be added was simply the volume which would result in re-submersion of the immersion heater, generally ± 10 cm³. Thereafter, successive runs could be performed using the same procedure detailed above.

3.3.4   Draining and Washing

At the end of a given day of experiments, the liquid mixture could be left in the still overnight to resume experimental runs the following day, according to Section 3.3.3 above. However, if experiments were to start from the other side of the composition space or indeed with a new binary system, it was necessary to drain and wash the still so as to flush any non-volatile liquids left over from the experiment and prevent contamination of the next experimental runs. In order to drain the still, it was necessary to allow the mixture to cool to ambient temperature before draining the contents via the discharge valve (1.4), and to remove the homogeniser to drain any accumulated liquid in its housing. Thereafter, the homogeniser was refitted and the discharge vial closed again so that wash acetone could be added to the

still. Acetone was chosen as it met both the solvation and volatility criteria for the wash solvent highlighted in Section 3.3.1 above. The still was then set to run at ambient pressure for *30* minutes to allow the acetone to circulate through and "wash" both the vapour and liquid arms of the still. During this time, the ports were flushed with the acetone as was done during the experimental runs to ensure the sampling wells were also washed. After running and being left to cool, the acetone could also be drained from the still and the unit left with all aeration valves open to dry overnight.

3.3.5   Analytical Procedure

The compositions of the equilibrium phases were quantified by means of gas chromatography using a Varian CP-3380 gas chromatograph fitted with a flame ionisation detector (FID). A ZB Wax capillary column (*30*m x *0.32*nm x *1*μm), with helium as the carrier gas, was operated using a graduated temperature programme of *17* minutes to quantify each analytical sample. These samples were prepared as follows:

- *2* mL sample vials were loaded with ±*1.5* mL of the analytical solvent, i.e. 2-ethyl-1-hexanol, and weighed.
- *30* μL of internal standard (2-heptanone) was pipetted into the solvent, with the sample again weighed to yield the mass of standard added.
- *15* μL of the experimental sample was added to the solvent, with the vial weighed a third time to yield the mass of sample added.

Two analytical samples were prepared from each equilibrium phase of each experimental sample, resulting in a total of four analytical samples per experimental run/equilibrium temperature. An average was taken of the two composition results for each phase at each temperature to produce a single datum point which is reported in this work.

Quantification of component concentrations using an internal standard was achieved by creating a calibration curve for each component. Using an appropriate temperature profile, the GC produces distinct peaks for each component, the area of which is directly proportional to the quantity of that component in the sample. The calibration curves relate the peak areas of the component and the standard to their quantities (here, masses) by the following simple proportionality equation:

$$\frac{Area_{std}}{Area_{i}} = k_{i}\frac{mass_{std}}{mass_{i}} \qquad 3.1$$

In equation 3.1, k_i is the response factor for component *i* with respect to the internal standard, and is unique for each component in a mixture, provided the same GC operating conditions are used throughout. The calibration curve for each component was thus created by preparing samples containing known masses of both components and the internal standard and inferring the value of the response factor for each component using the relationship in equation 3.1. Thus, for each of the ester/alkane and

ether/alkane mixtures of interest, five samples of known mass were prepared to construct the calibration curves. Each sample contained different ratios of the two components, such that the full composition spectrum of the binary mixture could be accounted for. Each known sample was analysed four times on the GC, with the averages used to produce the calibration curve and yield the response factor for each component in each mixture, detailed in Appendix C.

3.4 Compositional Error Analysis

While the pressure and temperature deviations were directly measurable through uncertainties of calibration and observable fluctuations during experimentation, the errors associated with reporting compositions of equilibrium samples have to be somewhat inferred. The two major factors in determining compositional uncertainty are the effects of experimental fluctuations and errors associated with the analytical procedure.

3.4.1 Experimental Uncertainty

The equilibrium sample compositions are outputs of the phase equilibria experiments, and, as such, are directly influenced by errors and fluctuations in the input variables. Within the experimental procedure, there are two such input variables; specifically the power setting to the immersion heater and the operating pressure set point. The heater power is maintained at a constant setting throughout the experimental run and thus its effect on the uncertainty in compositional measurement can be considered negligible. Given the manual throttling of the vacuum drawn from the system, and the inherent pressure oscillations mentioned in Section 3.3.2 previously, the effect of fluctuations in the system pressure cannot be similarly neglected and must be explicitly accounted for.

As detailed in Section 3.3.2, manual throttling of the vacuum drawn from the system maintains the system pressure to well within ± 2 mbar of the desired operating pressure throughout the experimental run. Thus it is desirable to determine the impact of this pressure oscillation on the resulting equilibrium composition. In lieu of a means of directly measuring this effect, the effect of the worst case scenario pressure fluctuations can be modelled and compared to the equivalent set point prediction, provided an accurate model of the system phase behaviour is used. As will be detailed later, the sPC-SAFT$_{GV}$ model yields an excellent prediction of the ethyl butanoate/n-octane system and can thus be used for the compositional error analysis here. The reason for choosing this system as reference is explained in the course of the discussion of the analysis results which follow. The results of modelling the system at the set point and at the two pressure fluctuation extremes are presented in Figure 3.3 [i.] and [ii.].
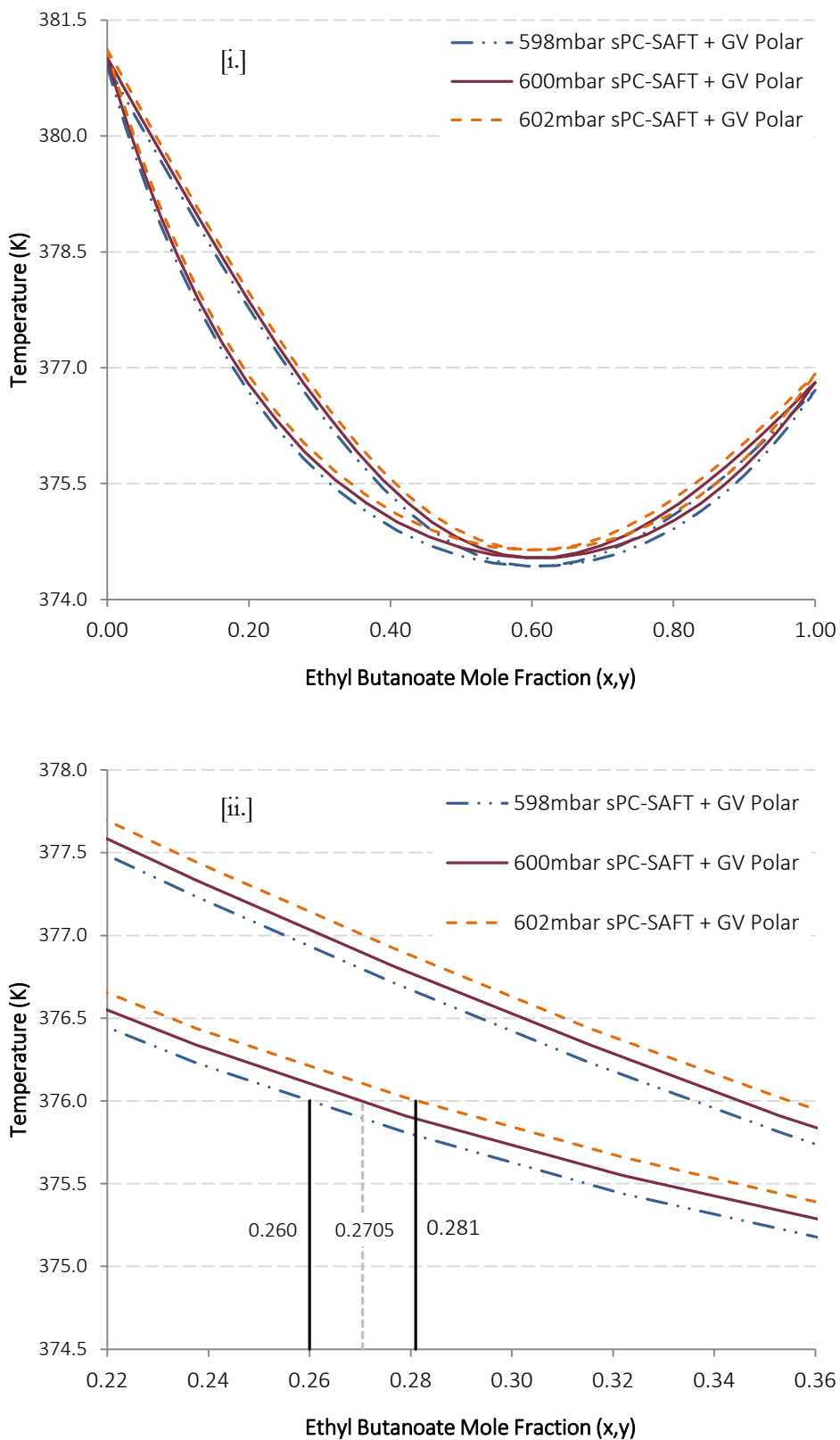
Figure 3.3: Effects of worst case pressure fluctuation on resulting equilibrium composition measurements. [i.] Entire phase envelope. [ii.] Representative section of the phase envelope, highlighting the compositional uncertainty.

In Figure 3.3 [ii.], a section of the full phase envelope in the region of *30* mole% ethyl butanoate is used for the purpose of the analysis. If the equilibrium temperature is taken as reference for all three phase envelopes, it can be seen that the *2* mbar pressure fluctuation has an associated compositional deviation of *0.011* mole fraction at a reference mixture composition of *~0.27* mole fraction. It can be argued that larger deviations would result if the section taken in Figure 3.3 [ii.] was closer to the azeotropic point; however it can similarly be argued that a smaller compositional deviation would be evident for sections closer to the pure component ends of the mixture spectrum. In the same way, performing the analysis on the vapour phase would also yield similar trends. Thus, the section presented is chosen to be representative of the average deviations across the entire composition range, for both equilibrium phases.

Figure 3.3 illustrates the effect of the maximum pressure oscillations, but as previously noted, the pressure was generally controlled to well within these maximums, particularly around the time of sampling. Thus, to get an idea of the representative effect of the average pressure fluctuations, we can consider its impact on the instantaneous experimental output; the vapour temperature. If it is assumed that the micro-fluctuations seen in the temperature are a direct result of the average pressure oscillations at any given time, the temperature fluctuations can be used to infer the average pressure oscillations. Thereafter, using a similar analysis to that performed in Figure 3.3, the effect of these average pressure oscillations on the compositional uncertainty can be inferred. This assumption can be justified by considering that the thermal equilibrium in the unit is slower than the mechanical equilibrium, with the chemical equilibrium slower still. Thus, the fluctuations in temperature and equilibrium composition caused by the pressure oscillations will be smaller than those in the pressure and will average out in a smaller range.

To perform this analysis, the average temperature fluctuations during sampling were considered, on average found to be *0.02* °C at the time of sampling. If Figure 3.3 [ii.] is reconsidered, the average pressure fluctuation will be inferred by modelling the system such that the phase envelope passes through the same composition (here, *0.2705* mole fraction) at temperatures *0.02*°C higher and lower (diamonds in Figure 3.4). The resulting average pressure fluctuation is *0.3*mbar; significantly less than the maximum *2* mbar listed previously. The associated effect on the composition, taken to be the true experimental uncertainty as a result of pressure fluctuations, is calculable from the model predictions at *600.3*mbar and *599.7*mbar (circles in Figure 3.4) and shown to be *0.0015* mole fraction.

As mentioned, the effect of pressure fluctuations on compositional measurements is largest around the azeotrope, with the fluctuations having a smaller influence moving further from the azeotropic point and closer to the pure component extremes. It is for this reason that it is important to perform this analysis on a system exhibiting azeotropic behaviour, specifically because the azeotrope exhibits the worst case scenario which is the goal of this analysis. Further, it is evident from Figure 3.4 that the gentler the slope of the phase envelope, or the smaller the temperature range of the system, the more pronounced the effect of the pressure fluctuations will be on the compositional deviations. Given that the ethyl butanoate/n-octane system exhibits azeotropic behaviour and the phase envelope is formed over a small temperature range mean that this system is suitable for the analysis performed here.
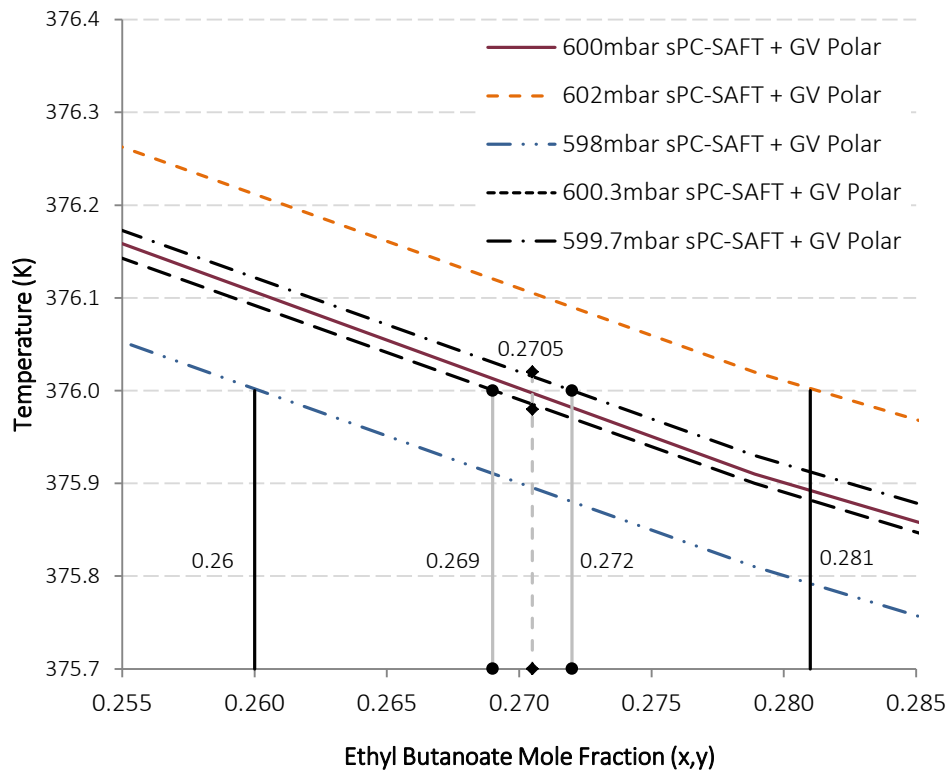
Figure 3.4: Representative section of bubble curve for the phase envelopes corresponding to the average pressure oscillations (0.3mbar). Associated uncertainty in compositional measurements (0.00105 mole fraction) inferred from deviations indicated.

3.4.2   Analytical Uncertainty

While the experimental procedure has been shown to produce small deviations in the compositional measurements, additional uncertainty is introduced by the analytical procedure. The highest degree of accuracy is ensured by making use of accurate calibration curves and performing the analysis for the entire system in the shortest possible time. The latter is of importance as the response of the GC may drift over time due to wearing of the column with successive runs, which would render even the most accurate of calibration curves inaccurate. Thus it is of importance to test the reproducibility of the calibration curves, and thus the GC itself, after each system has been run to quantify the effect of drift in the responses over time.

To this end, once all experimental samples for a given system had been analysed, samples of known composition were prepared in the same manner as those used to establish the calibration curve (see Section 3.3.5). These samples were then run through the GC four times each, with the compositions predicted using the same calibration curves. In this way, the predictions could be compared to the known concentrations for the samples, and the maximum deviation due to drift in the response factors could be quantified. Results of this procedure are presented in Appendix C, where the maximum deviation in the composition as a result of analytical uncertainty was found to be *±0.008* mole fraction.

3.4.3 Total Compositional Uncertainty

It is apparent from the analysis presented here that the contribution of the analytical effects to the compositional uncertainty is almost an order of magnitude greater than that for the experimental effects. However, the latter cannot be neglected in light of the former because these errors are additive; the errors introduced by the pressure fluctuations during the experimental runs are present before the samples are analysed and thus need to be added to the errors associated with the sample analysis. Thus, the total compositional uncertainty reported for equilibrium concentrations here is *±0.010* mole fraction.

Chapter 4:   PHASE EQUILIBRIA MEASUREMENTS

In this chapter, the results of the experimental study are presented. Initially, verification of the experimental setup and procedure is presented through comparison with an independently measured system from the literature. Thereafter, the new isobaric phase equilibria measurements for the two ether isomer/n-heptane systems and five ester isomer/n-octane systems are presented, with a discussion of the observable phase behaviour of these systems. Particular attention is paid to any azeotropic behaviour, as well as the changes in phase behaviour between isomers as the functional group of interest shifts along the carbon backbone.

4.1 Experimental Verification

Verification of the equilibrium still and experimental method are necessary to validate any new phase equilibrium measurements resulting from this study. Given the confirmed purities of the materials used in this study, measurement of pure component vapour pressures can serve to validate the temperature and pressure measurements from the equilibrium still. Verification of the method for binary systems is best achieved through the reproduction on an independently measured data set for a system similar to those under consideration in this work.

4.1.1   Pure Component Vapour Pressures

The phase diagram of a pure component indicates that for every pressure, there is a single temperature at which equilibrium between the vapour and liquid phases exists. This fundamental principle is used here to verify the temperature and pressure readings of the dynamic still used in this study. Figures 4.1 [i.] and [ii.] present a comparison between experimentally measured vapour pressures for each component and their literature counterparts, with the data tabulated in Appendix D.

The comparisons show excellent agreement between the experimentally measured vapour pressures and the literature data for all components. Statistically, *92*% of the measured data points across all components deviated by less than *3*% from the literature data with the largest deviation being *3.64*%. More importantly, these deviations are scattered rather than systematic, with both positive and negative deviations apparent. The high degree of agreement between the experimental and literature vapour pressures serve to validate the temperature and pressure measurements reported in this work
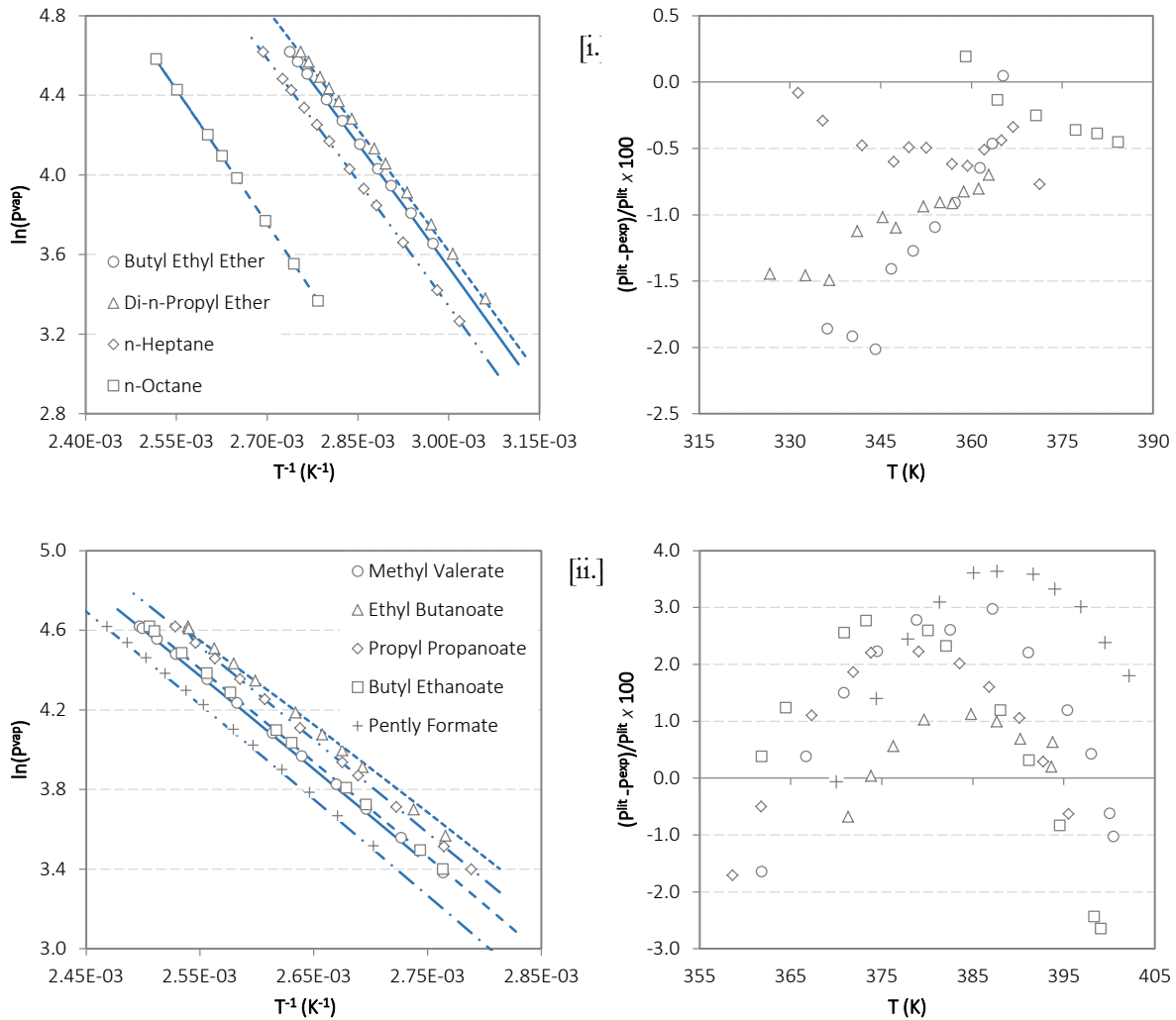
Figure 4.1: Comparison between experimentally measured and literature vapour pressures for [i.] n-alkanes and ethers, and [ii.] esters of interest to this study. Literature data (DIPPR) represented by a linear trend line through actual points to aid in readability.

4.1.2   Verification of Experimental Method

Within this study, the experimental focus is on binary systems comprising a polar component and an n-alkane of similar molecular weights, under isobaric conditions. To this end, use of the 2-butanone/n-heptane system at *94* kPa (Wisniak *et al,.* 1998) fits the criteria for a verification system. Furthermore, the thermodynamic consistency of the data and the large body of phase equilibrium measurements published by this group lend a degree of confidence to the reliability of the reference data set. The measured 2-butanone/n-heptane data are compared to the reference data in Figure 4.2.
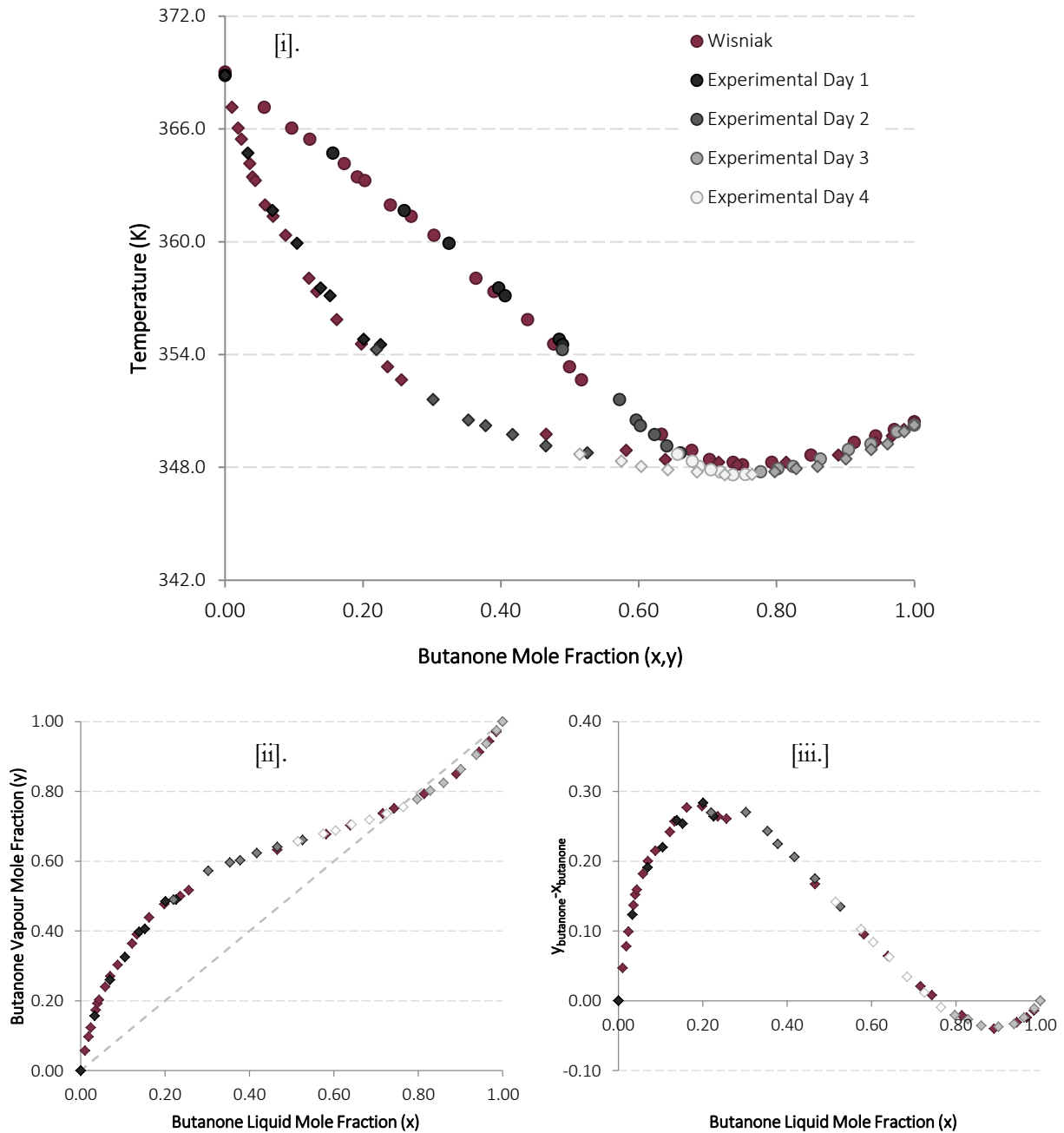
Figure 4.2: Comparison of measured data to that of Wisniak et al. (1998) for the 2-butanone/n-heptane system at 94.0 kPa. [i.] T-xy plot, [ii.] x-y plot, [iii.] y-x vs. x plot.

Excellent agreement between the measured data and the reference data is apparent in all three representations of the comparison. A particularly pleasing result is the reproducibility of the azeotropic composition as seen in the *x-y* plot (Figure 4.2 [ii.]) and highlighted in the *(y-x) vs. x* plot (Figure 4.2 [iii.]). The azeotropic composition reported by Wisniak *et al.* (1998) is *0.750* mole fraction 2-butanone, while that measured here is *0.745* mole fraction 2-butanone; the difference is well within the reported compositional uncertainty of *0.010* mole fraction.

The *T-xy* plot (Figure 4.2 [i.]) does however highlight a small degree of deviation between the measured and reference data, notably in the equal composition space tending towards higher

concentrations of 2-butanone, *viz.* *≥0.55* mole fraction 2-butanone. Given that these deviations are not apparent in the compositional plots, where the temperature effects are excluded, it can be deduced that these deviations are purely in the temperature measurement. The largest temperature difference is apparent around the azeotropic point, with deviations of approximately *0.2* K, which is of the same order of magnitude as the reported uncertainty in temperature. Furthermore, temperature measurements were validated through reproducing literature vapour pressures in the previous section where, in particular, deviations were found to be scattered rather than systematic. In light of these two points, the small temperature deviations apparent in the *T-xy* plot can be considered within acceptable experimental limits.

4.1.3   Verification Summary

By accurately reproducing both pure component vapour pressures and an independently measured binary system, a degree of confidence is given to the data generated in this study. Both the equipment and the procedure employed can thus be considered verified and focus can turn to the generation of new phase equilibrium data.

4.2 C$_6$ Ether/n-Heptane Systems

The experimental data for both the di-n-propyl ether and butyl ethyl ether systems are presented and their phase behaviour discussed separately. An analysis of the role of the shifting functional group on the associated mixture behaviour follows thereafter.

4.2.1   Phase Equilibrium Results

4.2.1.1   Di-n-Propyl Ether/n-Heptane

The phase equilibrium data for the di-n-propyl ether/n-heptane system at *60* kPa are plotted in Figure 4.3, with data tabulated in Appendix E. The reproducibility of the experimental data is good, as is evidenced by the agreement between *'Experimental Day 5'* data and that of the preceding days' runs. The system presents slight positive deviations from ideality, which results in a very narrow phase envelope, but not significant enough to produce azeotropic behaviour. This is verified by the fact that no temperature minimum was apparent experimentally and that the *x-y* plot does not cross the *x = y* line in Figure 4.3 [ii.] or equivalently the *x*-axis in Figure 4.3 [iii.]. The data reported were shown to be thermodynamically consistent by both the McDermott-Ellis and L/W consistency tests, exhibiting a D value of *4.28* (less than the recommended maximum of *5*).
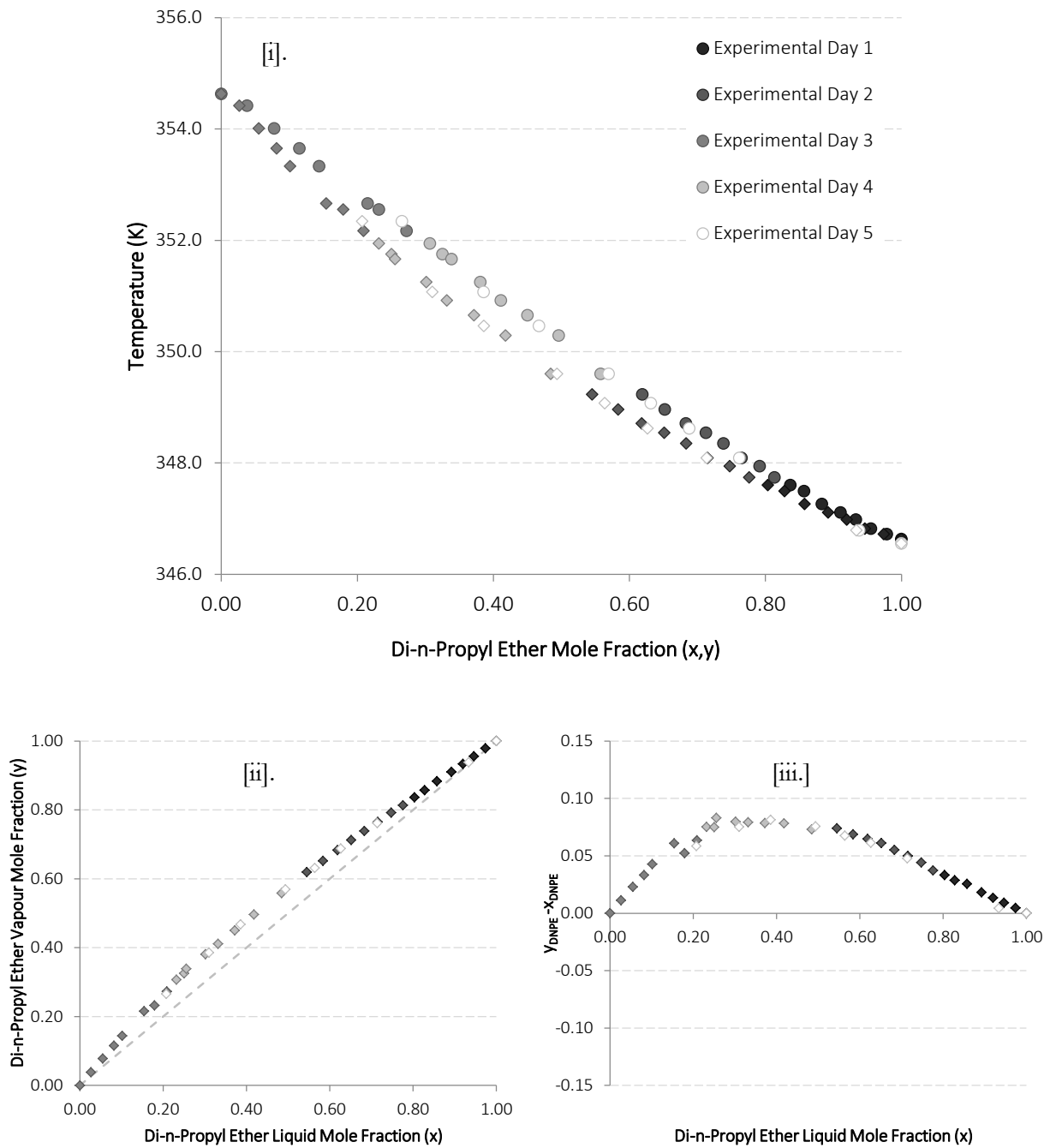
Figure 4.3: Experimental phase equilibrium data for the di-n-propyl ether/n-heptane system at 60 kPa. Equilibrium represented in [i.] T-xy, [ii.] x-y, and [iii.] y-x vs. x plot forms.

4.2.1.2   *Butyl Ethyl Ether/n-Heptane*

Like the di-n-propyl ether/n-heptane system before it, the butyl ethyl ether/n-heptane system at *60* kPa is seen to exhibit positive deviations from ideality with no azeotropic point, but a particularly narrow phase envelope in Figure 4.4. The lowest recorded temperature was the pure ether boiling point, which confirmed zeotropic behaviour in the system experimentally. Reproducibility of the data is evident while the data were found to be thermodynamically consistent by both the L/W (D = *3.15*) and McDermott-Ellis consistency tests.
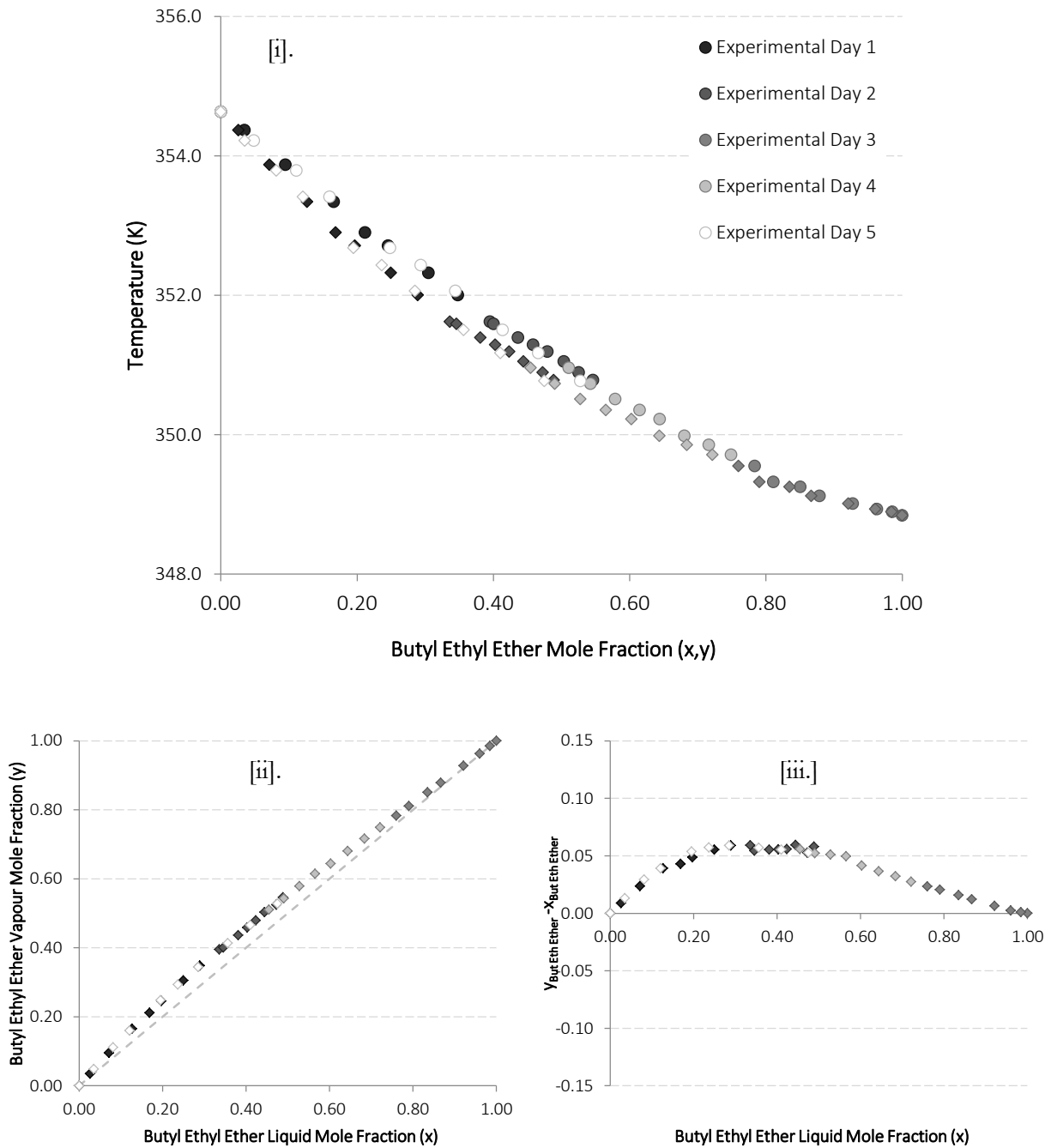
Figure 4.4: Experimental phase equilibrium data for the butyl ethyl ether/n-heptane system at 60 kPa. Equilibrium represented in [i.] T-xy, [ii.] x-y, and [iii.] y-x vs. x plot forms.

4.2.2   Role of Functional Group Location

With neither ether/n-heptane system exhibiting azeotropic behaviour, the difference in mixture behaviour between the two ethers manifests itself most readily in the pure component boiling points. As the polar oxygen atom moves further from the centre of the carbon backbone, the polar forces become more prominent, raising the boiling point of the ether, as demonstrated in Figure 4.5. Structurally, a C_6 ether is not dissimilar from n-heptane – the only difference being the substitution of a CH_2 group for the polar oxygen within the carbon backbone itself.
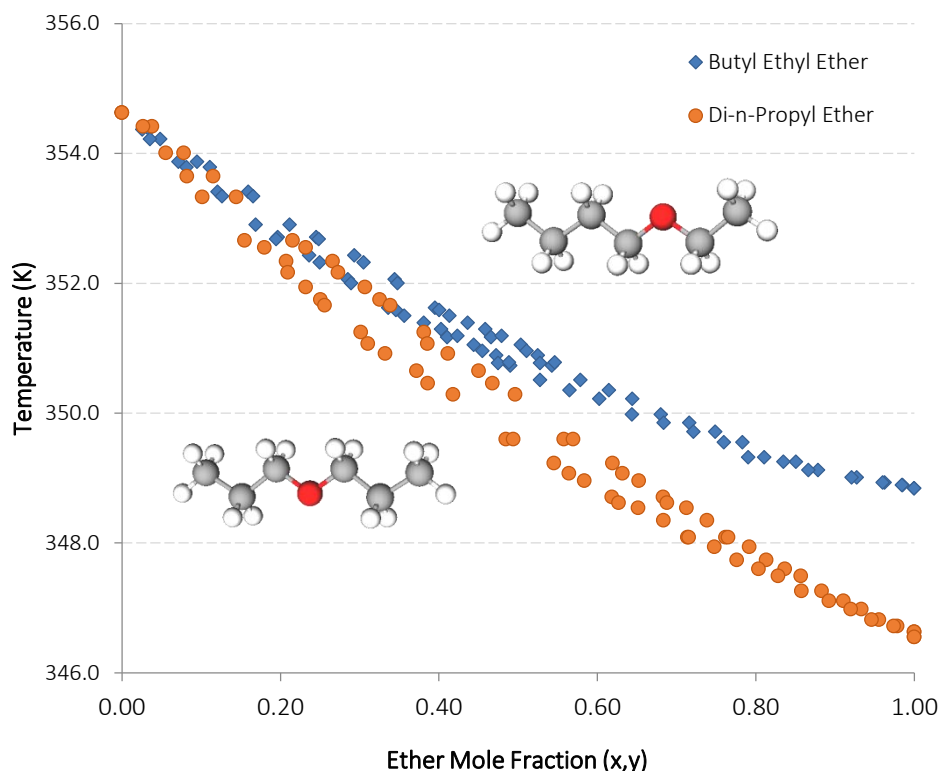
Figure 4.5: Combined T-xy plot for both ether/n-heptane systems at 60 kPa, highlighting the role of the polar functional group location in altering system behaviour. Molecular representations of the respective ethers are included for ease of reference.

Thus, what is interesting with the behaviour of the ethers is that as the polar ether group shifts toward the terminal methyl group, its influence increases and the boiling point of the ether *approaches* that of the equivalent sized nonpolar alkane. In fact, the boiling point of the final linear isomer (pentyl methyl ether – not measured here) at the experimental conditions is *355.3* K (DIPPR), a mere *0.6* K higher than that of n-heptane. One could thus argue that when the oxygen is located in the centre of the chain, the greatest "deviation" from nonpolar behaviour is apparent. That is, the greatest difference between the phase behaviour of the polar ether and the nonpolar alkane is in evidence for the mixture with di-n-propyl ether. This emphasises the subtle but important role that the polar oxygen plays in distinguishing the ether from a nonpolar alkane and the difficulty inherent in accurately describing the behaviour of components of this functional group.

4.3 C$_6$ Ester/n-Octane Systems

As with the ether systems in the previous section, the experimental data for and discussion of the phase equilibrium of the five ester/n-octane systems will be presented first. This will be followed by a discussion on the role of the shifting diatomic functional group on the associated phase behaviour.

4.3.1   Phase Equilibrium Results

The results of the vapour-liquid equilibrium experiments for each of the C$_6$ ester isomers with n-octane are presented in Figures 4.6 to 4.10 that follow. All five systems exhibited strong positive deviations from ideality and a minimum boiling azeotrope, with the experimentally observed azeotropic points listed in Table 41.

Table 4.1: Summary of experimentally measured azeotropic temperatures and compositions in the five ester/n-octane systems considered.

	Azeotropic Temperature	Azeotropic Composition
	K	mole fraction ester
methyl valerate/n-octane	377.53	0.409
ethyl butanoate/n-octane	374.60	0.605
propyl propanoate/n-octane	375.44	0.546
butyl acetate/n-octane	376.55	0.459
pentyl formate/n-octane	378.32	0.308

Reproducibility of the data was checked by performing repeat runs in all five systems, with excellent agreement between the runs performed on different days. Thermodynamic consistency of all the data was checked and confirmed by both the L/W and McDermott-Ellis consistency tests. In the case of the L/W test, the largest D value of any of the five systems was found to be *0.861* – well within the recommended maximum of 5. For the McDermott-Ellis consistency test, all data pairs exhibited deviations smaller than their respective D$_{max}$ values. Details of the thermodynamic consistency testing can be found in Appendix E.

4.3.1.1   Methyl Valerate/n-Octane
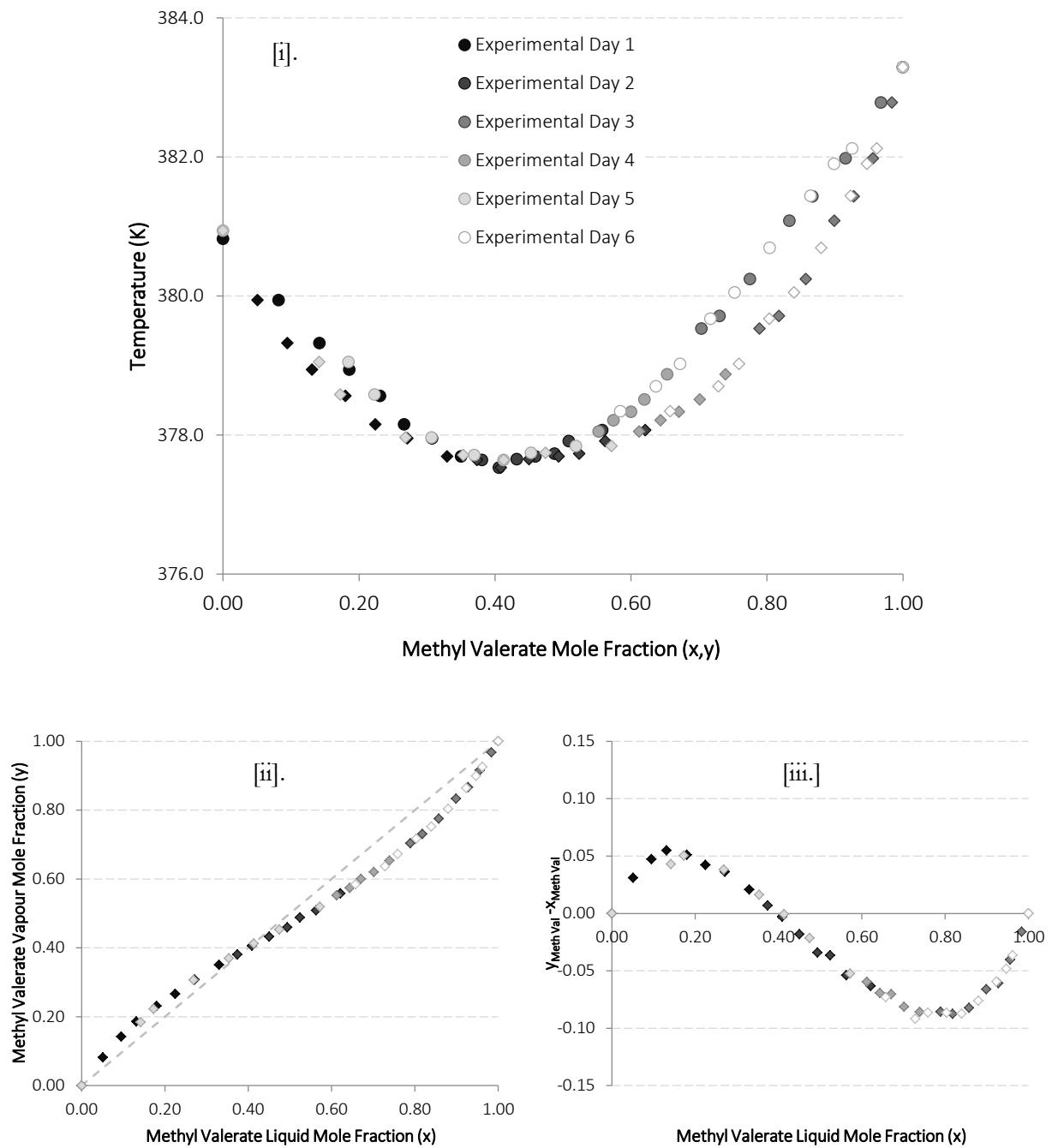
Figure 4.6: Experimental phase equilibrium data for the methyl valerate/n-octane system at 60 kPa. Equilibrium represented in [i.] T-xy, [ii.] x-y, and [iii.] y-x vs. x plot forms.

4.3.1.2   *Ethyl Butanoate/n-Octane*
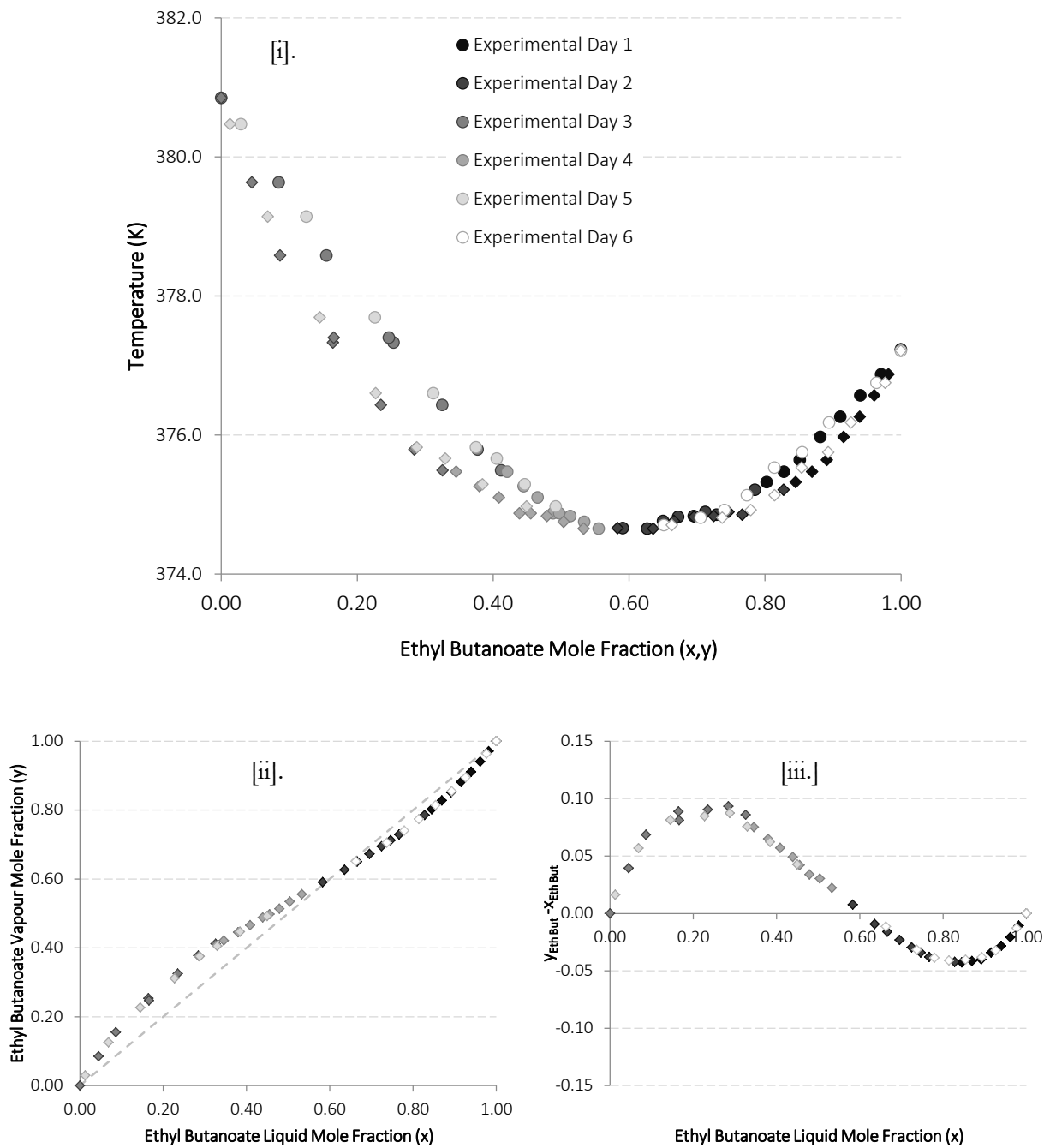
Figure 4.7: Experimental phase equilibrium data for the ethyl butanoate/n-octane system at 60 kPa. Equilibrium represented in [i.] T-xy, [ii.] x-y, and [iii.] y-x vs. x plot forms.

4.3.1.3   Propyl Propanoate/n-Octane
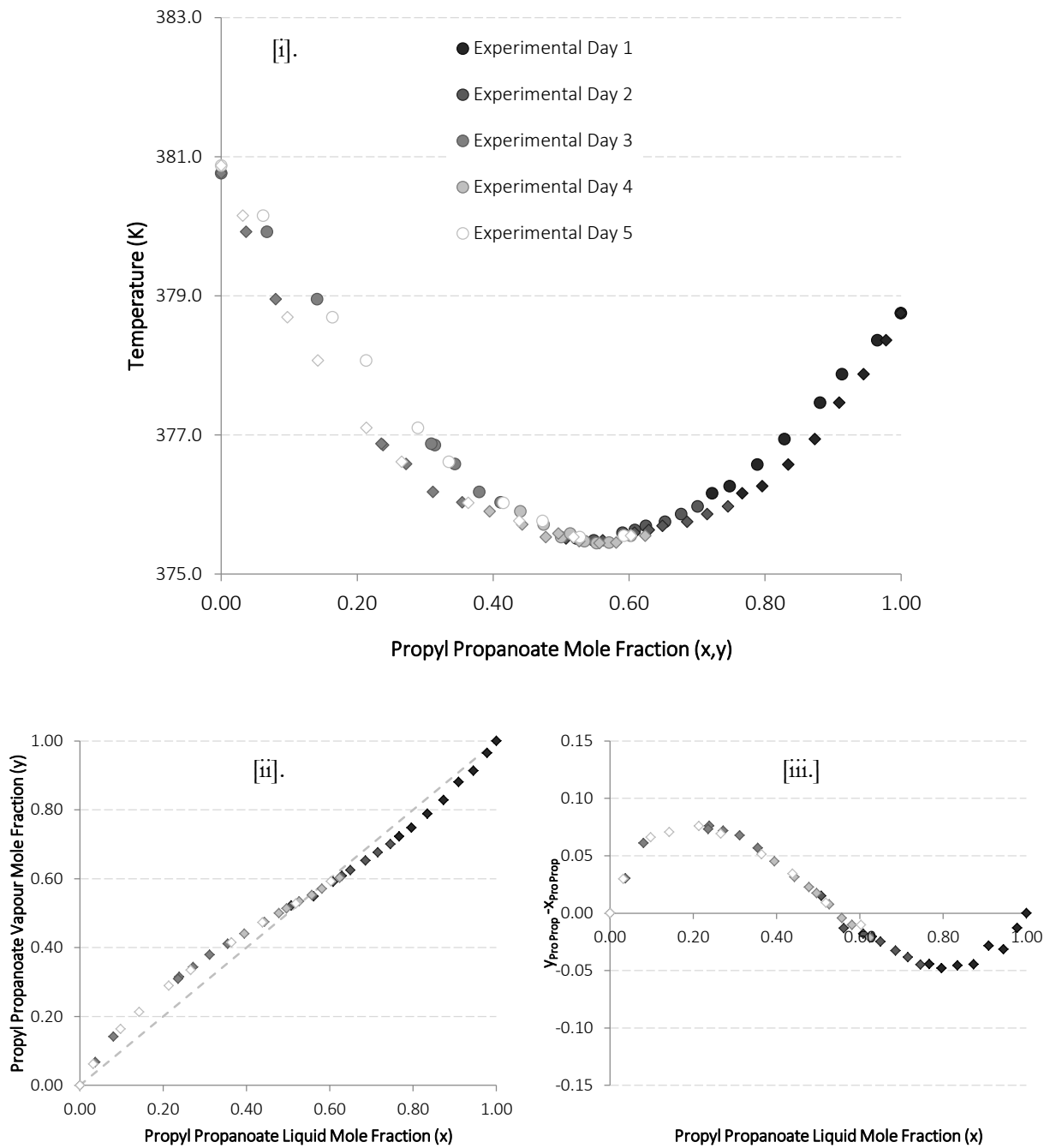
Figure 4.8: Experimental phase equilibrium data for the propyl propanoate/n-octane system at 60 kPa. Equilibrium represented in [i.] T-xy, [ii.] x-y, and [iii.] y-x vs. x plot forms.

4.3.1.4   *Butyl Acetate/n-Octane*
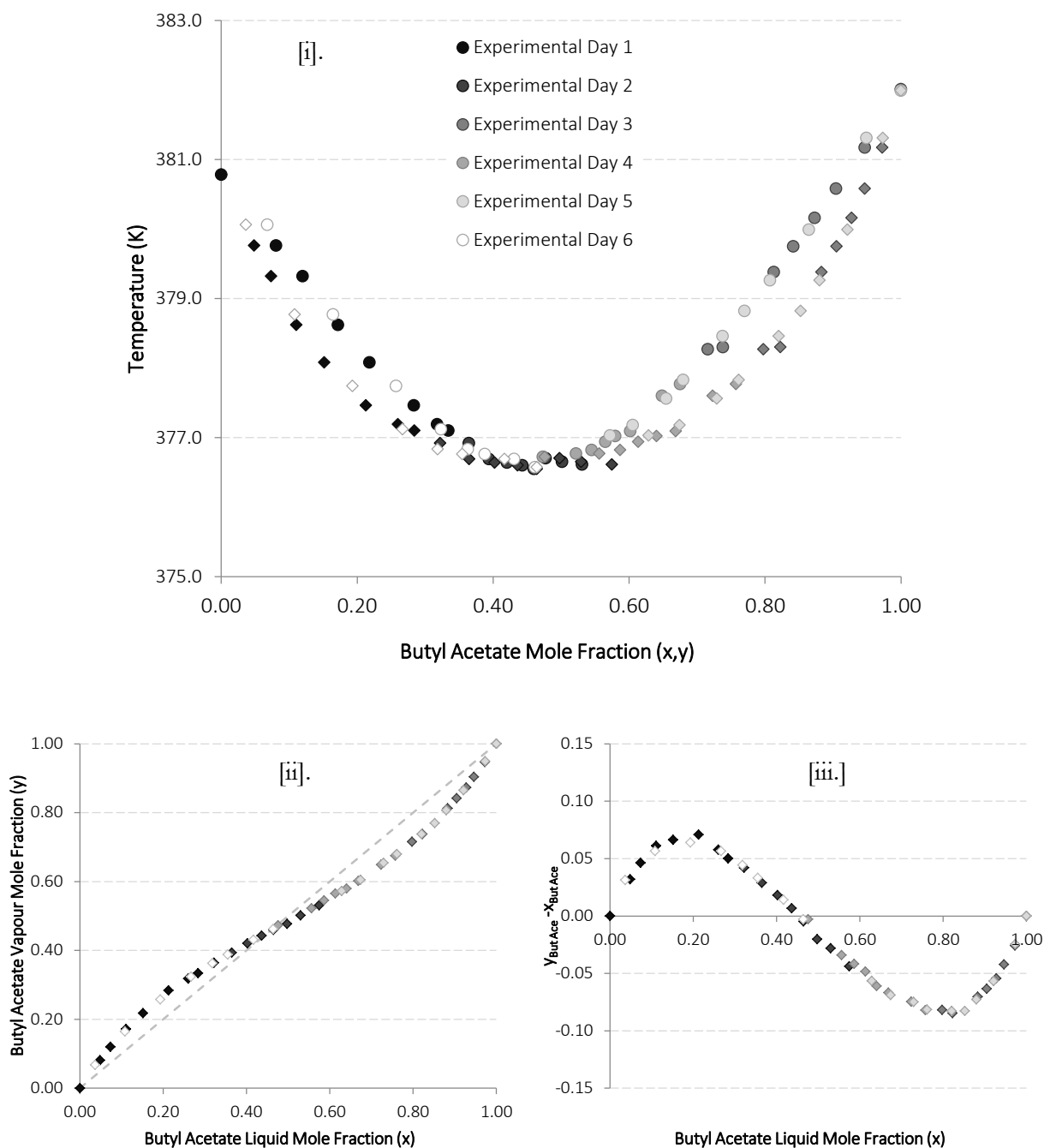
Figure 4.9: *Experimental phase equilibrium data for the butyl acetate/n-octane system at 60 kPa. Equilibrium represented in [i.] T-xy, [ii.] x-y, and [iii.] y-x vs. x plot forms.*

4.3.1.5   *Pentyl Formate/n-Octane*
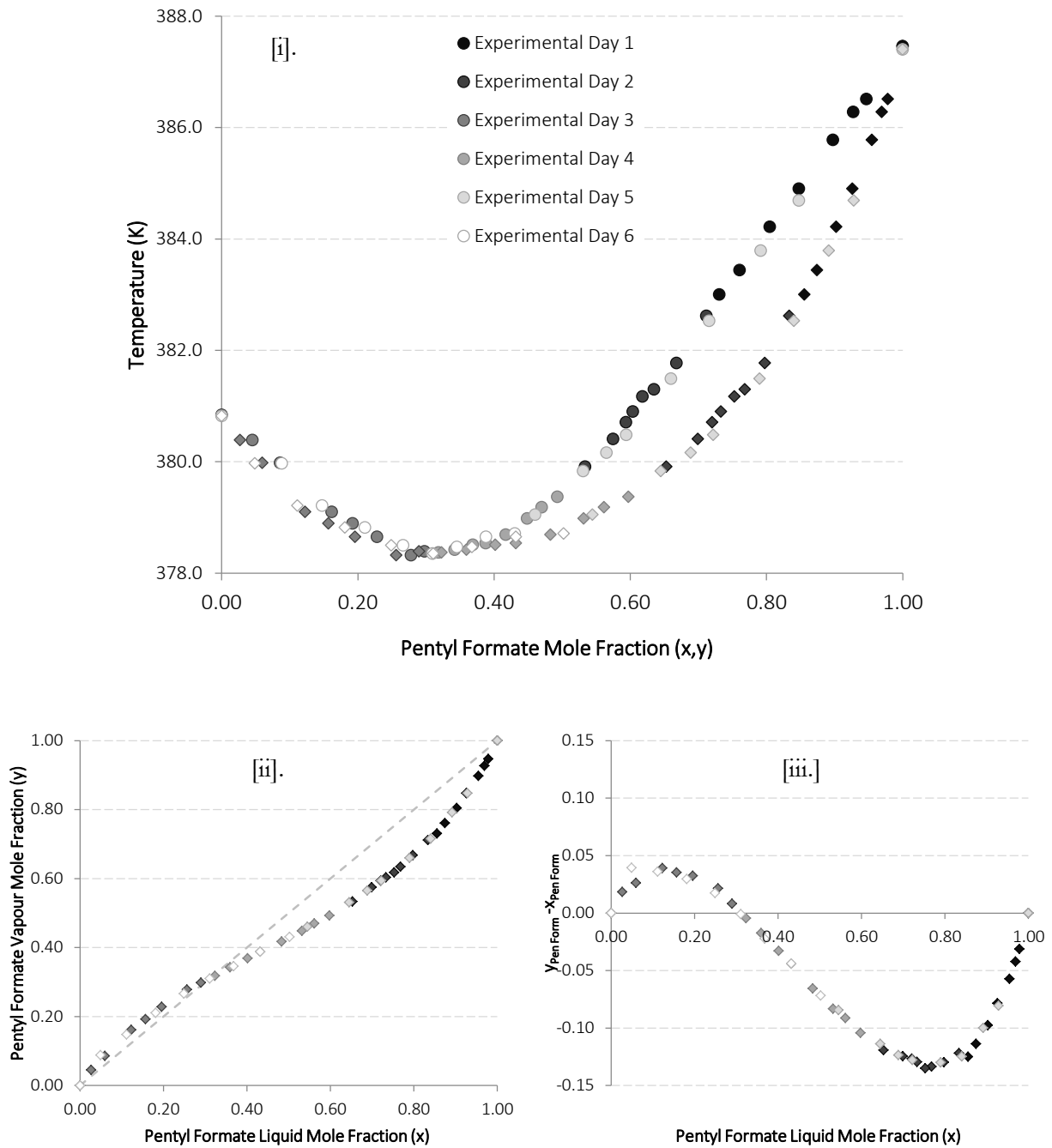
Figure 4.10: Experimental phase equilibrium data for the pentyl formate/n-octane system at 60 kPa. Equilibrium represented in [i.] T-xy, [ii.] x-y, and [iii.] y-x vs. x plot forms.

4.3.2 Role of Functional Group Location

The ester functional group comprises an alkoxy group in the carbon backbone of the molecule directly bonded to a carbonyl group, or simplistically, an ether group bonded to a ketone group. As a result, a given linear ester has roughly *1.5* times the number of structural isomers as an equivalent length ketone or ether, as well a larger scope for differences in their associated phase equilibrium. This is readily apparent from both the pure ester boiling points in Figure 4.1 as well as the mixture behaviour of each isomer with n-octane in Figures 4.6 to 4.10.

In ketones and ethers, it has already been shown that the strength of polar interactions is directly linked to the location of the single carbonyl or alkoxy group in the carbon chain; a terminally located polar functional group yields the most polar isomer with successively decreasing influence until the group is in the middle of the chain. For esters the situation is a little more nuanced; here it is the relative locations of the carbonyl and alkoxy subgroups in relation to each other and the *two* terminal methyl groups that impact the strength of the polar interactions and consequently their phase behaviour. The effect of these relative locations are highlighted in the combined *T-xy* and *x-y* plots for the five ester isomers in Figures 4.11 and 4.12 respectively.
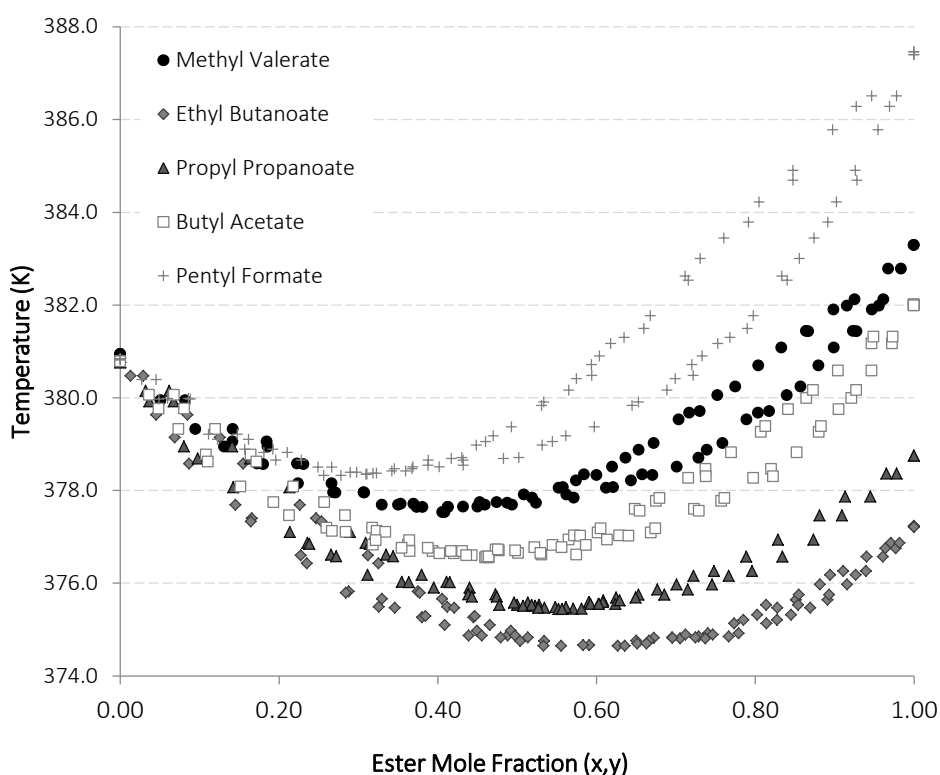
Figure 4.11: Combined T-xy plot for ester/n-octane systems at 60 kPa, highlighting the role of the polar functional group location in altering system behaviour.
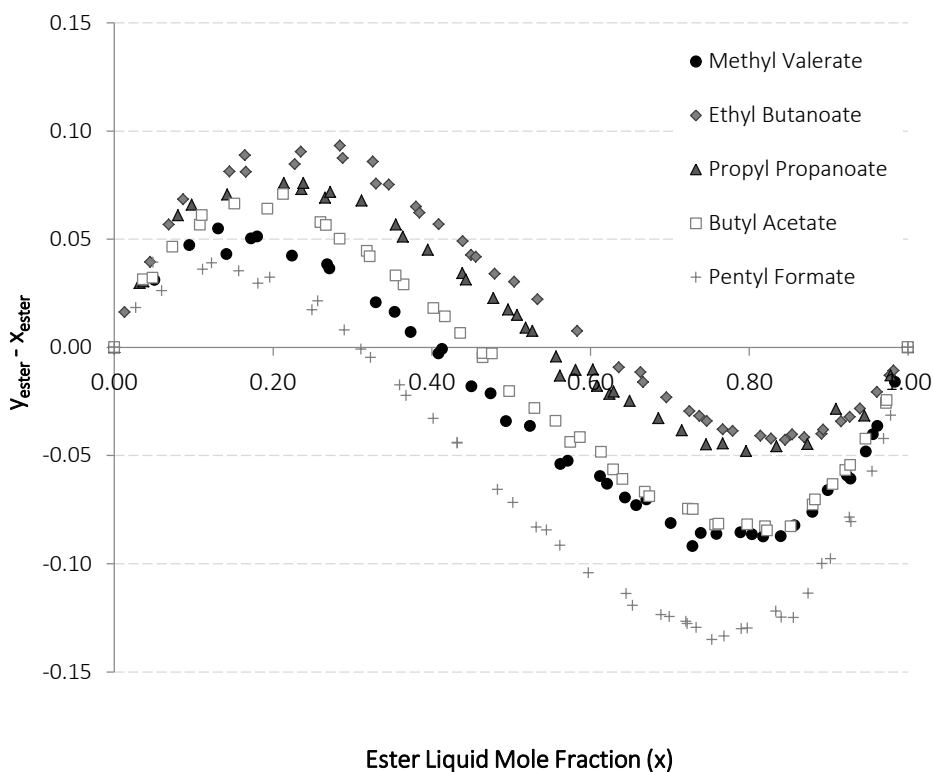
Figure 4.12: Combined (y-x) vs. x plot for ester/n-octane systems at 60 kPa, highlighting the role of the polar functional group location in altering system behaviour.

Given that the carbonyl subgroup is located at the end of the chain readily explains why pentyl formate is the most polar isomer with the highest boiling point. The interesting trend is the relative dipolar strength of the methyl valerate-butyl acetate and propyl propanoate-ethyl butanoate pairs. To clarify this point, the skeletal formulae of the esters considered here are presented in order of descending boiling point in Figure 4.13.
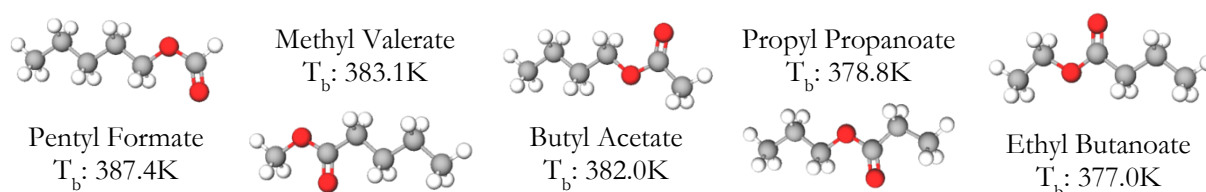
Figure 4.13: Skeletal formulae of the five linear C₆ structural isomers, presented from left to right in descending order of their boiling points at the experimental pressure (60 kPa). The aim is to highlight the location of carbonyl and alkyl subgroups of the ester group within the linear chain.

Given that ketones are more polar molecules than ethers, one might intuit that the more terminally located carbonyl subgroup of butyl acetate would make it more strongly polar than methyl valerate, but based on the experimental phase behaviour the opposite seems to be true. This trend is reversed for the latter pair, where the centrally located and thus sterically hindered carbonyl subgroup of ethyl butanoate results in more dampened dipolar interactions than propyl propanoate. Indeed, if the behaviour of methyl valerate is omitted, it is clear that a regular trend exists between the *acid* chain length

and the strength of the polar interactions: the shorter the *acid* chain length, the more polar the ester. The methyl ester is the clear exception, with its proximity to the terminal end of the *alkyl* chain increasing its asymmetry and thus polar interactions. Comparing the azeotropic points listed in Table 4.1 with the trend in Figure 4.13 confirms that the azeotropic temperatures and ester concentrations for each isomer decrease and increase respectively, following this same trend.

4.4 Chapter Summary

The goal of this chapter was the generation of new isobaric phase equilibrium data for the structural isomers of linear C_6 ethers and esters with a common n-alkane. These data supplement previously measured data for the isomers of linear C_7 ketones, also with a common n-alkane. The motivation behind this data generation was to fill the knowledge gap relating to the effect of polar functional group location on the observable phenomena in the phase behaviour of such binary mixtures.

The generated data indicate that, while the dipole strength of the ether and ester functional groups is much weaker than that of the ketones, the effect of these polar functional groups is significant in dictating the observable phase behaviour. **Furthermore, the difference in observable phase behaviour between different isomers is subtle, yet still substantial – from the narrow yet distinct phase envelopes of the ether isomers to the shifting azeotrope between ester isomers, accurately accounting for the differences in phase behaviour may prove difficult, but is clearly important.**

In the case of the ketone systems, accounting for differences in phase behaviour of constitutional isomers proved to be a stringent test for the predictive capacity of thermodynamic models. In the following chapters, the subtle variation in phase behaviour of the isomers of ethers and esters will be used to test the predictive capacity of SAFT-type thermodynamic models.

4.5 Scientific Contribution

The phase equilibrium data generated in this chapter have been published in two separate articles as detailed below:

Title:	Vapor–Liquid Equilibria Measurements for the Five Linear C_6 Esters with n–Octane
Authors:	J. T. Cripwell, C. E. Schwarz, A. J. Burger
Journal:	Journal of Chemical and Engineering Data, **2016** *61 (7)*, 2353-2362.

Title:	Vapor-Liquid Equilibria Measurements for Di-n-Propyl Ether and Butyl Ethyl Ether with n-Heptane
Authors:	J. T. Cripwell, C. E. Schwarz, A. J. Burger
Journal:	Journal of Chemical and Engineering Data, **2016** *62 (1)*, 204-209.

Chapter 5:   ASSESSING THE PREDICTIVE CAPACITY OF POLAR sPC-SAFT

In Chapter 2, an introduction to the field of SAFT modelling was presented, highlighting the development of the EoS, up to and including the simplified perturbed chain SAFT variant (sPC-SAFT) as well as the Jog & Chapman (JC) and Gross & Vrabec (GV) polar terms. In this chapter, the predictive capacity of sPC-SAFT, combined with each of these two polar terms, is assessed through the model's application to the vapour-liquid equilibrium data presented in Chapter 4.

Initially, the regression method is discussed. The results of the parameter regression are presented with reference to deviations from appropriate pure component properties given as an indication of the quality of fit. Thereafter, the pure predictions of the EoSs for the mixture phase behaviour are compared to experimental data, to assess the predictive capacity of the models. Particular attention is paid to trends in the success or failure of the models to accurately account for the differences in phase behaviour of each structural isomer of each homologous group under consideration. Finally, a summary of the overall predictive strengths and shortcomings of polar sPC-SAFT is presented.

5.1 Determining Polar sPC-SAFT Parameters

Modelling of mixture phase behaviour requires generation of pure component parameter sets for each component in question. For a thermodynamic model to be used in the prediction of mixture properties, the accurate representation of pure component properties is a prerequisite.

5.1.1   Choice of Pure Component Data Inclusion

Given that thermodynamic models are most widely used for the description of phase equilibria, emphasis is generally placed on accurate description of pure component properties that will yield the best account of the two phase region. To this end, the saturated liquid density (ρ_i^{sat}) and saturated vapour pressure (P_i^{sat}) are traditionally the pure component properties of choice. The vapour pressure dictates the *T-P* relationship between the vapour and liquid phases, while the liquid density provides a measure of the phase volumes and thus the volume roots of the EoS. The ultimate goal of thermodynamic modelling however, is the accurate description of any thermodynamic property using a single, component-specific parameter set. In the case of SAFT type models, defining the EoS with respect to the residual Helmholtz free energy allows determination of many other thermodynamic properties by appropriate differentiation. This interconnectivity was first presented in Chapter 1 (Figure 1.1).

Llovell *et al.* (2006) argued that the parameters of a physically sound thermodynamic model should be transferable, giving accurate predictions of all thermodynamic properties using the thermodynamic relationships illustrated in Figure 1.1. De Villiers (2011) refined this argument by stating that it is the *optimum* parameter set for such a model that should exhibit these characteristics. This is an important distinction; the mathematical nature of parameter regression means that by fitting component parameters against pure component data, one will always produce a parameter set capable of accurately representing the fitted properties. Thus it is important to select pure component properties that can provide the best balance of prediction for all properties to yield the optimum parameter set.

As is evident from Figure 1.1, incorporation of both saturated vapour pressure and saturated liquid densities of a pure component allows for regression to test both the first compositional and first volume derivatives of the residual Helmholtz energy function, *viz*: *dA/dn$_i$* & *dA/dV*. What is also evident however, is that the temperature dependency is not tested in this procedure (*dA/dT*). While a degree of temperature dependence is incorporated through the temperature range of the P_i^{sat} and ρ_i^{sat} data, some authors have elected to include other pure component properties in the regression procedure to yield a more balanced parameter set.

Lafitte *et al.* (2006) argued the merits of including pure component speed of sound data, while the same group later advocated for the inclusion of heats of vaporisation (Lafitte *et al.*, 2007) within a SAFT-VR framework. It is evident from Figure 1.1 that both suggestions would serve to incorporate temperature dependence into the resulting regressed parameter set and should yield accurate predictions of these previously excluded properties. However, the predictive capacity of thermodynamic models is traditionally measured in their application to mixture phase equilibrium. Thus, it is important that increased accuracy in the prediction of derivative properties does not compromise the ability of the model to yield accurate phase equilibrium predictions.

Within the sPC- and PC-SAFT frameworks respectively, de Villiers (2011) and de Villiers *et al.* (2013) performed extensive studies on using different combinations of pure component properties in the regression procedure. The goal of these studies was identifying the combination that would yield the optimum parameter set. The results indicated that regardless of the choice of pure component data included, no single combination of parameters could yield equally accurate predictions for phase equilibrium as well as derivative properties. The authors attributed this deficit to inherent shortcomings in the predictive behaviour of the hard sphere term, where the use of a Lennard-Jones potential function restricts the range of repulsive intermolecular interactions.

With the emphasis here on the sPC-SAFT framework, the conclusion of de Villiers (2011) is highlighted. In that work, the best combination of properties (with regression weights in parentheses) for accurate representation of phase equilibrium, and with fair correlation of derivative properties, was found to be:

- saturated vapour pressures, P^{sat}, (4),

- saturated liquid densities, ρ_i^{sat}, (2), and

- heats of vaporisation, H^{vap}, (1).

This combination of properties and regression weights was used to good effect in the previous study performed on ketones (Cripwell, 2014) and is similarly employed in the regression of polar sPC-SAFT parameter sets in this work.

Incorporating the correct pure component data is an important *initial* requirement for determination of the optimum parameter set. The challenge when regressing parameters of fundamental models like SAFT is the need to produce parameters that have physical meaning, e.g. non-negative segment numbers and realistic segment sizes. Being able to bridge the divide between the mathematical parameter space and their physical realism often presents the biggest challenges in the regression of SAFT parameters.

5.1.2   Regression Challenges

A majority of SAFT variants, including the original PC-SAFT and its simplified variant, support three pure component parameters – typically the segment diameter (σ - Å), the segment number (m - dimensionless) and the dispersion energy ($\varepsilon/k - K$). Regression of n pure component parameters can be seen as determining the global minimum in an n-dimensional space. Determination of the usual three parameters is thus performed in the visible three dimensional space and is readily achieved using a local optimisation type algorithm. The objective functions used in these algorithms are typically of the form presented in equation 5.1, using the aforementioned standard pure component properties, *viz.* saturated vapour pressure and liquid density data respectively.

$$OF = \sum_{i=1}^{np}\left[\left(\frac{P_i^{sat,calc} - P_i^{sat,ex}}{P_i^{sat,ex}}\right)^2 + \left(\frac{\rho_i^{sat,calc} - \rho_i^{sat,ex}}{\rho_i^{sat,ex}}\right)^2\right] \qquad 5.1$$

However, complications often arise once the number of parameters requiring fitting increases, as is the case for the introduction of polar terms to the SAFT framework. In this case, the *global* minimum needs to be found in a four-dimensional or higher space, where the existence of multiple *local* minima can cause the search algorithms to become trapped in false solutions. This degeneracy of the parameter space causes mathematical difficulties when trying to find the global minimum.

When applying PC-SAFT$_{JC}$ to ketones, ethers and esters, both Sauer & Chapman (2003) and Dominik *et al.* (2005) noted degeneracy of the parameter space, resulting in multiple minima in the objective function. This meant that, when parameters were fit only to pure component saturated vapour pressures and liquid densities, multiple parameter sets exist that could accurately represent the pure component properties. However, many of these sets were physically unrealistic (e.g. excessively large

segment numbers). This result highlighted the importance of stressing the physical significance of the regressed parameters in order to obtain optimum parameter sets.

Indeed, Gross & Vrabec (2006) went further to note that, when the four PC-SAFT$_{JC}$ parameters were fit to pure component data alone, the optimum parameter set was frequently that which had a zero polar contribution. Specifically, the zero polar contribution arose when the polar parameter x_p was forced to its lower physical limit of zero. This trend was supported by similar observations by de Villiers *et al.* (2011) and the precursor to this work (Cripwell, 2014), where both the Jog & Chapman and Gross & Vrabec polar terms were incorporated in the sPC-SAFT framework. This trend seems to suggest an inability of the polar term to distinguish between the anisotropic polar contribution and the isotropic dispersion forces in some cases. However, the problem up to this point is that no *trend* in parameter space degeneracy has yet been identified and so this suggestion has yet to be proven to be the case.

5.1.3 Proposed Solutions to Regression Challenges

In the original work for the GV polar term, Gross & Vrabec (2006) set the value of their additional polar parameter, n_p, equal to unity for molecules containing a single polar group, but it could be changed to *2* for diketones, diethers, etc. In this way, the problem of parameter multiplicity could be avoided and the authors claimed this to be a superior aspect of the GV term compared to the JC term. This example of employing physical considerations for fixing the value of one of the component parameters is the first of the suggested means in the literature for avoiding parameter multiplicity by reducing the dimensionality of the parameter space.

Such considerations were also made in the original works on the JC polar term (Jog *et al.,* 2001), where the value of the dipolar fraction, x_p, was expected to be equal to the inverse of the segment number. This was based on the physical consideration that the dipole moment is confined to a single group in the carbon chain in most common polar molecules. Later, Sauer & Chapman (2003) and Dominik *et al.* (2005) built on this physical consideration and showed that, for a given homologous group, the product of x_p and *m* is constant. This relatively simple re-working is an example of employing an empirical correlation based on the same physical observation, which still serves to fix the value of a given parameter. In this case, if the value of x_p could be successfully regressed for one member of a homologous series, the constant x_pm correlation could be used to determine unique parameters for other members of the homologous series, resulting in better representation of mixture behaviour.

In the same work that introduced the relationship between x_p and *m* as a means for fixing a parameter value, Dominik *et al.* (2005) also suggested the second means of overcoming problems in regressing unique parameter sets. The problem with multiple local minima in the objective function is that different regressed parameter sets can accurately model pure component properties but not all can account for mixture behaviour. Thus, Dominik *et al.*'s (2005) argument was that by incorporating mixture VLE data, a subtle bias could be afforded to the description of multicomponent phase equilibria, and the true global minimum in the objective function could be found. The choice of mixture data is important

however, as the second component in the mixture needs to have had its own parameters determined and tested, as well as being void of functionality beyond typical dispersion forces. This last point is particularly poignant; dipolar interactions only occur between polar molecules, while dispersion forces are common to all components. Thus, the inclusion of binary data with a nonpolar component helps differentiate between these different intermolecular forces.

As discussed in Chapter 2, de Villiers *et al.* (2011) argued that an accurate comparison between the performance of the JC and GV polar terms necessitates that each be assessed on an equal footing with the same number of regressed parameters. To this end, polar sPC-SAFT parameter sets were determined for a wide range of polar components where the value of n_p was allowed to vary in the regression procedure. Following the line of thought proposed by Dominik *et al.* (2005), de Villiers *et al.* (2011) similarly included VLE data in the regression procedure for both sPC-SAFT$_{JC}$ and sPC-SAFT$_{GV}$. This resulted in parameter sets that reproduced both pure component and mixture phase behaviour with a high degree of accuracy.

The problem with the reliance on incorporating mixture VLE data in the regression procedure is that, for many components of industrial and academic interest, accurate phase equilibrium data is simply not available. Indeed, one of the strongest arguments for using fundamental models like SAFT is the models' predictive capacity without the need for experimental data in the first place. Thus, in lieu of experimental data, it is vital that parameter multiplicity does not hinder the use and application of these models. De Villiers *et al.* (2011) acknowledged this point and looked to combine the approaches of fixing the value of a pure component parameter with the incorporation of VLE data in the regression procedure. Using Dominik *et al.*'s observation of the relationship between x_p and m for a given homologous series, de Villiers developed an empirical correlation for setting the value of both x_p and n_p, the form of which is presented in equations 5.2 and 5.3

$$x_p = \frac{K}{(A \cdot M_w + B) \cdot \mu^2} \tag{5.2}$$

$$n_p = \frac{K \cdot (A \cdot M_w + B)}{\mu^2} \tag{5.3}$$

The term in parenthesis is approximately equal to the segment number, while the molecular dipole moment introduces further component specific dependence in the correlation. The constants K, A and B are homologous group specific and are presented for ketones and esters in Table 5.1. Parameters for the ether functional group were not previously determined due to a lack of "good VLE data" for this homologous group (de Villiers *et al.*, 2011); so determination of equivalent constants for mono ethers was an objective of this work.

The same procedure as that adopted by de Villiers was thus to add the constants for ethers to those for ketones and esters in Table 5.1. The constants (K, A & B) of these equations are fit to parameter sets that have been successfully regressed using binary VLE data in the regression procedure. A and B are

determined by a least squares regression, using the segment number (*m*) of the **VLE** parameter sets as the fitted value. Thereafter, the value of *K* is similarly regressed by using the appropriate polar parameter (x_p/n_p) as the fitted value.

Table 5.1: Constants for correlations for setting value of polar parameters (de Villiers et al., 2011)

Variant	Group	*K*	*A*	*B*
sPC-SAFT$_{JC}$	Ketones	4.9316	0.02871	0.4754
x_p	Esters	4.3399	0.03182	-0.01459
	Ethers†	1.8492	0.02669	0.8455
sPC-SAFT$_{GV}$	Ketones	4.4208	0.02258	1.3821
n_p	Esters	3.6697	0.02364	1.2880
	Ethers†	1.3851	0.02517	1.0705

† Determined in this work

Predictions based on the correlations in equations 5.2 and 5.3 exhibit excellent agreement with those where VLE data are used in the regression procedure, even for components not used in the fitting of the constants of Table 5.1. In this way, accurate parameters can be determined with confidence, even for components for which no experimental data are available.

The final alternative for avoiding parameter multiplicity is by means of employing global optimisation (e.g. Simplex) methods rather than a local optimisation technique such as the Levenberg-Marquardt algorithm commonly used. This alternative, proposed by Al Saifi *et al.* (2008), is argued to be more robust at avoiding the multiple local minima present in four-dimensional parameter space due to the direct search nature of Simplex methods compared to the indirect search nature of Levenberg-Marquardt. The authors argued superiority of this method over the "arbitrary" choice of including VLE data in the regression procedure. The physical arguments of both Dominik *et al.* (2005) and de Villiers *et al.* (2011) make sense however, and including VLE data is no more arbitrary than fixing the value of a given parameter. Al Saifi *et al.* (2008) did also note that unrealistic parameter values may result through use of global optimisation techniques, with de Villiers (2011) noting that large errors in VLE prediction were still apparent using parameters generated by Al Saifi *et al.*'s technique.

5.1.4   Selected Regression Methods

Regression of model parameters in this work is achieved through use of the *TRSolutions* software package developed by de Villiers and subsequently modified for use in this study. The software employs the Levenberg-Marquardt algorithm and, as such, is the regression method of choice for this work. As has already been discussed, the work presented in this chapter builds upon a similar study performed for the ketone homologous series (Cripwell, 2014). The choice of regression method here is made upon the same basis as in that study and in light of the considerations presented above.

To this end, the following three regression procedures are performed:

i. Standard pure component regression

- Only pure component property data will be used, with all four parameters included in the regression procedure.

ii. Fixing polar parameter

- The value of x_p and n_p for sPC-SAFT$_{JC}$ and sPC-SAFT$_{GV}$ respectively will be fixed using the correlations of equations 5.2 and 5.3 with the constants in Table 5.1. Thereafter, the remaining three nonpolar parameters will be regressed against the same pure component property data as considered in the *Standard pure component regression* above.

iii. Inclusion of measured VLE data in regression procedure

- The appropriate isobaric VLE data for each ether and ester isomer, presented in Chapter 4, will be included in the regression procedure for that isomer's parameter set.

Pure component data used in the regression procedure includes saturated vapour pressures, liquid densities and heats of vaporisation. All such data are taken from appropriate correlations in the DIPPR database, or from retrofitted correlations of the form presented in DIPPR for any components not present in the database. Each component property comprises *30* equidistant data points over a temperature range of *0.5<T$_r$<0.9*. The objective function for regressions to pure component data alone is of the form in equation 5.4, where τ, υ, and ω are the regression weights for each pure component property (*viz. 4, 2* and *1* respectively):

$$OF = \sum_{i=1}^{np}\left[\tau\left(\frac{P_i^{sat,calc} - P_i^{sat,ex}}{P_i^{sat,ex}} \right)^2 + \upsilon\left(\frac{\rho_i^{sat,calc} - \rho_i^{sat,ex}}{\rho_i^{sat,ex}} \right)^2 + \omega\left(\frac{H_i^{vap,calc} - H_i^{vap,ex}}{H_i^{vap,ex}} \right)^2 \right] \qquad 5.4$$

For the regression cases involving VLE data inclusion, the measured ether/n-heptane and ester/n-octane data are included. The objective function for these cases takes the form presented in equation 5.5, where ψ is the VLE data regression weight, and the revised approximate weights are *10, 8, 2* and *1* successively as per the recommendation of de Villiers (2011) and also used in Cripwell (2014):

$$OF = \sum_{i=1}^{np}\left[\tau\left(\frac{P_i^{sat,calc} - P_i^{sat,ex}}{P_i^{sat,ex}} \right)^2 + \upsilon\left(\frac{\rho_i^{sat,calc} - \rho_i^{sat,ex}}{\rho_i^{sat,ex}} \right)^2 \right.$$
$$\left. + \omega\left(\frac{H_i^{vap,calc} - H_i^{vap,ex}}{H_i^{vap,ex}} \right)^2 + \psi\left(X_i^{VLE,error} \right)^2 \right] \qquad 5.5$$

5.2 Regressed Parameters

The results of the parameter regressions for each isomer of the considered ethers and esters are presented in this section. The parameter sets corresponding to each of the regression procedures highlighted in the previous section are reported, followed by a discussion of apparent trends in the results.

5.2.1 C_6 Ether Parameters

Parameters regressed for di-n-propyl ether and butyl ethyl ether are presented in Table 5.2, along with those used for n-heptane. Parameters for the latter are those originally derived by Gross & Sadowski (2000) and shown to be applicable in the sPC-SAFT framework (von Solms *et al.*, 2003). Given that n-heptane is a nonpolar molecule, it necessarily lacks a polar parameter and a zero polar contribution, meaning the same parameter set for sPC-SAFT applies to both sPC-SAFT$_{JC}$ and sPC-SAFT$_{GV}$.

Table 5.2: Regressed model parameters for n-heptane and each C_6 ether isomer using indicated regression procedures

	M_W	σ	m	ε/k	n_P/x_P	μ	P^{sat}	ρ^{sat}	H^{vap}
	g/mol	Å		K		D	AAD%	AAD%	AAD%
n-Heptane									
sPC-SAFT									
sPC-SAFT$_{GV}$	100.20	3.8049	3.4831	238.40	-	-	0.2545	0.8738	1.407
sPC-SAFT$_{JC}$									
Di-n-Propyl Ether									
sPC-SAFT	102.17	3.6960	3.4870	234.37	-	-	0.1663	0.0547	0.5951
sPC-SAFT$_{GV}$									
Std. Regression	102.17	3.7070	3.4576	234.05	2.6847	1.21	0.1529	0.0780	0.5947
n_p Correlation	102.17	3.7119	3.4444	233.70	3.4457	1.21	0.1503	0.1035	0.5946
Exp VLE Data	102.17	3.6745	3.5748	228.21	4.0082	1.21	1.211	1.316	1.104
sPC-SAFT$_{JC}$									
Std. Regression	102.17	3.7140	3.4442	235.00	0.2023	1.21	0.1485	0.0510	0.6073
x_p Correlation	102.17	3.7420	3.3789	235.84	0.3467	1.21	0.1534	0.0458	0.6328
Exp VLE Data	102.17	3.6995	3.5485	228.66	0.3708	1.21	1.602	2.227	1.354
Butyl Ethyl Ether									
sPC-SAFT	102.17	3.6020	3.7604	226.40	-	-	0.7402	0.5559	6.986
sPC-SAFT$_{GV}$									
Std. Regression	102.17	-	-	-	-	1.22	-	-	-
n_p Correlation	102.17	3.6162	3.7178	225.79	3.3895	1.22	0.7794	0.5410	6.958
Exp VLE Data	102.17	3.6273	3.7064	225.28	4.1182	1.22	0.7944	1.165	6.889
sPC-SAFT$_{JC}$									
Std. Regression	102.17	-	-	-	-	1.22	-	-	-
x_p Correlation	102.17	3.6538	3.6265	227.87	0.3411	1.22	0.9386	0.5534	7.084
Exp VLE Data	102.17	3.6622	3.6374	227.29	0.3518	1.22	0.9450	1.585	7.079

Regressed parameters for the nonpolar sPC-SAFT model are included for comparison and for illustration of the need to explicitly account for the polar forces. Starting with the parameters for di-n-propyl ether, unique parameter sets were determined for both sPC-SAFT$_{JC}$ and sPC-SAFT$_{GV}$, using all three regression cases. Analysis of the AADs for the considered pure component properties, defined in equation 5.6, indicate that excellent agreement with pure component properties is in evidence for all regression alternatives – even in the nonpolar sPC-SAFT case.

$$AAD = \frac{1}{np} \sum_{i}^{np} \frac{\left| x^{calc} - x^{\exp} \right|}{x^{\exp}} \times 100 \qquad\qquad 5.6$$

It is further apparent that the parameter sets regressed with the incorporation of VLE data exhibit AADs that are an order of magnitude higher than the cases where only pure component data were considered. These predictions are still very good however, but it remains to be seen in the prediction of mixture data whether this larger deviation is validated.

Considering the regressed parameters for butyl ethyl ether, one is immediately drawn to the lack of a reported parameter set for either sPC-SAFT$_{JC}$ or sPC-SAFT$_{GV}$ using the *Standard pure component regression* procedure. In this case, it was found that, regardless of initial guess, the value of the polar parameters were consistently forced to zero, yielding a zero polar contribution. This result suggests the presence of a broad minimum in the objective function, where no distinction can be made between the dispersion and weak polar forces at play in the ether. This argument is supported by the contributions of each term to the residual chemical potential predicted by each model, as typified by Figure 5.1.
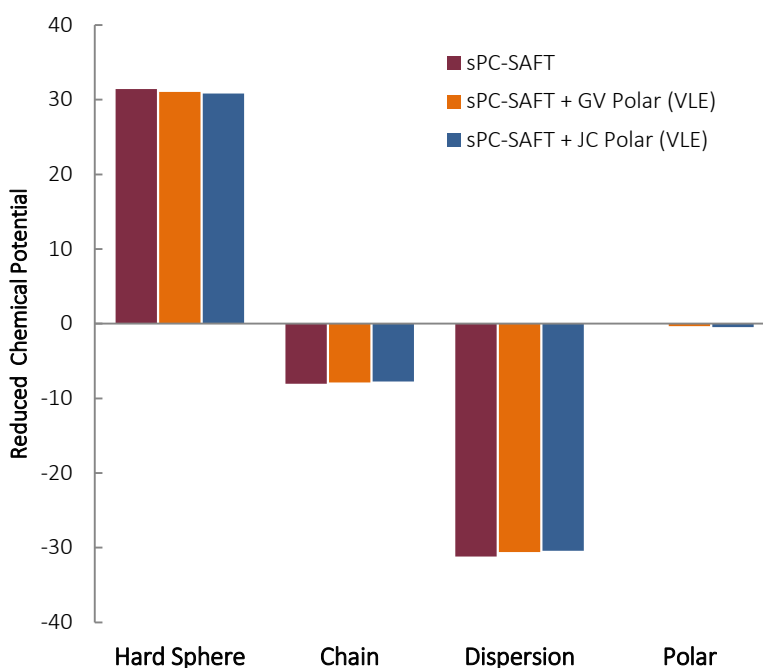
Figure 5.1: Contributions of each term to the reduced chemical potential of butyl ethyl ether at T = 298.15 K. The weak contribution of the polar term is stressed, supporting arguments for difficulties in accounting for its contribution.

In Figure 5.1, the sPC-SAFT$_{JC}$ and sPC-SAFT$_{GV}$ predictions are those using the parameter sets successfully fitted by incorporating VLE data. The figure highlights the weakness of the dipolar interactions in butyl ethyl ether, particularly when compared to the magnitude of the dispersion contribution and the similarity with the nonpolar model prediction. It also helps shed light on the difficulty in successfully accounting for this contribution. It should be stressed that term contributions of a similar magnitude to those presented in Figure 5.1 were in evidence for di-n-propyl ether, where a unique parameter set *could* be obtained without the need for including mixture data. The point being

stressed here is that including mixture VLE in the regression has the *potential* for a distinction to be made between dispersion forces and dipolar interactions. Given that no polar contribution was predicted for butyl ethyl ether *without* incorporating mixture behaviour, this line of thought appears to be validated.

A discussion on the superiority of any of the regression procedures as well as an explanation of their shortcomings is necessarily delayed until an assessment of the performance of the parameter sets in predicting mixture behaviour is made. This will be the primary focus of the remainder of this chapter, once the results of the parameter regression for the ester isomers are presented in the next section.

5.2.2 C_6 Ester Parameters

The regressed parameter sets for each of the five C_6 ester isomers are presented in Table 5.3. As with the ether systems previously, the parameters for the n-alkane used for generating mixture behaviour (*viz.* n-octane) are also included and are identical to those published by Gross & Sadowski (2000). As with n-heptane, identical parameter sets for the nonpolar sPC-SAFT as well as the sPC-SAFT$_{JC}$ and sPC-SAFT$_{GV}$ variants are reported for n-octane.

The immediately apparent result in Table 5.3 is the lack of reported sPC-SAFT$_{JC}$ parameters using the *Standard pure component regression* for either ethyl butanoate or propyl propanoate. In both cases, as was noted for butyl ethyl ether previously, the regression converged to a solution with a zero polar contribution. Specifically, the value of x_p was consistently forced to zero regardless of initial guess or changes in regression weights. This is a particularly interesting result given the molecular structure of these isomers, specifically the location of the functional group in the middle of the carbon backbone. It is worth noting that this is the same trend noted for 4-heptanone in the study of ketones (Cripwell, 2014), where a relationship between functional group location and parameter degeneracy was first suggested.

Assessing the polar parameters themselves, for sPC-SAFT$_{GV}$ there is no significant change in the magnitude of n_p for the different regression cases for methyl valerate, butyl acetate and pentyl formate. For ethyl butanoate and propyl propanoate in particular, n_p is *50%* and *100%* larger, respectively, for the *Standard pure component regression* when compared to the other two regression cases. Once again, this is true for the isomers where the functional group is centrally located. In the case of sPC-SAFT$_{JC}$, there is a marked difference in the value of x_p between the *Standard pure component regression* set and the other two regression cases for methyl valerate, butyl acetate and pentyl formate.

The AADs for the vapour pressures, liquid densities and heats of vaporisation are consistently within the *5%* range required to yield accurate phase equilibrium results (Sauer & Chapman, 2003). The smallest AAD values are evident when only pure component data are included in the regression procedure, and the inclusion of VLE data increases the pure component AADs in all cases. Whether this increase is indicative of a marked improvement in the prediction of mixture behaviour however, is the focus of the discussion in the following section.

Table 5.3: Regressed model parameters for n-heptane and each C6 ester isomer using indicated regression procedures

	M_W	σ	m	ε/k	n_P/x_P	μ	P^{sat}	ρ^{sat}	H^{vap}
	g/mol	Å		K		D	AAD%	AAD%	AAD%
n-Octane									
sPC-SAFT									
sPC-SAFT$_{GV}$	114.23	3.8213	3.8468	241.87	-	-	0.14	0.60	1.09
sPC-SAFT$_{JC}$									
Methyl Valerate									
sPC-SAFT	116.16	3.5693	3.8300	248.62	-	-	0.926	0.215	2.067
sPC-SAFT$_{GV}$									
Std. Regression	116.16	3.6067	3.7042	239.95	5.7062	1.62	0.890	0.333	1.784
n_P Correlation	116.16	3.6061	3.7077	240.90	5.4357	1.62	0.887	0.282	1.810
Exp VLE Data	116.16	3.6085	3.7039	239.91	5.7046	1.62	0.921	0.293	1.755
sPC-SAFT$_{JC}$									
Std. Regression	116.16	3.5933	3.7658	249.38	0.1345	1.62	0.935	0.240	2.034
x_P Correlation	116.16	3.7245	3.4380	251.68	0.4492	1.62	0.981	0.380	2.013
Exp VLE Data	116.16	3.6803	3.5754	245.16	0.4504	1.62	1.509	0.998	2.312
Ethyl Butanoate									
sPC-SAFT	116.16	3.6711	3.5818	252.68	-	-	0.786	0.860	2.421
sPC-SAFT$_{GV}$									
Std. Regression	116.16	3.7005	3.4707	231.16	6.5025	1.81	0.367	0.269	2.929
n_P Correlation	116.16	3.7093	3.4659	243.31	4.5147	1.81	0.657	0.371	2.468
Exp VLE Data	116.16	3.6340	3.6897	235.79	4.5450	1.81	2.202	0.975	1.513
sPC-SAFT$_{JC}$									
Std. Regression	116.16	-	-	-	-	1.81	-	-	-
x_P Correlation	116.16	3.8200	3.2355	256.79	0.3595	1.81	1.222	1.000	2.337
Exp VLE Data	116.16	3.7427	3.5383	240.96	0.3785	1.81	3.331	4.046	0.793
Propyl Propanoate									
sPC-SAFT	116.16	3.4814	4.1315	235.39	-	-	1.228	0.469	3.807
sPC-SAFT$_{GV}$									
Std. Regression	116.16	3.4971	4.0053	204.88	8.6588	1.79	0.693	1.417	2.678
n_P Correlation	116.16	3.5177	3.9963	227.85	4.6212	1.79	1.202	0.119	3.575
Exp VLE Data	116.16	3.5265	3.9802	228.81	4.5504	1.79	1.323	0.3284	3.668
sPC-SAFT$_{JC}$									
Std. Regression	116.16	-	-	-	-	1.79	-	-	-
x_P Correlation	116.16	3.6579	3.6439	238.23	0.3680	1.79	1.825	0.669	3.827
Exp VLE Data	116.16	3.6503	3.6997	237.36	0.3504	1.79	2.021	1.304	4.080
Butyl Acetate									
sPC-SAFT	116.16	3.4792	4.1549	237.39	-	-	0.577	0.461	0.901
sPC-SAFT$_{GV}$									
Std. Regression	116.16	3.5075	4.0554	233.99	3.1801	1.84	0.538	0.239	0.771
n_P Correlation	116.16	3.5145	4.0251	229.99	4.3688	1.84	0.607	0.112	0.668
Exp VLE Data	116.16	3.5062	4.0415	227.18	4.8216	1.84	1.098	0.200	0.517
sPC-SAFT$_{JC}$									
Std. Regression	116.16	3.5595	3.8128	239.73	0.2628	1.84	0.203	0.600	0.936
x_P Correlation	116.16	3.6519	3.6752	239.95	0.3479	1.84	0.189	0.653	0.993
Exp VLE Data	116.16	3.6547	3.7360	235.61	0.3727	1.84	0.875	2.240	1.050
Pentyl Formate									
sPC-SAFT	116.16	3.5360	4.0253	244.88	-	-	0.610	1.512	1.260
sPC-SAFT$_{GV}$									
Std. Regression	116.16	3.5727	3.8957	235.38	4.5525	1.90	0.689	1.021	1.492
n_P Correlation	116.16	3.5718	3.9018	237.50	4.0975	1.90	0.664	1.120	1.435
Exp VLE Data	116.16	3.5520	3.9431	231.82	4.9029	1.90	1.423	0.836	1.609
sPC-SAFT$_{JC}$									
Std. Regression	116.16	3.5521	3.9793	245.43	0.0743	1.90	0.584	1.528	1.233
n_P Correlation	116.16	3.7012	3.5837	248.30	0.3263	1.90	0.588	1.678	1.127
Exp VLE Data	116.16	3.6336	3.8149	236.23	0.3480	1.90	3.532	1.894	2.435

5.3 Application to Mixture Phase Behaviour

With the parameters regressed, focus now shifts to assessing the predictive capacity of the two polar sPC-SAFT terms through their ability to successfully predict the measured phase behaviour presented in the previous chapter. In the sections that follow for ethers and esters respectively, a general overview of the prediction results is presented, followed by an assessment of each polar model's performance within each regression procedure, to each system.

5.3.1 C$_6$ Ether Systems

The results of the pure predictions for the di-n-propyl ether/n-heptane and butyl ethyl ether/n-heptane systems are summarised in Table 5.4.

Table 5.4: Summary of deviations for pure prediction results of sPC-SAFT models applied to ether/n-heptane systems

Regression Case	sPC-SAFT		sPC-SAFT$_{GV}$		sPC-SAFT$_{JC}$	
	Δy (x10^2)^a	ΔT (K)^a	Δy (x10^2)^a	ΔT (K)^a	Δy (x10^2)^a	ΔT (K)^a
di-n-propyl ether/n-heptane						
Std. Regression			0.845	0.334	0.886	0.424
n_p/x_p Correlation	1.031	0.642	0.809	0.173	0.764	0.105
Exp VLE Data			0.728	0.069	0.734	0.110
butyl ethyl ether/n-heptane						
Std. Regression			-	-	-	-
n_p/x_p Correlation	0.846	0.534	0.411	0.081	0.265	0.138
Exp VLE Data			0.378	0.064	0.360	0.076

^{a} $\Delta z = \sum_i^{np} \left| z_i^{calc} - z_i^{exp} \right|$ where z is y or T and np is the number of data points.

The standard average deviations provided in Table 5.4 for the vapour phase composition and temperature indicate an excellent fit for all predictions using successfully regressed parameter sets. Average deviations in *y* are less than *0.01* mole fraction and those in *T* are below *0.5* K throughout. The true impact of these deviations however, requires an analysis of the predictions relative to the experimental data. To this end, reference is made to Figure 5.2 for the following discussion, where the predictions for the di-n-propyl ether/n-heptane system using the results of the *Standard pure component regression* are used as an example.
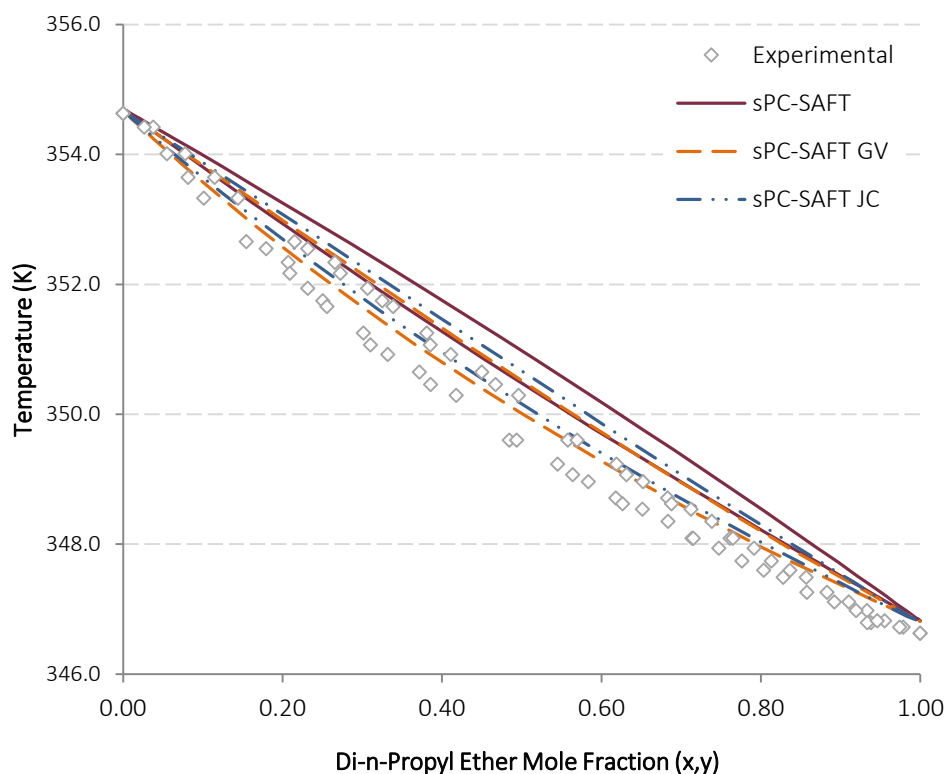
Figure 5.2: Predictions for the di-n-propyl ether/n-heptane systems at 60 kPa using parameter sets resulting from the standard pure component regression. Small but significant deviations of the model from the data are highlighted, with the prediction of nonpolar sPC-SAFT included for comparison.

It is readily apparent that while only small deviations between the predictions of both sPC-SAFT$_{JC}$ and sPC-SAFT$_{GV}$ with the experimental data exist, these small deviations actually result in the predictions completely missing the phase envelope. This is a consequence of how narrow the phase envelope is, resulting in a predicted liquid phase in agreement with the experimental vapour phase. This does not necessarily condemn the predictive capacity of the models, but rather serves to illustrate that the magnitude of average deviations in *y* and *T* should always be considered with respect to the system of interest. Further, it suggests and stresses that there is no universal scale for deviations in these properties that is indicative of an excellent model fit.

5.3.1.1   Standard Pure Component Regression

The results of the prediction based on the *Standard pure component regression* for each model applied to di-n-propyl ether/n-heptane have already been presented in Figure 5.2. The results of the same prediction applied to the *x-y* representation of the equilibrium data are presented in Figure 5.3. The zeotropic behaviour of the system is well predicted in the *x-y* plot for this system, where even the nonpolar sPC-SAFT prediction accurately represents the data. This suggests that errors in the model prediction are limited to deviations in the temperature prediction.
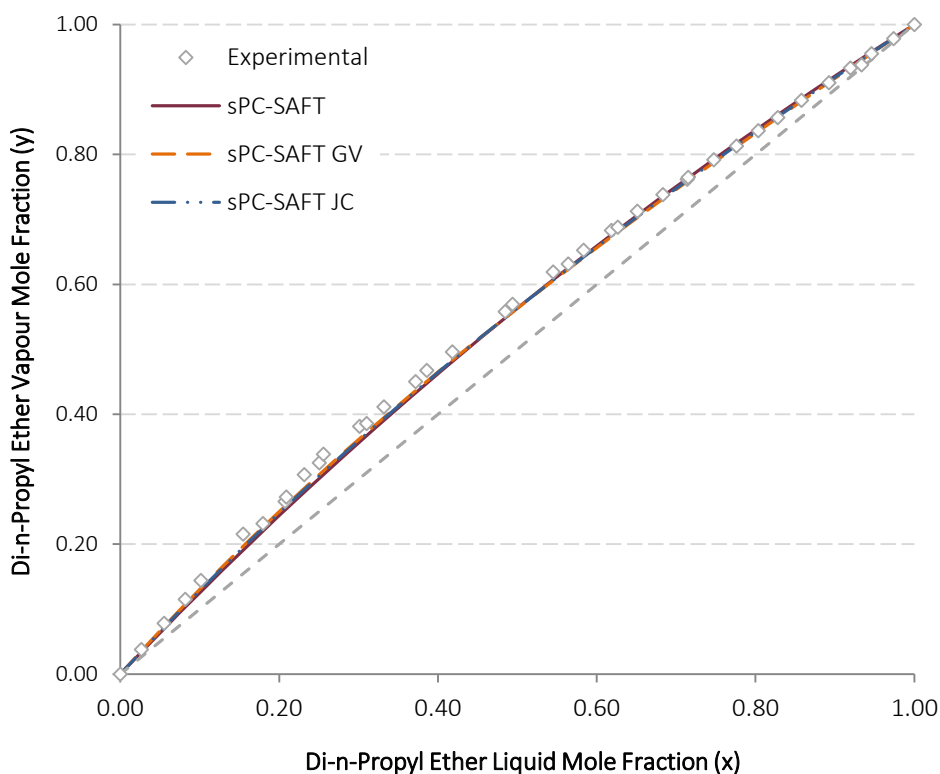
Figure 5.3: Predictions for the x-y behaviour of the di-n-propyl ether/n-heptane systems at 60 kPa using parameter sets resulting from the Standard pure component regression for sPC-SAFT$_{GV}$ and sPC-SAFT$_{JC}$. The prediction of nonpolar sPC-SAFT is included for comparison.

Although the temperature description of predictions based on the *Standard pure component regression* result in deviations from the experimental behaviour, the introduction of small binary interaction parameters (BIPs) can improve model performance. In the SAFT framework, these BIPs are introduced in the description of the mixture interaction energy as per equation 5.7:

$$\varepsilon_{ij} = \sqrt{\varepsilon_i \varepsilon_j}\left(1 - k_{ij}\right)$$

5.7

The introduction of BIPs improves the accuracy of model predictions, but because they are system specific, they diminish the predictive capacity of the model. Nevertheless, fitting k_{ij} to the ether systems here yield excellent correlations of the experimental data. This is true of both the two polar variants as well as nonpolar sPC-SAFT, as highlighted in Figure 5.4 where only very small BIPs are required to bring the model into agreement with the data. The correlations serve to improve the temperature description of the models, while maintaining the excellent prediction of the *x-y* behaviour. Further correlation results are presented in Appendix F.

Given that unique parameter sets could not be determined for butyl ethyl ether using either polar model, it was not possible to generate either predictions or correlations for the butyl ethyl ether/n-heptane system.
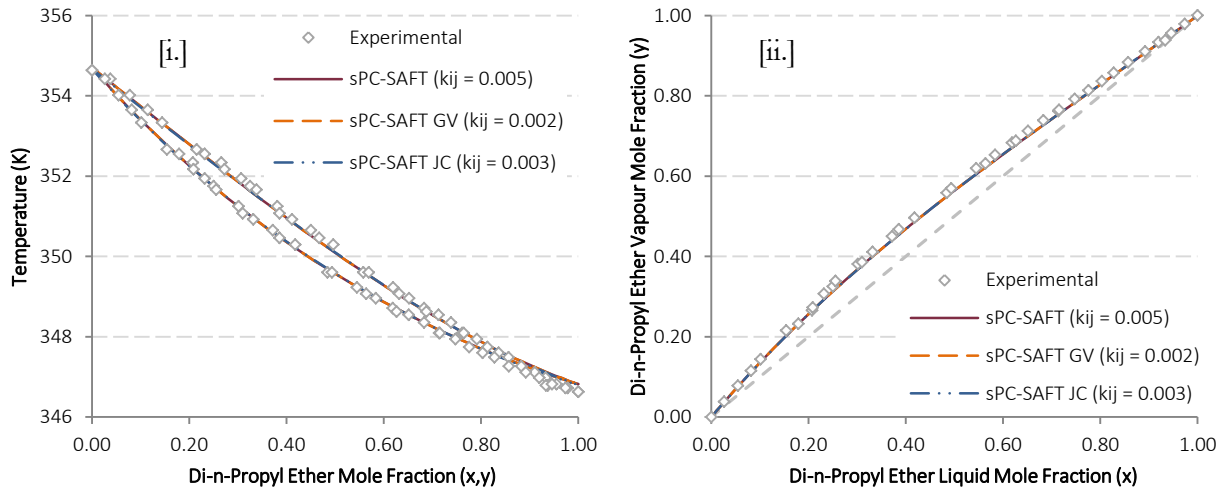
Figure 5.4: Correlation results for di-n-propyl ether/n-heptane system at 60 kPa. [i.] Deviations in the temperature predictions are rectified. [ii.] The x-y prediction is largely unchanged.

5.3.1.2 n_p/x_p *Correlation Regression*

The resulting model predictions for the parameter sets where the polar parameters were fixed using the correlations in equations 5.2 and 5.3 and the updated ether parameters in Table 5.1 are presented in Figures 5.5 and 5.6 for the di-n-propyl ether/n-heptane and butyl ethyl ether/n-heptane systems respectively. The improvement over the *Standard pure component regression* predictions is immediately apparent, with both the *T-xy* and *x-y* representations in excellent agreement with the experimental data.
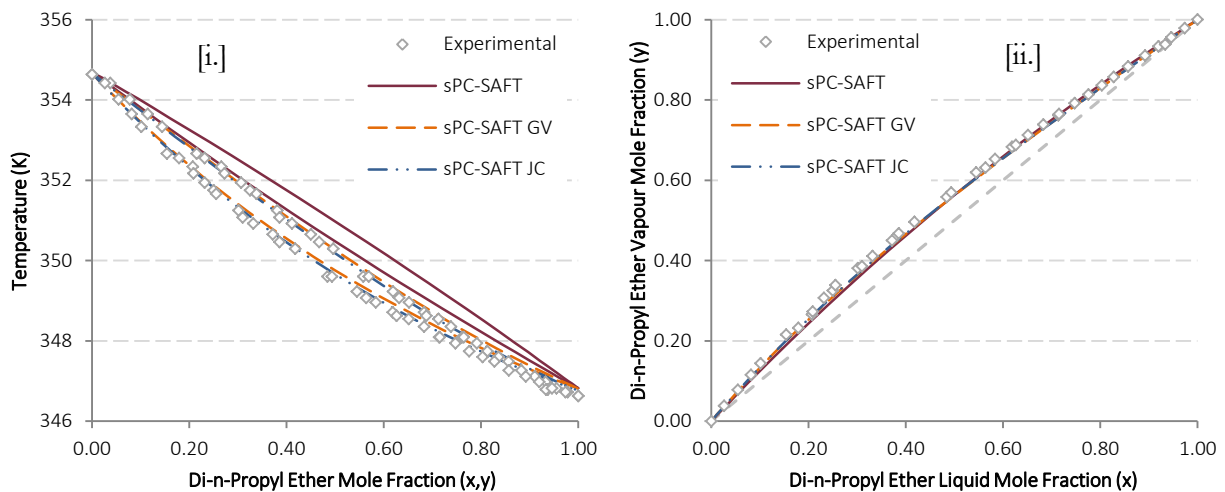
Figure 5.5: [i.]T-xy and [ii.] x-y pure predictions for the di-n-propyl ether/n-heptane system at 60 kPa using the parameter set obtained by fixing the value of polar parameter (n_p, x_p) and regression to pure component data. The prediction of nonpolar sPC-SAFT is included for comparison.

For the di-n-propyl ether/n-heptane system, both polar terms produce an excellent prediction of the phase behaviour across the whole compositional range. For the butyl ethyl ether/n-heptane system, sPC-SAFT$_{GV}$ similarly maintains the quality of its prediction throughout, while that of sPC-SAFT$_{JC}$ tends

to drift slightly as the ether concentration increases. This final observation is overly critical however, given that no prediction was possible for this system using the results of the *Standard pure component regression*.
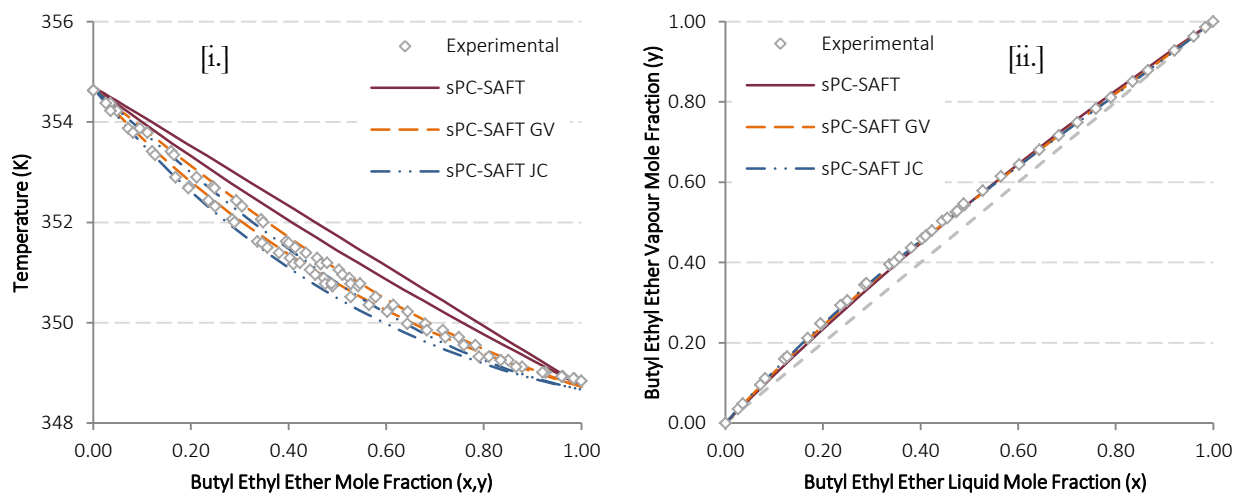
Figure 5.6: [i.]T-xy and [ii.] x-y pure predictions for the butyl ethyl ether/n-heptane system at 60 kPa using the parameter set obtained by fixing the value of polar parameter (n_P, x_P) and regression to pure component data. The prediction of nonpolar sPC--SAFT is included for comparison.

5.3.1.3   VLE Data Regression

The final results for the ether systems considered are those for the parameter sets determined with the inclusion of VLE data in the regression procedure. The results for the di-n-propyl ether/n-heptane and butyl ethyl ether/n-heptane systems using these parameter sets are presented in Figures 5.7 and 5.8 respectively. The predictions of both sPC-SAFT$_{JC}$ and sPC-SAFT$_{GV}$ are identical and in excellent agreement with the experimental data.
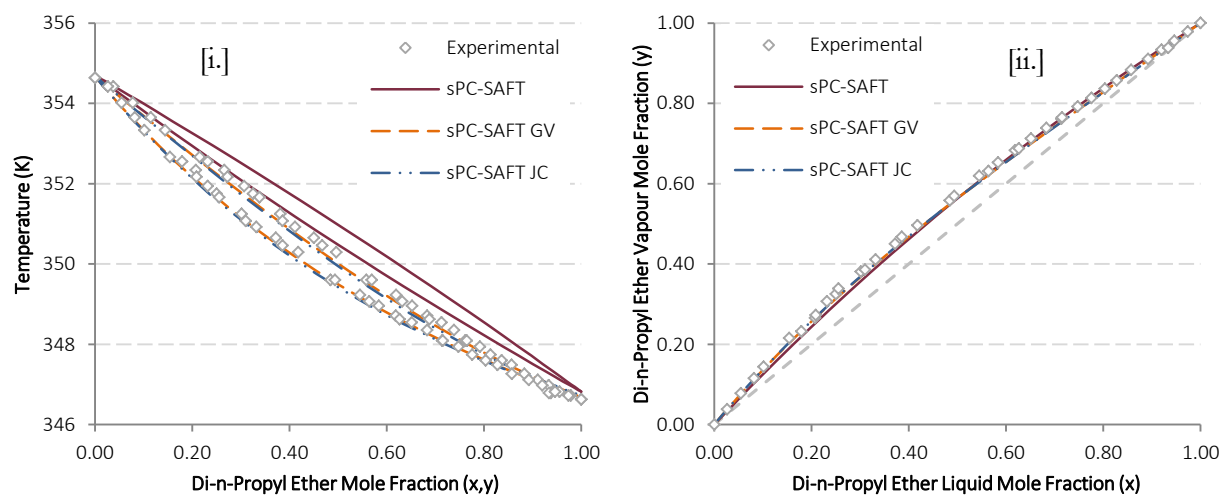
Figure 5.7: [i.]T-xy and [ii.] x-y pure predictions for tthe di-n-propyl ether/n-heptane system at 60 kPa using the parameter set obtained by incorporating VLE data in the regression procedure. The prediction of nonpolar sPC-SAFT is included for comparison.

That this regression case provides the best prediction of the phase equilibrium results should be no surprise, considering the parameters were fit to these data sets to begin with. The true test of these parameter sets will be in their applicability to independently measured phase equilibria for systems other than those considered here. This will be a focus of the discussion that follows in Section 5.4.
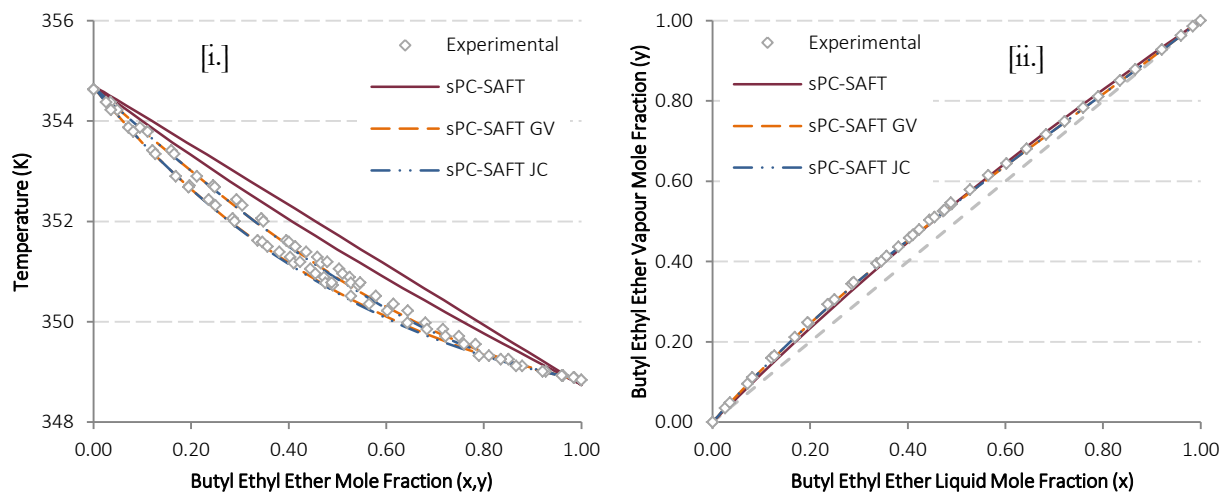
Figure 5.8: [i.]T-xy and [ii.] x-y pure predictions for the butyl ethyl ether/n-heptane system at 60 kPa using the parameter set obtained by incorporating VLE data in the regression procedure The prediction of nonpolar sPC--SAFT is included for comparison.

5.3.2 C_6 Ester Systems

Discussion of the results of applying the regressed parameters for the five C_6 ester isomers to the measured mixture behaviour follows the same course as was presented for the ethers previously. The results of the modelling exercise are summarised in Table 5.5.

Assessing the Predictive Capacity of Polar sPC-SAFT

Table 5.5: Summary of deviations for pure prediction results of sPC-SAFT models applied to ester/n octane systems

Regression Case	sPC-SAFT		sPC-SAFT$_{GV}$		sPC-SAFT$_{JC}$	
	Δy $(x10^2)^a$	ΔT $(K)^a$	Δy $(x10^2)^a$	ΔT $(K)^a$	Δy $(x10^2)^a$	ΔT $(K)^a$
methyl valerate/n-octane						
Std. Regression			0.970	0.083	3.665	2.198
n_p/x_p Correlation	3.972	2.494	1.192	0.205	1.582	0.261
Exp VLE Data			1.009	0.080	1.251	0.094
ethyl butanoate/n-octane						
Std. Regression			2.018	2.072	-	-
n_p/x_p Correlation	3.724	2.377	0.770	0.115	1.556	0.565
Exp VLE Data			0.785	0.083	0.770	0.154
propyl propanoate/n-octane						
Std. Regression			5.402	5.035	-	-
n_p/x_p Correlation	3.060	2.295	0.437	0.296	0.638	0.552
Exp VLE Data			0.515	0.083	0.585	0.130
butyl acetate/n-octane						
Std. Regression			2.374	1.609	2.052	1.216
n_p/x_p Correlation	3.929	2.960	1.183	0.628	1.021	0.295
Exp VLE Data			0.658	0.088	0.568	0.100
pentyl formate/n-octane						
Std. Regression			1.322	0.630	4.438	3.078
n_p/x_p Correlation	4.643	3.263	1.876	1.059	2.031	0.936
Exp VLE Data			1.087	0.097	1.274	0.104

^{a} $\Delta z = \sum_{i}^{np}\left|z_i^{calc} - z_i^{exp}\right|$ where z is y or T and np is the number of data points.

Differences between the average deviations in y and T reported in Table 5.5 for nonpolar sPC-SAFT and the two polar variants are more pronounced in the prediction of ester/n-alkane VLE than for the ethers in the previous section. This is due to the presence of the minimum boiling azeotrope in all five systems resulting from the strong positive deviations in these mixtures. The larger deviations in y and T for the nonpolar sPC-SAFT model are due to the inability of the model to account for the azeotropic behaviour in the system. The largest deviations are apparent for the sPC-SAFT$_{GV}$ prediction of the propyl propanoate/n-octane system using the *Standard pure component regression*, although the nature of the deviations is different. sPC-SAFT$_{GV}$ still accounts for the positive deviations in the mixture, but the strength of these deviations are overestimated and the azeotropic temperature is under predicted, as illustrated in Figure 5.9 [i.].
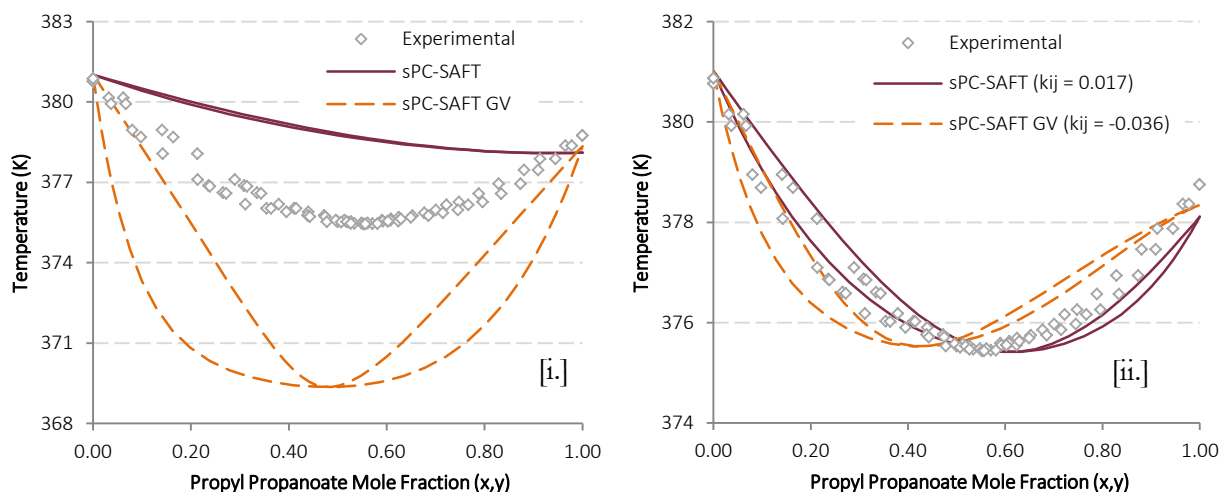
Figure 5.9: [i.] Pure prediction and [ii.] correlation of the propyl propanoate/n-octane system at 60 kPa using results of the standard pure component regression. The difference in the nature of the deviations in y and T of nonpolar sPC-SAFT and polar sPC-SAFT are highlighted.

In cases where accurate pure predictions were not possible, BIPs were fit using the experimental data. Figure 5.9 [ii.] highlights that even the nonpolar sPC-SAFT model can produce a qualitative fit of the experimental data using appropriate binary interaction parameters. For the propyl propanoate example provided, the correlation for sPC-SAFT$_{GV}$ provides a qualitative fit of the data, but the overall fit is not good. This case was the exception rather than the rule in terms of successfully correlating the experimental data, as is demonstrated in the supplementary correlation results in Appendix F. However, the relatively poor quantitative fit of these correlations stresses the importance of generating the optimum parameter set to begin with.

The assessment of correlation fits raises a further important point in the context of this work. The example provided in Figure 5.9 lacks a corresponding correlation fit for sPC-SAFT$_{JC}$. However, given that no parameters could be regressed for propyl propanoate using the *Standard pure component regression*, no prediction for this system was possible. Without a prediction to improve upon, or an interaction energy parameter to fit k_{ij} to, a correlation of the system is not possible. The problem of parameter degeneracy thus does not only affect the *predictability* of a system, but the ability to *correlate* that system as well.

The presence of the azeotrope provides the most stringent test of the predictive capacity of the thermodynamic models as accurate prediction of the azeotropic point is vital in industrial applications. In light of this, the predicted azeotropic point for each model in each system, using each regression procedure, is presented in Table 5.6. Discussion of the performance of each parameter set in representing the azeotropic point is reserved for the following sections, where the performance of each parameter set will be discussed as was the case for the ethers previously.

Assessing the Predictive Capacity of Polar sPC-SAFT

Table 5.6: Comparison between experimentally determined azeotropic points and the pure predictions of each model and regression case for ester/n-octane systems

Experimental		Regression Case	sPC-SAFT$_{GV}$		sPC-SAFT$_{JC}$	
Comp (mole% ester)	Temp (K)		Comp (mole% ester)	Temp (K)	Comp (mole% ester)	Temp (K)
methyl valerate/n-octane						
40.9%	377.53	Std. Regression	41%	377.5	28%	380.7
		n_p/x_p Correlation	41%	377.8	41%	378.0
		Exp VLE Data	41%	377.5	40%	377.7
ethyl butanoate/n-octane						
60.5%	374.60	Std. Regression	55%	371.8	-	-
		n_p/x_p Correlation	61%	374.5	68%	375.2
		Exp VLE Data	61%	374.6	63%	374.6
propyl propanoate/n-octane						
54.6%	375.44	Std. Regression	47%	369.4	-	-
		n_p/x_p Correlation	58%	375.2	59%	374.8
		Exp VLE Data	58%	375.5	58%	375.4
butyl acetate/n-octane						
45.9%	376.55	Std. Regression	45%	378.7	45%	378.2
		n_p/x_p Correlation	45%	377.3	45%	376.9
		Exp VLE Data	45%	376.5	45%	376.5
pentyl formate/n-octane						
30.8%	378.32	Std. Regression	31%	378.9	NP*	NP*
		n_p/x_p Correlation	28%	379.5	29%	379.5
		Exp VLE Data	32%	378.3	32%	378.4

NP* - No azeotrope predicted

5.3.2.1   *Standard Pure Component Regression*

The results for the predictions of the parameter sets determined using the *Standard pure component regression* procedure are presented graphically in Figures 5.10 to 5.14 for the five C$_6$ ester/n-octane systems. Starting with the predictions for the methyl valerate system in Figure 5.10, the first consideration is that the sPC-SAFT$_{GV}$ model produces an excellent pure prediction of the experimental data, in both the *T-xy* and *x-y* representations of the data. The quality of this fit is reflected in the accuracy with which the azeotropic point is predicted in Table 5.6. Considering the sPC-SAFT$_{JC}$ prediction however, there is barely an improvement over the nonpolar sPC-SAFT prediction. While the model does predict azeotropic behaviour, the azeotropic point is poorly predicted and this is reflected in the large deviations in *y* and *T* reported in Table 5.5.

The predictions for the ethyl butanoate system in Figure 5.11 show a decline in the quality of the sPC-SAFT$_{GV}$ prediction compared to the methyl valerate case. The increased deviation appears to be predominantly in the representation of the temperature as Figure 5.11 [ii.] shows that the *x-y* data are still fairly predicted. This is supported by the prediction of the azeotropic point, where the extent of the positive deviations is over exaggerated, and the azeotropic temperature is under-predicted as a result. This

is still better than the case for sPC-SAFT$_{JC}$ where the inability to successfully generate a unique parameter set meant that no prediction could be made.

Figure 5.10: [i.]T-xy and [ii.] x-y pure predictions for the methyl valerate/n-octane system at 60 kPa using the standard pure component regression procedure. The prediction of nonpolar sPC-SAFT is included for comparison.

Figure 5.11: [i.]T-xy and [ii.] x-y pure predictions for the ethyl butanoate/n-octane system at 60 kPa using the standard pure component regression procedure. The prediction of nonpolar sPC-SAFT is included for comparison.

The significant deviation of the sPC-SAFT$_{GV}$ prediction for the propyl propanoate mixture in Figure 5.12 has already been highlighted previously. The azeotropic temperature is under-predicted by *5* K and the *x-y* plot shows that these deviations are not limited to the prediction of the temperature. As with the ethyl butanoate system however, the quality of this prediction is still an improvement over the case of sPC-SAFT$_{JC}$, where no prediction was possible given that no parameters could be regressed.

Predictions for the butyl acetate system in Figure 5.13 show a significant improvement in the predictive capacity of the sPC-SAFT$_{JC}$ model, where the positive deviations are only slightly understated, resulting in an over predicted azeotropic temperature. A similar trend is apparent for the sPC-SAFT$_{GV}$

prediction and this is the only case where sPC-SAFT$_{JC}$ outperforms sPC-SAFT$_{GV}$. The azeotropic composition is well correlated by both models as shown in Table 5.6 and the *x-y* behaviour in general is well captured by both models in Figure 5.13 [ii.].
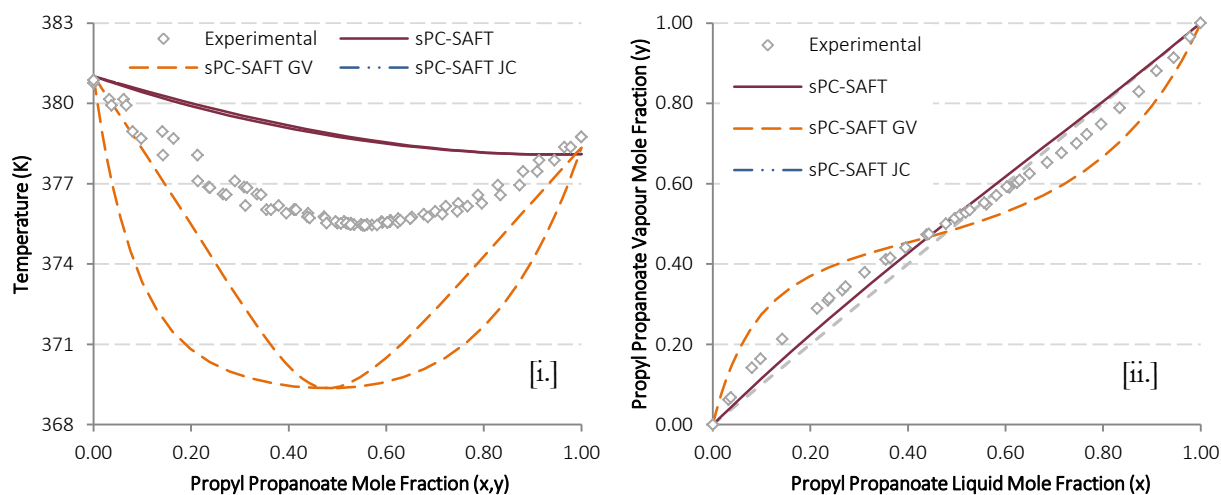
Figure 5.12: [i.]T-xy and [ii.] x-y pure predictions for the propyl propanoate/n-octane system at 60 kPa using the standard pure component regression procedure. The prediction of nonpolar sPC-SAFT is included for comparison.

Figure 5.13: [i.]T-xy and [ii.] x-y pure predictions for the butyl acetate/n-octane system at 60 kPa using the standard pure component regression procedure. The prediction of nonpolar sPC-SAFT is included for comparison.

Finally, the results for the pentyl formate/n-octane mixture are presented in Figure 5.14, where the sPC-SAFT$_{GV}$ model can be seen to maintain its good predictive capacity with an excellent prediction of the observed equilibrium behaviour. While the azeotropic temperature is slightly over predicted, the predicted composition is exactly right, with the *x-y* prediction underpinning this excellent fit. The sPC-SAFT$_{JC}$ prediction on the other hand offers little improvement over the nonpolar sPC-SAFT model predictions; no azeotrope is predicted and overall prediction of the phase behaviour is poor.
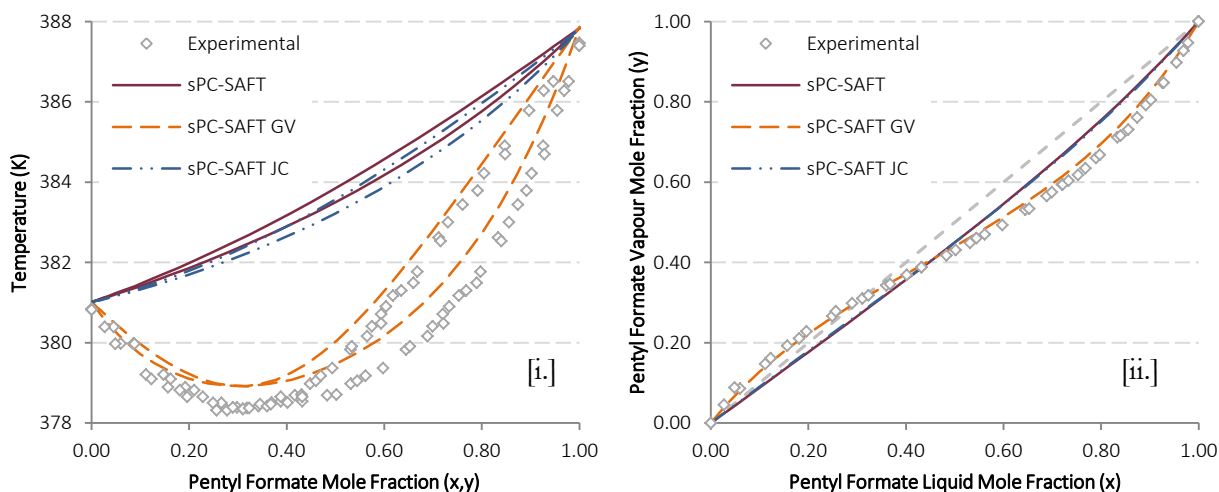
Figure 5.14: [i.]T-xy and [ii.] x-y pure predictions for the pentyl formate/n-octane system at 60 kPa using the standard pure component regression procedure. The prediction of nonpolar sPC-SAFT is included for comparison.

As previously highlighted, where poor pure predictions were in evidence, the introduction of BIPs resulted in successful correlation of these systems. This is typified by the *T-xy* correlations for the methyl valerate and pentyl formate systems in Figure 5.15 [i.] and [ii.] respectively. In particular, successful correlation served to address the relatively poor overall predictive capacity of the sPC-SAFT$_{JC}$ parameter sets based on the *Standard pure component regression* procedure. The correlation results and binary interaction parameters for all systems are presented in Appendix F.
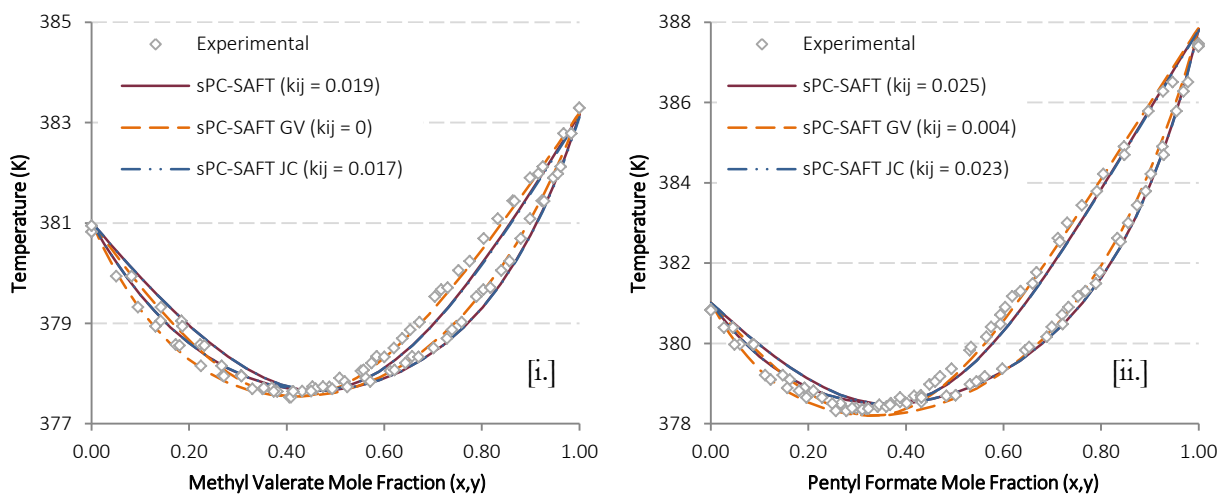
Figure 5.15: Correlation results for both models applied to the [i.] methyl valerate/n-octane and [ii.] pentyl formate/n-octane systems, highlighting the ability to introduce binary interaction parameters to produce excellent correlation fits.

5.3.2.2 n_p/x_p Correlation Regression

Employing the correlations developed by de Villiers (2011) for fixing the values of x_p and n_p for sPC-SAFT$_{JC}$ and sPC-SAFT$_{GV}$ respectively result in the VLE predictions of Figures 5.16 to 5.20. Applied to the methyl valerate system in Figure 5.16, the improvement of the sPC-SAFT$_{JC}$ prediction over its *Standard pure component regression* counterpart in Figure 5.10 is significant, to the point where the

azeotropic point is successfully correlated to within *0.5* K. For sPC-SAFT$_{GV}$, correlation of the azeotropic point is only slightly deteriorated, maintaining good predictive capacity using this regression procedure.
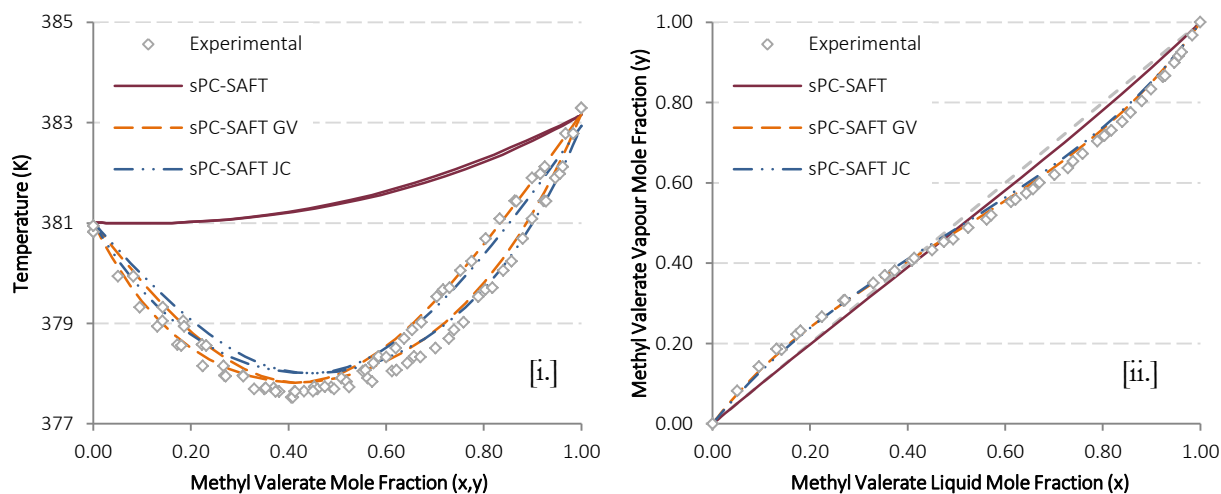
Figure 5.16: [i.]T-xy and [ii.] x-y pure predictions for the methyl valerate/n-octane system at 60 kPa using the parameter set obtained by fixing the value of polar parameter (n_P, x_P) and regression to pure component data. The prediction of nonpolar sPC-SAFT is included for comparison.
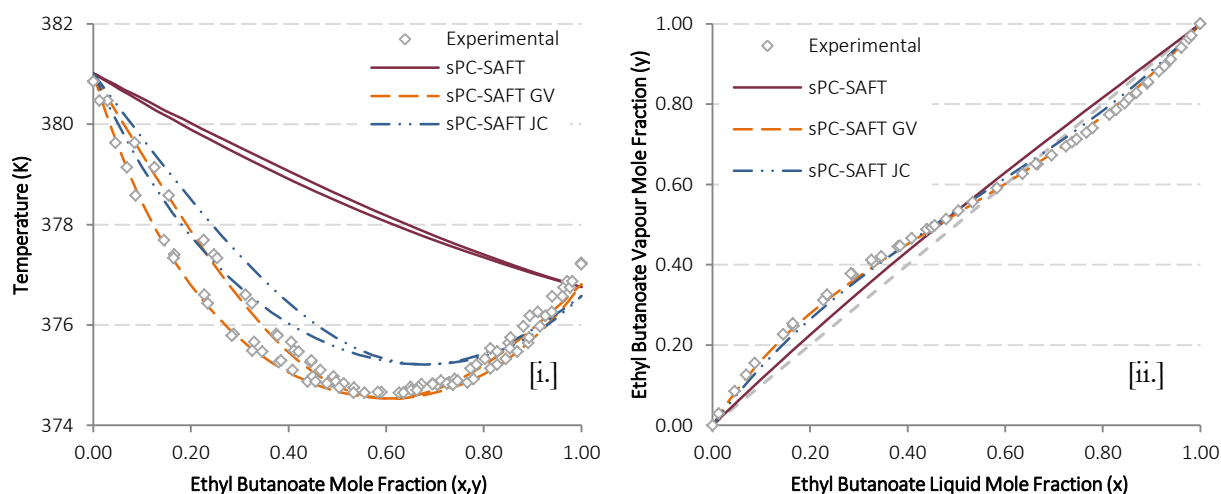
Figure 5.17: [i.]T-xy and [ii.] x-y pure predictions for the ethyl butanoate/n-octane system at 60 kPa using the parameter set obtained by fixing the value of polar parameter (n_P, x_P) and regression to pure component data. The prediction of nonpolar sPC-SAFT is included for comparison.

The predictions for ethyl butanoate and propyl propanoate in Figures 5.17 and 5.18 respectively offer particularly pleasing results. There is significant improvement in the performance of sPC-SAFT$_{GV}$ in both cases, where the azeotropic point is no longer overshot and the data is almost perfectly predicted. Further, sPC-SAFT$_{JC}$ is allowed to make good qualitative predictions for both isomers where none were possible using the *Standard pure component regression* procedure. In both cases, the models slightly under predict the pure component boiling points (consistent with the marginally increased AADs for the vapour pressures in Table 5.3) which serve to skew their predictions in the high ester concentration space. However, these small temperature deviations (*~0.6* K) only appear significant due to the small temperature range of the phase envelopes as a whole.
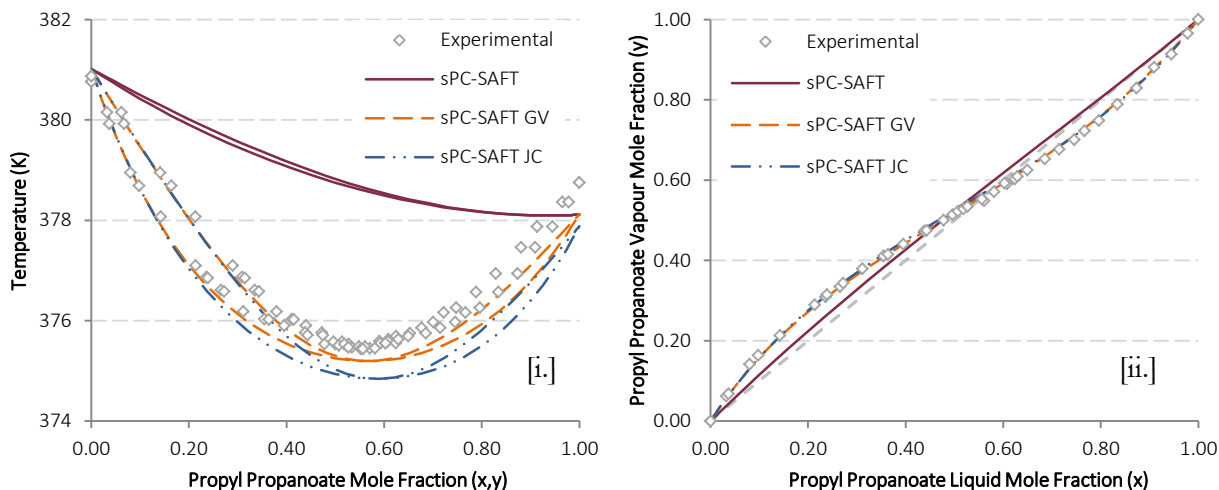
Figure 5.18: [i.]T-xy and [ii.] x-y pure predictions for the propyl propanoate/n-octane system at 60 kPa using the parameter set obtained by fixing the value of polar parameter (n_P, x_P) and regression to pure component data. The prediction of nonpolar sPC-SAFT is included for comparison.
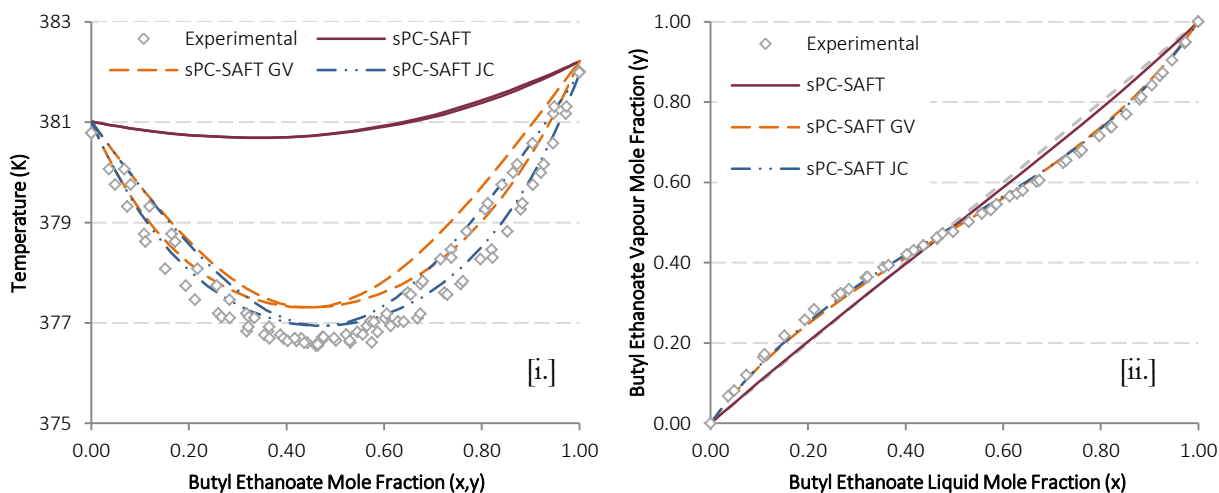
Figure 5.19: [i.]T-xy and [ii.] x-y pure predictions for the butyl acetate/n-octane system at 60 kPa using the parameter set obtained by fixing the value of polar parameter (n_P, x_P) and regression to pure component data. The prediction of nonpolar sPC-SAFT is included for comparison.
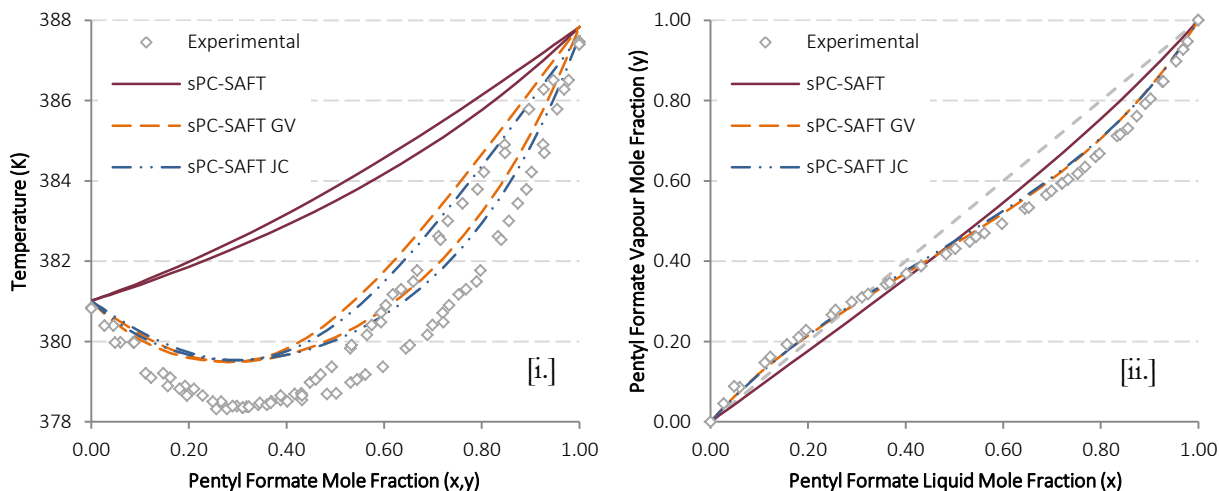
Figure 5.20: [i.]T-xy and [ii.] x-y pure predictions for the pentyl formate/n-octane system at 60 kPa using the parameter set obtained by fixing the value of polar parameter (n_P, x_P) and regression to pure component data. The prediction of nonpolar sPC-SAFT is included for comparison.

The phase behaviour in the butyl acetate system was qualitatively well predicted by both models using the *Standard pure component regression* parameter sets and Figure 5.19 shows further improvement in the temperature description of the predictions of both models when the values of the polar parameters are fixed. As was the case for the previous regression procedure, it is the only system for which the prediction of sPC-SAFT$_{JC}$ outperforms that of sPC-SAFT$_{GV}$, but both models still accurately account for the azeotropic point.

Predictions of the pentyl formate/n-octane phase behaviour present some mixed results. The prediction of sPC-SAFT$_{GV}$ is noticeably inferior to the previous regression case, but the prediction is still qualitatively correct. The *x-y* behaviour is well predicted, it is just the temperature dependence which is has suffered using this regression alternative. This is reflected in the model's description of the azeotropic point in Table 5.6 where the composition is correct but the temperature is *1.5* K too high. sPC-SAFT$_{JC}$ offers an identical prediction, but in this case the prediction is a marked improvement over the *Standard pure component regression* case in Figure 5.14, where no azeotropic behaviour was predicted.

5.3.2.3 VLE Data Regression

The prediction results for the parameter sets determined by including the measured VLE data for the respective ester/n-octane systems are presented in Figures 5.21 to 5.25. It is apparent that inclusion of the VLE data brings the predictions of both sPC-SAFT$_{JC}$ and sPC-SAFT$_{GV}$ into precise agreement with the experimental data for all five systems considered. Even the prediction of the propyl propanoate system, where increased deviations in the pure component vapour pressure tended to skew the predictions of both models previously, can be seen to be brought into agreement with the experimental data.
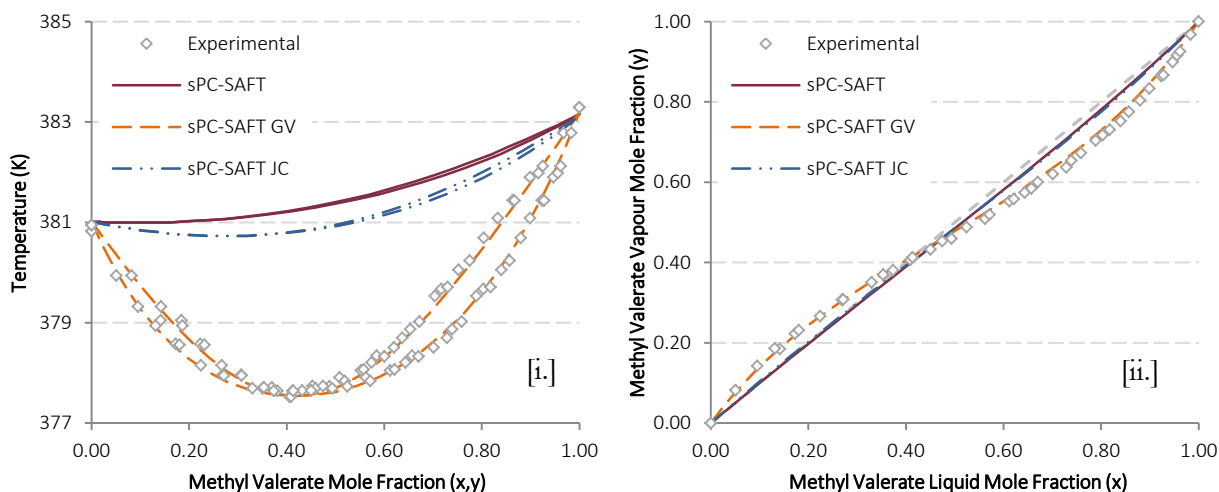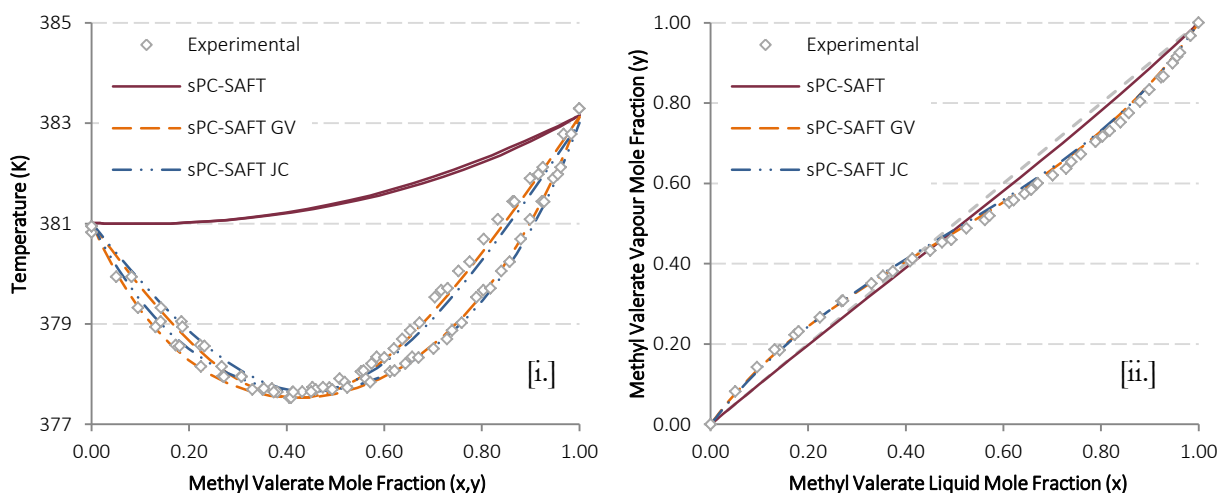

Figure 5.21: [i.]T-xy and [ii.] x-y pure predictions for the methyl valerate/n-octane system at 60 kPa using the parameter set obtained by incorporating VLE data in the regression procedure The prediction of nonpolar sPC-SAFT is included for comparison.
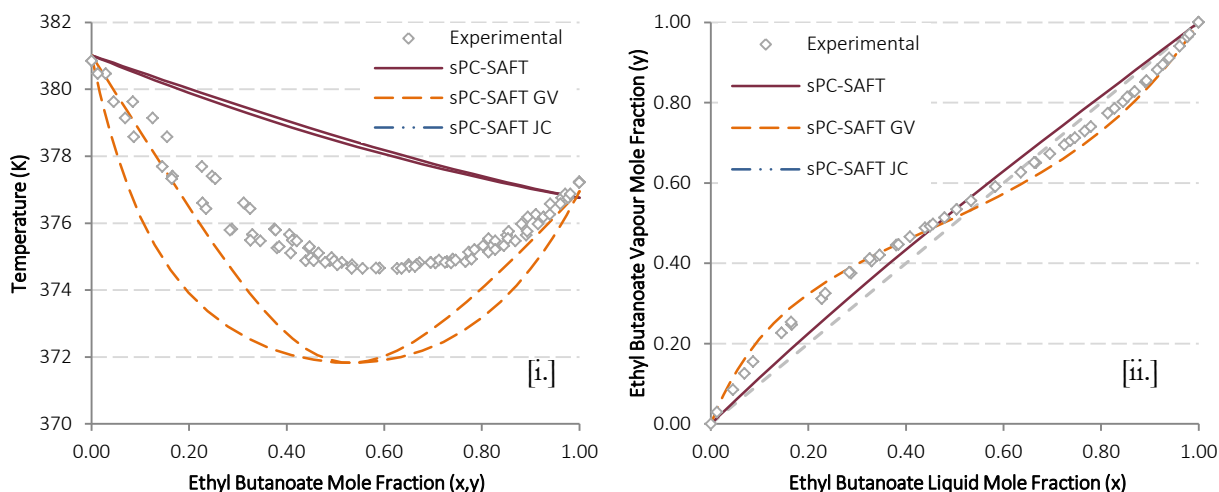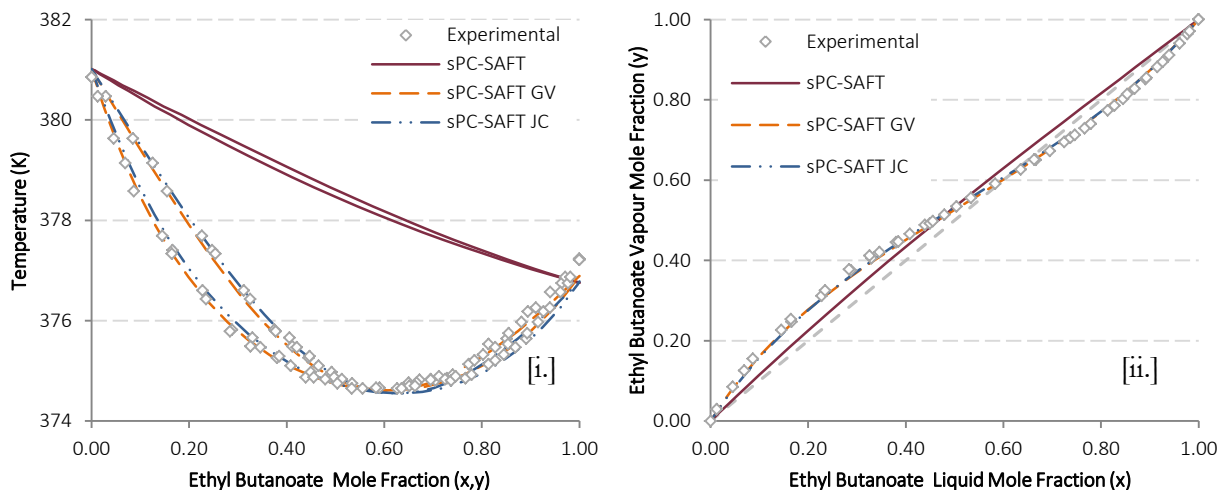
Figure 5.22: [i.]T-xy and [ii.] x-y pure predictions for the ethyl butanoate/n-octane system at 60 kPa using the parameter set obtained by incorporating VLE data in the regression procedure The prediction of nonpolar sPC-SAFT is included for comparison.
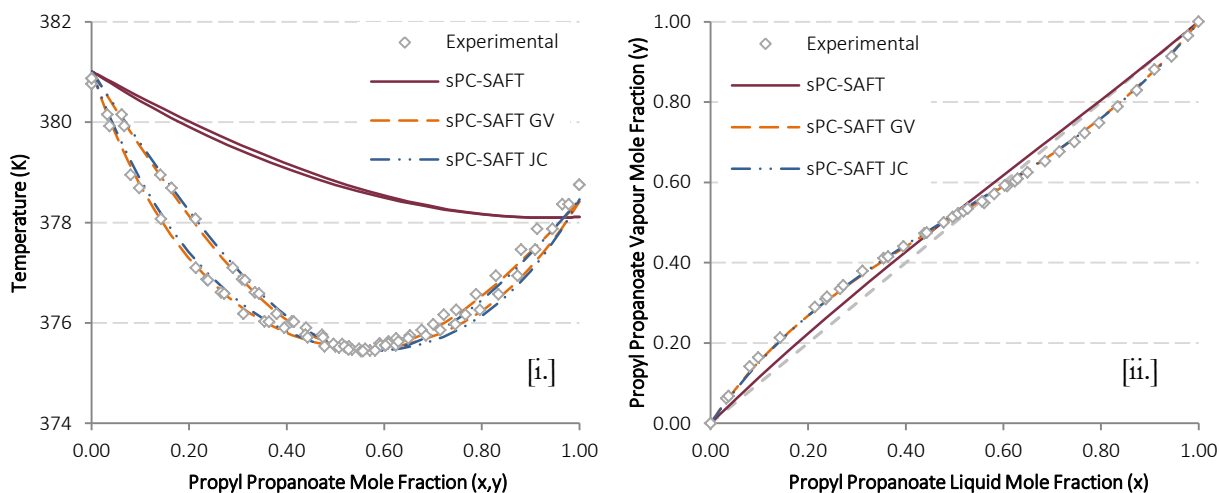
Figure 5.23: [i.]T-xy and [ii.] x-y pure predictions for the propyl propanoate/n-octane system at 60 kPa using the parameter set obtained by incorporating VLE data in the regression procedure The prediction of nonpolar sPC-SAFT is included for comparison.
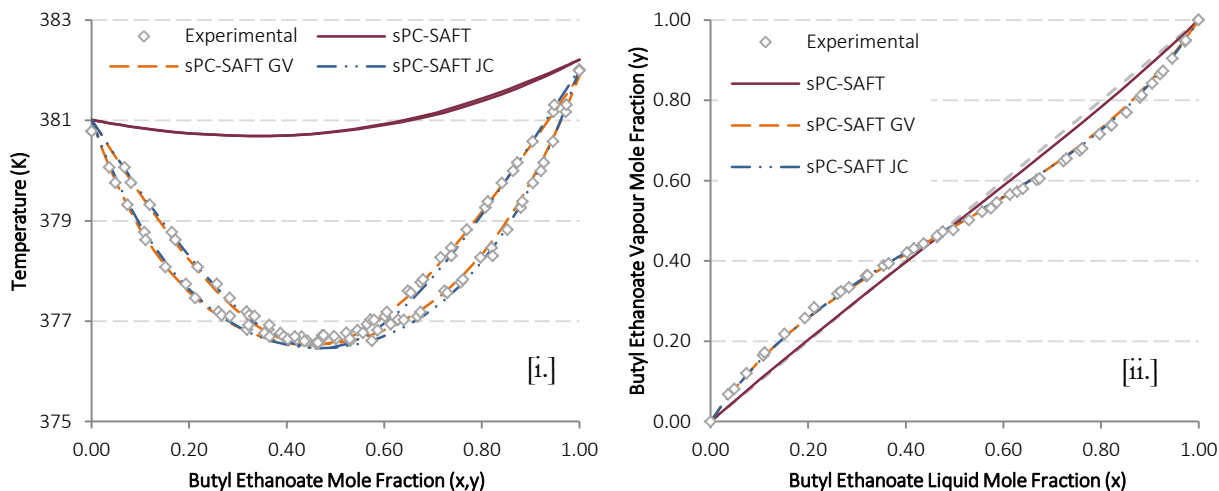
Figure 5.24: [i.]T-xy and [ii.] x-y pure predictions for the butyl acetate/n-octane system at 60 kPa using the parameter set obtained by incorporating VLE data in the regression procedure The prediction of nonpolar sPC-SAFT is included for comparison.
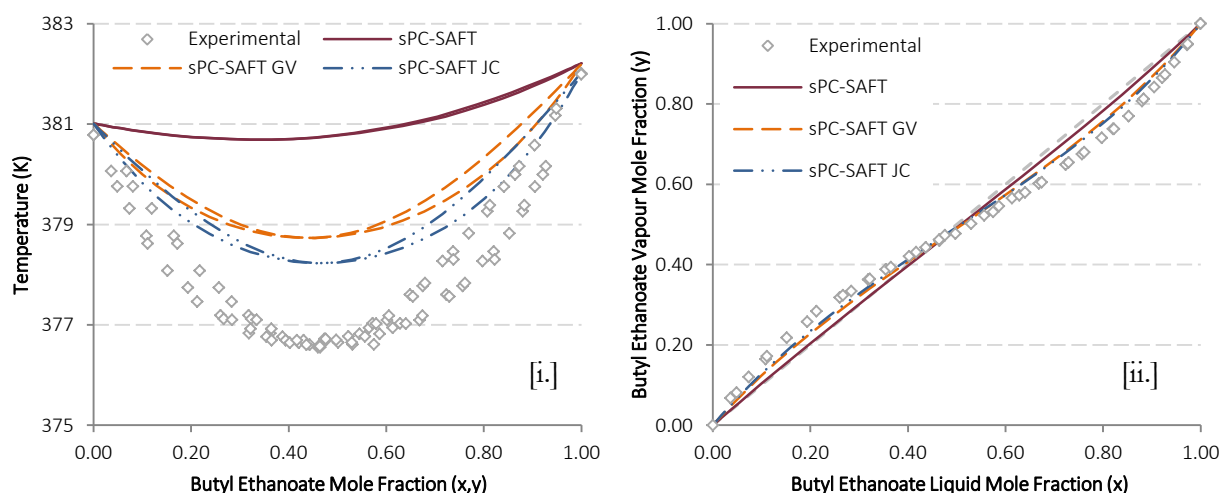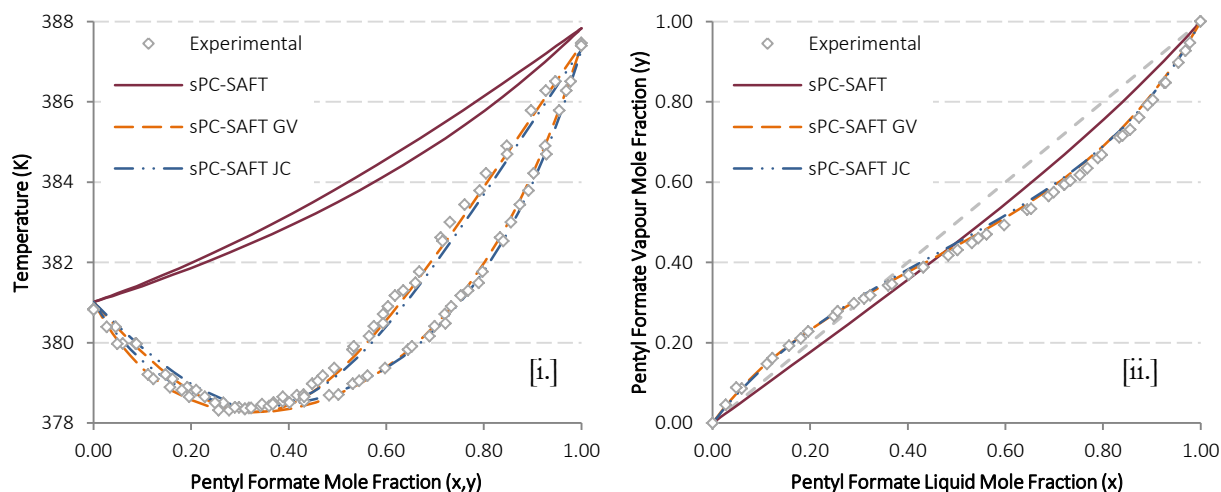
Figure 5.25: [i.]T-xy and [ii.] x-y pure predictions for the pentyl formate/n-octane system at 60 kPa using the parameter set obtained by incorporating VLE data in the regression procedure The prediction of nonpolar sPC-SAFT is included for comparison.

As with the results for the ethers previously, parameter sets of this regression procedure produced the best predictions for all the ester mixtures considered as a group. This result is to be expected however, as it was these same systems that were included in the regression procedure to begin with. A true test of these parameter sets however, will be their successful application to independently measured systems comprising these isomers, which is highlighted in the next section.

5.4 Performance of Polar sPC-SAFT Applied to Structural Isomers

With application of the regressed parameter sets to the phase equilibrium data performed in the previous section, it is possible to highlight and discuss observed trends in the predictive capacity of the polar sPC-SAFT models here. As with the structure of this chapter thus far, the discussion of the ether systems will be presented first, followed by that of the esters.

5.4.1 C$_6$ Ether Systems

Ethers are considered particularly difficult components to model due to the very small, but still significant contribution of this functional group's dipole moment. The validity of this argument was highlighted in the modelling procedure here, where the positive deviations from ideality of the di-n-propyl ether/n-heptane and butyl ethyl ether/n-heptane systems were not easily accounted for. The emphasis of this phase of the study however, was on the ability of the models to accurately account for the differences in phase behaviour between different structural isomers of polar molecules. This focus was most readily addressed in the results of the *Standard pure component regression* procedure.

5.4.1.1   *Shortcomings of the Standard Pure Component Regression*

The inability of either polar sPC-SAFT variant to generate unique parameter sets for butyl ethyl ether using only pure component data in the regression procedure serves to re-enforce trends witnessed for heptanone isomers previously (Cripwell, 2014). In the case of the ketones, a systematic trend was observed for the deterioration of model predictions and the associated ability to generate unique component parameters (the latter specifically for sPC-SAFT$_{JC}$). This trend was attributed to the shifting of the carbonyl group from the terminal end to the centre of the carbon chain. In the case of the ethers considered here, it is difficult to establish a trend when only two isomers are considered. Through consultation of Figure 5.26 however, it is apparent that the "trend" for ethers is juxtaposed to that for ketones. Here, the direction of the graduated red lines indicate deterioration of model predictions relative to the different functional group locations.
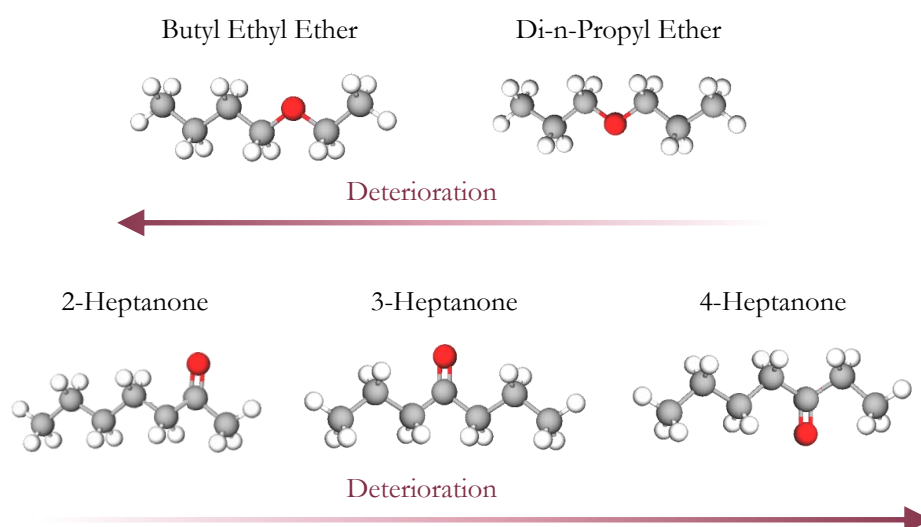
Figure 5.26: Observable trend in the deterioration of model predictions using the standard regression procedure for ethers (top) and ketones (bottom) as a function of functional group location. Skeletal structures presented from left to right following shift of respective functional groups from terminal end to centre of the chain.

For ketones previously, a unique parameter set could not be determined for the isomer with the centrally located functional group, *viz.* 4-heptanone. For ethers here however, it is the isomer with the more terminally located functional group, *viz.* butyl ethyl ether, which presents this problem. This suggests that the trend in parameter degeneracy being linked to functional group location needs to be reassessed and restructured.

The starting point here is the line of thought introduced in Chapter 4. It was remarked upon that as the alkoxy group shifts from the centre of the molecule (di-n-propyl ether) to the terminal methyl group (pentyl methyl ether), the boiling point of the ether *approaches* the boiling point of the equivalent weight n-alkane. If a similar analysis is performed for the heptanone isomers, we find that as the carbonyl group shifts from the centre of the molecule (4-heptanone) to the terminal ethyl group (2-heptanone), the boiling point of the ketone *departs* from that of the equivalent weight n-alkane, as highlighted in Table 5.7.

Table 5.7: Trends in normal boiling points of C_6 ether and C_7 ketone isomers compared to those of equivalent weight n-alkanes. Data taken from DIPPR.

Component	M_W	T_b	Component	M_W	T_b
	g/mol	K		g/mol	K
n-Heptane	100.20	371.58	n-Octane	114.23	398.83
Di-n-Propyl Ether	102.17	363.23	4-Heptanone	114.19	417.15
Butyl Ethyl Ether	102.17	365.35	3-Heptanone	114.19	420.55
Pentyl Methyl Ether	102.17	372.00	2-Heptanone	114.19	424.18

Viewed in light of the trend in Table 5.7, the trend in degeneracy of the parameter space illustrated in Figure 5.26 can be redefined: **the deterioration depends on the extent of the departure of the polar component from the behaviour of that for the equivalent sized nonpolar molecule**. Specifically, increased predictive capacity is apparent for polar components where there is a pronounced difference between the phase behaviour of that component and its nonpolar analogue (*viz.* n-alkane). The inability to distinguish between the dipolar and normal dispersion forces, responsible for the inability to determine optimum parameter sets (see Figure 5.1), supplements this argument.

It is worth emphasising here that the role of structural isomerism in this observed phenomenon is still central to the performance of the models. While the assertion that the predictive capacity of the polar sPC-SAFT models decreases as the polar functional group shifts centrally (Cripwell, 2014) is disproved by the case for ethers, Figure 5.26 shows that the influence of that polar functional group is still dependent on its location in the carbon chain. The case for ethers simply indicates that the polar functional group shifting centrally does not necessitate a decreased departure from nonpolar behaviour, as it did for ketones. Rather, it simply serves to show that the graduated red arrows in Figure 5.26 indicate the tendency to approach nonpolar behaviour for each homologous group as a function of the polar group location, in addition to their original purpose of indicating deterioration of predictive capacity.

While the ether case redefined the trend, polar sPC-SAFT modelling of ether isomers indicated that the observed systematic shortcoming of the *Standard pure component regression*, seen first for the ketone functional group, is maintained here. The significance of this result is that alternative means of regressing pure component parameters for all structural isomers of polar components still needs to be addressed. This is the focus of the role of fixing the polar parameter and incorporating VLE data in the regression procedure, discussed in the following section.

5.4.1.2   *The Role of Regression Alternatives*

The quality of the phase equilibria predictions using the parameter sets where the value of the polar parameters were fixed, or those determined where VLE data were used in the regression indicate that viable alternatives to the *Standard pure component regression* exist. The ability to generate pure component parameters without needing to turn to mixture VLE data is the ultimate goal for thermodynamic models. Ethers in particular are an underrepresented functional group with limited mixture data available in the literature. **The success of the predictions for the case of fixing the values of**

x_p/n_p **is thus a particularly important result**. Improvement of the prediction behaviour compared to the *Standard pure component regression* case and comparable performance with the parameter set where VLE data were included in the regression procedure serve to validate this regression alternative.

Given that the constants for ethers (Table 5.1) were determined and applied here for the first time is of further significance. The values for n_p larger than *1* again serve to validate the decision to make the parameter adjustable in the regression, as was the case for other functional groups. This correlation has already been shown to yield good results for aliphatic ketones, cyclic ketones, esters and aldehydes, so its successful extension to the ether functional group is a significant next step.

The ability to successfully generate a unique parameter set does not necessarily imply universal applicability however. This is an important point, particularly for the parameter set determined by including the respective ether/n-heptane data sets in the regression procedure. Successful prediction of the data used in the regression of the parameters does not guarantee that similar success will be achieved when applied to other mixtures. To this end, the applicability of the regressed parameters was tested through prediction of the di-n-propyl ether/acetone and di-n-propyl ether/2-butanone data of Resa *et al.* (1995) and Garriga *et al.* (1999) respectively, the results of which are presented in Figure 5.27. A similar test of the butyl ethyl ether parameters was not possible given the lack of mixture data for this component.
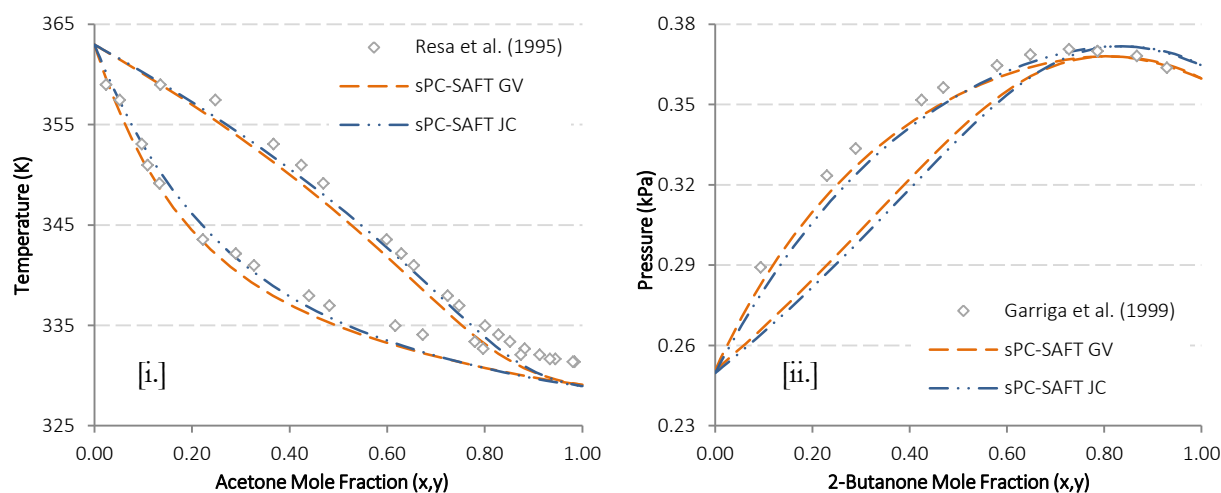
Figure 5.27: Application of the VLE Data parameter set for di-n-propyl ether to the independently measured [i.] acetone/DNPE and [ii.] 2-butanone/DNPE data. Universal applicability of the parameter set is highlighted.

The parameters for the ketones in these systems are those published by de Villiers *et al.* (2011), with the parameter set based on the inclusion of the measured VLE data chosen for di-n-propyl ether. Predictive capacity in these polar/polar systems is maintained for both models with excellent predictions in evidence, and the behaviour in the high ether composition space is particularly good. The quality of these pure predictions demonstrates that the regressed parameters are in fact appropriate beyond the system to which they were fit and gives a measure of confidence to the universal applicability of the parameter set.

5.4.2 C_6 Ester Systems

The structure of the ester functional group inherently allows for a greater degree of structural isomerism. This results in a less intuitive relationship with the functional group location for determining the most and least polar isomers. These characteristics thus provide the greatest scope for testing the predictive capacity of the polar sPC-SAFT models using structural isomerism as the assessment criterion. As with the ether case, the predictive capacity of sPC-SAFT$_{JC}$ and sPC-SAFT$_{GV}$ were most stringently tested by the results of the *Standard pure component regression*.

5.4.2.1   *Shortcomings of the Standard Pure Component Regression*

The sPC-SAFT$_{JC}$ predictions using the *Standard pure component regression* parameter sets provide the most compelling results here. Broad minima in the regression function were encountered for both ethyl butanoate and propyl propanoate, resulting in an inability to generate a prediction of the mixture data at all. Of the remaining three isomers for which parameters could be regressed, only the prediction of butyl acetate was in qualitative agreement with the experimental data. For methyl valerate and pentyl formate, the strength of the polar forces was underestimated (Figure 5.28) leading the model to yield only slightly better predictions than the nonpolar sPC-SAFT model. Analysis of the regressed parameters (Table 5.3) reinforce this argument, where the regressed values of x_p (*0.13* for methyl valerate, *0.07* for pentyl formate) are significantly smaller than those for the other two regression cases (*~0.45* and *~0.34*, respectively) which yielded significantly improved predictions of the mixture behaviour.
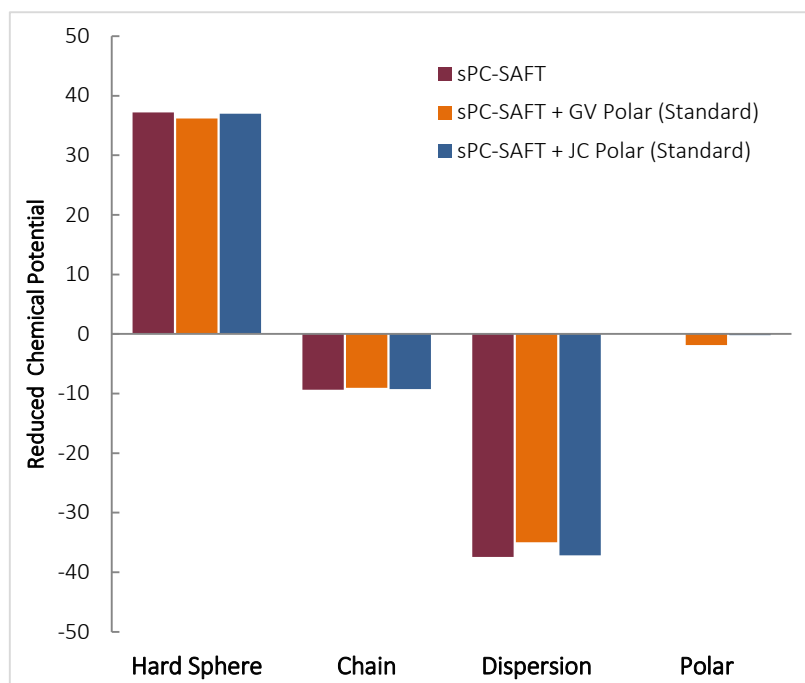
Figure 5.28: Contributions of each term to the reduced chemical potential of pentyl formate at T = 298.15 K using parameters of the standard pure component regression. Underestimation of the polar contribution for sPC-SAFT$_{JC}$ is highlighted.

Considering the performance of the sPC-SAFT$_{GV}$ model, the notably superior predictive capacity of these predictions is evident, although a trend is apparent in the prediction quality. In fact, the quality of

the predictions follows much the same trend as the boiling point/polar strength trend for the isomers presented in Figure 4.13 of the previous chapter. Specifically, the best predictions are in evidence for the two most polar isomers and deteriorate systematically with decreasing strength of the polar forces as depicted in Figure 5.29.
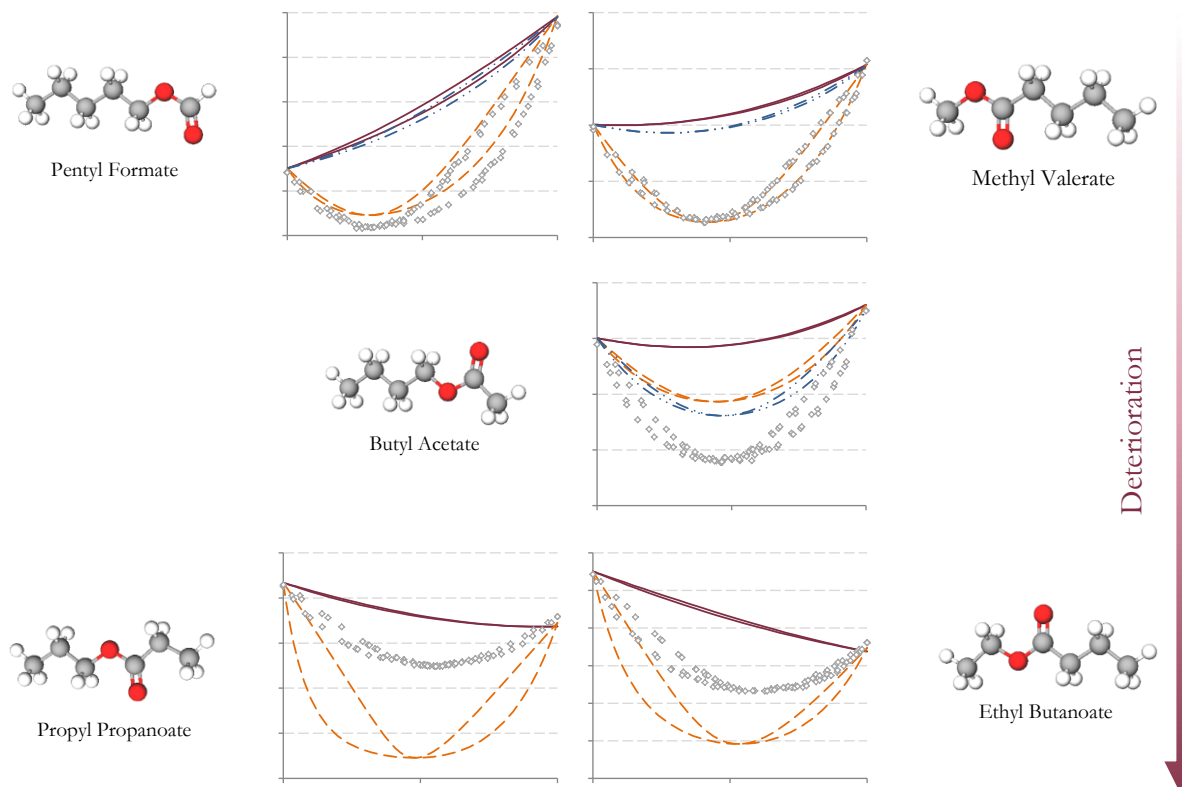
Figure 5.29: Deterioration of model predictions using the standard regression procedure for esters as a function of functional group location and polar strength. Structures presented from top to bottom follow shift of functional groups from terminal end to centre of the chain and following boiling point trend.

The systematic decline in the accuracy of sPC-SAFT$_{GV}$'s predictions with the shifting functional group maintains the trends seen for ketones and ethers previously. The same conclusion can be drawn from the degeneracy of the parameter space for sPC-SAFT$_{JC}$ when considering the least polar isomers. **Specifically, the quality of the model predictions and the ability to generate unique parameter sets is shown to once again be dependent on the polar strength of the isomer in question.** Furthermore, the case for esters mirrors that for ketones where the poorest predictions and broad minima in objective functions are apparent for the isomers where the functional group is located in the middle of the chain. These results lend a degree of confidence to the assertion that these trends can now be considered a systematic problem for all polar functional groups.

5.4.2.2   The Role of Regression Alternatives

It has already been demonstrated that deviations in the model predictions based on parameters from the *Standard pure component regression* can largely be overcome by the introduction of a small binary interaction parameter to yield accurate correlation results. However, the need for accurate phase equilibrium data to fit the binary interaction parameters to is the same caveat for including VLE data in

the regression procedure to begin with. To this end, the results for predictions using the parameter sets where the value of the polar parameters were fixed, or those determined by incorporating VLE data in the regression, offer more viable and reliable alternatives.

The results based on the parameter sets where x_p/n_p are fixed produce particularly interesting results, given that parameter sets for other esters based on this correlation were not included in the previous published work (de Villiers, 2011; de Villiers *et al.* 2014). The parameters based on the correlations in equations 5.2 and 5.3 provide consistent qualitative predictions for all five isomers with improved predictions in evidence for most cases. Some small bias is apparent however for isomers with more centrally located functional groups. This can be readily explained by the nature of the generation of the constants for the esters in Table 5.1.

The lack of experimental data for all isomers of a given molecular weight ester, and indeed other polar functional groups, has already been cited as motivation for performing this study. Where such data exists, it is largely limited to smaller components or systems of industrial interest (e.g. acetates). Furthermore, the functional group constants for the correlations in equations 5.2 and 5.3 were fit to parameter sets that were successfully regressed using such available VLE data in the regression procedure. Thus, considering the case of esters here, de Villiers (2011) only incorporated parameters sets for components up to C_6 in the determination of the functional group constants. Of these largest esters, only propyl propanoate and butyl acetate were considered given data availability. This work has already shown that *methyl* and *formate* type esters exhibit notably different phase behaviour compared to the other, less polar isomers. Thus application of these correlations to the likes of pentyl formate yields an extrapolation of the correlation results, rather than interpolation for the more prevalent *acetates* and *ethyl* esters, which produce larger deviations in the witnessed predictions.

Nevertheless, these deviations do not markedly dissuade the quality of the predictions given that only pure component data are included in the regression. **The ability of this regression alternative to offer unique parameters yielding excellent predictions of mixture phase behaviour, in lieu of available experimental data, is necessarily emphasised.**

As with the ketones and ethers previously, parameter sets where VLE data is incorporated in the regression procedure yield the best prediction of the measured phase behaviour, although their applicability beyond the systems measured here need to be tested. To this end, the parameters were used to predict independently measured phase behaviour, the results of which are summarised in Table 5.7.

Table 5.8: Deviations for the predictions obtained by applying the parameter sets determined here to independently measured ester/n-alkane and ester/ester VLE data.

System	sPC-SAFT$_{GV}$		sPC-SAFT$_{JC}$		Data Reference
	Δy (x10^2)[a]	ΔT (K)[a]	Δy (x10^2)[a]	ΔT (K)[a]	
Ester/n-Alkane Systems					
methyl valerate/n-heptane	0.833	0.326	1.028	0.397	Ortega *et al.* (2003)
ethyl butanoate/n-nonane	0.267	0.350	0.189	0.347	Ríos *et al.* (2012)
propyl propanoate/n-heptane	0.888	0.220	0.911	0.284	Ortega *et al.* (2001)
butyl acetate/n-hexane	1.233	1.181	1.483	1.331	Feng *et al.* (1998)
Ester/Ester Systems					
butyl acetate/ethyl acetate	0.487	0.464	0.573	0.462	Shono & Kanazawa (1969)
butyl acetate/butyl formate	0.917	0.528	0.951	0.569	Shaburov *et al.* (1971)

[a] $\Delta z = \sum_i^{np} \left| z_i^{calc} - z_i^{exp} \right|$ where z is y or T and np is the number of data points.

The parameters for ethyl acetate and butyl formate in these systems are those determined by de Villiers *et al.* (2011), with their applicability thus tested in a similar fashion. From the model fits in Figures 5.30 and 5.31, where selected systems from Table 5.8 are presented for both ester/n-alkane and ester/ester systems respectively, it is clearly demonstrated that the determined parameters for the esters are applicable beyond the system to which they were fit. Predictive capacity is maintained in both ester/n-alkane systems as well as ester/ester mixtures. This incorporates the effects of both nonpolar/polar and polar/polar interactions between different components.
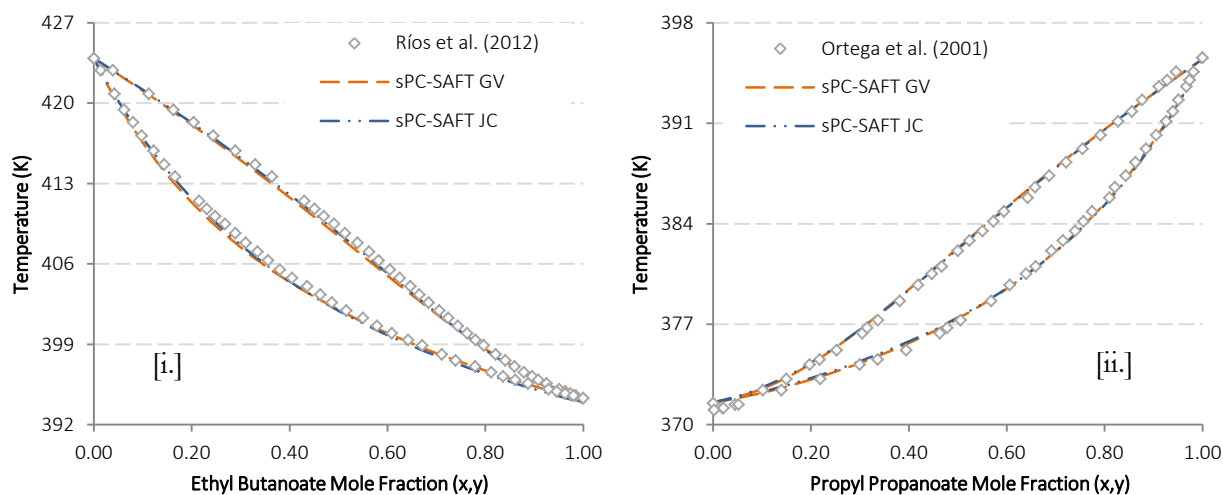
Figure 5.30: Application of the VLE Data parameter sets for C$_6$ esters to independently measured ester/n-alkane data: [i.] ethyl butanoate/n-nonane and [ii.] propyl propanoate/n-heptane. Universal applicability of the parameter sets is highlighted.
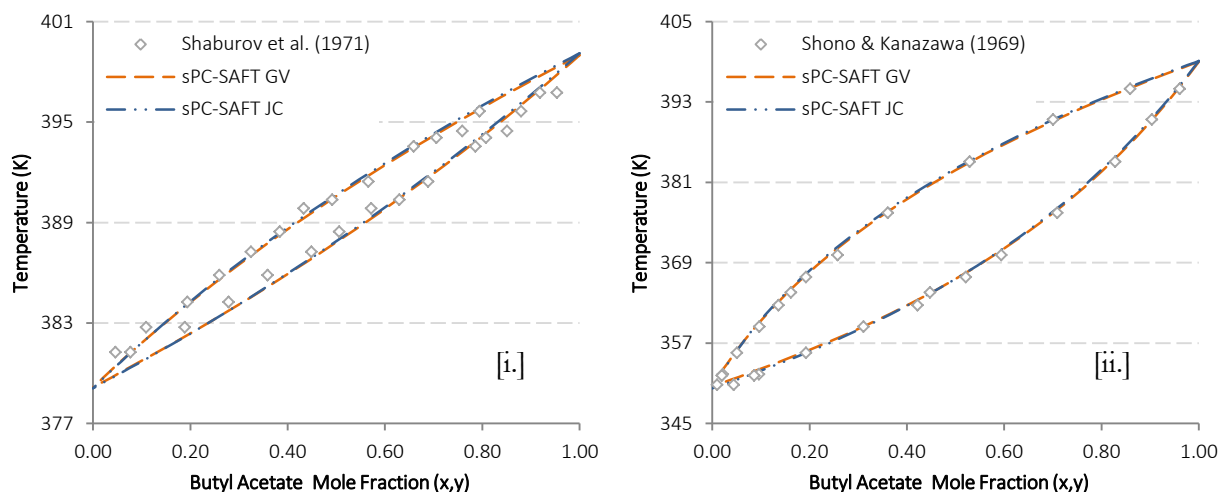
Figure 5.31: Application of the VLE Data parameter sets for C_6 esters to independently measured ester/ester data: [i.] butyl acetate/ethyl acetate and [ii.] butyl acetate/butyl formate. Universal applicability of the parameter sets is highlighted.

5.5 Chapter Summary

The aim of this chapter was to test the predictive capacity of polar sPC-SAFT using the effects of structural isomerism on mixture phase behaviour as the judgement criterion. The main objective was to determine whether systematic deterioration of the prediction quality for both sPC-SAFT$_{JC}$ and sPC-SAFT$_{GV}$ would result when considering structural isomers of ethers and esters, as had been the case for ketones previously.

When attempting to regress pure component parameters using the *Standard pure component regression*, the minimum in the objective function of some isomers was found to be more pronounced than for others. The procedure for ethers and esters verified that the link between parameter space degeneracy and polar functional group location did extend beyond the instance apparent for ketones. However these results further demonstrated that the deterioration of the prediction quality was not simply a result of the functional group shifting centrally.

The case for ethers in particular clarified that **model predictions deteriorated as the behaviour of the isomer approached that of an equivalent sized nonpolar molecule**. This was argued to result from a decreasing ability to distinguish between polar forces, unique to these components, and the dispersion forces common to all polar and nonpolar molecules. For ketones and esters, this behaviour is associated with decreasing polar interactions when the functional group shifts from the terminal end to the centre of the molecule. Ethers are clearly the exception however, as shifting of the functional group *towards* the terminal end results in the isomer's phase behaviour *approaching* that of a nonpolar molecule, despite indicating an increase in polar interactions. What remains clear from the results for all functional groups

considered is that **parameter degeneracy and prediction accuracy of polar sPC-SAFT models are intrinsically related to functional group location when considering different structural isomers**.

The relative performance of both models using the *Standard pure component regression* parameters was particularly interesting. The rapid deterioration of the JC polar term's predictions, first noted for ketones, was shown to extend to ethers and esters. Indeed, the sPC-SAFT$_{JC}$ model could only produce a qualitatively good fit for the binary phase behaviour of one of the five considered ester isomers and no parameters could be regressed for the two least polar esters. **The sPC-SAFT$_{GV}$ model on the other hand, when used with an adjustable polar parameter, produced consistently better predictions** than its counterpart and demonstrated the same robustness that was apparent in the investigation of ketones. The accuracy of the predictions could be seen to decrease systematically as the influence of the polar group diminished however, and suggests that there remains room for improvement.

The considered regression alternatives of fixing the value of x_p/n_p or including mixture data in the regression procedure illustrated that means of circumventing the problems associated with determining the optimum parameter set from pure component data alone do exist. The inclusion of mixture data in the regression, *if such data are available*, was shown to yield parameter sets which produce the best predictions of phase equilibrium beyond merely the system to which they were fit. The caveat of availability of accurate phase equilibrium data is sizable however, and thus the significant result is clearly the performance of parameters determined by fixing the value of the polar parameter. **The empirical correlations derived for this purpose have physical significance and allow for the accurate prediction of mixture phase behaviour in lieu of actual data.** This last point is of particular significance for the predictive capacity of polar sPC-SAFT and its application to more complex and physically obscure systems.

Chapter 6: SAFT-VR Mie: A Potential Holistic Approach

The modelling results of the previous chapter highlighted that there are still predictive shortcomings in the polar sPC-SAFT framework when accurately accounting for phase equilibrium of all polar molecules. In recent studies, a particularly prominent deficiency of the sPC-SAFT model has been brought to light: the inability to accurately account for derivative properties (Lafitte *et al.* 2006, de Villiers *et al.* 2011, Lafitte *et al.* 2013). The development of thermodynamic models has shifted to an ever more fundamental basis. With it, the focus of application has similarly gradually shifted from exclusively accounting for phase equilibrium, to providing well balanced predictions for the full spectrum of thermodynamic properties illustrated in Figure 1.1 of Chapter 1.

The SAFT-VR Mie model has garnered much attention recently due to its ability to seemingly provide this holistic approach to thermodynamic properties. While not itself a *new* SAFT variant, the most recent version of SAFT-VR Mie developed by Lafitte *et al.* (2013) has shown much promise in the short time since its initial publication. The goal of this chapter is to summarise the development of this SAFT variant to provide context to the modelling exercise that will follow within this model framework.

6.1 Development of SAFT-VR Mie

The SAFT-VR Mie EoS has its roots in SAFT-VR (SAFT for potentials of variable range), a SAFT variant pioneered by Alejandro Gil-Villegas and co-workers (Gil-Villegas *et al.,* 1996, Galindo *et al.,* 1998). The variant differs from SAFT$_{HR}$ that came before it, and PC-SAFT which came after, in the choice and treatment of the intermolecular potential.

6.1.1   SAFT-VR

An equation of state's reference pair potential has a significant effect on the model's predictive capacity. It is one of the first and biggest assumptions inherent in the development of any EoS as it is the mathematical approximation of the fundamental forces between molecules. In the SAFT-0, SAFT$_{HR}$ and sPC-SAFT EoSs, the square well and Lennard-Jones potentials used account for the different magnitudes of interaction for different molecules. The inherent assumption of these potentials however, is that all molecules interact over the same range of intermolecular distances. The former is accounted for through the dispersion energy parameter, ε, represented by the potential well depth, but the range of interactions, associated with the well width, is constant.

The previously asserted assumption of a universal potential range, known since the 1950s to be highly simplified (Lafitte *et al.*, 2013), was the reason for the development of a SAFT-type EoS for potentials of variable range (Gil-Villegas *et al.,* 1996, Galindo *et al.,* 1998). In this new SAFT-VR framework, the monomer reference fluid comprised the traditional hard spheres interacting with a simple square well potential, but of variable width through the introduction of a new parameter, λ. This new parameter characterises the range of the potential, as illustrated in Figure 6.1. While the square well potential of SAFT$_{HR}$ was also characterised by a well width, that range was constant while the λ of SAFT-VR is an additional, regressed pure component parameter.
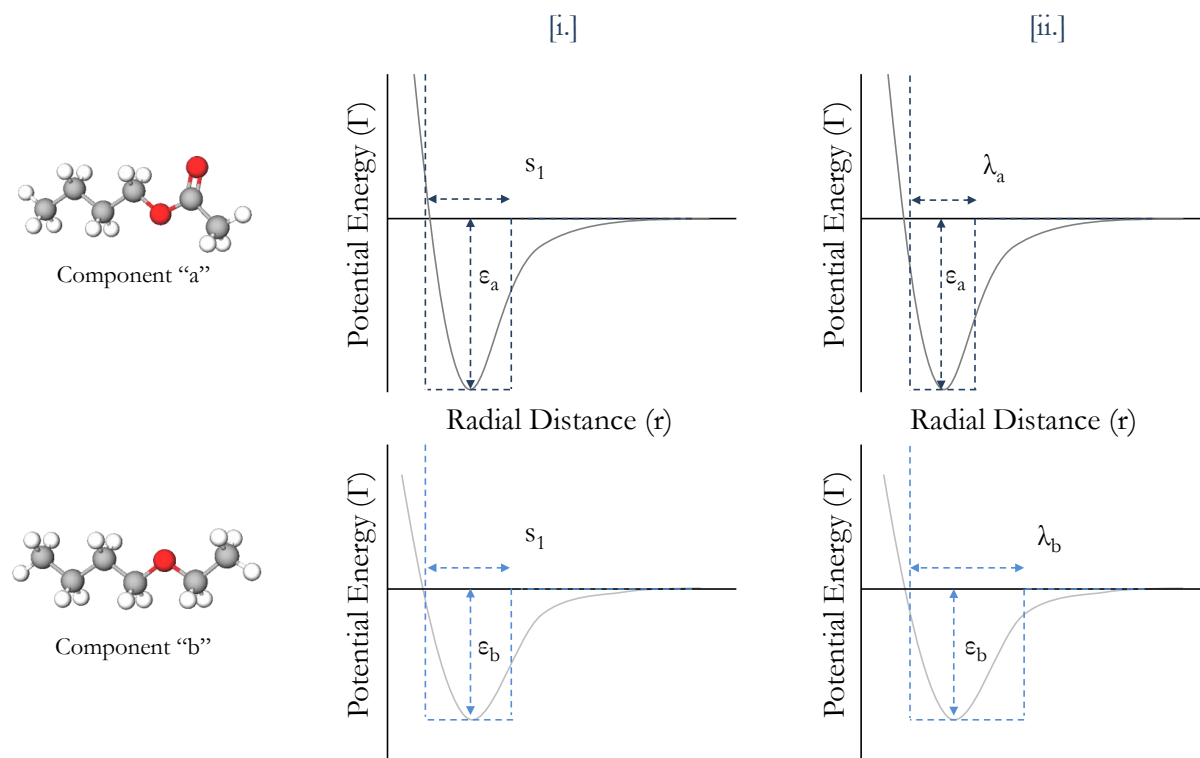
Figure 6.1: Accounting for the range of intermolecular interactions. [i.] SAFT$_{HR}$ accounts for the different magnitudes of interaction of two species (ε_a & ε_b), but simplistically assumes their range to be equal (s_1) [ii.] SAFT-VR accounts for both the difference in magnitude and range, yielding better overall approximation of the true potentials.

One may argue that the incorporation of an additional, regressed parameter merely allows more room for flaws in the theory to be compensated for by curve fitting – even purely empirical equations can be fit to highly non-ideal system behaviour if enough parameters are included. However, the widely held view that a universal potential function would not be truly applicable to the different intermolecular forces of all substances (Lafitte *et al.*, 2013) supports, and arguably necessitates, the inclusion of a further regressed parameter. This inclusion results in SAFT-VR's four pure component parameters for non-associating components (σ, m, ε and λ) compared to its contemporaries' three.

SAFT-VR employs the full statistical mechanical theory of Barker & Henderson (1967a, b), where a hard sphere fluid is considered the reference and the attractive term is considered a perturbation. In the theory, a high temperature expansion can be used to approximate the dispersive free energy of the system,

which is typically truncated at the second term, as in the case of PC-SAFT. Further however, an nth order expansion in the free energy corresponds to a $(n\text{-}1)^{th}$ order expansion in the fluid structure, or more specifically, the radial distribution function (Gil-Villegas *et al.*, 1996). Thus truncating the dispersion term at second-order necessitates the use of a first-order expansion in the radial distribution function. This term is important for the calculation of the contribution of the chain term to the residual Helmholtz free energy according to equation 6.1:

$$\frac{A^{chain}}{NkT} = -\sum_i x_i \left(m_i - 1\right) \ln g_{ii}{}^{mon}\left(\sigma_{ii}\right)$$

$$g_{ii}{}^{mon}\left(\sigma_{ii}\right) = g_{ii}{}^{hs}\left(\sigma_{ii}\right) + g_1\left(\sigma_{ii}\right)$$

6.1

This full application of the Barker-Henderson perturbation theory is not explicitly employed in the PC-SAFT framework. As is traditionally the case, only the zeroth order radial distribution function (i.e. hard sphere g^{hs} of Boublik (1970) and Mansoori *et al.* (1971)) is used in the chain term of PC-SAFT. Thus, the use of a higher order approximation should arguably result in better correlation of chain effects, even if a simpler monomer geometry is used.

Using the mean value theorem and the local compressibility approximation, Gil-Villegas *et al.* (1996) present analytical functions for the first and second order dispersion terms respectively. The first order structural term in equation 6.1 (i.e. g_1) is determined analytically by a self-consistent method equating the monomer compressibility factor from the Clausius virial theorem and the density derivative of the Helmholtz energy. The strength of SAFT-VR is thus the theoretically derived, yet analytically simple expressions for each term in the residual Helmholtz free energy, incorporating the range variability of intermolecular interactions. Further, and perhaps critically, while Gil-Villegas *et al.* (1996) presented predictions and correlations of SAFT-VR using a square-well potential, they showed that the procedure for determining these analytical expressions is readily and easily generalizable to any pair potential.

6.1.2   Original SAFT-VR Mie

Application of the SAFT-VR framework using generalised Mie potentials, typified by equation 6.2, was the next major advancement for the variant as a whole. The Mie (λ_a - λ_r) potentials, of which the *6 - 12* Lennard-Jones potential is the most recognisable, are generalised potentials which accurately capture the curvature and magnitude of the potential energy between molecules as a function of their intermolecular distance.

$$u^{Mie}\left(r\right) = C\epsilon\left(\left(\frac{\sigma}{r}\right)^{\lambda_r} - \left(\frac{\sigma}{r}\right)^{\lambda_a}\right)$$

$$C = \frac{\lambda_r}{\lambda_r - \lambda_a}\left(\frac{\lambda_r}{\lambda_a}\right)^{\frac{\lambda_a}{\lambda_r - \lambda_a}}$$

6.2

The λ_a and λ_r parameters are representative of the ranges of the attractive and repulsive interactions, respectively. With the advent of quantum mechanics, it was shown that attractive interactions were a result of fluctuating electric dipoles, later referred to as London dispersion interactions. The contribution of these interactions to the pair potential function is proportional to the inverse sixth power in the intermolecular distance (Lafitte *et al.*, 2013). This physical description serves as a fundamental basis for setting the value of the attractive range parameter (λ_a) to *6*, but there exists no unique value for λ_r which is universally applicable. This ties in to the original assertion of this section that the popular *6 - 12* Lennard-Jones potential is oversimplified, and that the repulsive range should be a component specific parameter.

Using this notion, and the generalised SAFT-VR framework established by Gil-Villegas *et al.* (1996), Lafitte *et al.* (2006, 2007) proposed the SAFT-VR Mie EoS using the Mie (λ_a - λ_r) potential of equation 6.2. In an extensive comparative study, the new EoS was found to outperform its square-well SAFT-VR counterpart for the prediction of phase equilibria of both associating and non-associating components and their mixtures, with these predictions comparable with those of PC-SAFT. A more significant result however, was the ability of the SAFT-VR Mie EoS to accurately predict derivative properties, including speed of sound as well as isobaric and isochoric heat capacities. Generally accepted to be a stern test for any thermodynamic model, the ability to predict these second derivative properties (compare Figure 6.2 [i.] with [ii.]) suggests that SAFT-VR Mie has a strong fundamental basis.

SAFT-VR Mie: A Potential Holistic Approach
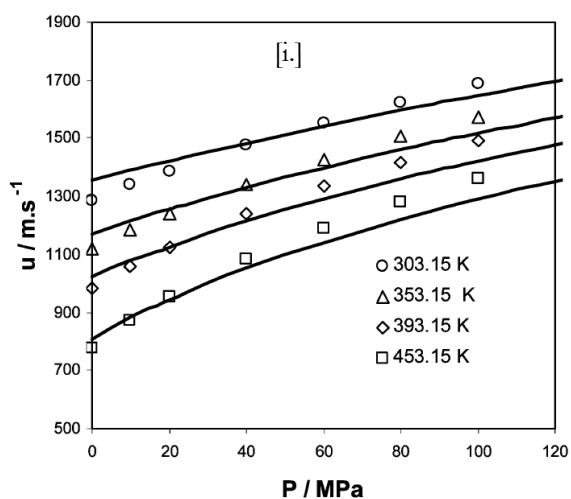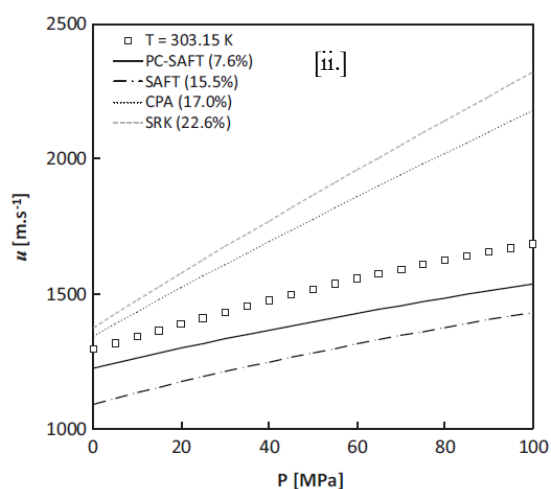
Figure 6.2: Predictions for the speed of sound through 1-hexanol at 303.15 K using [i.] SAFT-VR Mie[3], & [ii.] SAFT_{HR}, PC-SAFT and two cubic EoSs[4].

The authors attributed the success of the model in this regard to the use of a variable repulsive term in the intermolecular potential. They further claimed that EoSs for which the repulsive range was fixed, like PC-SAFT, were unable to match the accuracy of the prediction of these second derivative properties (Lafitte *et al.,* 2007). This claim was supported by the work of de Villiers *et al.,* (2013), who showed that, using sPC-SAFT, good correlation of second derivative properties was not possible while maintaining the quality of phase equilibria predictions. Indeed, in the case of pressure-volume derivative properties like speed of sound, a good fit of experimental data was not possible under any conditions (Figure 6.2 [ii.]), suggesting the terms of the sPC-SAFT EoS could not accurately describe the physical interactions governing these properties.

[3] [i.] Reprinted (adapted) with permission from T. Lafitte, M. M. Piñeiro, J. Daridon & D. Bessières, "A Comprehensive Description of Chemical Association Effects on Second Derivative Properties of Alcohols through a SAFT-VR Approach", Journal of Physical Chemistry B, 2007, 111(13), pg 3447-3461. Copyright 2007 American Chemical Society.

[4] [ii.] Reprinted from Fluid Phase Equilibria, 338, A. J. de Villiers, C. E. Schwarz, A. J. Burger & G. M. Kontogeorgis, "Evaluation of the PC-SAFT, SAFT and CPA equations of state in predicting derivative properties of selected nonpolar and hydrogen-bonding compounds", 1-15, Copyright 2013, with permission from Elsevier.

6.2   Current SAFT-VR Mie

Lafitte *et al.* (2013) later further modified the SAFT-VR Mie EoS to consider a third order expansion in the residual Helmholtz free energy and a second order expansion in the molecular structure. Including these higher order terms in the Barker & Henderson perturbation theory has allowed even better correlation of real fluid properties, without introducing more component specific parameters than in the previous manifestation. Application of the refined EoS has not been limited to the aforementioned phase equilibria and derivative properties, but includes accurate description of the supercritical region (Lafitte *et al.*, 2013). Such a description has previously been considered beyond the capabilities of an EoS type thermodynamic model without employing a cross-over treatment (Tan *et al.* 2008), but highlights the strength and potential of this new SAFT variant.

The apparent holistic predictive strength of this most recent SAFT-VR Mie EoS suggests that it is a promising fundamental model moving forward. To date, application of the refined EoS to real components has largely been limited to n-alkanes as well as smaller chain alcohols, fluoroalkanes, carbon dioxide and water (Lafitte *et al.* 2013; Dufal *et al., 2015*). Application to mixture data has been even more limited, with a focus on industrially relevant reservoir fluid and carbon capture mixtures (Dufal, 2013). In fact, recent work by the originators of SAFT-VR Mie suggest its inception may have been originally envisioned as a starting point for the group contribution type γ-SAFT EoS (Papaioannou *et al.*, 2011; Papaioannou *et al.*, 2014) as much of their subsequent work has been focused on this model framework.

6.3   Accounting for Polarity with SAFT-VR

According to the most recent review of progress made in the SAFT literature, Tan *et al.,* (2008) highlight the fact that most research into accounting for polar interactions has been made in the PC-SAFT formalism. Only a select few attempts at accounting for polar interactions have been made using the SAFT-VR EoS as a basis.

The only attempt to account for dipolar interactions explicitly using SAFT-VR is in the work of Zhao & McCabe (2006) and Zhao *et al.* (2007). Rather than considering an additional dipolar term in the residual Helmholtz free energy expansion, the SAFT-VR+D EoS attempts to account for dipolar interactions implicitly through their influence on molecular structure. Specifically, the dipolar segments are considered part of the reference fluid, appropriately accounted for in the monomer term, and the radial distribution function of these dipolar segments is considered in the chain term. In this way, the influence of the dipolar segments on their nonpolar neighbours and next-nearest neighbours is accounted for. The theory further distinguishes both the orientation of specific dipoles as well as their location in the chain (Zhao & McCabe, 2006), features unaccounted for in PC-SAFT$_{JC}$ and PC-SAFT$_{GV}$.

While the SAFT-VR+D EoS showed good results when compared to molecular simulations data of dipolar associating and non-associating fluids, application to the properties of real fluids and their mixtures was limited to the vapour pressure and saturated liquid density of water (Zhao *et al.,* 2007). Due to the lack of further published results, the ability of SAFT-VR+D, or any SAFT-VR EoS where dipolar interactions are explicitly accounted for, to predict the properties of polar organics and their mixtures, remains untested. Whether it is thus far assumed that dipolar interactions can be assimilated into the potential range parameter (λ) in SAFT-VR's standard form is unclear. However, having improved the predictive capacity of nonpolar SAFT$_{HR}$ and PC-SAFT, it is reasonable to assume that explicitly accounting for polar interactions could result in a similar improvement in SAFT-VR.

6.4 Opportunities

The model in its most recent incarnation (Laffitte *et al.*, 2013) can be considered still to be in its infancy compared to the well-developed frameworks of PC-SAFT and sPC-SAFT considered previously. To date, no attempt has been made to explicitly account for polar interactions using SAFT-VR Mie as the model framework. This provides a unique opportunity to take the model in a direction in which it has yet to see application; the prediction of thermodynamic properties of polar components and their mixtures.

Chapter 7:   DEVELOPMENT OF POLAR SAFT-VR MIE

The unique opportunity to expand the existing application of SAFT-VR Mie to the properties of real polar components and their mixtures provides the basis and rationale behind the work done in this chapter. To this end, the approach taken to account for the polar interactions is initially discussed, followed by a renewed analysis of the regression procedure alternatives in a SAFT-VR Mie framework. Successfully regressed parameter sets are then applied to thermodynamic properties of pure component as well as their mixtures where the suitability and applicability of polar SAFT-VR Mie will be assessed.

7.1   The Question of Accounting for Polarity

Whether it is necessary to explicitly account for polar interactions as distinct from their dispersion counterparts has been a central thread in the work presented here. This is a common theme in the thermodynamic modelling and SAFT literature as well. Use of advanced mixing rules have shown to yield adequate results for traditional EoSs (Dahl & Michelsen 1990, Kontogeorgis & Folas 2010) while assuming pseudo-self-association of polar components has shown similar results for SAFT-type models (von Solms *et al.*, 2004).

In Chapter 5, the three pure component parameters of nonpolar sPC-SAFT have already been shown to be unable to account for the differences between polar and dispersion forces. In order to maintain physical realism, this necessitated the incorporation of explicit polar terms. This question takes on added significance in the SAFT-VR Mie framework due to the way in which the ranges of intermolecular forces are treated in this model.

7.1.1   Is There Need for a Polar Term?

The use of the Mie potential introduces the possibility of an additional two pure component parameters in the form of the attractive and repulsive range exponents, *viz.* λ_a and λ_r respectively. The previous chapter highlighted that fixing the value of λ_a to a value of *6* has physical significance related to the range of the London dispersion forces common to all molecules. It is the adjustable value of λ_r that is frequently cited as being responsible for the model's superiority in accounting for a wider range of properties than other variants. The poignant question here is thus whether this variable repulsive range can, and should be allowed to, account for dipolar interactions.

A crude mathematical argument would say that, given that the addition of a fourth (polar) parameter to sPC-SAFT allowed for accurate description of polar components, then the fourth parameter of SAFT-VR Mie should facilitate similar capability. The physical significance of these models and their

parameters is what elevates this above a simple mathematical argument however, and adherence of the parameters to physically meaningful values is of paramount importance in the SAFT framework. In light of this physical emphasis, expecting the repulsive range parameter to account for dipolar interactions immediately raises a red flag: dipolar interactions by their nature are *attractive* forces. Thus relying exclusively on a variable *repulsive* range parameter to account for these additional forces is physically flawed.

A physically sound alternative may be to allow the dipolar interactions to be accounted for through a variable *attractive* range parameter, λ_a. To this end, a particularly significant result is the work of Dufal *et al.*, (2015) who assessed different parameter sets considering λ_a as either adjustable or fixed for nonpolar components. Leaving λ_a adjustable often yielded better correlation of component properties, but the resulting values of λ_a were frequently at odds with the physical understanding of the quantity. As a result, those parameter sets based on the London *dispersion* attractive range (*viz*. $\lambda_a = 6$) were favoured. Thus, allowing SAFT-VR Mie to regress physically dubious parameter values to account for polar interactions does not adhere to the emphasis placed on physical significance in the SAFT framework. Nonpolar sPC-SAFT artificially exaggerates values of the dispersion energy parameter to accommodate the fundamentally different polar forces. In the same way, allowing λ_a to vary from its London force value would be tantamount to lumping dispersion and polar forces together, erroneously suggesting the nature of these forces is the same.

In light of these considerations, it was decided to maintain the physical significance of a constant ($\lambda_a = 6$) attractive range in the polar SAFT-VR Mie framework presented here. Polar interactions will be treated separately, as befits their fundamentally different nature, through the incorporation of a polar specific term as in the case of previous SAFT variants:

$$\frac{A^r}{NkT} = \frac{A^{seg}}{NkT} + \frac{A^{disp}}{NkT} + \frac{A^{chain}}{NkT} + \frac{A^{polar}}{NkT} \qquad 7.1$$

7.1.2   Polar Terms for SAFT-VR Mie

In lieu of a SAFT-VR Mie specific polar term, it is necessary to assess whether existing polar terms can be used within the refined SAFT-VR Mie framework. The Jog & Chapman and Gross & Vrabec polar terms have been the focus of the modelling exercise in this work thus far and present logical starting points for this consideration. Whether these terms can be assimilated into SAFT-VR Mie is a question of compatibility of the reference fluids and intermolecular potentials.

The common thread in many SAFT variants, including PC-SAFT, sPC-SAFT and SAFT-VR Mie, is the thermodynamic perturbation theory (TPT) treatment of a chain reference fluid comprised of tangentially bonded spheres. Thus incorporation of terms into the SAFT framework necessitates similar treatment of the reference fluid. The GV term was developed on the basis of a two-centre Lennard-Jones fluid rather than a tangent-sphere model, but Gross & Vrabec (2006) formulated correlations for

successfully applying the model results to such fluids. This facilitated the term's successful incorporation into the PC-SAFT and sPC-SAFT models. Development of the JC term on the other hand, employed an identical reference fluid geometry of tangent-sphere chains (Jog & Chapman, 1999) and was readily applicable to the SAFT$_{HR}$ framework for which it was developed. In this way, the physical representation of the molecules was maintained when considering additional terms.

The question of intermolecular potential is a little more nuanced as this is frequently the basis for distinguishing SAFT variants and terms in the first place. This is particularly true of the SAFT-VR Mie model, where the variable description of the potential is at the core of the model's development. Thus, whether polar terms rooted in a given intermolecular potential can be employed within a model framework based on a different potential function is of particular significance here. The JC term was developed based on a simple hard sphere potential, but was successfully employed in the SAFT$_{HR}$ framework which used a square well potential (Jog *et al.,* 2001). The same is true of the GV term, where the Lennard-Jones based polar term is seamlessly incorporated into the modified square well PC-SAFT framework (Gross & Vrabec, 2006). Indeed, extension of the JC term to the PC-SAFT (Tumakaka *et al.*, 2004) and sPC-SAFT (de Villiers *et al.* 2011) frameworks without appreciable difference in predictive capacity supports this argument and serves to allay concerns over the mixing of terms based on different pair potentials.

In light of these considerations, there appears to be no reason why the JC and GV terms shouldn't fit seamlessly into a polar SAFT-VR Mie framework. The modular nature of terms within the SAFT family facilitates the unique opportunity to improve parent models with previously developed and well tested terms. Use is made of this opportunity to propose the following polar SAFT-VR Mie models:

- SAFT-VR Mie with the Jog & Chapman polar term (SAFT-VR Mie[JC]); and
- SAFT-VR Mie with the Gross & Vrabec polar term (SAFT-VR Mie[GV]).

Given the lack of previous applications of the base nonpolar SAFT-VR Mie model to polar components, nonpolar SAFT-VR Mie is considered in addition to these two polar models. This serves to test the predictive capacity of the nonpolar variant in a novel environment, but also allows for the assessment of the difference made by the explicit inclusion of polar terms in SAFT-VR Mie[JC] and SAFT-VR Mie[GV]. These three models provide the basis of the extensive thermodynamic modelling procedure presented in the remainder of this chapter.

7.2   Determining Polar SAFT-VR Mie Parameters

With the means by which dipolar interactions will be accounted for in the newly defined polar SAFT-VR Mie framework, attention turns to the determination of pure component parameters. As with the sPC-SAFT framework, the accurate description of pure component properties is a necessary and significant starting point.

7.2.1   Choice of Pure Component Properties

The line of thought followed in the similarly-named section in Chapter 5 is applicable for determining the appropriate choice of pure component properties to be considered in regressing polar SAFT-VR Mie parameters. Addressing this issue using the already discussed case for sPC-SAFT as both reference and juxtaposition provides a suitable starting point. In the case of sPC-SAFT, a trade-off in predictive capacity between phase equilibria and derivative properties was apparent: *either* phase equilibrium *or* derivative properties could be accurately described, but not both using a single parameter set. As a result, the best combination of properties for determining the optimum parameter set in sPC-SAFT for application to phase equilibria was found to be that which omitted derivative properties in their entirety, *viz.* saturated vapour pressure, saturated liquid density, and heat of vaporisation. The resulting parameters were shown to be capable of producing accurate predictions of phase equilibria. Given the success of this combination of properties in regressing accurate sPC-SAFT parameter sets, it stands to reason that the same combination should yield similar results when applied to SAFT-VR Mie.

The proven superiority of SAFT-VR Mie however, is in its ability to simultaneously and accurately predict *both* phase equilibrium and derivative properties using a single parameter set. Thus a revaluation of the choice of pure component properties is warranted. The good holistic predictions reported for SAFT-VR Mie suggest that the inclusion of derivative properties in the regression procedure would augment the predictive capacity of the model, rather than hinder it as was the case with sPC-SAFT. In the original SAFT-VR Mie formulation, Lafitte *et al.* (2006) argued that the optimum parameter set was obtained with the inclusion of compressed liquid density (ρ^{liq}) and speed of sound (u^{liq}) data, over and above the standard saturated vapour pressure and liquid density. Considering the interconnectivity of thermodynamic properties using the residual Helmholtz free energy, reintroduced in Figure 7.1, illustrates the merit in this argument.
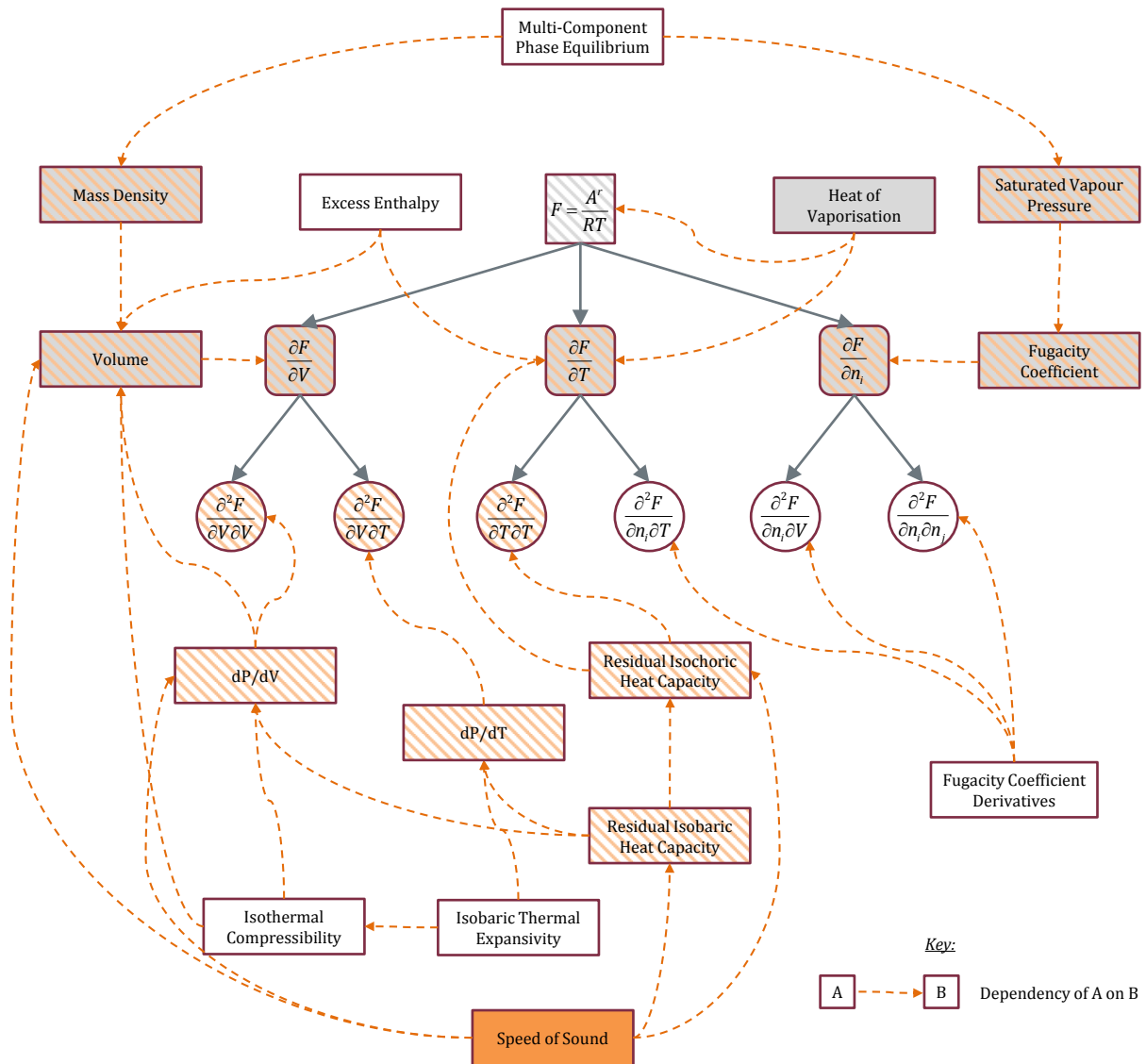
Figure 7.1: Schematic representation of the interconnectivity of thermodynamic properties using the residual Helmholtz energy as a reference point. Figure redrawn and adapted from de Villiers (2011)

The argument for including speed of sound is particularly poignant: equation 7.2 shows that u^{liq} is explicitly dependent on the *dP/dV* derivative as well as the isochoric (C_V) and isobaric (C_P) heat capacities. These properties are themselves derivative properties of physical significance and are of practical interest. This means that accurately accounting for these properties is not only necessary for describing u^{liq}, but is a priority in its own right, given the holistic approach adopted with SAFT-VR Mie. Following the arrows and orange-shaded properties stemming from *Speed of Sound* in Figure 7.1, we can see that this dependency can be traced all the way to the second derivatives of *F* in temperature and volume.

$$u^{liq} = \sqrt{-\frac{V^2}{M_w}\frac{C_P}{C_V}\left(\frac{\partial P}{\partial V}\right)_{T,n}}$$

7.2

A similar analysis of the grey shaded properties stemming from *Heat of Vaporisation* shows that incorporating this property over speed of sound yields only explicit dependence on A^r and its temperature

derivative, the latter of which is already tested by including u^{liq}. Similarly, since both regression procedures incorporate P^{sat} and ρ^{sat}, those properties that are accounted for through dependencies by both property inclusion alternatives are shaded with both colours. Tracing these dependencies illustrate that the incorporation of speed of sound in the regression procedure inherently allows for testing of a wider range of thermodynamic derivatives without the need to include these properties in the regression explicitly. This quality is clearly lacking for the case of including H^{vap} and it is thus expected that parameter sets determined through inclusion of u^{liq} will produce more balanced predictions than those determined by including H^{vap}.

7.2.2   The Role of Speed of Sound

The intrinsic link between phase equilibrium and P^{sat}, ρ^{sat} and even H^{vap} means that research of the former goes hand-in-hand with generating experimental data for the latter. Combined with the industrial significance of distillation in the modern era, this has resulted in the plethora of available experimental phase equilibrium-related data for both pure components and mixtures. Unlike distillation and phase equilibrium however, the interest in acoustic speeds in fluids and their mixtures is a relatively new endeavour with far more limited industrial application. As a result, available experimental data is not as abundant for u^{liq}, nor do there exist the extensive databases of measurements and correlations that are available for saturation properties; the DIPPR database for example does not contain any speed of sound data. Thus while the inclusion of pure component speed of sound data in the regression of SAFT-VR Mie parameters promises to yield balanced predictions of thermodynamic properties, a potential stumbling point is the nature of the property itself.

7.2.2.1   The Identified Problem

The source of pure component speed of sound data used by Lafitte *et al.* (2013) for the determination of SAFT-VR Mie parameters for the real components considered in that work was the NIST Standard Reference Database Number 69 (Linstrom & Mallard, 2016). Consultation of this database showed that, while there are indeed data available for the components of interest in Lafitte *et al.*'s study, the component database is severely limited and devoid of data for even a single ketone, ester or ether. This is not meant as an indictment of the database, but rather serves to highlight the difficulty of finding pure component speed of sound data. To this end, use of NIST's ThermoLit report builder (Kroenlein *et al.,* 2016) proved invaluable in the compilation of Table 7.1, which summarises the pure component speed of sound data available in the literature for polar components of interest to this study.

Table 7.1: Summary of available pure component speed of sound data for ketones, esters and ethers of interest in this study. Listed data sources necessarily included more than a single datum point.

Component	Property Specification	Range	No. of Data Points	Reference
Ketones				
acetone	Isothermal		28	Azevedo *et al.*, (2004)
2-butanone	Isobaric	(293.15-323.15)K	7	Varfolomeev *et al.* (2014)
	Isobaric	(293.15-303.15)K	3	Cobos *et al.* (2016)
2-pentanone	Isobaric	(293.15-303.15)K	3	Cobos *et al.* (2016)
2-heptanone	Isobaric	(293.15-303.15)K	3	González*et al.* (2011)
	Isobaric	(293.15-303.15)K	3	Cobos *et al.* (2016)
Esters				
methyl acetate	Isobaric	(288.15-308.15)K	5	Pal *et al.* (2013)
ethyl formate	Isobaric	(298.15-313.15)K	4	Rathnam *et al.* (2010)
methyl propanoate	Isobaric	(308.15-318.15)K	2	Sastry *et al.* (1999)
	Isobaric	(298.15-308.15)K	2	Sastry *et al.* (2013)
ethyl acetate	Isobaric	(288.15-308.15)K	5	Pal *et al.* (2013)
methyl butanoate	Isobaric	(308.15-318.15)K	2	Sastry *et al.* (1999)
ethyl propanoate	Isobaric	(308.15-318.15)K	2	Sastry *et al.* (1999)
	Isobaric	(298.15-308.15)K	3	Oswal *et al.* (2004)
	Isobaric	(298.15-308.15)K	2	Sastry *et al.* (2013)
propyl acetate	Isobaric	(298.15-313.15)K	4	Patwari *et al.* (2009)
ethyl butanoate	Isobaric	(293.15-343.15)K	11	Freitas *et al.* (2013)
butyl acetate	Isobaric	(288.15-308.15)K	5	Pal *et al.* (2013)
Ethers				
diisopropyl ether	Isobaric	(279.15-323.15)K	23	Gonzalez-Olmos *et al.* (2008)
ethyl *tert*-butyl ether	Isobaric	(279.15-323.15)K	23	Gonzalez-Olmos *et al.* (2008)
tert-amyl methyl ether	Isobaric	(279.15-323.15)K	23	Gonzalez-Olmos *et al.* (2008)

Table 7.1 demonstrates that there is not only a lack of published speed of sound data available in the literature for polar components, but also that data sets which have been generated typically only have *2* to *3* data points each. The reason for this is that the focus of the published data is generally towards mixture behaviour at varying conditions, with the pure component property happening to fall in this spectrum. Of particular significance to this study is the lack of data for all structural isomers of any given sized functional group. For the considered ketones, only data for 2-heptanone are available; for the C_6 esters there is data for ethyl butanoate and butyl acetate, while for the ethers, no data set comprising more than a single point has been published for linear ethers at all. The viability of incorporating speed of sound data into the regression of polar SAFT-VR Mie parameter sets is thus clearly in question.

7.2.2.2   The Proposed Solution

An analysis of that data which are available may yield an improvised solution to the problem posed by a lack of data for all isomers. Table 7.1 shows that published pure component speed of sound data are available for three C_5 ester isomers as well as two C_6 esters. These cases provide the best context for this discussion and thus these data sets are presented in Figures 7.2 [i.] and [ii.] respectively. The

notable similarity in the magnitude of u^{liq} for each isomer in both figures leads to the following provisional proposal:

For those components where no pure component speed of sound data are available, available data for isomers of that component may be used in the regression of SAFT-VR Mie parameters.

Justification of this proposed solution starts with consideration of Figures 7.2 [i.], which shows that the largest relative difference between the three C_5 linear esters considered is *3%,* and that data for each component follow a similar trend with temperature. Lafitte *et al.* (2006) demonstrated that typical deviations in speed of sound predictions for models other than SAFT-VR Mie are of the order of *10%*. In a later work, Lafitte *et al.* (2013) present SAFT-VR Mie parameter sets with deviations in u^{liq} of *ca. 3%*, where note is made of the "very small overall deviation" for speed of sound and other second derivative thermodynamic properties. In light of this, a *3%* variation between u^{liq} of different isomers can be considered small, as it is of the same order of magnitude as the expected deviation of a good thermodynamic prediction. A flaw in this consideration however is the small number of data points in these data sets, as well as the small range of physical (*viz. T & P*) conditions for which these measurements were made.
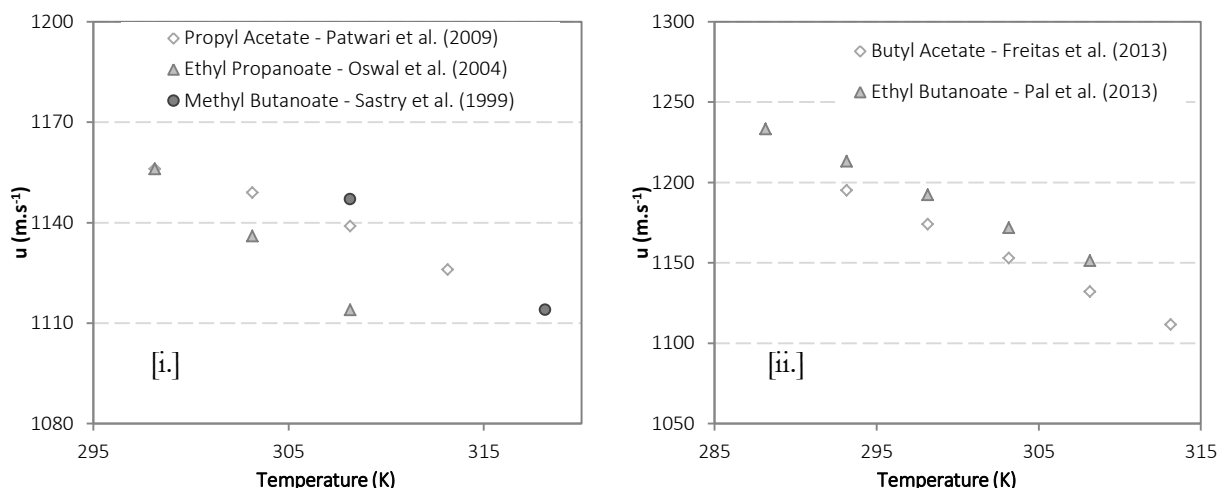
Figure 7.2: Available pure component speed of sound data for [i.] three structural isomers of C_5 ester, and [ii.] two isomers of C_6 ester. Small relative differences between isomers and apparent adherence to same trend are highlighted.

These points are addressed by considering the data for ethyl butanoate and butyl acetate in Figures 7.2 [ii.]. Data for these components, exhibiting similarly small relative differences, were tested over larger temperature ranges than for the C_5 esters and visibly follow the same trend over this increased range. This serves to alleviate concern over markedly different behaviour for different isomers at the same conditions, even if question marks remain over the extent of data measurement for any one component.

A similar analysis cannot be made for either ketones or the linear ethers of interest to this study as data are simply not available for more than a single given isomer. Table 7.1 does however indicate that extensive data are available for branched C_6 ethers, which can be used for testing the proposed solution. The speed of sound data of diisopropyl ether, ethyl *tert*-butyl ether and *tert*-amyl methyl ether are plotted in

Figure 7.3. While it is reassuring to see that the data for all three isomers follow the same trend over the extended range of temperature considered, it is also clear that the relative differences between the components is well in excess of the aforementioned *3%*. These significantly larger differences between the pure component properties throw doubt over the viability of the proposed solution.
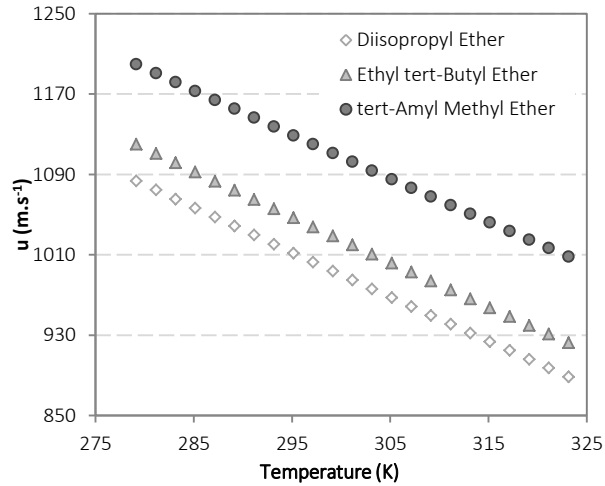
Figure 7.3: Pure component speed of sound data available for three branched C_6 ether structural isomers. The noticeably larger relative differences in the property between branched isomers are highlighted. Experimental data is that of Gonzalez-Olmos et al. (2008).

In order to address this concern, it is necessary to start by reconsidering the thermodynamic description of speed of sound in equation 7.2, which shows that u^{liq} is strongly dependent on the system volume, or more specifically its density. This suggests that fluids of similar densities should exhibit similar values of speed of sound, and that as the densities converge, so too should u^{liq}. Figure 7.4 [i.] shows that the densities of the five linear C_6 esters considered throughout this study are practically identical over the full range of temperature of practical interest. Combined with the small differences in u^{liq} for ethyl butanoate and butyl acetate presented in Figure 7.2 [ii.], this line of thought is evidently supported.
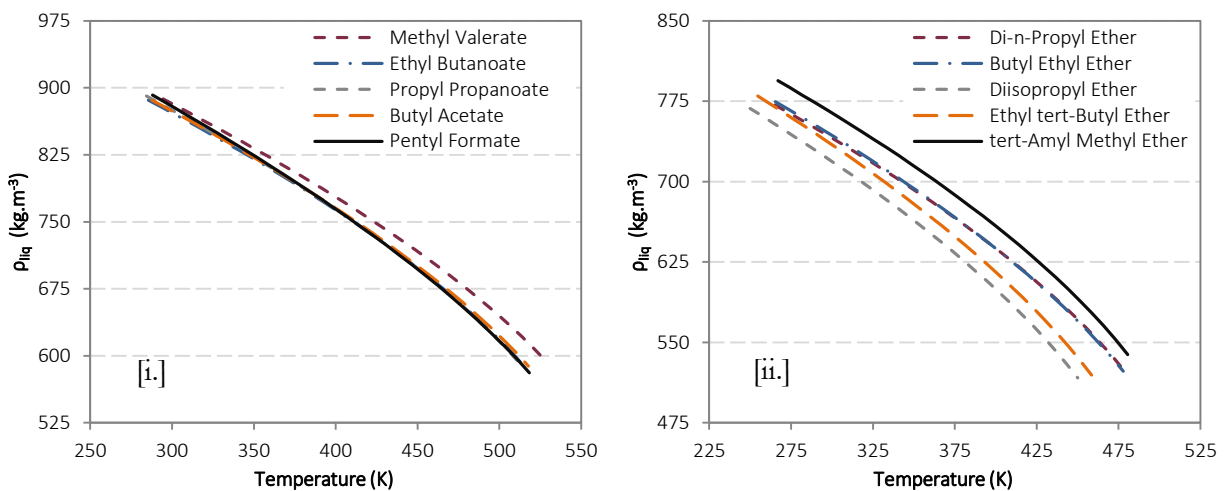
Figure 7.4: Pure component saturated liquid densities for [i.] the five C_6 linear ester isomers and [ii.] two linear (di-n-propyl ether & butyl ethyl ether) with three of their branched isomers. Combined with previous figures, these plots illustrate the strong link between u^{liq} and ρ^{liq}. Curves are correlations taken from DIPPR.

Comparing the density trends in Figure 7.4 [ii.] with the u^{liq} trends in Figure 7.3 show that almost identical differences between the respective properties of the isomers are apparent and also helps explain the differences in u^{liq} for the branched isomers. The addition of side alkyl groups serve to significantly alter the nature of the intermolecular forces in these isomers due to the more prominent role played by steric hindrance. These differences manifest themselves in the significantly altered physical properties of these isomers compared to each other, and when compared to the two linear isomers. As with the linear esters in Figure 7.4 [i.], the density correlations of di-n-propyl ether and butyl ethyl ether lie on top of one another and thus suggest that similar values of u^{liq} would result.

The arguments presented here serve to validate the proposed solution to the problem of lack of speed of sound data. In order to reflect the results of Figures 7.2 to 7.4, the following small adjustment is made to the original proposal:

*For those **linear** components where no pure component speed of sound data are available,*
*available data for **linear** isomers of that component may be used in the regression of SAFT-VR*
Mie parameters.

If the amount of published speed of sound data follows its current upward trend, use of this improvisation may and necessarily will be negated. In light of what data is currently available however, successful determination of SAFT-VR Mie parameter sets using speed of sound as a regressed property necessitates an improvised solution. This proposal will form the basis for the determination of polar SAFT-VR Mie parameter sets for polar components using speed of sound data. The success of these parameter sets will be assessed in order to verify this proposal in subsequent sections.

7.2.3   Addressing Potential Regression Challenges

Given the fairly recent publication of the revised SAFT-VR Mie equation of state, the amount of published work reporting SAFT-VR Mie parameters, or the regression challenges facing this EoS have been limited. Further, given that the new SAFT-VR Mie[JC] and SAFT-VR Mie[GV] polar models are proposed here for the first time, no previous attempts in dealing with this parameter space have been reported.

Considering the base nonpolar variant, recent work by Dufal *et al.* (2015) demonstrated that familiar problems of parameter degeneracy and multiple local minima in the objective function are present when regressing SAFT-VR Mie parameters. A particularly interesting approach was taken in addressing the problem of multiple local minima in this work, by projecting the contours of the objective function onto different α-β planes. Here, α and β correspond to each of the five nonpolar SAFT-VR Mie parameters and each such plane provides an analysis of the objective function for discrete values of α and β. These contour plots provided visual confirmation of the existence of multiple local minima, particularly for the case where all parameters were considered adjustable.

Dufal *et al.* (2015) demonstrated that using physical considerations to fix the values of different parameters mitigated the problem of multiple minima, removing them in some cases while confining them to physically unrealistic α-β combinations in others. The problem was not completely removed however, and different parameter sets exhibiting a sliding bias to different considered properties were still presented. These results emphasised the need to choose appropriate pure component data and to attach appropriate regression weights to these different properties.

7.2.4   Selected Regression Methods

Given the novelty of a polar SAFT-VR Mie framework, it is necessary to generate a collection of parameter sets for different homologous groups, which will constitute a solid core for the model moving forward. In light of the work done here, the initial homologous groups of interest will be linear ketones, esters and ethers. To this end, it is desirable to generate parameters starting with the smallest component of each functional group and systematically work up to longer chain molecules, considering all relevant structural isomers.

As has already been discussed, the value of the attractive range parameter, λ_a, is fixed to the London dispersion value of *6* for all components. The value of the remaining four nonpolar parameters (σ, m, ε/k and λ_r) will be left adjustable in the regression procedure for all cases. For the SAFT-VR Mie[JC] and SAFT-VR Mie[GV] models, the value of the polar parameters (x_p/n_p) is kept adjustable to allow for a fair comparison of the terms, as was done for sPC-SAFT. The case for fixing n_p equal to *1* as per the original term is also considered to provide a comparison with the regressed n_p case.

Use was made of available pure component speed of sound data tabulated in Table 7.1 and employing the improvised solution above for components whose isomers have available data. In this way, polar SAFT-VR Mie parameters can be regressed for a number of polar components, using the following properties, with weightings in parentheses, as suggested by Lafitte *et al.* (2013):

- saturated vapour pressures, P^{sat}, (4),
- saturated liquid densities, ρ^{sat}, (4), and
- speed of sound, u^{liq}, (1).

The problem however, is that for some components (e.g. methyl formate and the linear ethers) u^{liq} data are not available for either the component or its isomers. Thus, an alternative combination of pure component properties needs to be considered. To this end, the same property combination as was employed for polar sPC-SAFT will be considered for polar SAFT-VR Mie, *viz*:

- saturated vapour pressures, P^{sat}, (4),
- saturated liquid densities, ρ^{sat}, (2), and
- heats of vaporisation, H^{vap}, (1).

This regression alternative will also provide a comparison of the performance of those regressed parameter sets incorporating speed of sound with those that do not.

Incorporating mixture VLE data in the regression procedure proved to be a viable means of mitigating the problem of parameter degeneracy in the polar sPC-SAFT framework. It also facilitated the generation of the empirical correlations of equations 5.2 and 5.3 to fix the values of x_p and n_p and allow accurate parameter generation in lieu of experimental data. The success of these alternatives in improving the predictive capacity of the polar sPC-SAFT models advocates that similar procedures should be considered for SAFT-VR Mie[JC] and SAFT-VR Mie[GV]. Application of these alternatives require determination of parameter sets using mixture VLE data before the SAFT-VR Mie equivalents of the homologous group constants can be determined. Thereafter, the predictive capacity of parameter sets determined using these correlations can be assessed.

The approach adopted to the regression of SAFT-VR Mie, SAFT-VR Mie[JC] and SAFT-VR Mie[GV] parameters for polar components is summarised in Figure 7.5.
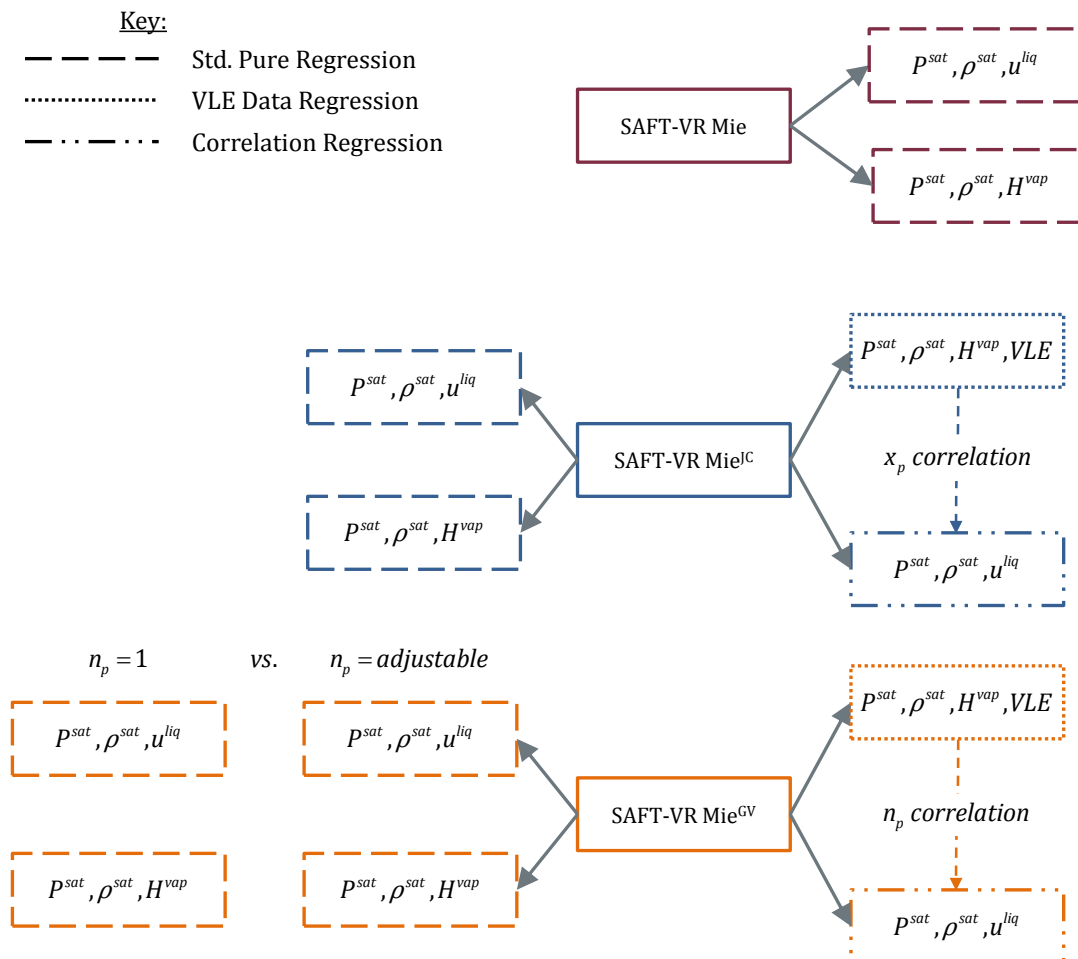
Figure 7.5: Schematic representation of the approach adopted to the regression of polar SAFT-VR Mie parameters illustrating the three models and the different regression procedures appropriate to each case.

Regression of component parameters following the outline of Figure 7.5 yields up to *12* parameter sets for each component considered. The regression procedures will be assessed according to the predictive capacity of their parameter sets when tested against thermodynamic and phase equilibrium properties of pure components and their mixtures. This is the goal of the sections that follow.

7.3 Validation of Coded SAFT-VR Mie

Before parameters can be regressed for polar components within the new polar SAFT-VR Mie framework and the predictive capacity of this model can be tested, it is necessary to validate the coding of the SAFT-VR Mie EoS to corroborate modelling results presented in this chapter.

Thermodynamic modelling using SAFT type EoSs is conducted by means of the in-house developed software, *TRSolutions*. The software was originally written by A.J. de Villiers to conduct predominantly sPC-SAFT focused research and had this functionality coded and validated already. In order to conduct the SAFT-VR Mie focused modelling suggested here, it was necessary to first code the EoS and its derivatives in order to add them to the *TRSolutions* framework. Thus, starting with the model framework presented by Lafitte *et al.* (2013), the appropriate thermodynamic derivatives were determined in analytical form (the working equations are presented in Appendix G) and added to the software.

The additional code requires validation, which is achieved by:

i.   *Numerical Differentiation*
        Appropriate numerical differentiation of each term can be used to compare with the coded analytical derivative. This allows for any error in the analytical differentiation of the EoS terms to be identified and fixed as they arise.

ii.   *Reproducing Published Predictions*
        Using parameter sets published by Lafitte *et al.*, (2013) and Dufal *et al.,* (2015) to predict pure component properties allows for direct comparison of published predictions with literature data and deviations reported by these authors; and

iii.   *Regression of Published Parameters*
        Regressing parameters for the same components for which Lafitte *et al.*, (2013) and Dufal *et al.,* (2015) published parameters allow for validation of the regression engine in the software, the goal of which is to determine significantly similar parameter sets.

The numerical differentiation validation was written into each unit of the code, each of which was checked via a step-through procedure of the program. Deviations between the analytical and numerical derivatives indicated an erroneously-coded analytical derivative function, which was amended immediately. To this end, all coded functions were verified by this numerical differentiation procedure and modelling results presented here are mathematically correct. Details of this numerical differentiation are provided in Appendix H.

Development of Polar SAFT-VR Mie

Validation of the model predictions was performed by considering the three n-alkanes of particular interest to this study, *viz.* n-heptane, n-octane and n-nonane. The parameter sets published by Lafitte *et al.* (2013) and those of Dufal *et al.* (2015) were used to generate the same pure component predictions as were reported in those works. The results of these comparisons are provided in Table 7.2, where the AADs of the predictions generated using *TRSolutions* are listed, followed by the values reported by the original authors in parentheses. It is clear that all generated predictions yield deviations of the same order of magnitude as those reported by the original authors. It should be noted that different sources were used for these properties (DIPPR vs. NIST) which should account for the small discrepancies between the values. Also, where Lafitte *et al.* (2013) and Dufal *et al.* (2015) considered u^{liq} data over a surface of temperatures and pressures, only those of the saturated liquid were considered here. The comparison is adequate however as these saturation values fall within the T and P ranges considered by those authors.

Table 7.2: Comparison of parameter sets regressed in this work and those of Lafitte et al. (2013) and Dufal et al., (2015) for the n-alkanes of interest in this study. Deviations obtained in this work, through use of the indicated published parameters, are compared to those reported in parentheses.

	σ	m	ε/k	λ_a	λ_r	$P^{sat *}$	ρ^{sat*}	$u^{sat} \dagger$	H^{vap*}
	Å		K			AAD%	AAD%	AAD%	AAD%
n-Heptane									
Lafitte *et al.* (2013)	4.4282	2.3949	358.510	6	17.0920	0.886 (0.91)	0.489 (0.45)	0.922 (0.67)	2.186 (1.79)
Dufal *et al.* (2015	4.5427	2.2413	381.420	6	18.2520	0.462 (0.27)	0.109 (0.19)	0.339 (0.92)	2.015 (1.65)
Regressed	4.4811	2.3185	369.295	6	17.5886	0.230	0.086	0.526	2.191
n-Octane									
Lafitte *et al.* (2013)	4.4696	2.6253	369.180	6	17.3780	0.983 (0.96)	0.683 (.052)	0.488 (0.75)	1.651 (.158)
Dufal *et al.* (2015	4.5708	2.4777	391.870	6	18.6540	0.386 (0.29)	0.139 (0.36)	1.954 (1.79)	1.705 (1.59)
Regressed	4.4816	2.5944	370.997	6	17.2990	0.347	0.100	0.432	1.716
n-Nonane									
Lafitte *et al.* (2013)	4.5334	2.8099	387.550	6	18.3240	0.758 (0.82)	0.549 (0.60)	1.640 (0.45)	1.398 (1.60)
Dufal *et al.* (2015	4.6236	2.6665	404.830	6	19.1160	0.587 (0.34)	0.140 (0.41)	0.753 (0.60)	1.280 (1.48)
Regressed	4.5672	2.7490	394.826	6	18.6445	0.448	0.117	1.137	1.427

† u^{liq} deviations reported by Lafitte *et al.* & Dufal *et al.* for compressed liquid; presented here for the saturated liquid
* AADs based on DIPPR Correlations;
† AADs based on NIST Data

The same three components were considered for validating the regression procedure, where the P^{sat}- ρ^{sat}- u^{liq} property combination was selected to mirror the procedures followed by Lafitte *et al.* (2013) and Dufal *et al.* (2015). The results of the regression are also listed in Table 7.2 along with their respective AADs in the considered pure component properties. The regressed parameters are in consistent agreement with those previously generated, with the resulting AADs exhibiting similar agreement. Indeed, the AADs of the parameter sets regressed here are frequently the smallest of the three considered.

With the numerical, predictive and regressive validations for the base nonpolar SAFT-VR Mie case completed, focus shifts to the application of the model to polar components by incorporating the JC and GV polar terms. Verification of the SAFT-VR Mie[JC] and SAFT-VR Mie[GV] models can only be achieved by the numerical differentiation step in the validation procedure highlighted above and was performed as such. The fully validated model could now be applied to the regression of parameter sets for real polar components, the results of which are discussed in the following section.

7.4 Polar SAFT-VR Mie Parameters

The regression alternatives considered in Figure 7.5 illustrate the sheer volume of generated parameter sets resulting from the regression exercise. As a result, not every parameter set generated is reported here. Rather, regressed parameter sets that exhibit good predictive capacity are tabulated, before a detailed assessment of the regression results is provided in the proceeding section.

As was the case with the sPC-SAFT framework, the inclusion of polar component/n-alkane VLE data in the regression procedure yielded parameter sets that exhibited the best predictions for mixture phase behaviour. For this reason, these parameter sets are considered the ideal starting point for the analysis of regression results and will provide an ideal reference with which to compare the results of the other regression cases. To this end, the parameters for the SAFT-VR Mie[JC] and SAFT-VR Mie[GV] models regressed as a result of incorporating mixture VLE data in the regression procedure are tabulated in Tables 7.3 and 7.4 respectively.

It is perhaps most notable that, in Table 7.3, the value of the polar parameter is listed as zero for a number of the considered components. This is a result of the inability to successfully regress a parameter set for these components with a nonzero x_p, despite the inclusion of VLE data in the regression procedure. This was particularly prevalent amongst the considered ketones although selected instances were apparent for esters and ethers. The result was regression of a "nonpolar" parameter set for SAFT-VR Mie[JC] and the reported parameter sets for these components are thus the best fit nonpolar SAFT-VR Mie parameters for those components. This appears to be a continuation of the problem of broad minima in the objective function for the JC polar term, but will be discussed at length in subsequent sections.

The SAFT-VR Mie[GV] model exhibits no such problems, with notable polar contributions regressed for all components considered. Analysis of the parameters themselves indicate that they are well behaved and follow the expected trends with changes in molecular weight; *viz.* molecular sizes (product of σ and m) and dispersion energy increase as the molecular size increases. Trends in the value of the regressed range parameters are also noteworthy; smaller values of λ_r are in evidence for smaller components with a steady increase in the parameter value for larger molecules. This trend is similar to that reported for nonpolar components by Lafitte *et al.,* (2013) and Dufal *et al.,* (2015). This serves to further support the physical arguments behind allowing λ_r to deviate from its traditional fixed Lennard-Jones value.

Development of Polar SAFT-VR Mie

Table 7.3: SAFT-VR Mie^{JC} parameters for ketones, esters and ethers determined by regression incorporating the indicated polar/n-alkane VLE data in the regression.

	M_W g.mol^{-1}	σ Å	m	ε/k K	λ_a	λ_r	x_p	μ D	VLE Data Reference	Paired Alkane	P^{sat} * AAD%	ρ^{sat} * AAD%	u^{liq} † AAD%	H^{vap} * AAD%
Ketones														
acetone	58.08	3.8102	1.9162	258.370	6	11.0337	0.3052	2.88	Acosta *et al.* (2002)	n-hexane	1.918	2.275	5.783	3.035
2-butanone	72.11	4.0215	2.2107	258.347	6	11.2061	0.3517	2.76	Wisniak *et al.* (1998)	n-heptane	3.741	11.51	0.449	1.280
2-pentanone	86.13	4.0571	2.3194	375.912	6	16.7737	0 [b]	2.77	Geiseler *et al.* (1968)	n-heptane	0.359	0.479	7.537	3.322
3-pentanone	86.13	4.0341	2.3322	369.083	6	16.2708	0 [b]	2.82	Fuchs *et al.* (1984)	n-heptane	1.513	0.770	_[a]	3.097
2-heptanone	114.1	3.9158	3.3015	307.272	6	12.9282	0 [b]	2.61	Cripwell *et al.* (2015)	n-nonane	0.190	0.094	3.551	1.983
3-heptanone	114.1	3.9878	3.1163	290.571	6	12.4634	0.2222	2.81	Cripwell *et al.* (2015)	n-nonane	0.112	0.477	_[a]	2.330
4-heptanone	114.1	4.3051	2.6032	392.799	6	17.2198	0 [b]	2.68	Cripwell *et al.* (2015)	n-nonane	0.553	0.559	_[a]	1.440
Esters														
methyl formate	60.05	3.4037	2.1266	221.529	6	10.2165	0.4741	1.77	Ortega *et al.* (2003)	n-heptane	0.694	0.799	_[a]	2.864
ethyl formate	74.08	3.9950	1.7900	294.511	6	13.1830	0.7996	1.93	Ortega *et al.* (2015)	n-heptane	0.743	0.940	0.884	3.285
methyl acetate	74.08	3.5142	2.4784	238.061	6	10.9886	0.4665	1.68	Fernández *et al.* (2013)	n-heptane	0.691	0.134	2.436	2.232
propyl formate	88.11	3.6807	2.6705	244.235	6	10.8966	0.3847	1.91	Galván *et al.* (1994)	n-heptane	0.326	0.361	_[a]	2.197
ethyl acetate	88.11	3.7299	2.6011	263.106	6	12.2552	0.4747	1.78	Fernández *et al.* (2010)	n-heptane	0.437	0.247	2.859	2.373
methyl propanoate	88.11	3.4126	3.1969	230.184	6	10.7439	0.1997	1.70	Ortega *et al.* (2003)	n-heptane	0.486	0.987	6.355	1.809
butyl formate	102.1	4.0953	2.3897	324.482	6	14.3963	0.5131	2.02	Ortega *et al.* (2015)	n-heptane	1.375	0.204	_[a]	2.380
propyl acetate	102.1	3.7258	3.0506	257.864	6	11.8194	0.3642	1.79	Fernández *et al.* (2013)	n-heptane	0.442	0.380	6.047	2.968
ethyl propanoate	102.1	3.9842	2.5737	306.267	6	14.1383	0.5589	1.75	Ríos *et al.* (2014)	n-heptane	0.370	0.355	1.675	3.820
methyl butanoate	102.1	4.0057	2.5066	313.159	6	13.9857	0.5801	1.72	Ríos *et al.* (2012)	n-heptane	0.204	0.179	3.408	2.245
pentyl formate	116.2	4.1631	2.6676	323.241	6	14.0702	0.5868	1.90	This work	n-octane	0.947	1.264	_[a]	1.273
butyl acetate	116.2	4.0492	2.8374	310.894	6	14.0149	0.5105	1.84	This work	n-octane	0.636	0.216	3.398	1.408
propyl propanoate	116.2	4.0740	2.7941	360.848	6	17.2044	0 [b]	1.79	This work	n-octane	1.728	0.182	_[a]	4.345
ethyl butanoate	116.2	4.2815	2.4425	332.077	6	14.0531	0.6091	1.81	This work	n-octane	1.376	0.712	4.315	2.163
methyl valerate	116.2	4.2810	2.4602	355.743	6	15.7938	0.6939	1.62	This work	n-octane	0.923	1.420	_[a]	2.581
Ethers														
diethyl ether	74.12	3.7964	2.4531	245.859	6	12.1527	0.5461	1.15	Klon-Palczewska *et al.* (1980)	n-hexane	0.335	0.196	_[a]	1.920
di-n-propyl ether	102.18	4.1355	2.6406	302.892	6	14.0232	0.3826	1.21	This work	n-heptane	0.373	0.506	_[a]	1.183
butyl ethyl ether	102.18	4.0085	2.8776	294.033	6	14.1005	0.2023	1.22	This work	n-heptane	1.287	0.694	_[a]	7.745
dibutyl ether	130.23	4.3424	2.9612	362.723	6	17.3716	0 [b]	1.17	March *et al.,* (1980)	n-hexane	0.446	0.601	_[a]	1.582

† AADs in u^{liq} calculated with reference to corresponding pure component data sets as indicated in Table 7.1

* AADs based on DIPPR Correlations

[a] No AADs possible due to lack of published data

[b] Nonpolar SAFT-VR Mie parameters listed (*viz.* zero polar contribution) due to tendency of regression to drive x_p to zero regardless of initial guess

Table 7.4: SAFT-VR Mie^{GV} parameters for ketones, esters and ethers determined by regression incorporating the indicated polar/n-alkane VLE data in the regression.

	M_W g.mol^{-1}	σ Å	m	ε/k K	λ_a	λ_r	n_P	μ D	VLE Data Reference	Paired Alkane	P^{sat} * AAD%	ρ^{sat} * AAD%	u^{liq} † AAD%	H^{vap} * AAD%
Ketones														
acetone	58.08	3.4778	2.3593	251.047	6	12.3835	1.2389	2.88	Acosta *et al.* (2002)	n-hexane	0.127	0.248	9.413	1.195
2-butanone	72.11	3.6394	2.5585	260.956	6	12.3040	1.5638	2.76	Wisniak *et al.* (1998)	n-heptane	0.279	0.195	4.079	1.097
2-pentanone	86.13	3.8494	2.6093	297.363	6	13.8669	1.7869	2.77	Geiseler *et al.* (1968)	n-heptane	0.131	0.589	3.327	2.485
3-pentanone	86.13	3.9840	2.3771	329.238	6	16.8726	2.216	2.82	Fuchs *et al.* (1984)	n-heptane	0.541	0.885	_^{a}	1.974
2-heptanone	114.1	3.8386	3.4465	276.968	6	11.9113	1.9211	2.61	Cripwell *et al.* (2015)	n-nonane	0.359	0.564	6.006	1.663
3-heptanone	114.1	3.8101	3.4857	293.744	6	12.7967	0.6449	2.81	Cripwell *et al.* (2015)	n-nonane	0.320	0.958	_^{a}	2.176
4-heptanone	114.1	4.1391	2.7414	332.124	6	14.6402	2.1229	2.68	Cripwell *et al.* (2015)	n-nonane	0.500	0.040	_^{a}	1.048
Esters														
methyl formate	60.05	3.1162	2.6170	208.666	6	10.3869	1.9084	1.77	Ortega *et al.* (2003)	n-heptane	0.269	1.303	_^{a}	1.566
ethyl formate	74.08	3.3775	2.7158	221.984	6	10.8664	2.3195	1.93	Ortega *et al.* (2015)	n-heptane	0.312	1.395	2.285	2.140
methyl acetate	74.08	3.2320	3.0310	216.275	6	10.5774	2.2498	1.68	Fernández *et al.* (2013)	n-heptane	0.405	1.242	3.082	1.461
propyl formate	88.11	3.4336	3.1523	226.314	6	10.5945	2.1136	1.91	Galván *et al.* (1994)	n-heptane	0.457	1.529	_^{a}	1.611
ethyl acetate	88.11	3.5434	2.9332	254.629	6	12.7101	3.2674	1.78	Fernández *et al.* (2010)	n-heptane	0.239	0.992	2.201	1.452
methyl propanoate	88.11	3.2761	3.5254	216.018	6	10.3199	1.094	1.70	Ortega *et al.* (2003)	n-heptane	0.517	1.634	7.819	1.606
butyl formate	102.1	3.9668	2.5794	332.046	6	16.5322	3.4987	2.02	Ortega *et al.* (2015)	n-heptane	0.403	1.134	_^{a}	2.037
propyl acetate	102.1	3.6507	3.1868	260.878	6	12.5111	3.5139	1.79	Fernández *et al.* (2013)	n-heptane	0.502	1.009	5.436	2.406
ethyl propanoate	102.1	3.6671	3.1451	267.250	6	12.8094	3.1965	1.75	Ríos *et al.* (2014)	n-heptane	0.335	0.807	3.845	3.345
methyl butanoate	102.1	3.6918	3.0564	272.843	6	12.6336	3.06612	1.72	Ríos *et al.* (2012)	n-heptane	0.255	1.067	5.887	1.734
pentyl formate	116.2	3.8661	3.1884	288.207	6	13.2007	4.1093	1.90	This work	n-octane	0.904	0.220	_^{a}	1.627
butyl acetate	116.2	3.8501	3.1907	293.024	6	13.8230	4.0503	1.84	This work	n-octane	0.553	0.865	3.788	0.865
propyl propanoate	116.2	4.0225	2.8671	331.304	6	16.2168	4.2672	1.79	This work	n-octane	1.478	0.684	_^{a}	4.123
ethyl butanoate	116.2	4.1891	2.5736	335.846	6	15.3695	4.3293	1.81	This work	n-octane	0.681	0.201	3.185	2.208
methyl valerate	116.2	4.0646	2.7511	332.541	6	15.2862	4.3386	1.62	This work	n-octane	0.681	0.914	_^{a}	2.186
Ethers														
diethyl ether	74.12	3.7032	2.6069	239.234	6	12.0284	2.2558	1.15	Klon-Palczewska *et al.* (1980)	n-pentane	0.374	0.514	_^{a}	1.784
di-n-propyl ether	102.18	4.3583	2.3226	356.304	6	17.3103	3.4305	1.21	This work	n-heptane	0.441	0.543	_^{a}	0.963
butyl ethyl ether	102.18	4.0139	2.8687	295.481	6	14.1883	1.6563	1.22	This work	n-heptane	1.219	0.712	_^{a}	7.745
dibutyl ether	130.23	4.3564	2.9364	363.111	6	17.4393	3.9749	1.17	March *et al.,* (1980)	n-hexane	0.486	0.621	_^{a}	1.604

† AADs in u^{liq} calculated with reference to corresponding pure component data sets as indicated in Table 7.1

* AADs based on DIPPR Correlations

^{a} No AADs possible due to lack of published data

Development of Polar SAFT-VR Mie

Apart from the SAFT-VR Mie[JC] exceptions, the polar SAFT-VR Mie variants are clearly able to accurately model the pure component properties under consideration. The reported AADs are of the expected order of magnitude for SAFT type thermodynamic models, with particularly good correlation of the saturation properties in evidence. The AADs in pure component speed of sound are of specific interest in the SAFT-VR Mie framework and warrant particular attention. The magnitudes of some of the deviations for u^{liq} reported in Tables 7.3 and 7.4 are disappointingly high given SAFT-VR Mie's renown for accurate prediction of this property. A fair assessment of these AADs however, requires direct comparison with equivalent deviations exhibited by polar sPC-SAFT; this comparison is provided in Figure 7.6.
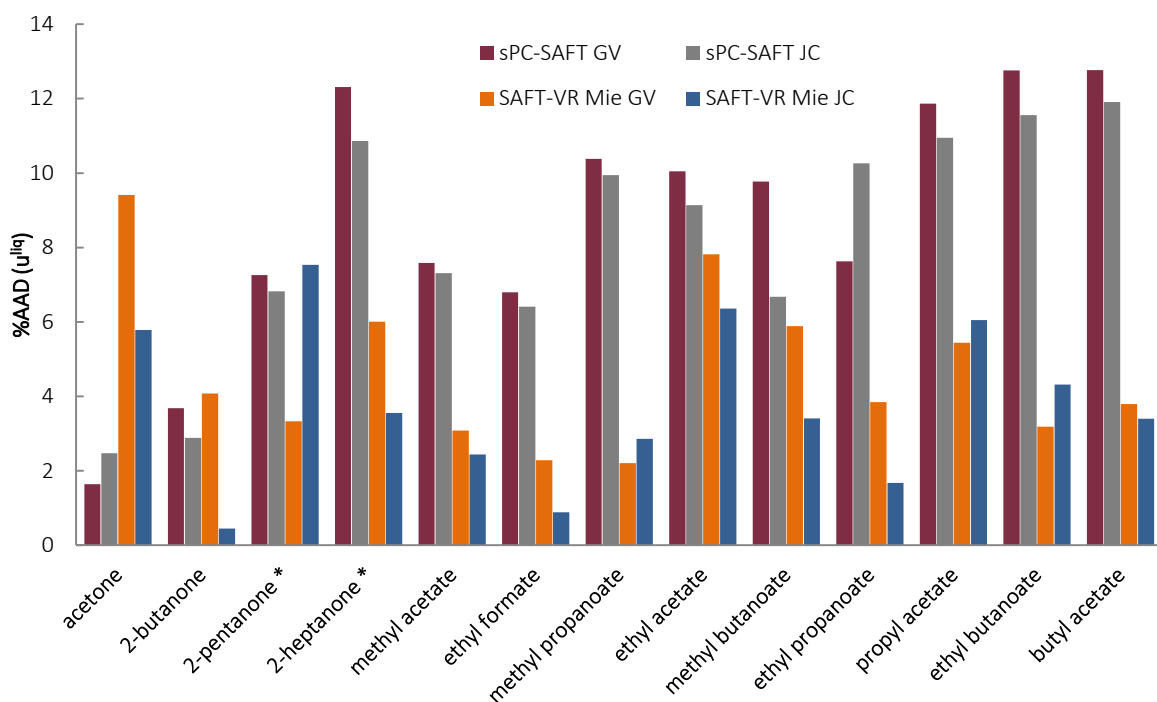
Figure 7.6: Comparison of AADs in u^{liq} for both polar SAFT-VR Mie and polar sPC-SAFT considering ketones and esters with available reference data. Reference data are those presented in Table 7.1. *SAFT-VR Mie[JC] predictions are those of nonpolar variant, given the inability to regress appropriate SAFT-VR Mie[JC] parameters for these components.

Comparison between the polar SAFT-VR Mie predictions and those of polar sPC-SAFT illustrate that, apart from the smaller ketone molecules, significant improvement in the prediction of pure component u^{liq} is apparent for the polar SAFT-VR Mie models. The arguments of Lafitte *et al.,* (2006, 2013) appear to hold for the polar variants of SAFT-VR Mie: explicitly accounting for variable repulsive range serves to improve accuracy in the prediction of speed of sound. The significance of this improvement is made even more apparent when considering that the parameter sets reported in Tables 7.3 and 7.4 were generated without speed of sound data being included in the regression procedure to begin with.

Inclusion of speed of sound data in the objective function offers just one alternative to the regression procedures used to determine the parameters presented in Tables 7.3 and 7.4. The good predictive capacity of these parameters however, makes them an excellent reference with which to compare the results of these alternative regression procedures. This is the aim of the following section.

7.5   Analysis of Regression Results

The analysis performed in this section is limited to the generalised results of the different regression procedures and how these results compare with each other. Such an analysis is necessarily supplemented by example cases of application to pure component data and selected application to mixtures. A more rigorous and thorough assessment of the performance of these parameter sets to mixture data is reserved for Chapter 8, where only the optimum parameter sets will be considered.

7.5.1   Results of the Standard Pure Component Regression

Results of the *Standard pure component regression* constitute the largest proportion of the regression results, with eight different cases under consideration according to Figure 7.5. As highlighted in the Chapter 5, regression procedures of this kind are the literature standard for determination of pure component properties given the relative availability of pure component property data.

7.5.1.1   *Multiple Minima and Parameter Degeneracy*

The work of Dufal *et al.* (2015) highlighted the prevalence of multiple, discreet local minima in the SAFT-VR Mie objective function. It was emphasised that this was sensitive to the choice of pure component properties, their relative regression weights, as well as initial guesses for the parameter values. Results of the *Standard pure component regression* show that the problem of multiple minima extends to the polar SAFT-VR Mie models as well.

Choosing initial values proved to be the most influential aspect in determining the parameter set resulting from the regression. This was particularly true for the determination of the polar parameter (*viz.* x_p and n_p) as the largest adjustments between regression iterations were made to this parameter value. This was most prevalent and problematic when initial parameter values far from those corresponding to the objective function minimum were chosen. In these cases, the initial adjustments were largest for x_p/n_p and frequently resulted in the parameter being pushed to the bounded lower value of zero before significant changes were made to the other nonpolar parameters. Once pushed in this direction, the x_p/n_p value would approach zero asymptotically for the remainder of the assigned iterations and yield "nonpolar" SAFT-VR Mie[JC] and SAFT-VR Mie[GV] parameter sets.

In the case of SAFT-VR Mie[GV], this tendency was the result of multiple discrete local minima of the kind demonstrated by Dufal *et al.* (2015). This conclusion was drawn based on the fact that careful selection of parameter initial values and altering regression weightings frequently mitigated the problem of

n_p tending to zero. However, the presence of these discrete local minima meant that some regressed parameter sets were non-optimum and exhibited significant AADs in pure component properties as a result. This is typified by the case of methyl valerate in Table 7.5, where the results of the parameter set regressed using the sPC-SAFT$_{GV}$ parameter values as the initial guess are compared to those resulting from using the SAFT-VR Mie^{GV} parameters in Table 7.3 as the initial values. The results emphasise the importance of an accurate initial guess in mitigating the effect of multiple local minima in the objective function.

Table 7.5: SAFT-VR Mie^{GV} parameters regressed for methyl valerate using different initial value guesses (regressed sPC-SAFT$_{GV}$ vs. regressed SAFT-VR Mie^{GV} using VLE in regression) for model parameters. Importance of good initial guess in mitigating multiple local minima is highlighted.

Initial Value Basis	σ Å	m	ε/k K	λ_a	λ_r	x_p/n_p	P^{sat} * AAD%	ρ^{sat} * AAD%	u^{liq} AAD%	H^{vap} * AAD%
Methyl Valerate										
sPC-SAFT$_{GV}$	4.0485	2.7793	327.584	6	15.0511	5.3223	15.50	1.090	-[a]	4.724
VR Mie^{GV} (VLE)	4.3800	2.7733	328.919	6	15.0950	4.3800	0.659	0.924	-[a]	2.187

* AADs based on DIPPR Correlations;
[a] No AADs possible due to lack of published data

An exception to this successful mitigation strategy was the regression of parameters for the ether components. The difficulty in successfully modelling these weakly polar components had already been encountered in the polar sPC-SAFT modelling chapter, and this difficulty was found to extend to the polar SAFT-VR Mie framework. Irrespective of initial guess, the value of n_p approached its lower bound of zero asymptotically, suggesting the presence of a broad minimum in a flat objective function space when using pure component data alone. Unlike the case for sPC-SAFT$_{GV}$ however, this problem was not limited to a single ether and prevented the regression of polar parameter sets for all four ethers considered. In the case of SAFT-VR Mie^{GV}, this problem was confined to the ether functional group.

The presence of broad minima was particularly problematic for the JC polar term in the sPC-SAFT framework. The results of the *Standard pure component regression* demonstrated that this problem transcends the parent framework and extends to the SAFT-VR Mie^{JC} model as well. In the case of sPC-SAFT$_{JC}$, this deterioration was systematic and was successfully linked to the prominence of the polar interactions as a result of functional group location. For SAFT-VR Mie^{JC} however, the trend is more widespread, with the majority of components considered exhibiting this behaviour when pure component data alone were incorporated in the objective function. Unlike the problem of multiple discrete local minima in SAFT-VR Mie^{GV}, regression of a zero x_p could not be mitigated by careful selection of the initial values or altering regression weights. Indeed, even choosing the optimum model parameters determined by incorporating VLE data in the regression procedure (Table 7.3) as the initial guess could not allay this problem when only pure component data were considered.

The likely cause for this pronounced degeneracy problem is the increased number of regressed parameters in the SAFT-VR Mie framework – the additional parameter complicates the regression space

further and increases the difficulty of finding a unique parameter set. Given the prevalence of this deterioration in polar sPC-SAFT, where four pure component parameters are considered, **the addition of a fifth parameter appears to increase the occurrence of this problem when using SAFT-VR Mie**.

7.5.2   Explicit vs. Implicit: Effect of Accounting for Polarity

Perhaps the most important consideration in proposing a polar SAFT-VR Mie framework is whether the explicit polar dependence is necessary in light of the enhanced predictive capacity of this model. Thus the focus of the discussion presented here is a comparison of the relative performance of nonpolar SAFT-VR Mie vs. the proposed polar variants. Given the regression difficulties for the SAFT-VR Mie[JC] model demonstrated in the previous section, the discussion here will centre on a comparison of nonpolar SAFT-VR Mie and SAFT-VR Mie[GV]. Evaluation of the polar model is further divided into the cases where $n_p = 1$ as per the original Gross & Vrabec formulation, and the case where this parameter is variable. To this end, due consideration is given to successfully generated parameter sets for representative components of each functional groups of interest, followed by a summary of the overall comparison.

7.5.2.1   Ketones

Acetone is undeniably the first choice reference ketone in the literature, given the relative abundance of pure and mixture data for this component compared to other members of the ketone family. Due to acetone's small molecular mass and large dipole moment however, its properties are not necessarily representative of the ketone family as a whole. Thus, a reference component for the linear ketones should be a longer chain molecule and is chosen to be 2-pentanone for the purposes of illustration here. Regressed parameters of both ketones for nonpolar SAFT-VR Mie and SAFT-VR Mie[GV] are provided in Table 7.6. The reported parameter sets are based on the *Standard pure component regression* procedure using the H^{vap} alternative, which thus allows for a direct comparison of the model performance.

Development of Polar SAFT-VR Mie

Table 7.6: Regressed parameters for acetone and 2-pentanone for nonpolar SAFT-VR Mie and SAFT-VR Mie^GV. Results are those of the Standard Regression Procedure using the same reference pure component data (P^{sat}, ρ^{sat}, H^{vap})

	σ	m	ε/k	λ_a	λ_r	x_p/n_p	P^{sat} *	ρ^{sat} *	u^{liq}	H^{vap} *
	Å		K				AAD%	AAD%	AAD%	AAD%
Acetone										
SAFT-VR Mie	3.5596	2.2518	304.452	6	13.1896		0.919	1.291	13.24 [a]	2.822
SAFT-VR Mie^GV (n_p=1)	3.6142	2.1544	294.291	6	14.0449	1.0000	0.123	0.439	13.94 [a]	1.784
SAFT-VR Mie^GV (n_p variable)	3.4854	2.3472	253.350	6	12.4778	1.2289	0.122	0.206	9.681 [a]	1.228
2-Pentanone										
SAFT-VR Mie	4.0571	2.3194	375.912	6	16.7737		0.359	0.479	7.537 [b]	3.322
SAFT-VR Mie^GV (n_p=1)	4.1701	2.1667	394.584	6	18.5786	1.0000	0.205	0.185	10.42 [b]	2.968
SAFT-VR Mie^GV (n_p variable)	3.8381	2.6275	294.266	6	13.7247	1.8037	0.130	0.624	2.997 [b]	2.462

* AADs based on DIPPR Correlations;
[a] AADs based on data of Azevedo *et al.*, (2004)
[b] AADs based on data of Cobos *et al.* (2016)

Considering the AADs in the indicated pure component properties, it is clear that both models are capable of reproducing the pure properties of acetone and 2-pentanone with a high degree of accuracy. However, the SAFT-VR Mie^GV predictions exhibit consistently smaller deviations than the nonpolar variant. The exception to these accurate predictions is that for the speed of sound data, where deviations in excess of 7% are apparent for nonpolar SAFT-VR Mie for both ketones. This problem is not limited to the nonpolar model case however, as similarly large AADs in u^{liq} are reported for both SAFT-VR Mie^GV parameter sets. As will be demonstrated, this is more a result of the choice of component properties used in the regression procedure (H^{vap} vs. u^{liq}) than a reflection of the relative performance of the polar and nonpolar variants.

Comparing the parameters of nonpolar SAFT-VR Mie and SAFT-VR Mie^GV with variable n_p, it is readily apparent that the nonpolar variant exhibits a significantly larger dispersion energy parameter than the polar term. There is also a clear difference in the regressed values of λ_r between the polar and nonpolar models. There appears to be a cooperative relationship between these parameters; larger differences in ε/k between the polar and nonpolar model correspond to similarly large differences in the λ_r parameter. For the case of sPC-SAFT, it was argued that the nonpolar model attempts to account for the additional dipolar interactions by exaggerating the dispersion energy parameter. If similar arguments are held here, it would appear that nonpolar SAFT-VR Mie compensates for this exaggeration in ε/k by similarly increasing the range of these interactions for polar molecules.

Application of the regressed parameter sets to mixture phase behaviour should help clarify whether the inclusion of the explicit polar term is warranted within a SAFT-VR Mie framework. To this end, the parameter sets presented in Table 7.6 were used to generate predictions of the binary phase behaviour of the acetone/n-hexane and 2-pentanone/n-heptane systems presented in Figures 7.7 and 7.8 respectively.
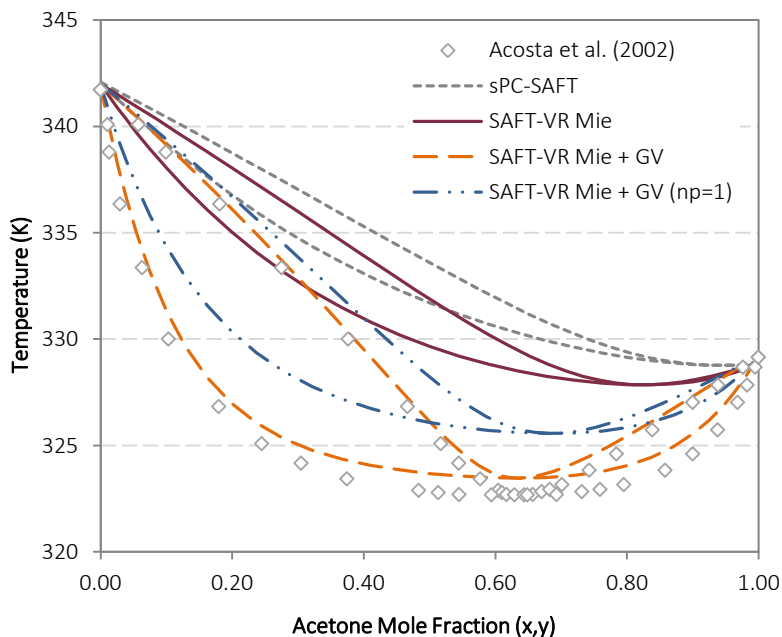
Figure 7.7: Application of nonpolar SAFT-VR Mie and SAFT-VR Mie ^{GV} (n_p = 1 & variable) to phase behaviour of the acetone/n-hexane (Acosta et al., 2002) mixture at 101.3kPa. Nonpolar sPC-SAFT prediction equivalent included for reference.

It is clear from Figures 7.7 and 7.8 that the inclusion of the GV polar term improves the prediction accuracy in both ketone/n-alkane systems. It is also notable that a constant n_p = *1* parameter set fails to accurately capture the effects of the strong positive deviations in these ketone molecules. This is consistent with similar trends in sPC-SAFT that lead to the consideration of a variable n_p to begin with. Fixing the value of n_p in this fashion limits the ability to account for dipolar interactions, resulting in exaggerated dispersion energy parameters in the same fashion as that described for the nonpolar case. In the same vein, the apparent cooperativity between ε/k and λ_r results in similarly larger values of the repulsive range. These exaggerated values of λ_r are clearly responsible for the notable difference in the predictability of u^{liq} by the two SAFT-VR Mie^{GV} cases in Table 7.6.
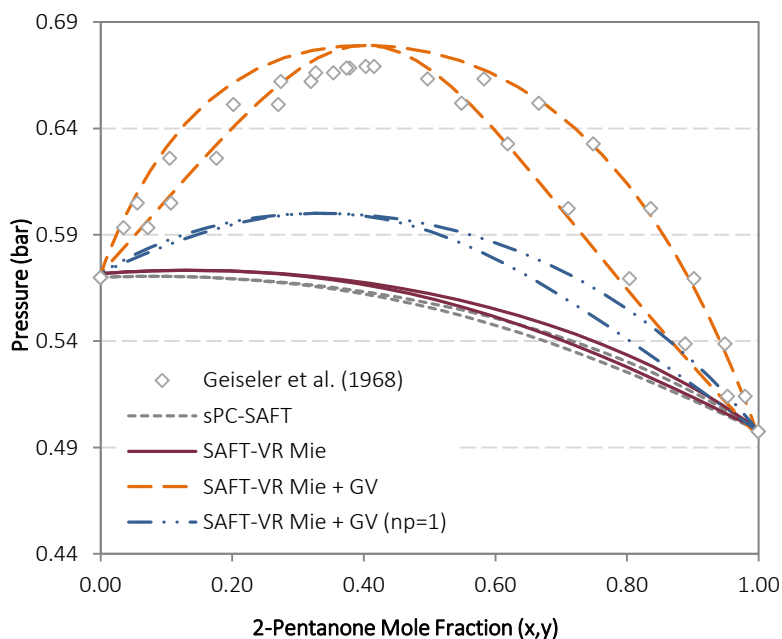
Figure 7.8: Application of nonpolar SAFT-VR Mie and SAFT-VR Mie ^{GV} (n_p = 1 & variable) to phase behaviour of the 2-pentanone/n-heptane (Geiseler et al., 1968) mixture at 353.15K. Nonpolar sPC-SAFT prediction equivalent included for reference.

The quality of the nonpolar SAFT-VR Mie prediction should not so quickly be dismissed however, as comparison with the equivalent nonpolar sPC-SAFT predictions (based on the parameters of de Villiers (2011)) shows an improvement in prediction accuracy. **Based on the predictions for the representative ketones however, it is readily apparent that explicitly accounting for the polar interactions is necessary to yield a good fit of their phase equilibria.**

7.5.2.2   Esters

Studies on esters are generally limited to smaller ($C_4 \geq$) members of this homologous group with limited attention paid to larger components where wider ranges of behaviour are exhibited for the different isomers. The ester functional group's capacity for extensive structural isomerism has already been highlighted in previous chapters. For these reasons it is necessary to consider multiple reference components for this functional group. Here ethyl acetate and methyl valerate are selected to be representative of different chain lengths as well as different functional group locations. Parameters regressed for these components for the nonpolar SAFT-VR Mie model and the SAFT-VR Mie^{GV} polar variant are listed in Table 7.7. As with the ketones, parameter sets are results of the *Standard pure component regression* procedure using H^{vap} instead of u^{liq} in the regression, allowing for direct comparison of the predictions.

Table 7.7: Regressed parameters for ethyl acetate and methyl valerate for nonpolar SAFT-VR Mie and SAFT-VR Mie^{GV}. Results are those of the Standard Regression Procedure using the same reference pure component data (P^{sat}, ρ^{sat}, H^{vap})

	σ Å	m	ε/k K	λ_a	λ_r	x_p/n_p	P^{sat} * AAD%	ρ^{sat} * AAD%	u^{liq} AAD%	H^{vap} * AAD%
Ethyl Acetate										
SAFT-VR Mie	3.6095	2.8246	289.604	6	13.7377		0.094	0.274	0.435 [a]	2.089
SAFT-VR Mie^{GV} (n_p=1)	3.5646	2.9109	275.455	6	13.0879	1.0000	0.088	0.295	0.451 [a]	2.058
SAFT-VR Mie^{GV} (n_p variable)	3.5746	2.8837	271.202	6	13.0501	1.9467	0.096	0.461	0.850 [a]	1.902
Methyl Valerate										
SAFT-VR Mie	4.0524	2.7925	346.100	6	15.2997		0.768	0.372	_[b]	2.455
SAFT-VR Mie^{GV} (n_p=1)	4.0627	2.7741	347.228	6	15.3720	1.0000	1.006	0.370	_[b]	2.546
SAFT-VR Mie^{GV} (n_p variable)	4.0753	2.7380	337.270	6	15.3785	3.8597	0.682	0.778	_[b]	2.267

* AADs based on DIPPR Correlations;
[a] AADs based on data of Pal *et al.*, (2013)
[b] No available experimental data with which to compare model predictions

The AADs reported in Table 7.7 illustrate that the difference between the prediction accuracy of the polar and nonpolar SAFT-VR Mie variants is much smaller for esters than was the case for ketones. Deviations in pure component properties are almost identical throughout and there is no marked improvement of the model when explicitly accounting for the polar effects. Numerically, the values of the regressed parameters for the polar and nonpolar models are very similar, with larger values of ε/k and λ_r once again in evidence for the nonpolar variant and the constant n_p case. The smaller difference between the dispersion energies in the polar and nonpolar models is likely a result of the markedly weaker dipole moment of the ester functional group compared to the ketones.

The predictive capacity of these model parameters is tested against mixture phase equilibrium data in Figures 7.9 and 7.10, where the ethyl acetate/n-heptane and methyl valerate/n-octane systems are considered respectively.
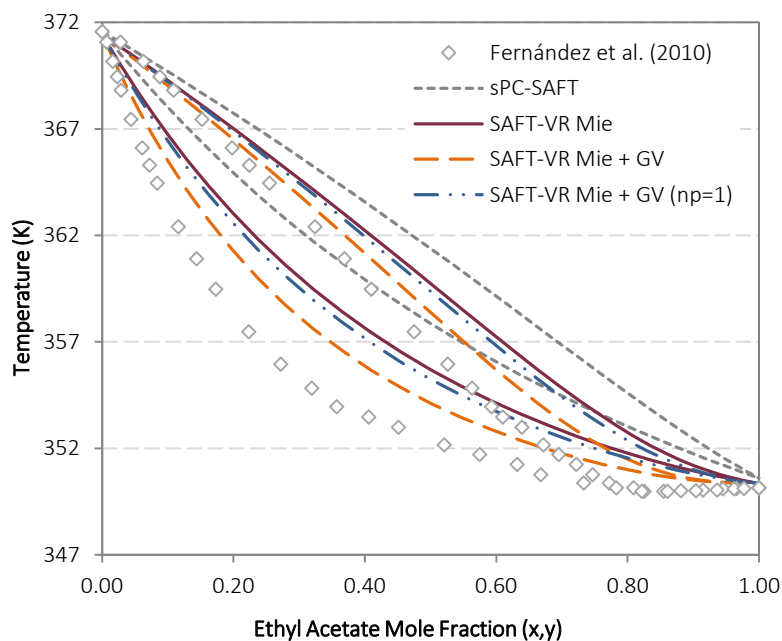
Figure 7.9: Application of nonpolar SAFT-VR Mie and SAFT-VR Mie ^{GV} (n_p = 1 & variable) to phase behaviour of the ethyl acetate/n-heptane (Fernández et al., 2010) mixture at 101.3kPa. Nonpolar sPC-SAFT prediction equivalent included for reference.

In the ethyl acetate/n-heptane case, the nonpolar SAFT-VR Mie model fit is only slightly worse than the variable n_p SAFT-VR Mie^{GV} prediction. The poorest correlation of the data is visible in the high ester concentration range, where the nonpolar model fails to account for the azeotrope at ~*0.86* mole fraction ethyl acetate. This is remedied in the case of the polar variant predictions, albeit at higher ester concentrations (*ca. 0.92* mole fraction). In Figure 7.10 the nonpolar variant similarly fails to accurately capture the temperature dependence of the azeotrope in the methyl valerate/n-octane system and is clearly outperformed by SAFT-VR Mie^{GV} in this system. However, the SAFT-VR Mie prediction can be seen to maintain its superiority over nonpolar sPC-SAFT for the prediction of the phase equilibria of ester mixtures.
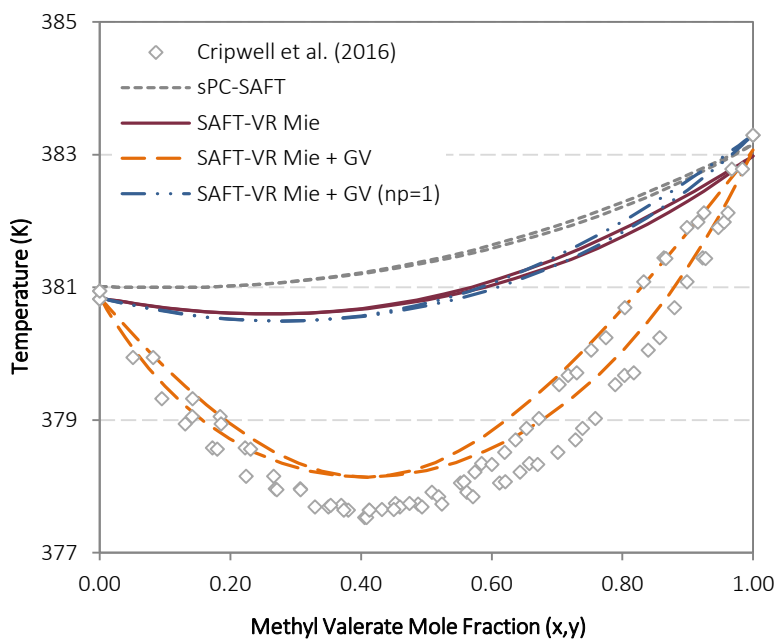
Figure 7.10: Application of nonpolar SAFT-VR Mie and SAFT-VR Mie ^{GV} (n_p = 1 & variable) to phase behaviour of the methyl valerate/n-octane (This work) mixture at 60.0kPa. Nonpolar sPC-SAFT prediction equivalent included for reference.

The notable result from Figures 7.9 and 7.10 is the negligible improvement offered by the constant n_p SAFT-VR Mie^{GV} case compared to the predictions of the nonpolar model. This is reflected in the similarity of the two parameter sets and emphasises the need to accurately capture the polar contribution in a variable fashion. **The parameter set for the regressed n_p case is not markedly different apart from the value of n_p itself, but the effect of limiting this parameter on the associated predictive capacity is made clear in the ester functional group.**

7.5.2.3   Ethers

The problem of broad minima in the objective functions of the ethers means that comparison of the polar and nonpolar models can only be performed by using the SAFT-VR Mie^{GV} parameter sets of Table 7.3. This necessitates comparing parameter sets determined by different regression procedures; *viz. Standard pure component regression* for both the nonpolar model and fixed n_p case vs. the inclusion of VLE data for SAFT-VR Mie^{GV} with variable n_p. However, the comparison still provides insight into the question of whether polar interactions need to be explicitly accounted for. Diethyl ether and butyl ethyl ether are used as reference components for this functional group, with their respective parameters listed in Table 7.8.

As with the ketones and esters previously, AADs reported in Table 7.8 suggest that there is little to distinguish between the predictive capacities of nonpolar SAFT-VR Mie and SAFT-VR Mie^{GV}. The similarity of the parameters themselves highlights the small contribution of polar interactions to the phase behaviour of the ethers. The exception is the variable n_p parameter set for butyl ethyl ether, where smaller dispersion energy and repulsive range parameters are in evidence. The same trend is found for the other

functional groups. In those cases, the most apparent manifestation of this difference was the description of u^{liq} but the lack of such data for ethers means the only appreciable difference will be noted in the description of mixture behaviour.

Table 7.8: Regressed parameters for diethyl ether and butyl ethyl ether for nonpolar SAFT-VR Mie and SAFT-VR Mie^{GV}. Results are those of the Standard Regression Procedure for SAFT-VR Mie with those for SAFT-VR Mie^{GV} relisted from Table 7.3.

	σ Å	m	ε/k K	λ_a	λ_r	x_p/n_p	P^{sat} * AAD%	ρ^{sat} * AAD%	u^{liq} AAD%	H^{vap} * AAD%
Diethyl Ether										
SAFT-VR Mie	3.7120	2.5952	245.350	6	12.2809		0.370	0.383	-ª	1.863
SAFT-VR Mie^{GV} (n_p=1)	3.7018	2.6120	242.328	6	12.1424	1.0000	0.368	0.436	-ª	1.831
SAFT-VR Mie^{GV} (n_p variable)	3.7032	2.6069	239.234	6	12.0284	2.2558	0.374	0.514	-ª	1.784
Butyl Ethyl Ether										
SAFT-VR Mie	4.2397	2.5159	349.734	6	17.4652		1.116	0.620	-ª	7.659
SAFT-VR Mie^{GV} (n_p=1)	4.2414	2.5129	349.511	6	17.4559	1.0000	1.117	0.623	-ª	7.656
SAFT-VR Mie^{GV} (n_p variable)	4.0139	2.8687	295.481	6	14.1883	1.6563	1.219	0.712	-ª	7.745

* AADs based on DIPPR Correlations;
ª No available experimental data with which to compare model predictions

The parameter sets of Table 7.8 are used to predict VLE for the binary diethyl ether/n-pentane and butyl ethyl ether/n-heptane in Figures 7.11 and 7.12.
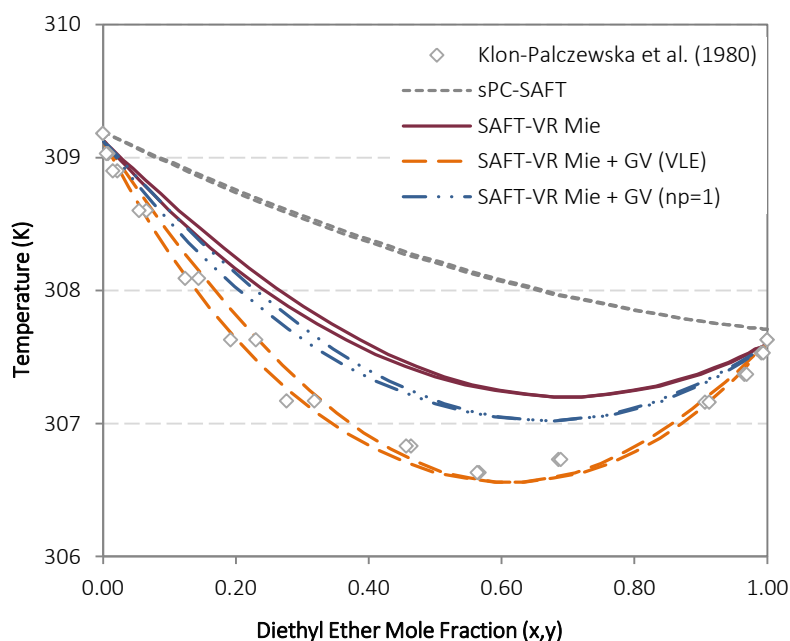
Figure 7.11: Application of nonpolar SAFT-VR Mie and SAFT-VR Mie ^{GV} (n_p = 1 & variable fit to VLE data) to phase behaviour of the diethyl ether/n-pentane (Klon-Palczewska et al., 1980) mixture at 101.3kPa. Nonpolar sPC-SAFT prediction equivalent included for reference.

The diethyl ether/n-pentane system highlights the improvement of nonpolar SAFT-VR Mie over its nonpolar sPC-SAFT counterpart, qualitatively accounting for the azeotropic behaviour in the system. The prediction of the fixed n_p parameter set goes a step further in improving the temperature description of the azeotrope, but the variable n_p case once again clearly provides the superior prediction. This is more subtly demonstrated in the butyl ethyl ether/n-heptane system where all but the variable n_p parameter sets produce near identical predictions, shifted away from the experimental data.
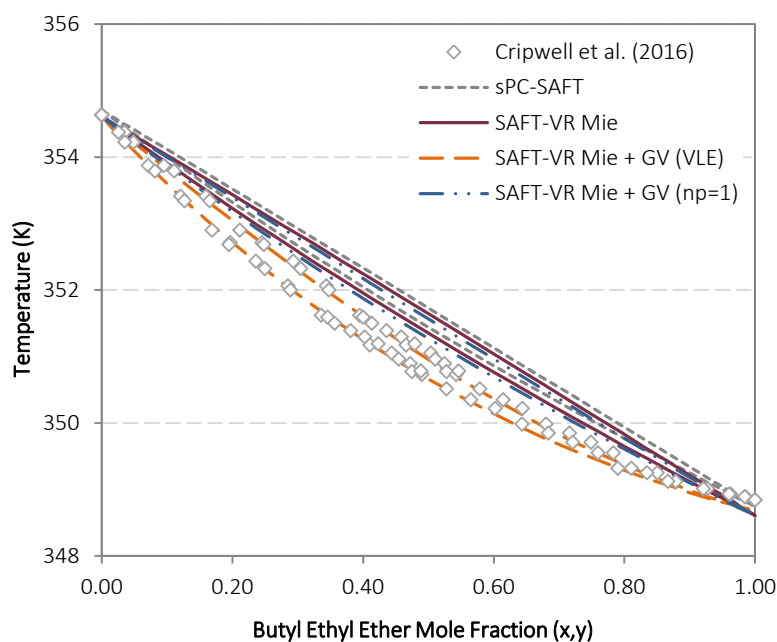
Figure 7.12: Application of nonpolar SAFT-VR Mie and SAFT-VR Mie ^{GV} (n_p = 1 & variable fit to VLE data) to phase behaviour of the butyl ethyl ether/n-heptane (This work) mixture at 60.0kPa. Nonpolar sPC-SAFT prediction equivalent included for reference.

7.5.2.4   Summary

When considering the prediction of pure component properties, the nonpolar and polar SAFT-VR Mie models exhibited similar predictive capacities, regardless of the functional group considered. Analysis of the parameters themselves however, showed that the dispersion energy and repulsive range parameters of nonpolar SAFT-VR Mie are systematically larger than their SAFT-VR Mie^{GV} equivalents when n_p is regressed. These differences were most obvious for the ketones, with systematically smaller differences as the more weakly polar ester and ether groups were considered. The larger values of ε/k and λ_r in the nonpolar variant are indicative of the tendency of the model to artificially exaggerate the contribution of the dispersion term in order to accommodate the polar interactions. This same argument applies to the fixed n_p = 1 case, where limiting the value of the polar parameter leads to exaggerated dispersion parameters. Indeed, this explains why the nonpolar SAFT-VR Mie and SAFT-VR Mie^{GV} parameters are significantly different for the strongly polar ketones, yet almost identical for the very weakly polar ethers.

The clearest distinction between polar and nonpolar model performances was in their application to selected phase equilibria. As the most strongly polar of the functional groups under consideration, the ketone homologous group most ardently demonstrated the need to account for polar interactions explicitly. While the nonpolar SAFT-VR Mie model captured the azeotropic behaviour in the ketone/n-alkane systems, and exhibited marked improvement over its nonpolar sPC-SAFT counterpart, the fits were still only qualitatively correct. This functional group also most clearly showed the effect of fixing the value of the polar parameter to *1*: improved prediction of mixture behaviour is in evidence compared to the nonpolar model, but the limitation on n_p similarly limits the predictive capacity of the model.

While the difference in predictive capacity between the polar and nonpolar SAFT-VR Mie models is smaller when considering the ester and ether functional groups, there is still a clear distinction between them. Nonpolar SAFT-VR Mie cannot accurately capture the temperature dependence of the positive deviations in these systems, with the fixed n_p case offering minimal improvement. For the esters, a consistent trend is apparent in the predictions of these models: higher accuracy is apparent in the nonpolar model prediction of mixture data for less polar esters (*viz.* acetates, propanoates) than for more strongly polar members (*viz.* methyl esters, formates). This makes sense considering the less strongly polar isomers will exhibit a smaller *polar* contribution to the overall system behaviour. This results in a smaller distinction between polar and dispersion forces, the latter of which is well correlated by the nonpolar model. This last point is even more pronounced in application to the ether functional group. As with sPC-SAFT previously, the nonpolar SAFT-VR Mie and fixed n_p cases can't account for the subtle deviations resulting from the ether's weak dipole.

Lafitte *et al.*'s SAFT-VR Mie exhibits an enhanced predictive capacity compared to nonpolar sPC-SAFT when applied to polar components and their mixtures. While the improved theory underpinning SAFT-VR Mie and its **variable range parameter allow for better description of derivative properties, this improvement is clearly insufficient to accurately account for dipolar interactions in the model's original framework**. Indeed, trying to shoehorn the effects of dispersion and polar interactions into a single contribution is fundamentally erroneous and has been proven as such by the model predictions in this section.

7.5.3   Role of Speed of Sound

The role of speed of sound in setting SAFT-VR Mie apart from its predecessors has already been extensively detailed in this work. The question of importance here is whether its explicit inclusion in the regression procedure yields improved performance when applied to properties of polar components and their mixtures. The inclusion of u^{liq} is not itself a novel suggestion; there was a demonstrated trade-off in predictive accuracy between phase equilibrium properties and derivative properties in the sPC-SAFT framework (de Villiers, 2011). This meant that its inclusion in the regression procedure only served to

deteriorate the overall predictive capacity of the resulting parameter set. Whether such a trade-off exists in SAFT-VR Mie is thus of particular interest in this section.

7.5.3.1 H^{vap} *vs.* u^{liq}

The role of speed of sound was tested by considering the results of the different cases where heats of vaporisation and speeds of sound were incorporated into the regression procedure (Figure 7.5) respectively. Given the problems of broad minima prevalent in SAFT-VR Mie[JC] detailed previously, this variant could not be considered and this discussion is therefore limited to the *Standard pure component regression* results for nonpolar SAFT-VR Mie and SAFT-VR Mie[GV]. The resulting parameter sets are listed for selected components in Table 7.9.

Table 7.9: Different parameter sets for selected components resulting from the Standard pure component regression when considering either H^{vap} or u^{liq} in the regression procedure.

	σ Å	m	ε/k K	λ_a	λ_r	x_p/n_p	P^{sat} * AAD%	ρ^{sat} * AAD%	u^{liq} AAD%	H^{vap} * AAD%
2-Heptanone										
SAFT-VR Mie										
H^{vap}	3.9158	3.3015	307.272	6	12.9282		0.190	0.094	3.551	1.983
u^{liq}	3.9972	3.1382	326.337	6	13.7518		0.171	0.233	2.221	2.056
SAFT-VR Mie[GV]										
H^{vap}	3.9584	3.1936	299.001	6	13.0118	2.3731	0.219	0.359	4.000	1.658
u^{liq}	4.0789	2.9756	333.902	6	14.3778	1.7342	0.235	0.098	1.492	1.926
Ethyl Formate										
SAFT-VR Mie										
H^{vap}	3.5468	2.4324	285.975	6	12.9425		0.327	0.229	4.345	3.032
u^{liq}	3.4997	2.5116	275.387	6	12.4691		0.389	0.061	3.443	2.988
SAFT-VR Mie[GV]										
H^{vap}	3.5362	2.4318	262.900	6	12.5671	2.0117	0.057	0.560	2.424	2.637
u^{liq}	3.5340	2.4380	267.572	6	12.4831	1.5807	0.159	0.317	2.633	2.801

* AADs based on DIPPR Correlations;

Perhaps the most notable result from Table 7.9 is that the AADs in u^{liq} are not significantly different for the different regression cases. There is improvement in the description of u^{liq} when speed of sound is included in the regression procedure, but the AAD is of the same order of magnitude as when H^{vap} is used instead. This is a subtle but important result; it suggests that the SAFT-VR Mie theory itself is responsible for the accurate description of this property rather than a bias afforded by its incorporation into the parameter fitting. It is important to note that there is no significant trade-off in the description of the other pure component properties (specifically, saturation properties) which might result from a simple fitting exercise.

The two fitting procedures do yield different parameter sets however, most notably in the dispersion energy and range parameters of the nonpolar model, and in the polar parameter when SAFT-VR Mie[GV] is considered. **That the incorporation of the GV term does not deteriorate the quality of**

the SAFT-VR Mie prediction of the derivative property is also an important result. In fact, the best description of u^{liq} is apparent when the polar interactions are explicitly accounted for. This serves to further allay concerns over the compatibility of the Lennard-Jones based GV polar term and the SAFT-VR Mie framework.

While the inclusion of speed of sound data in the regression procedure does not result in a poorer description of the pure component saturation properties, its effect on the description of mixture phase behaviour has to be assessed. The parameters for 2-heptanone and ethyl formate in Table 7.9 were used to generate predictions for the 2-heptanone/n-nonane and ethyl formate/n-heptane systems in Figures 7.13 and 7.14 respectively.
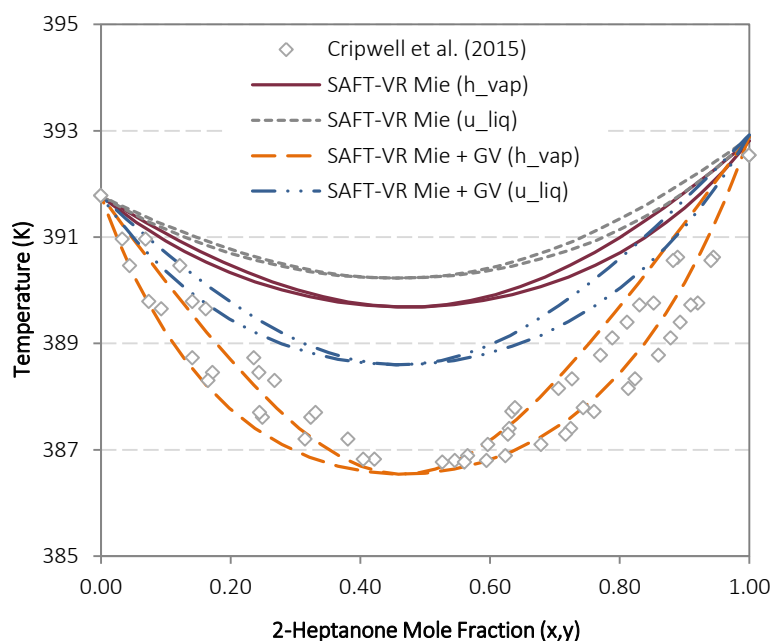
Figure 7.13: SAFT-VR Mie and SAFT-VR Mie ^{GV} predictions of the system 2-heptanone/n-nonane at 40.0kPa using parameter sets regressed using either H^{vap} or u^{liq} in the objective function.

It is clear from Figures 7.13 and 7.14 that better prediction of mixture phase behaviour is achieved when H^{vap} is used in the objective function rather than u^{liq}. The largest differences between these predictions are in evidence for the SAFT-VR Mie^{GV} model, and in application to more strongly polar systems: the two SAFT-VR Mie^{GV} predictions are in better agreement with the data of the weaker ethyl formate/n-heptane system than in the strongly polar 2-heptanone/n-nonane case. This suggests that there is still some trade-off in prediction accuracy between phase equilibria and derivative properties using SAFT-VR Mie. In light of the equivalent compromise exhibited in the sPC-SAFT framework however, the all-round predictive capacity of SAFT-VR Mie can be considered particularly well balanced. It is worth stressing however, that the small pool of pure component speed of sound data for polar components, highlighted in Table 7.1, makes a true assessment of the all-round predictive capacity of the models difficult.
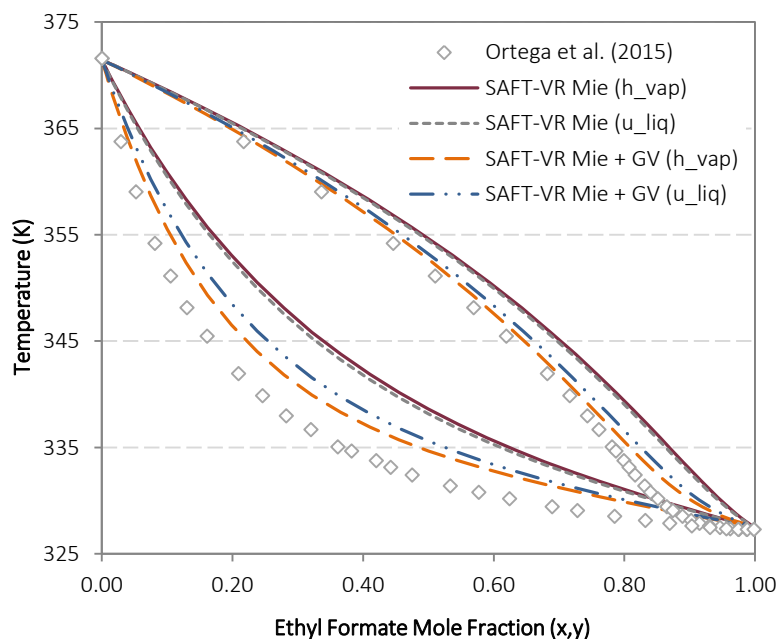
Figure 7.14: SAFT-VR Mie and SAFT-VR Mie ^{GV} predictions of the system ethyl formate/n-heptane at 101.3kPa using parameter sets regressed using either H^{vap} or u^{liq} in the objective function.

7.5.3.2   *Using u^{liq} of Isomers in Regression*

In Section 7.2 and Table 7.1, the lack of pure component speed of sound data for polar components was highlighted. Given the central role that this property plays in the reported SAFT-VR Mie framework, physical arguments were made to support the following claim to account for speed of sound data for those isomers where no experimental data have been published:

For those linear components where no pure component speed of sound data are available,
available data for linear isomers of that component may be used in the regression of SAFT-VR
Mie parameters.

Here, the aim is to test the validity of this argument by testing the predictions of the parameter sets determined using the *Standard pure component regression* and employing this premise. Given the demonstrated need to incorporate the explicit dipolar term, and the evidence given in the previous section that including speed of sound data does not significantly improve the accuracy of phase equilibria predictions in the nonpolar model, this discussion is limited to the results for SAFT-VR Mie^{GV}. To this end, selected parameter sets determined in this manner are presented in Table 7.10.

Development of Polar SAFT-VR Mie

Table 7.10: Regressed parameter sets for selected components using the pure component u^{liq} data of their linear structural isomers. Parameter sets following the H^{vap} regression alternative listed for comparison.

	σ Å	m	ε/k K	λ_a	λ_r	x_p/n_p	P^{sat} * AAD%	ρ^{sat} * AAD%	u^{liq} AAD%	H^{vap} * AAD%
3-Pentanone										
SAFT-VR Mie^{GV}										
H^{vap}	3.9689	2.3972	324.476	6	16.5943	2.2401	0.529	0.916	6.627 [a]	1.952
u^{liq}	3.9689	2.4019	326.997	6	15.8260	1.8739	0.783	0.408	5.362 [a]	2.417
4-Heptanone										
SAFT-VR Mie^{GV}										
H^{vap}	4.7438	2.0747	469.593	6	26.7097	4.7438	0.093	0.237	15.21 [b]	0.150
u^{liq}	4.3476	2.5293	389.852	6	18.1491	4.3476	0.237	0.094	0.723 [b]	0.919
Pentyl Formate										
SAFT-VR Mie^{GV}										
H^{vap}	4.4929	2.2472	437.890	6	24.3903	5.0077	0.654	0.360	14.43 [c]	1.591
u^{liq}	4.1976	2.6248	373.041	6	18.5101	4.4138	0.819	0.317	4.577 [c]	1.623
Methyl Acetate										
SAFT-VR Mie^{GV}										
H^{vap}	3.4361	2.6119	264.106	6	12.6665	2.0504	0.119	0.308	2.213 [d]	1.671
u^{liq} *(isomer)*	3.4188	2.6478	264.830	6	12.5191	1.5344	0.093	0.181	2.095 [d]	1.858
u^{liq} *(self)*	3.4258	2.6363	268.487	6	12.6291	1.2984	0.113	0.094	2.441 [d]	1.916

* AADs based on DIPPR Correlations;
[a] AADs based on u^{liq} data of 2-pentanone;
[b] AADs based on u^{liq} data of 2-heptanone;
[c] AADs based on u^{liq} data of butyl acetate;
[d] AADs based on u^{liq} data of ethyl formate

In similar fashion to that demonstrated in the previous section, incorporating the u^{liq} data of a linear isomer yields a SAFT-VR Mie^{GV} parameter set which differs from the H^{vap} alternative primarily in the values of n_p and ε/k. The same trends in the numerical values of these parameters are also apparent, with smaller dispersion energies and repulsive ranges in evidence when the isomer u^{liq} data are considered. The reported AADs for the u^{liq} regression alternative are of the same order of magnitude as those in Table 7.9 for those components where their own speed of sound data were available. The most notable difference is the vastly improved prediction of u^{liq}. Although the AADs are calculated with reference to the respective isomer data, the equivalent data for these components are expected to be numerically similar, making the improved predictions a significant result.

Table 7.10 contains two parameter sets for methyl acetate; the first of which was regressed using u^{liq} data of methyl acetate while the second was determined using equivalent data for ethyl formate. The similarity of the resulting parameter sets confirm that the regression procedure is not sensitive enough to distinguish between the numerically similar data of the two isomers. This is further reflected in the prediction of both the pure component speed of sound data as well as mixture phase equilibrium data in Figures 7.15 [i.] and [ii.] respectively.
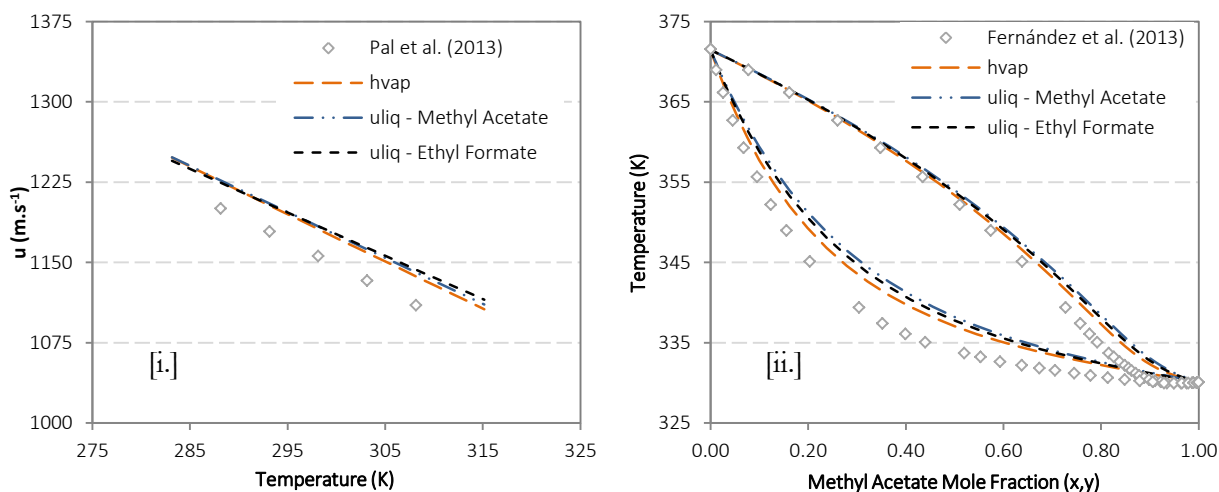
Figure 7.15: Comparing the performance of parameter sets for methyl acetate regressed against H^{vap}, its own u^{liq} data and that of its linear isomer, ethyl formate. Predictions for [i.] u^{liq} and [ii.] methyl acetate/n-heptane VLE (Fernández et al., 2013) at 101.3kPa.

Predictions for mixture phase behaviour of 3-pentanone, 4-heptanone and pentyl formate using the parameter sets in Table 7.10 are shown in Figures 7.16 [i.] to [iii.]. It is clear that there is no significant deterioration of the VLE prediction quality when incorporating the isomer u^{liq} data in the regression procedure. Combined with the improved description of the isomer u^{liq} data, these results suggest that including data of linear isomers in the regression objective function is indeed a viable regression alternative.

7.5.4   Accounting for Structural Isomerism

The major focus of the experimental and sPC-SAFT modelling chapters was the role of functional group location on mixture phase behaviour and the predictability of these systems. It was here that the numerical deficiencies of the JC polar term were systematically highlighted, and the relationship between structural isomerism and prediction accuracy was first established. Having considered and developed a polar SAFT-VR Mie model, a pertinent consideration is whether such trends are maintained or indeed improved upon in the SAFT-VR Mie framework.

The superiority of sPC-SAFT$_{GV}$ over its sPC-SAFT$_{JC}$ counterpart became evident in the determination of parameter sets using the *Standard pure component regression* for different isomers. The difficulties experienced using the JC polar term came as a result of a broad flat minimum for those isomers that exhibit behaviour closest to that of the equivalent weight nonpolar component. This resulted in an inability to distinguish between the polar and dispersion contributions. The more general problems encountered by SAFT-VR Mie[JC] as a result the same numerical issues have already been discussed. Thus of particular interest is whether the GV polar term maintains its predictive accuracy for isomers moving from sPC-SAFT to SAFT-VR Mie.
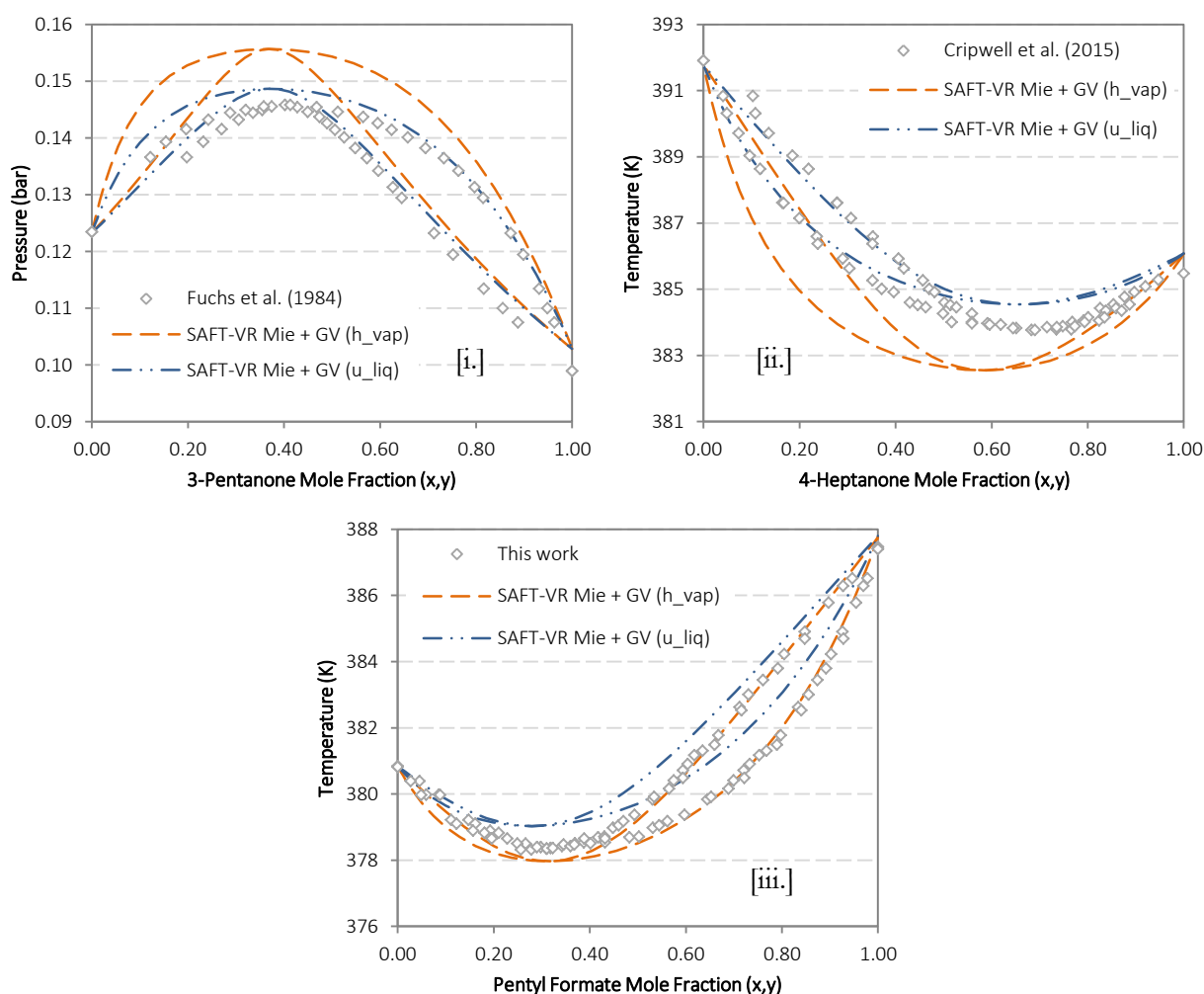
Figure 7.16: Assessment of the predictive capacities of parameter sets based on u^{liq} data for linear isomers given that no such data are available for the components in question. Predictions are compared to the H^{vap} alternatives in the systems [i.] 3-pentanone/n-heptane (Fuchs et al., 1984) at 363.15K, [ii.] 4-heptanone/n-nonane (Cripwell et al., 2015) at 40.0kPa and [iii.] pentyl formate/n-octane (This work) at 60.0kPa.

The comparison between sPC-SAFT$_{GV}$ and SAFT-VR Mie^{GV} predictions, with parameters regressed by the *Standard pure component regression*, for the three heptanone/n-nonane mixtures is presented in Figures 7.17 [i.] to [iii.]. There is clear improvement in the predictions of SAFT-VR Mie^{GV} for the more strongly polar 2-heptanone and 3-heptanone isomers. **Predictions for the least polar 4-heptanone isomer on the other hand are practically identical**. This is an important result, given the need to regress an additional pure component parameter in the SAFT-VR Mie framework.
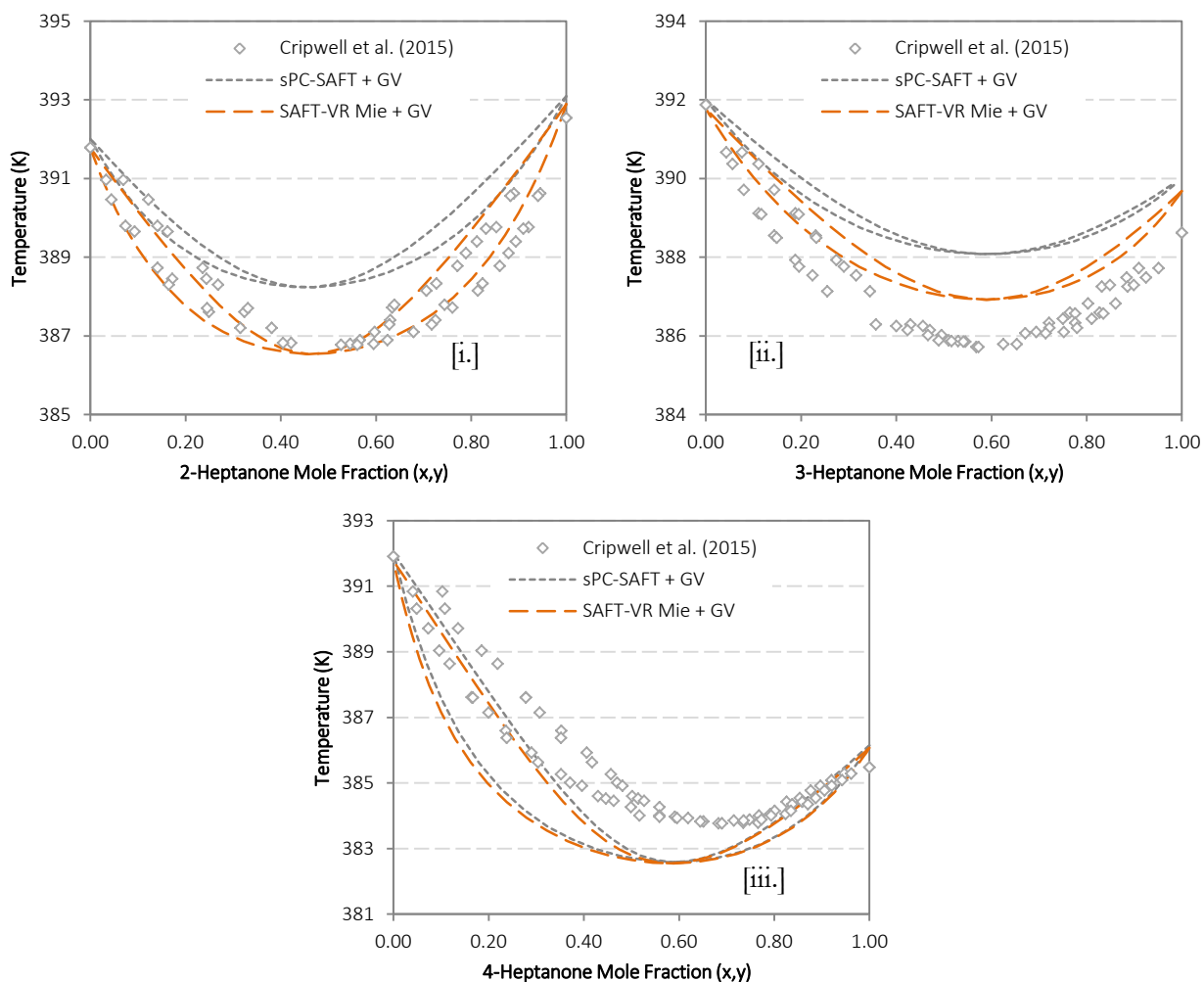
Figure 7.17: Comparison of the sPC-SAFT_{GV} and SAFT-VR Mie^{GV} predictions for the phase behaviour of [i.] 2-heptanone, [ii.] 3-heptanone and [iii.] 4-heptanone with n-nonane at 40.0kPa (Cripwell et al., 2015).

Predictions for the phase behaviour of the five C_6 ester isomers with n-octane are presented in Figures 7.18 [i.] to [v.]. Predictive capacity of the GV polar term is maintained in the strongly polar pentyl formate and methyl valerate cases, while a qualitatively good prediction is in evidence for ethyl butanoate. The predictions in these systems are on par with their sPC-SAFT_{GV} counterparts with more equal performance of the models in evidence for the weaker ester than in the ketones previously.

The distinct difference between the models however, is in the cases of butyl acetate & propyl propanoate and indeed both C_6 ether isomers, where the presence of a broad minimum prevented successful regression of a unique polar parameter set for SAFT-VR Mie^{GV}. In sPC-SAFT_{GV}, this problem was only evident for the case of butyl ethyl ether, but the problem extends to the remainder of the ether family and a number of weakly polar esters in SAFT-VR Mie^{GV}. This is a clear demonstration of the increased prevalence of broad minima in the regression space of higher dimensionality using SAFT-VR Mie, which as has already been discussed.
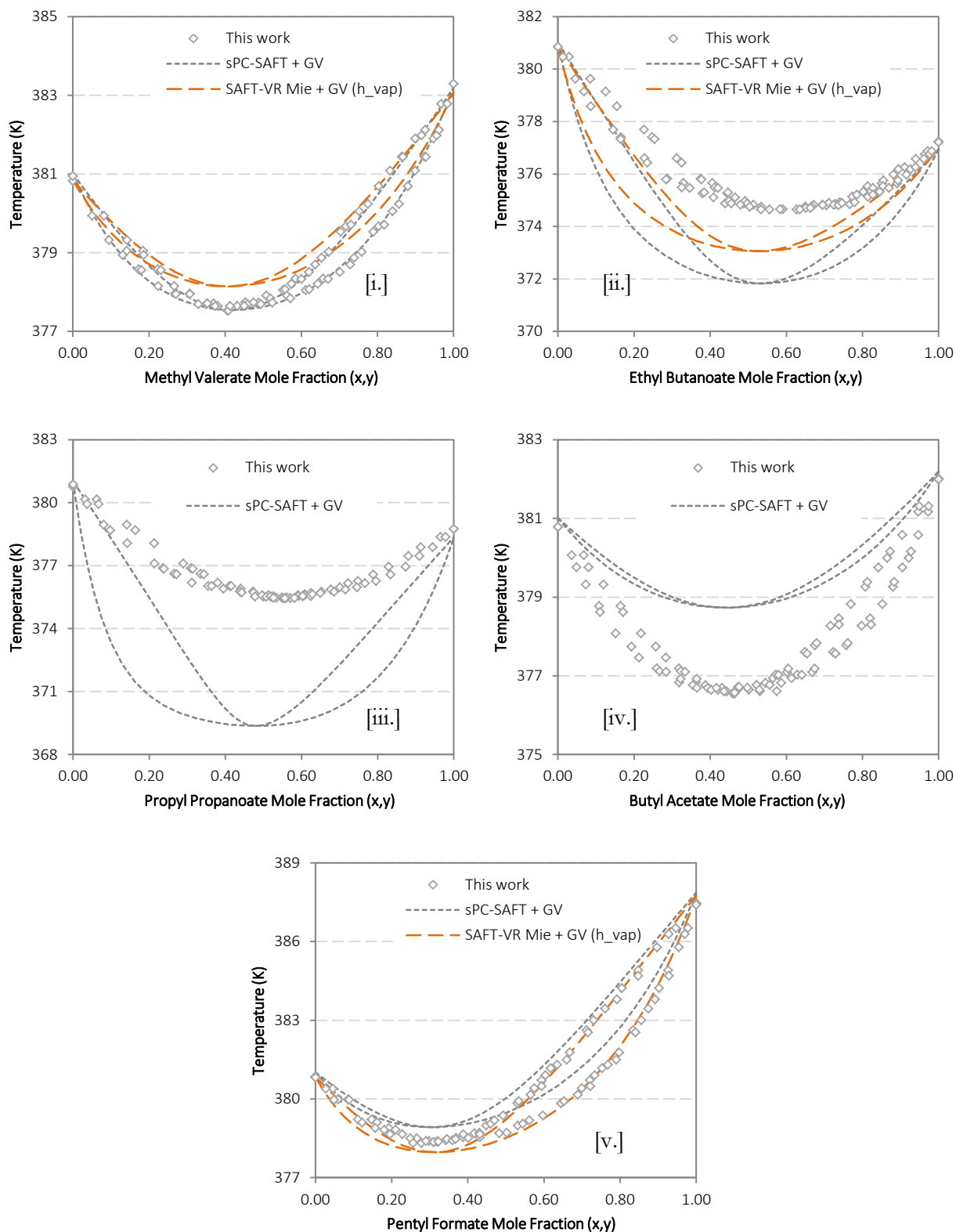
Figure 7.18: Comparison of the sPC-SAFT_GV and SAFT-VR Mie^GV predictions for the phase behaviour of [i.] methyl valerate, [ii.] ethyl butanoate, [iii.] propyl propanoate, [iv.] butyl acetate and [v.] pentyl formate with n-octane at 60.0 kPa (This work).

That polar SAFT-VR Mie could not make up for the deficiencies in describing the phase behaviour of polar structural isomers demonstrated in polar sPC-SAFT is a disappointing result, but one which demonstrates that the fault does not lie with the parent EoS. **Rather, it is inherently linked to the prominence of the dipolar behaviour and thus its description by the polar term as distinct from an equivalent nonpolar molecule.** Extension to the SAFT-VR Mie framework has also demonstrated the robustness of the GV polar term in a mathematically challenging regression space and clearly established its superiority over the JC polar term in this regard. This last point is notable as it addresses a primary aim of this study.

As with polar sPC-SAFT before it, the numerical difficulties of determining unique parameter sets in polar SAFT-VR Mie can be bypassed through incorporation of mixture phase behaviour in the regression function. The resulting optimum parameter sets were presented and used as reference earlier in this chapter. Though demonstrably accurate, a fundamental flaw in the process of determining these parameters is the need for reliable mixture data. In lieu of such data, it is necessary to improve the regression results based on pure component data alone.

7.6 Addressing the Dependence of Optimal Parameters on VLE Data

In the polar sPC-SAFT framework, the reliance of accurate parameter sets on incorporating mixture VLE data in the regression was mitigated by using the correlations of equations 5.2 and 5.3. These functional group specific, empirical correlations fix the values of the polar parameters to physically meaningful constant values, allowing the dimensionality of the regression space to be reduced. This allows for determination of the remaining nonpolar parameters by regression using pure component data alone. The success of this procedure was extensively demonstrated in Chapter 5, producing parameter sets exhibiting comparable predictions with those where VLE data were incorporated.

$$x_p = \frac{K}{\left(A \cdot M_w + B\right) \cdot \mu^2} \qquad \text{5.2}$$

$$n_p = \frac{K \cdot \left(A \cdot M_w + B\right)}{\mu^2} \qquad \text{5.3}$$

The dependence of these correlations on pure component properties alone (*viz.* molecular weight and dipole moment) suggests that employing this approach using polar SAFT-VR Mie is a viable alternative. In polar sPC-SAFT, the equivalent constants of equations 5.2 and 5.3 were fit to values of x_p and n_p that had been successfully regressed as a result of incorporating VLE data in the regression procedure. The details of this fitting procedure were given in Section 5.1.3. Extending this to polar SAFT-VR Mie means that these functional group specific constants require refitting using the successfully

regressed parameters of Tables 7.3 and 7.4. The results of this fitting procedure are presented in Table 7.11.

Table 7.11: Functional group specific constants determined for Equations 5.2 & 5.3 for polar SAFT-VR Mie

Variant	Group	*K*	*A*	*B*
SAFT-VR Mie^{JC}	Ketones	-	-	-
x_p	Esters	3.8062	0.01056	1.4819
	Ethers	1.0597	0.00668	1.9578
SAFT-VR Mie^{GV}	Ketones	4.3725	0.02014	1.0405
n_p	Esters	3.6506	0.00693	2.3156
	Ethers	1.9224	0.00587	2.0837

The inability to successfully determine unique SAFT-VR Mie^{JC} parameter sets for all but two of the ketones considered means that correlation constants could not be determined for this functional group. **This omission further reinforces the apparent superiority of the GV term over its JC counterpart in the SAFT-VR Mie framework**. With the constants of Table 7.11 successfully determined, polar SAFT-VR Mie parameter sets could be regressed with a fixed polar parameter.

7.6.1   Choice of Pure Component Properties

An alternative regression procedure once again raises the question of which pure component properties should be considered. In the case of polar sPC-SAFT, after fixing the value of the polar parameter, the remaining nonpolar parameters were fit to the standard combination of saturated vapour pressure, saturated liquid density and heat of vaporisation. This same procedure could be followed using polar SAFT-VR Mie, but a more promising alternative exists.

The incorporation of speed of sound data in the regression procedure has already shown to improve the description of this property by the resulting SAFT-VR Mie parameter sets. More importantly, this improved description of u^{liq} does not come at the expense of a notable loss in prediction accuracy of saturation properties and phase equilibria. Thus, the final polar SAFT-VR Mie regression alternative (Figure 7.1) is fixing the value of the polar parameter and regressing the nonpolar parameters using the following pure component properties with approximate regression weightings as indicated:

- saturated vapour pressures, P^{sat}, (4),
- saturated liquid densities, ρ^{sat}, (4), and
- speed of sound, u^{liq}, (1).

The demonstrated ability to use the speed of sound data of isomers when no such data are available for the component in question means that this regression procedure is applicable to the majority of the polar components of interest. A clear exception is the case of the ether components, for which the

lack of data has been discussed, and methyl formate which has no available u^{liq} data nor does it have any linear isomers. In these cases, the same procedure used for polar sPC-SAFT will be used, *viz.*:

- saturated vapour pressures, P^{sat}, (4),
- saturated liquid densities, ρ^{sat}, (2), and
- heats of vaporisation, H^{vap}, (1).

The resulting parameter sets for this regression alternative are listed in Table 7.12 for SAFT-VR Mie[JC] and in Table 7.13 for SAFT-VR Mie[GV]. Combined with the *"VLE"* parameter sets of Tables 7.3 and 7.4, these "*Correlation*" parameters represent the optimum parameter sets generated in this work. These two parameter sets are extensively applied to mixture data for phase equilibria and other thermodynamic properties in Chapter 8, where a detailed assessment of the predictive capacities of these models is performed.

7.6.2   Fixed x_p/n_p Parameter Sets

Table 7.12: "Correlation" SAFT-VR Mie^{JC} parameters for ketones, esters and ethers determined by fixing x_p according to equation 5.2.

	M_W	σ	m	ε/k	λ_a	λ_r	x_p	μ	P^{sat} *	ρ^{sat} *	u^{liq} †	H^{vap} *
	g.mol^{-1}	Å		K				D	AAD%	AAD%	AAD%	AAD%
Esters												
methyl formate	60.05	3.4617	2.0248	220.010	6	10.1708	0.5742	1.77	0.646	0.365	_^{a}	2.937
ethyl formate	74.08	3.7224	2.1468	264.689	6	11.7418	0.4513	1.93	0.814	0.483	0.397	2.982
methyl acetate	74.08	3.6334	2.2751	225.079	6	11.7172	0.5956	1.68	0.613	0.462	1.379	2.418
propyl formate	88.11	3.7861	2.4830	267.264	6	11.7890	0.4325	1.91	0.319	0.041	_^{a}	2.338
ethyl acetate	88.11	3.8449	2.4078	295.263	6	13.7644	0.4980	1.78	0.273	0.386	0.378	2.444
methyl propanoate	88.11	3.7792	2.4793	277.077	6	12.5843	0.5460	1.70	0.148	0.209	3.386	2.262
butyl formate	102.1	4.1453	2.3269	365.456	6	16.6977	0.3643	2.02	1.183	0.126	_^{a}	2.356
propyl acetate	102.1	3.9702	2.6012	312.972	6	14.3533	0.4640	1.79	0.345	0.229	1.803	3.152
ethyl propanoate	102.1	4.0606	2.4588	340.302	6	16.0320	0.4855	1.75	0.195	0.301	1.088	3.800
methyl butanoate	102.1	4.0274	2.4732	329.877	6	14.8501	0.5026	1.72	0.140	0.137	2.126	2.181
pentyl formate	116.2	4.2601	2.5354	380.295	6	17.3048	0.3892	1.90	0.812	1.155	_^{a}	1.288
butyl acetate	116.2	4.2030	2.5955	370.436	6	17.3950	0.4150	1.84	0.404	0.113	1.094	1.289
propyl propanoate	116.2	4.1905	2.5990	361.945	6	17.0019	0.4385	1.79	1.947	0.117	_^{a}	4.367
ethyl butanoate	116.2	4.4051	2.2844	387.611	6	17.0853	0.4289	1.81	1.205	0.617	0.916	2.233
methyl valerate	116.2	4.2663	2.4539	367.882	6	16.2246	0.5354	1.62	0.903	0.106	_^{a}	2.464
Ethers												
diethyl ether	74.12	3.7784	2.4826	245.136	6	12.1411	0.4812	1.15	0.337	0.236	_^{a}	1.900
di-n-propyl ether	102.18	4.3519	2.3350	355.558	6	17.0543	0.3504	1.21	0.214	0.405	_^{a}	1.121
butyl ethyl ether	102.18	4.2650	2.4785	351.041	6	17.4838	0.3446	1.22	1.172	0.590	_^{a}	7.681
dibutyl ether	130.23	4.3577	2.9356	363.617	6	17.3944	0.3139	1.17	0.505	0.572	_^{a}	1.550

† AADs in u^{liq} calaculated with reference to corresponding pure component data sets as indicated in Table 7.1

* AADs based on DIPPR Correlations

^{a} No AADs possible due to lack of published data

Table 7.13: "Correlation" SAFT-VR Mie^{GV} parameters for ketones, esters and ethers determined by fixing n_p according to equation 5.3.

	M_W g.mol^{-1}	σ Å	m	ε/k K	λ_a	λ_r	n_p	μ D	P^{sat} * AAD%	ρ^{sat} * AAD%	u^{liq} † AAD%	H^{vap} * AAD%
Ketones												
acetone	58.08	3.4290	2.4452	240.214	6	11.6448	1.1651	2.88	0.287	0.273	7.712	1.318
2-butanone	72.11	3.6138	2.6027	257.887	6	11.9565	1.4308	2.76	0.462	0.149	3.498	1.260
2-pentanone	86.13	3.8842	2.5546	309.096	6	14.2015	1.5814	2.77	0.121	0.368	4.043	2.698
3-pentanone	86.13	4.0097	2.3494	342.831	6	16.1235	1.5258	2.82	1.000	0.036	_ª	2.703
2-heptanone	114.1	4.0856	2.9591	331.839	6	14.4697	2.1428	2.61	0.302	0.052	1.440	1.854
3-heptanone	114.1	3.9978	3.0839	325.042	6	14.6525	1.8486	2.81	0.766	0.924	_ª	2.215
4-heptanone	114.1	4.3515	2.5258	390.102	6	18.0162	2.0323	2.68	0.307	0.069	_ª	1.023
Esters												
methyl formate	60.05	3.1099	2.5942	181.232	6	10.1684	3.1829	1.77	1.000	2.981	_ª	1.468
ethyl formate	74.08	3.5601	2.3787	259.101	6	13.0798	2.7723	1.93	0.617	1.075	2.814	2.287
methyl acetate	74.08	3.4420	2.5811	251.306	6	12.9906	3.6587	1.68	0.717	1.099	2.224	0.913
propyl formate	88.11	3.5942	2.8047	253.338	6	12.0292	2.9279	1.91	0.870	1.199	_ª	1.708
ethyl acetate	88.11	3.6430	2.7384	276.945	6	13.9637	3.3711	1.78	0.514	0.811	0.282	1.509
methyl propanoate	88.11	3.6282	2.7273	273.539	6	13.4408	3.6959	1.70	0.917	0.903	2.121	1.677
butyl formate	102.1	4.0182	2.5070	349.901	6	17.0089	2.7043	2.02	0.614	0.769	_ª	2.223
propyl acetate	102.1	3.8141	2.8611	298.740	6	14.4316	3.4440	1.79	0.648	0.629	1.979	2.544
ethyl propanoate	102.1	3.8377	2.8128	304.552	6	14.9307	3.6032	1.75	0.375	0.583	0.352	3.472
methyl butanoate	102.1	3.8523	2.7494	306.395	6	14.5124	3.7230	1.72	0.608	0.900	2.968	1.815
pentyl formate	116.2	4.1418	2.7116	363.389	6	17.1037	3.1226	1.90	0.804	0.636	_ª	1.499
butyl acetate	116.2	4.0617	2.8140	349.339	6	16.8933	3.3646	1.84	0.454	0.505	0.655	1.052
propyl propanoate	116.2	4.0945	2.7459	353.492	6	17.3547	3.5553	1.79	1.543	0.504	_ª	4.194
ethyl butanoate	116.2	4.3367	2.3711	378.372	6	17.5426	3.4771	1.81	0.779	0.126	0.552	2.282
methyl valerate	116.2	4.0648	2.7509	332.653	6	15.2902	4.3406	1.62	0.659	0.910	_ª	2.206
Ethers												
diethyl ether	74.12	3.7181	2.5763	237.444	6	12.0503	3.6616	1.15	0.408	0.633	_ª	1.695
di-n-propyl ether	102.18	4.3646	2.3167	357.437	6	17.3943	3.5238	1.21	0.147	0.538	_ª	1.026
butyl ethyl ether	102.18	4.2600	2.4820	349.730	6	17.6002	3.4662	1.22	1.082	0.658	_ª	7.597
dibutyl ether	130.23	4.3581	2.9326	363.107	6	17.4657	4.3989	1.17	0.572	0.646	_ª	1.464

† AADs in u^{liq} calaculated with reference to corresponding pure component data sets as indicated in Table 7.1

* AADs based on DIPPR Correlations

ª No AADs possible due to lack of published data

7.7 Chapter Summary

The aim of this chapter was the development of a new polar SAFT model using the newly proposed SAFT-VR Mie as a parent framework. Initially, the question of whether polar interactions needed to be explicitly accounted for using SAFT-VR Mie was conceptually addressed using the physical considerations of the model. Thereafter, the suitability of the Jog & Chapman and Gross & Vrabec polar terms being incorporated into this new framework was assessed and **the new SAFT-VR Mie[JC] and SAFT-VR Mie[GV] models were proposed**.

The effect of choosing different pure component properties to include in the parameter regression was assessed. While the use of saturation properties is considered standard, the role of speed of sound data in the SAFT-VR Mie framework was identified as a key factor in potentially setting the proposed models apart from their sPC-SAFT counterparts. The lack of pure component u^{liq} data available in the literature however, represented a potential hurdle to testing this hypothesis. To address this obstacle, using the speed of sound data of linear isomers as a pseudo pure component property for the regression of model parameters was shown to be a viable alternative in lieu of data for the component of interest.

The successful incorporation of mixture VLE data in the parameter regressions of polar sPC-SAFT in the previous chapter lead to similar regression procedures being considered here. The development of correlations for fixing the value of the polar parameters in the same vein as done by de Villiers (2011) was also proposed to provide an alternative for parameter regression using pure component data alone. The result was an extensive regression exercise producing up to *12* different parameter sets for a range of small to medium length ketones, esters and ethers, including those isomers of interest in earlier chapters and previous work.

Regression results demonstrated that the newly proposed polar **SAFT-VR Mie[GV] performs at least as well as its sPC-SAFT[GV] counterpart in the description of isomeric systems**. However, problems of parameter degeneracy and multiple minima were shown to be prevalent in the *Standard pure component regression* for the polar SAFT-VR Mie framework as well, most notably for SAFT-VR Mie[JC]. This served as confirmation that these regression problems are inherently linked to the polar terms considered, as suggested in the previous chapter. **The increased occurrence in SAFT-VR Mie[GV] however also suggests the problem is intrinsically linked to the dimensionality of the parameter space**. As with the polar sPC-SAFT framework, it was demonstrated that these problems could be circumvented by the *VLE* and *Correlation* regression procedures, for which optimum parameter sets were presented for a variety of components.

Having developed this new model framework in this chapter and put forward two sets of optimum parameters, the predictive capacity of SAFT-VR Mie[JC] and SAFT-VR Mie[GV] will be tested using a range of mixture data in the following chapter.

Chapter 8:   APPLICATION OF POLAR SAFT-VR MIE TO MIXTURE PROPERTIES

The merits and flaws of the respective "pure component" regression alternatives have been presented in Chapter 7, culminating in the *Correlation* parameter sets presented in Tables 7.12 and 7.13. In this chapter, predictions based on these parameter sets are compared to those of the optimum *VLE* parameter sets of Tables 7.3 and 7.4 with reference to experimental mixture data. This evaluation initially focuses on the prediction of mixture VLE to assess the validity of the polar parameter correlations of equations 5.2 and 5.3, and to determine whether these parameter sets are in fact comparable. The analysis is subsequently extended to other thermodynamic mixture properties to test the holistic predictive capacity of the newly proposed polar SAFT-VR Mie. Here, the applicability of the *VLE* and *Correlation* parameter sets are further tested, while the predictions of the polar SAFT-VR Mie models are also compared to their sPC-SAFT counterparts.

8.1 Vapour-Liquid Equilibrium

In this section, predictions for the phase equilibrium of a number of binary systems are considered using both *VLE* and *Correlation* parameter sets. These systems include those polar/n-alkane systems used to determine the parameters of Tables 7.3 and 7.4, as well as a number of other polar/n-alkane and polar/polar systems to test the applicability of these parameter sets beyond the systems to which the parameters were fit. The results are summarised in Table 8.1, where the equivalent results for nonpolar SAFT-VR Mie are provided for reference.

Application of Polar SAFT-VR Mie to Mixture Properties

Table 8.1: Summary of deviations in predictions of binary VLE using nonpolar SAFT-VR Mie and the VLE and Correlation variants of SAFT-VR Mie[GV] and SAFT-VR Mie[JC]

	T(K)/P(bar)	SAFT VR Mie Δy (x10²)[a]	SAFT VR Mie $\Delta P(\%)$[b]/$\Delta T(K)$[a]	SAFT VR Mie[GV] VLE Δy (x10²)[a]	VLE $\Delta P(\%)$[b]/$\Delta T(K)$[a]	Correlation Δy (x10²)[a]	Correlation $\Delta P(\%)$[b]/$\Delta T(K)$[a]	SAFT VR Mie[JC] VLE Δy (x10²)[a]	VLE $\Delta P(\%)$[b]/$\Delta T(K)$[a]	Correlation Δy (x10²)[a]	Correlation $\Delta P(\%)$[b]/$\Delta T(K)$[a]	Reference
Polar/Nonpolar Systems												
2-butanone/n-heptane	0.94 bar	8.31	4.26	0.94	0.28	1.39	0.39	1.15	0.29	-	-	Wisniak et al. (1998)
2-pentanone/n-heptane	353.15 K	4.53	9.61	0.34	0.76	0.78	1.69	-	-	-	-	Geiseler et al. (1968)
3-pentanone/n-heptane	313.15 K	6.41	12.30	1.41	4.69	2.06	2.69	-	-	-	-	Fuchs et al. (1984)
2-heptanone/n-nonane	0.40 bar	4.60	2.10	1.30	0.20	2.58	1.02	-	-	-	-	Cripwell et al. (2015)
3-heptanone/n-nonane	0.40 bar	2.14	1.22	1.94	1.09	0.81	0.38	1.33	1.22	-	-	Cripwell et al. (2015)
4-heptanone/n-hexane	338.15 K	0.85	8.26	0.27	4.26	0.26	2.62	-	-	-	-	Maripuri & Ratcliff (1972)
4-heptanone/n-nonane	0.40 bar	4.26	2.61	0.94	0.19	1.95	0.86	-	-	-	-	Cripwell et al. (2015)
methyl formate/n-heptane	1.013 bar	7.03	6.74	1.56	1.07	1.68	2.10	1.72	1.07	1.82	2.25	Ortega et al. (2003)
ethyl formate/n-heptane	1.013 bar	5.69	5.30	0.33	0.36	0.84	0.79	0.33	0.26	1.65	1.38	Ortega et al. (2015)
methyl acetate/n-heptane	1.013 bar	3.68	3.23	0.43	0.27	1.56	1.00	0.39	0.25	0.50	0.25	Fernández et al. (2013)
propyl formate/n-heptane	1.013 bar	2.18	2.61	0.29	0.26	0.57	0.43	0.34	0.34	0.26	0.64	Galvan et al. (1994)
ethyl acetate/n-heptane	1.013 bar	4.06	2.30	0.46	0.27	0.95	0.29	0.80	0.30	1.80	0.66	Fernández et al. (2010)
methyl propanoate/n-heptane	1.013 bar	2.07	2.09	1.69	0.65	2.66	1.15	1.41	0.75	2.02	0.84	Ortega et al. (2003)
butyl formate/n-heptane	1.013 bar	4.15	3.03	0.76	0.17	1.96	1.03	1.37	0.18	2.89	1.70	Ortega et al. (2015)
propyl acetate/n-heptane	1.013 bar	3.20	1.92	0.65	0.26	1.63	0.71	1.00	0.14	2.02	0.91	Fernández et al. (2013)
ethyl propanoate/n-heptane	1.013 bar	1.96	1.86	0.33	0.10	0.45	0.49	0.26	0.07	1.04	1.06	Ríos et al. (2014)
methyl butanoate/n-heptane	1.013 bar	2.16	2.33	0.23	0.62	0.46	0.80	0.22	0.64	0.98	1.35	Ríos et al. (2012)
pentyl formate/n-octane	0.60 bar	4.64	3.08	0.95	0.11	2.80	1.67	1.18	0.06	3.39	2.01	This work
butyl acetate/n-octane	0.60 bar	3.93	2.74	0.70	0.08	2.10	1.25	0.81	0.07	2.61	1.58	This work
propyl propanoate/n-octane	0.60 bar	3.05	2.12	0.64	0.14	1.35	0.59	-	-	1.82	0.89	This work
ethyl butanoate/n-octane	0.60 bar	3.69	2.23	0.91	0.10	1.89	0.79	0.98	0.20	2.73	1.43	This work
methyl valerate/n-octane	0.60 bar	3.68	2.08	1.06	0.09	1.04	0.09	1.21	0.07	2.21	0.80	This work
diethyl ether/n-pentane	1.013 bar	0.50	0.31	0.41	0.06	0.59	0.33	0.44	0.20	0.43	0.12	Klon-Palczewska et al. (1980)
diethyl ether/n-hexane	1.013 bar	0.50	0.17	0.66	0.40	1.09	0.77	0.78	0.54	0.70	0.46	Klon-Palczewska et al. (1980)
di-n-propyl ether/n-heptane	0.60 bar	1.01	0.54	0.73	0.06	0.79	0.10	0.71	0.05	0.88	0.38	This work
butyl ethyl ether/n-heptane	0.60 bar	0.84	0.46	0.34	0.05	0.37	0.06	0.41	0.93	0.64	0.27	This work
dibutyl ether/n-hexane	308.15 K	0.17	1.78	0.22	0.25	0.17	0.19	-	-	0.11	1.01	March et al. (1980)
Polar/Polar Systems												
dibutyl ether/2-heptanone	363.15 K	1.10	2.08	0.31	0.74	0.75	1.50	-	-	0.75	1.23	Wu & Sandler (1988)
dibutyl ether/3-heptanone	363.15 K	0.22	1.09	0.29	1.38	0.35	1.37	-	-	0.24	1.10	Wu & Sandler (1988)
dibutyl ether/4-heptanone	363.15 K	1.286	2.463	0.29	1.63	0.59	1.25	-	-	0.95	1.87	Wu & Sandler (1988)
ethyl formate/2-butanone	313.15 K	0.80	0.94	0.78	0.48	1.16	1.47	0.56	0.78	0.78	1.20	Macedo et al. (1984)
methyl acetate/ethyl acetate	353.15 K	0.39	1.07	0.15	0.56	0.25	1.47	0.15	0.40	0.15	0.40	Lee et al. (1997)
ethyl acetate/butyl acetate	1.013 bar	1.61	1.69	0.48	0.43	0.43	0.38	0.44	0.32	0.48	0.45	Shono & Kanazawa (1969)
acetone/dibutyl ether	1.013 bar	0.74	0.41	0.85	0.77	0.86	0.55	-	-	1.69	4.94	Resa et al. (1999)
acetone/2-butanone	3.447 bar	1.46	0.42	1.76	0.54	1.72	0.46	0.60	1.34	1.60	0.46	Othmer et al. (1952)
acetone/3-pentanone	1.013 bar	0.48	0.58	0.57	0.59	0.96	0.87	-	-	3.75	3.34	Glukhareva et al. (1974)

[a] $\Delta z = \sum_i^{np} \left| z_i^{calc} - z_i^{exp} \right|$ where z is y or T and np is the number of data points. [b] Deviations as %AAD

The phase equilibrium prediction results can be systematically assessed by considering the same homologous group basis followed in previous chapters. Beginning with the ketones, the deviations for the *VLE* and *Correlation* parameter sets are clearly comparable in Table 8.1. This is supported by the plots for the representative 3-pentanone/n-heptane and 4-heptanone/n-nonane systems in Figures 8.1 [i.] and [ii.], where the superiority of SAFT-VR Mie[GV] is clearest. The predictions of both the *VLE* and *Correlation* parameter sets are not only comparable, but in good agreement with the experimental data. For SAFT-VR Mie[JC] on the other hand, the lack of parameters for the ketone functional group in Table 7.12 necessarily implies that no predictions for mixture properties can be made using this regression alternative.
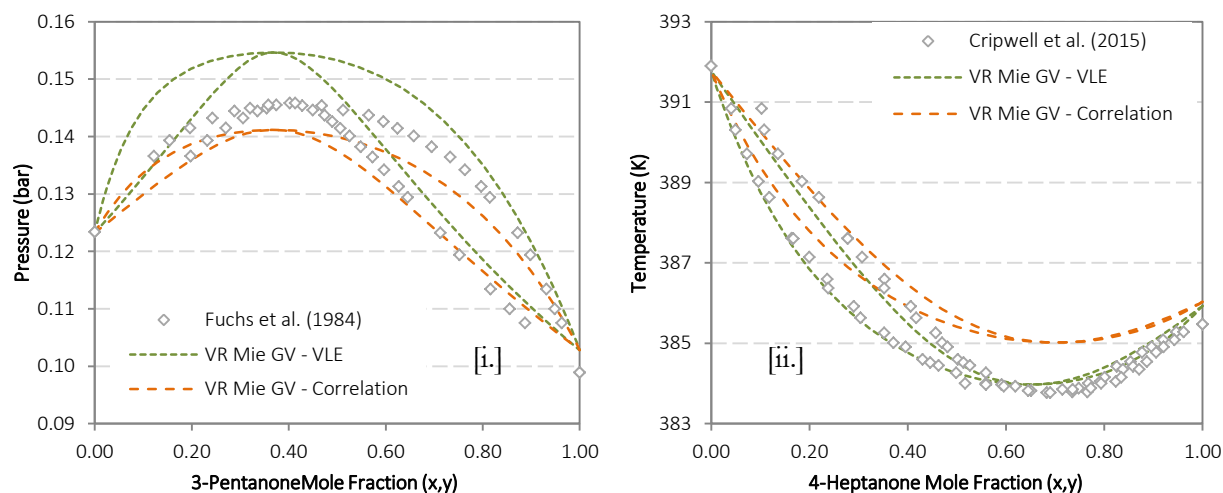
Figure 8.1: Comparison of the "VLE" and "Correlation" parameter set predictions using the SAFT-VR Mie[GV] model – application to VLE of ketone/alkane mixtures: [i.] 3-pentanone/n-heptane at 313.15 K and [ii.] 4-heptanone/n-nonane at 40.0 kPa.

Consideration of the ester functional group allows for comparison between polar variants, as well as between regression procedures. The deviations in Table 8.1 suggest that for both polar variants, predictions of the *Correlation* parameter sets do not show significant deviation from the optimum *VLE* parameters. As with the ketones, representative examples are plotted in Figures 8.2 [i.] to [iv.].

Application of Polar SAFT-VR Mie to Mixture Properties
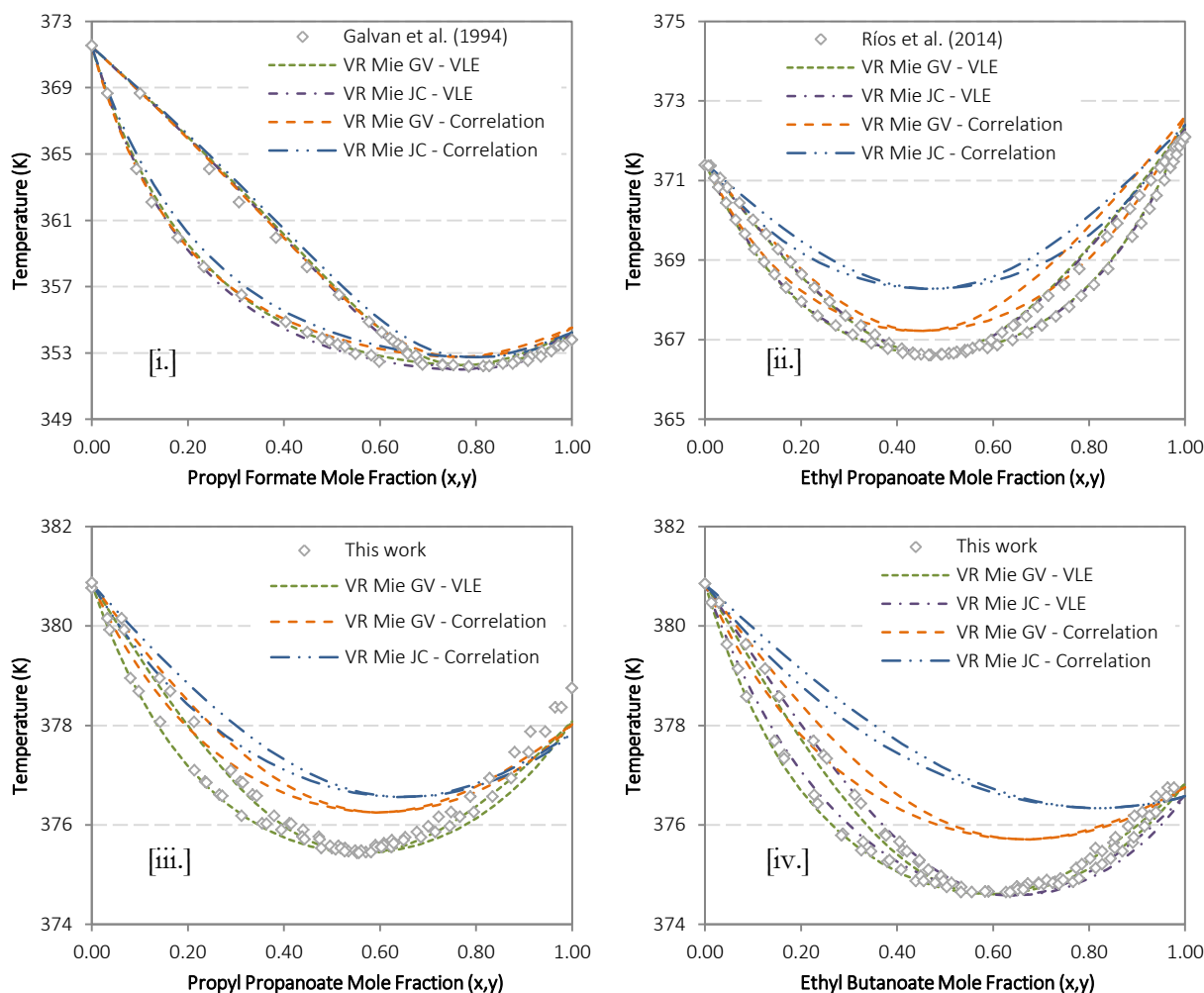
Figure 8.2: Comparison of the "VLE" and "Correlation" parameter set predictions using the SAFT-VR Mie^{GV} and SAFT-VR Mie^{JC} models – application to VLE of ester/alkane mixtures: [i.] propyl formate/n-heptane at 101.3 kPa, [ii.] ethyl ropanoate/n-heptane at 101.3 kPa, [iii.] propyl propanoate/n-octane at 60.0 kPa and [iv.] methyl valerate/n-octane at 60.0 kPa.

In all cases, the *VLE* parameter sets of both SAFT-VR Mie^{GV} and SAFT-VR Mie^{JC} necessarily fit the experimental data best, having been considered in the regression of the parameters to begin with. The case of propyl formate/n-heptane in Figure 8.2 [i.] shows that the predictions of the *Correlation* parameter sets show negligible deviations from their optimum *VLE* equivalents in azeotropic systems established over larger temperature ranges. The discrepancies between the *VLE* and *Correlation* parameter predictions are more notable in Figures 8.2 [ii.] to [iv.], where the azeotropic phase envelope is established in a much smaller temperature range, providing a more stringent test of the predictive capacity. The n_p *Correlation* predictions for SAFT-VR Mie^{GV} exhibit only small deviations from the data and the *VLE* parameter fits, in keeping with the trends seen for ketones previously – the azeotropic compositions are well correlated, even if the azeotropic temperatures are slightly over predicted in all three cases. The equivalent x_p *Correlation* predictions for SAFT-VR Mie^{JC} exhibit much larger deviations; the prediction of the ethyl butanoate/n-octane system (Figures 8.2 [iv.]) is particularly notable in this respect as the predicted azeotropic point is far removed from the experimental value. The method is validated by the prediction of the propyl propanoate/n-octane system (Figures 8.2 [iii.]) however, as the inability to regress a unique *VLE* parameter set for this component meant that no SAFT-VR Mie^{JC} prediction for this system would be

possible. In light of this, the x_p *Correlation* prediction provides a fair description of a difficult system, even if the prediction remains inferior to its SAFT-VR Mie^{GV} counterpart.

Comparison of the *VLE* and *Correlation* parameter predictions for ether systems yields similar results to that seen for esters, with smaller differences in the model predictions for these systems. The diethyl ether/n-pentane and butyl ethyl ether/n-heptane system are given in Figures 8.3 [i.] and [ii.] as representative systems, where the former offers a particularly rigorous test of the model performance. Here, the deviation of the n_p *Correlation* prediction from its *VLE* prediction counterpart is larger than that for the x_p *Correlation* prediction, but given the temperature range of the system, all four predictions can be considered excellent. The x_p *Correlation* prediction of the butyl ethyl ether/n-heptane system exhibits the same tendency as the *Standard pure component regression,* where a near ideal prediction is in evidence that oversights the experimental phase envelope.

Figure 8.3: Comparison of the "VLE" and "Correlation" parameter set predictions using the SAFT-VR Mie^{GV} and SAFT-VR Mie^{JC} models – application to VLE of ether/alkane mixtures: [i.] diethyl ether/n-pentane and [ii.] butyl ethyl ether/n-heptane.

Figures 8.1 to 8.3 clearly demonstrate that the *VLE* and *Correlation* parameter sets are suitable for the prediction of polar/n-alkane mixture VLE, but their applicability to other industrially relevant mixtures needs to be tested. In Figures 8.4 [i.] to [iv.], these parameter sets are used to predict the experimental phase behaviour of the three binary systems comprising dibutyl ether and one of the three heptanone isomers. The analysis is necessarily limited to the predictions of the SAFT-VR Mie^{GV} alternatives, with the data presented on the same scale axes in Figures 8.4 [i.] to [iii.]. An appropriately scaled representation of the 4-heptanone/dibutyl ether system is given in Figures 8.4 [iv.]. The model predictions are in excellent agreement with the experimental data, with the exception of the n_p *Correlation* prediction of the 2-heptanone system, where the presence of azeotrope in the low 2-heptanone concentration region is not predicted by the model. Both the *VLE* and *Correlation* predictions of the 4-heptanone system are shifted from the data, but given the narrowness of the phase envelope and the small (*4* kPa) pressure range, the predictions can still be considered excellent. Accurate prediction of these systems further serves to show that both regression alternatives, and in particular the case of fixing n_p,

yield SAFT-VR Mie^{GV} parameter sets capable of differentiating between the phase behaviour of different structural isomers.
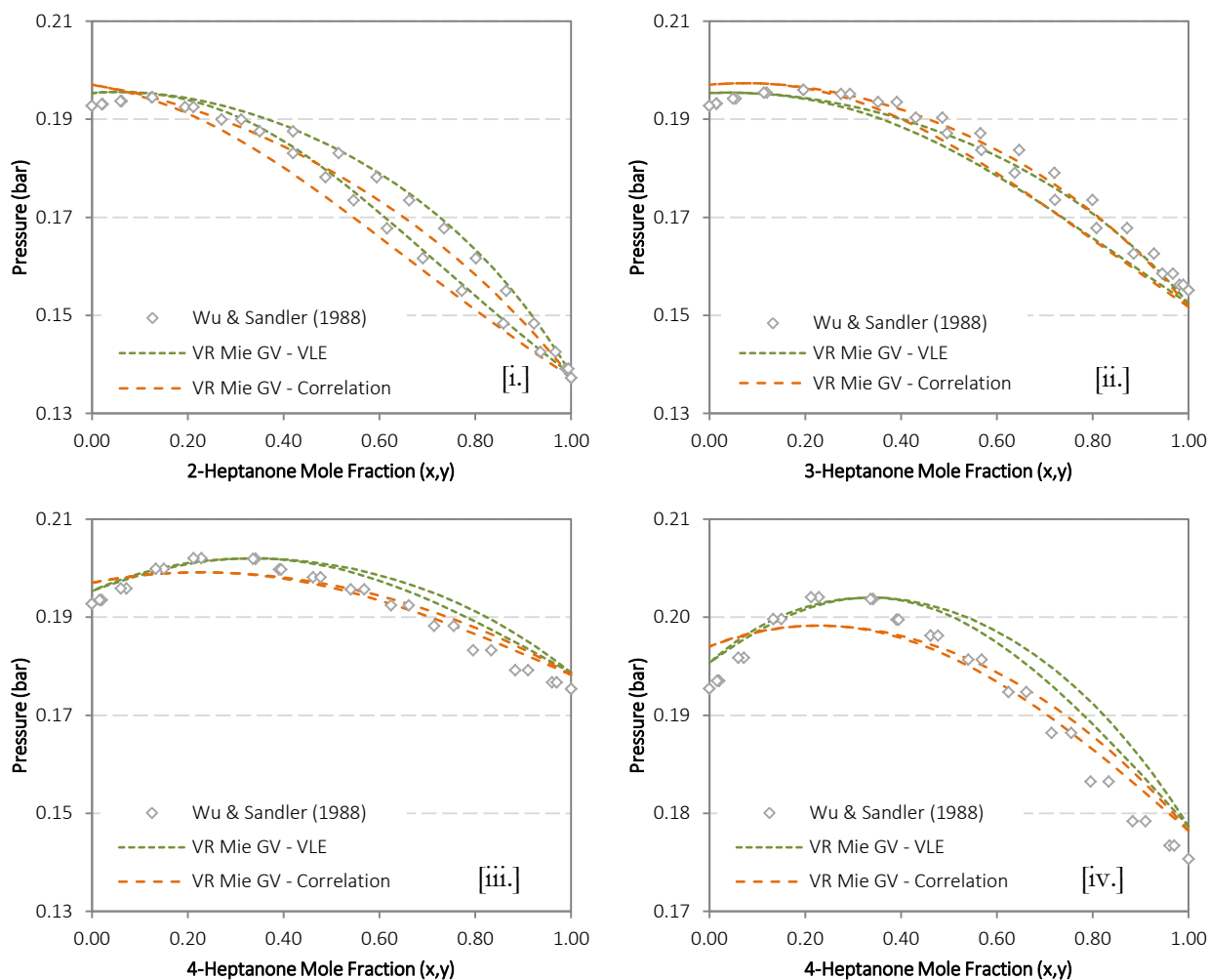
Figure 8.4: Comparison of the "VLE" and "Correlation" parameter set predictions using the SAFT-VR Mie^{GV} model – application to VLE of x-heptanone/dibutyl ether mixtures: [i.] 2-heptanone/dibutyl ether, [ii.] 3-heptanone/dibutyl ether, [iii.] and [iv.] 4-heptanone/dibutyl ether at 363.15 K.

Applicability of the regressed ester parameters beyond polar/n-alkane systems is tested in the representative ethyl formate/2-butanone and ethyl acetate/butyl acetate systems in Figures 8.5 [i.] and [ii.] respectively. The phase behaviour of both systems is well predicted by all applicable parameter sets, although the lack of x_p *Correlation* parameters for 2-butanone once again limit the applicability of the SAFT-VR Mie^{JC} model. These results, combined with those of Figure 8.4, demonstrate the applicability of polar SAFT-VR Mie parameters beyond the simple polar/n-alkane mixtures considered in their regression.
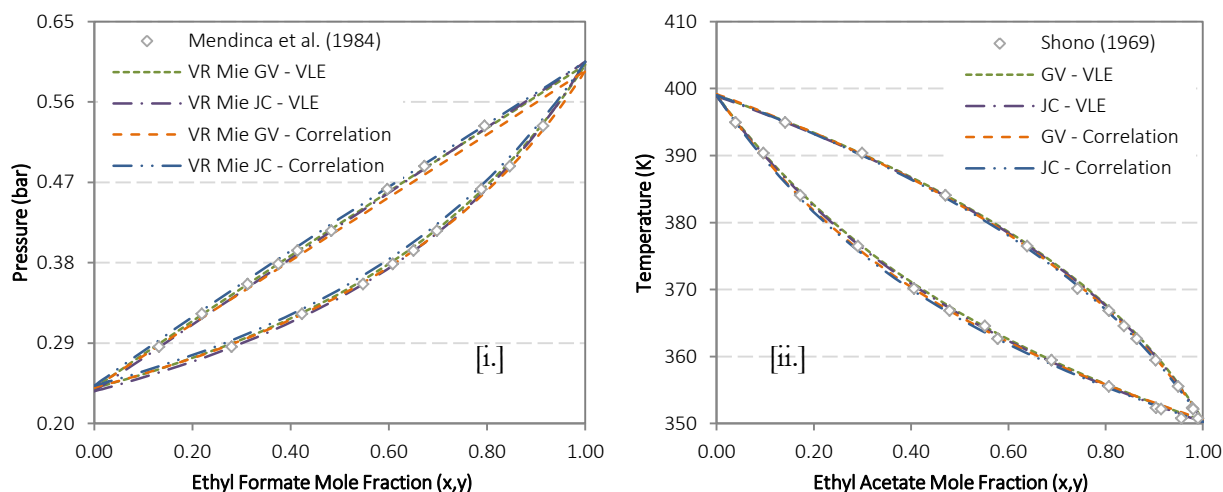
Figure 8.5: Comparison of the performance of the optimum parameter set fit to VLE data and that regressed using the polar parameter correlations – application to VLE of polar/polar mixtures: [i.] ethyl formate/2-butanone at 313.15 K and [ii.] ethyl acetate/butyl acetate 101.3 kPa.

Accurate description of mixture phase equilibria is of primary importance in assessing the performance of thermodynamic models. The results of this section show polar SAFT-VR Mie to be an accurate and predictive thermodynamic model on par with polar sPC-SAFT for the description of mixture phase behaviour. **Further, the comparable predictions of the *VLE* and *Correlation* parameter sets serve not only to validate the *Correlation* regression procedure, but also prove it to be a viable alternative for parameter determination for components for which there are no experimental VLE data available.**

The success of the predictions of the *Correlation* parameter sets are all the more important when the nature of the regression procedure is considered. The inclusion of pure component speed of sound data served only to deteriorate the predictive capacity of polar sPC-SAFT when mixture phase behaviour is considered, but the integrity of polar SAFT-VR Mie's predictions is maintained here. SAFT-VR Mie's ability to predict speed of sound and other derivative properties has been a constant thread in the development of polar SAFT-VR Mie in this work. Thus, testing the proposed polar model's ability to accurately predict speed of sound in polar mixtures is the logical next step in assessing the predictive capacity of the model.

8.2 Speed of Sound

Compared to the amount of published pure component data, there is a relative abundance of mixture speed of sound data for polar components of interest to this study. In this section, the same *VLE* and *Correlation* parameter sets used for the successful description of mixture phase behaviour are used for the prediction of ultrasonic speed in these polar mixtures. The results are summarised in Table 8.2 below.

Table 8.2: Summary of AADs for model predictions of speed of sound in polar/n-alkane mixtures. Both the "VLE" and "Correlation" parameter sets for polar SAFT-VR Mie are considered as indicated.

	SAFT-VR Mie	sPC-SAFT$_{GV}$	SAFT-VR Mie^{GV}		sPC-SAFT$_{JC}$	SAFT-VR Mie^{JC}		Reference
			VLE	Corr		VLE	Corr	
Ketone Systems								
acetone/n-hexane	1.90	7.65	5.26	4.22	7.21	-	-	Marino et al. (2001)
2-butanone/n-heptane	0.90	9.10	1.62	1.95	8.82	1.95	-	Ohomuro et al. (1987)
3-pentanone/n-heptane	2.85	10.84	2.21	1.97	10.60	-	-	Ohomuro et al. (1987)
Ester Systems								
methyl acetate/n-heptane	0.88	11.04	3.80	1.97	10.72	3.02	2.34	Sastry et al. (1999)
ethyl acetate/n-hexane	1.98	10.12	0.99	0.49	9.78	1.14	0.75	Acosta et al. (2001)
methyl propanoate/n-heptane	2.08	11.17	5.00	1.93	10.87	4.16	2.34	Sastry et al. (1999)
ethyl propanoate/n-heptane	0.40	11.62	3.02	1.19	11.48	1.77	0.65	Sastry et al. (1999)
methyl butanoate/n-heptane	0.67	12.18	3.66	1.93	11.57	2.27	1.35	Sastry et al. (1999)
butyl acetate/n-heptane	2.09	11.83	1.83	1.02	11.53	1.59	1.41	Sastry et al. (2009)
ethyl butanoate/n-heptane	1.08	12.28	6.58	0.82	11.65	2.89	0.91	Sastry et al. (1999)
Ether Systems								
diethyl ether/n-hexane	1.31	9.53	1.89	2.24	9.29	1.67	1.63	Canosa et al. (1999)
di-n-propyl ether/n-heptane	0.65	12.07	0.81	0.76	11.94	2.57	0.75	Ohomuro et al. (1987)

In Figures 8.6 to 8.11 that follow, the predictions of the optimum *VLE* parameter sets initially compared to their polar sPC-SAFT equivalents. The polar sPC-SAFT parameters are those determined by de Villiers (2011) which were similarly determined by incorporating mixture VLE data in their regression. Thereafter, the effect of incorporating pure component u^{liq} data in the *Correlation* regression procedure is considered by comparing the *VLE* and *Correlation* predictions directly.
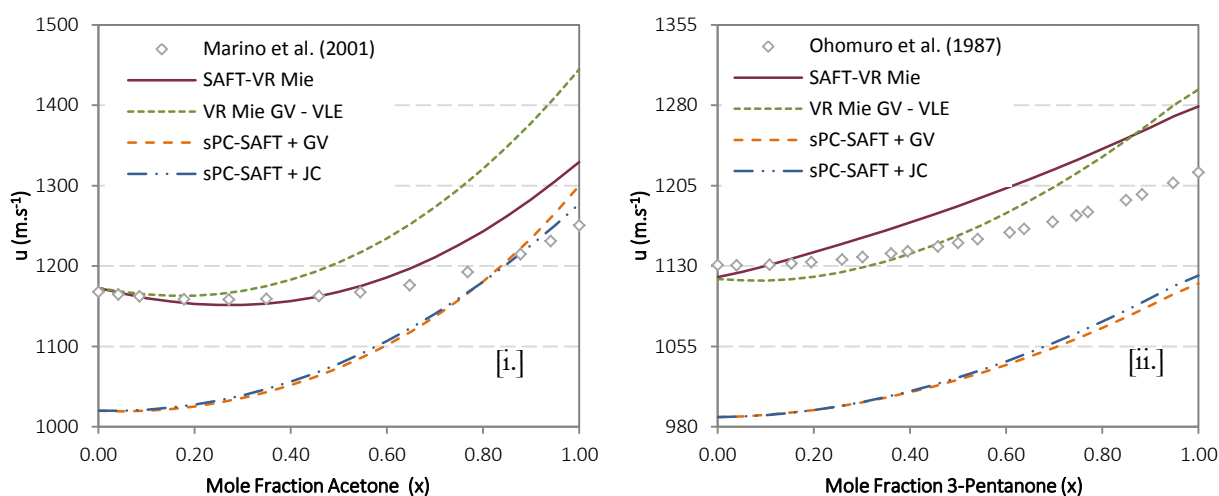
Figure 8.6: Predictions of mixture speed of sound using polar sPC-SAFT and polar SAFT-VR Mie– application to ketone/alkane mixtures: [i.] acetone/n-hexane at 273.15K and [ii.] 3-pentanone/n-heptane at 298.15K.

Figures 8.6 [i.] and [ii.] compare the polar SAFT-VR Mie models with their sPC-SAFT counterparts for the speed of sound in ketone mixtures. The case of acetone is particularly interesting as the prediction quality varies distinctly over the composition range. The alkane rich region is well correlated by the SAFT-VR Mie variants, but the prediction quality decreases as the acetone concentration increases. The pure acetone property is surprisingly best correlated by the sPC-SAFT variants, while incorporation of the GV polar term results in a worsened prediction compared to nonpolar SAFT-VR Mie. As the AADs of Table 8.2 and subsequent figures show however, acetone proves to be the exception to the trend.

Figure 8.6 [ii.] for the 3-pentanone/n-heptane system is more representative of this predictive trend, where there is notable improvement in the prediction quality of polar SAFT-VR Mie compared to polar sPC-SAFT. Incorporation of the polar term allows for the curvature apparent in the data to be better captured by the model compared to the nonpolar variant, even if the prediction of the pure ketone value is slightly worse. **It should be noted that these predictions are the result of parameter sets regressed without consideration of u^{liq}. Thus the innate superiority of SAFT-VR Mie in the prediction of speed of sound is highlighted and shown to be unaffected by inclusion of the polar term.**
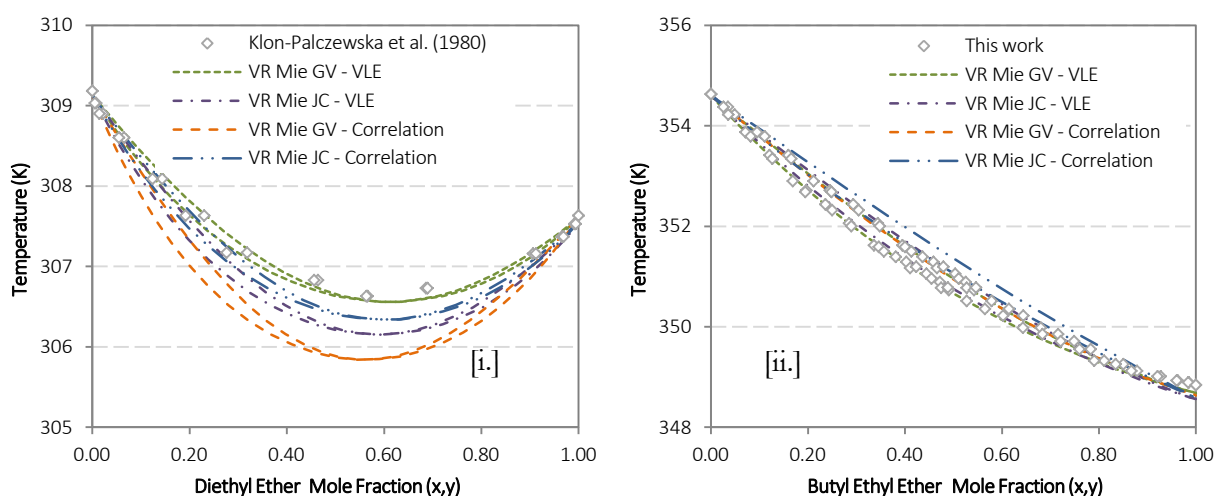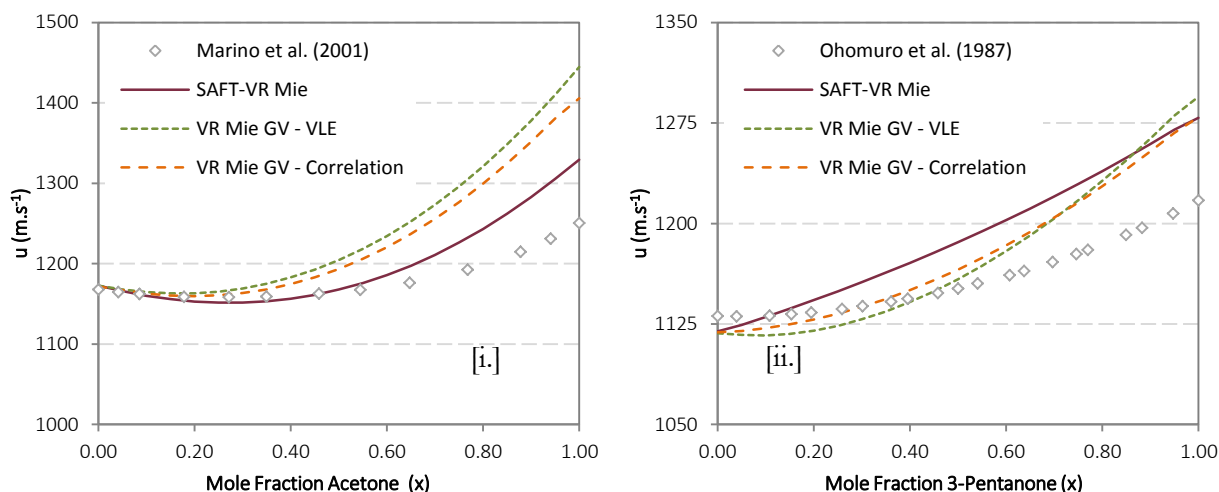

Figure 8.7: Comparison of the "VLE" and "Correlation" parameter set predictions using the SAFT-VR Mie^{GV} model – application to speed of sound of ketone/alkane mixtures: [i.] acetone/n-hexane at 273.15K and [ii.] 3-pentanone/n-heptane at 298.15K.

The effect of incorporating pure component u^{liq} data in the *Correlation* regression procedure on the prediction quality is demonstrated for the same two ketone systems in Figures 8.7 [i.] and [ii.]. In both systems, the model prediction is brought into closer agreement with the experimental data by using these parameter sets. Indeed, for the 3-pentanone/n-heptane system, the pure ketone property is correlated with the same accuracy as the nonpolar SAFT-VR Mie variant, but the curvature of the data is correctly captured by the polar model. Considered in conjunction with the successful VLE prediction in Figure 8.1 [i.], and the fact that the parameters were fitted to pure component data alone, the predictive promise of SAFT-VR Mie^{GV} is demonstrated in these ketone systems.

Application of Polar SAFT-VR Mie to Mixture Properties

The ester functional group allows for a more extensive analysis to be performed. Predictions of the *VLE* parameter sets of SAFT-VR Mie[GV] and SAFT-VR Mie[JC] are compared to their polar sPC-SAFT counterparts in the four representative systems of Figures 8.8 [i.] to [iv.]. These representative systems allow us to assess the model predictions applied to the range of molecular weights of linear esters under consideration, different functional group locations as well as differences between structural isomers. Across all four figures, a notable result is the significant improvement of prediction quality for the SAFT-VR Mie models compared to the sPC-SAFT equivalents; the latter clearly capture the trends but are consistently shifted quantitatively.

Figure 8.8: Predictions of mixture speed of sound using polar sPC-SAFT and polar SAFT-VR Mie– application to ester/alkane mixtures: [i.] methyl acetate/n-heptane at 298.15K, [ii.] ethyl propanoate/n-heptane at 308.15K, [iii.] ethyl butanoate /n-heptane at 308.15K, and [iv.] butyl acetate/n-hexane at 298.15K.

The esters also allow for direct comparison of the two polar SAFT-VR Mie models, which was not possible for ketones previously. Such a comparison suggests that the predictions of SAFT-VR Mie[JC] are marginally better than for SAFT-VR Mie[GV], although a similar analysis of the sPC-SAFT predictions yields the same conclusions. As with the ketones, inclusion of the polar term appears to worsen the correlation of the pure ester property, but allows for more accurate description of the curvature in the mixture space. This is particularly notable in the ethyl butanoate/n-heptane system of Figure 8.8 [iii.] where the nonpolar SAFT-VR Mie prediction is quantitatively much more accurate than

SAFT-VR Mie[GV]'s prediction, but the polar model captures the presence of the property minimum. Indeed, the minimum is well over predicted, but as with acetone previously, this case is the exception to the rule.

Comparing the results of the *VLE* and *Correlation* predictions for the same ester systems in Figures 8.9 [i.] to [iv.] shows a more significant improvement in the prediction quality using the latter parameter set. This improvement is more pronounced than was the case for the two ketone systems, most notably for the n_p *Correlation* predictions of the ethyl butanoate/n-heptane (Figure 8.9 [iii.]) and butyl acetate/n-heptane (Figure 8.9 [iv.]) systems. The case of ethyl butanoate demonstrates the significance of being able to use speed of sound data of isomers in the regression procedure; without following this procedure, the relatively poor *VLE* parameter set prediction would offer the best hope of a simultaneous prediction of both phase equilibrium and speed of sound in mixtures. The drastic difference in curvature also illustrates the complexity in describing u^{liq} of mixtures, despite the similarity of the *VLE* and *Correlation* parameter sets themselves.
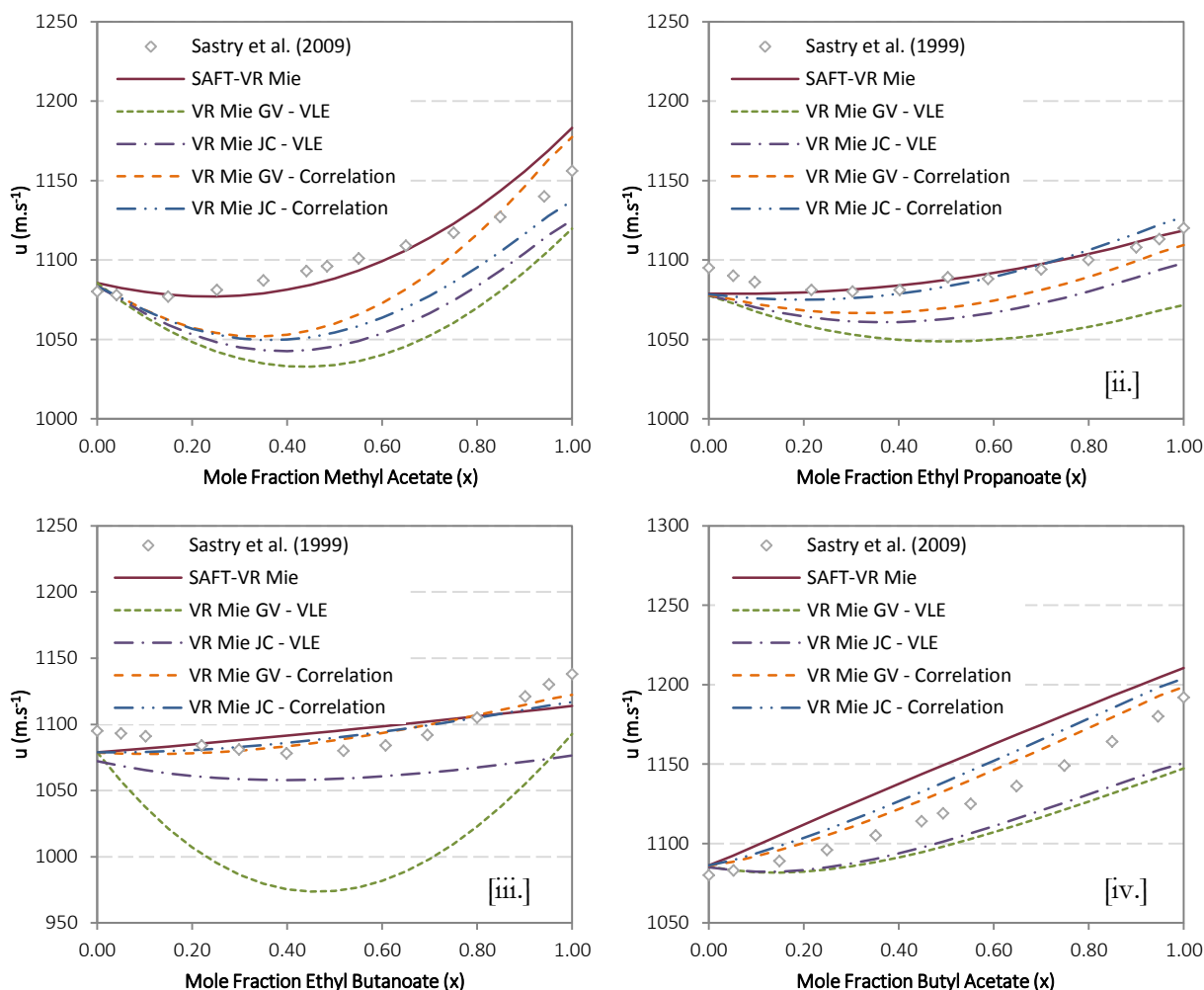
Figure 8.9: Comparison of the "VLE" and "Correlation" parameter set predictions using the SAFT-VR Mie[GV] and SAFT-VR Mie[JC] models – application to speed of sound of ester/alkane mixtures: [i.] methyl acetate/n-heptane at 298.15K, [ii.] ethyl propanoate/n-heptane at 308.15K, [iii.] ethyl butanoate /n-heptane at 308.15K, and [iv.] butyl acetate/n-hexane at 298.15K.

While the lack of pure ether u^{liq} data has already been highlighted, there are some mixture data available in the literature with which to compare the model predictions. Figures 8.10 [i.] and [ii.] illustrate that the same innate superiority of the SAFT-VR Mie models over their sPC-SAFT counterparts in predicting speed of sound data is maintained for this functional group. The plots further highlight the small influence of the ether functional group, with the polar predictions yielding much more similar results to the nonpolar case than for the ketones and esters previously.
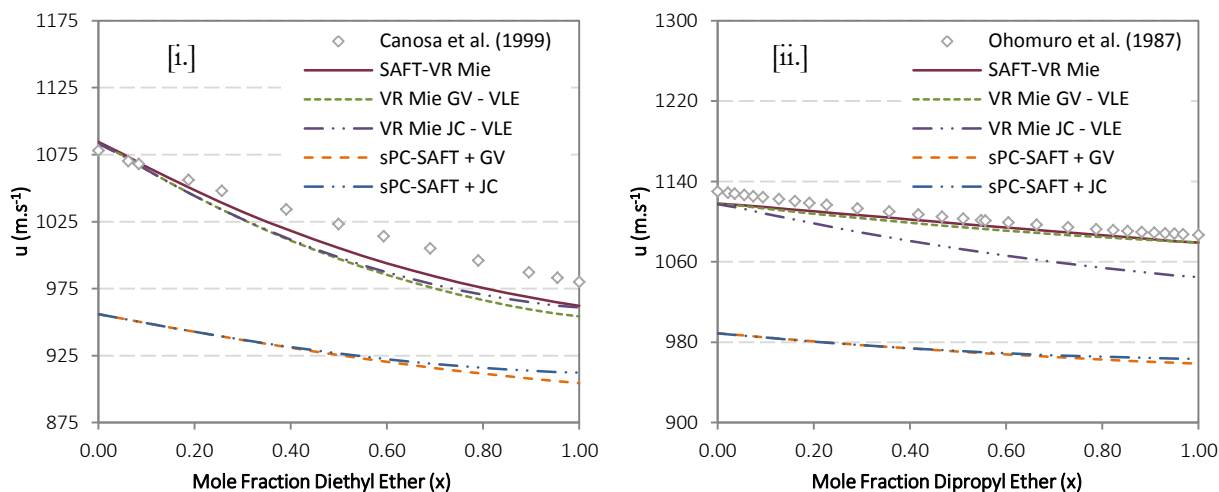
Figure 8.10: Predictions of mixture speed of sound using polar sPC-SAFT and polar SAFT-VR Mie– application to ether/alkane mixtures: [i.] diethyl ether/n-heptane at 298.15K and [ii.] di-n-propyl ether/n-heptane at 298.15K.

For the ketones and esters previously, notable improvement in mixture speed of sound predictions were apparent as a result of including u^{liq} data in the *Correlation* parameter regression. The lack of pure ether u^{liq} data necessitated that the *Correlation* fits for this functional group be fitted to heat of vaporisation data instead. The necessary change in regression procedure does not negatively affect the prediction quality however, as shown in Figures 8.11 [i.] and [ii.], where we see near identical predictions for the *Correlation* parameter sets as for the *VLE* sets. **This is still an important result however; it shows that the prediction integrity, for both speed of sound and phase equilibrium, can be maintained using only pure component saturation properties without the need for mixture phase equilibria data.**

Figure 8.11: Comparison of the "VLE" and "Correlation" parameter set predictions using the SAFT-VR Mie^{GV} and SAFT-VR Mie^{JC} models – application to speed of sound of ether/alkane mixtures: [i.] diethyl ether/n-heptane at 298.15K and [ii.] di-n-propyl ether/n-heptane at 298.15K.

8.3 Excess Properties

The results of the previous section clearly demonstrate the superiority of the polar SAFT-VR Mie models over their polar sPC-SAFT counterparts in the description of mixture speed of sound. Considered in conjunction with the phase equilibrium results of Section 8.1, the advantage of using a polar SAFT-VR Mie EoS for application to the properties of real fluid mixtures becomes apparent. However, it is important to remember the fundamental basis upon which the success of SAFT-type modelling has been based. An improvement in the prediction of one property at the expense of another does not mean that the model has been improved – even a completely empirical model can fit one property well. Thus, while it is not the focus of the work presented here, it is necessary to assess the application of the new model framework to other important thermodynamic properties of mixtures such as excess properties. Indeed, such an analysis has yet to be performed for real fluids using the SAFT-VR Mie EoS.

The purpose of the following sections is thus to perform a preliminary analysis of the predictive capacity of the proposed polar SAFT-VR Mie models. The aim of these analyses is to assess the holistic predictive capacity of polar SAFT-VR Mie using polar sPC-SAFT as a benchmark. The viability of the parameters resulting from the *Correlation* regression procedure are also further tested, using the *VLE* parameter predictions as a similar reference.

8.3.1   Excess Enthalpy

Assessing the interconnectivity of thermodynamic properties in Figure 7.1 shows that excess enthalpy provides a good indication of the temperature dependence of the system Helmholtz energy. More specifically, this property is defined as per equations 8.1 and 8.2, which are an extension of the framework of Michelsen & Mollerup (2007), with $F = A^r/NkT$:

Application of Polar SAFT-VR Mie to Mixture Properties

$$H^{ex} = H^{res}\left(T,P,\mathbf{n}\right) - \sum_{i=1}^{nc} H_i^{res}\left(T,P,n_i\right) \tag{8.1}$$

$$H^{res}\left(T,P,\mathbf{n}\right) = -RT^2\left(\frac{\partial F}{\partial T}\right)_{V,\mathbf{n}} + PV - nNkT \tag{8.2}$$

Equation 8.2 in particular shows that accurate description of mixture excess enthalpy is strongly dependent on the accurate model description of the temperature dependence of F. Thus, an assessment of the model predictions of excess enthalpy will provide some insight into how the SAFT-VR Mie framework models the F-T relationship and test the accuracy of this representation.

The acetone/n-hexane and 3-heptanone/n-heptane systems are used as representative examples for the ketone functional group, with the corresponding sPC-SAFT and SAFT-VR Mie predictions plotted in Figures 8.12 [i.] and [ii.]. These systems account for both the size distribution of the ketones, as well as the relative strength of the dipolar interactions of the components of interest to this study. The difference between the nonpolar SAFT-VR Mie prediction and those of the other four models clearly demonstrates the need to explicitly account for dipolar interactions to account for H^{ex} in these ketone/alkane mixtures. This large discrepancy comes as a result of the interactional contribution to H^{ex} arising from the significant difference between like and unlike energetic interactions (Costas & Patterson, 1987).
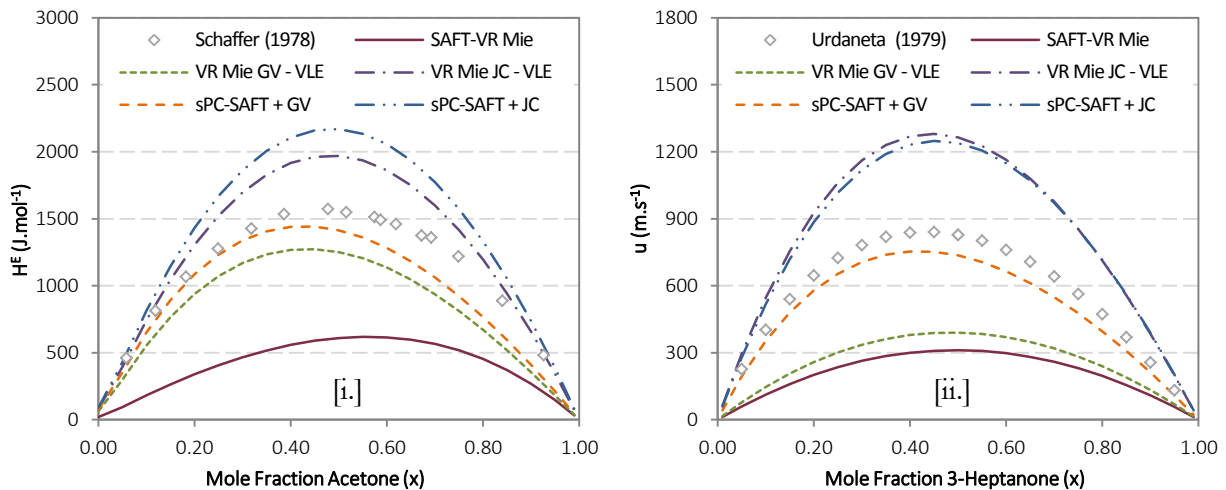
Figure 8.12: Predictions of mixture excess enthalpy using polar sPC-SAFT and polar SAFT-VR Mie– application to ketone/alkane mixtures: [i.] acetone/n-hexane at 293.15K and [ii.] 3-heptanone/n-heptane at 298.15K.

The choice of dipolar term, rather than model framework, appears to have the largest effect on the prediction accuracy, with the sPC-SAFT and SAFT-VR Mie version of the respective polar terms exhibiting similar predictions. It is further evident that the predictions of the GV variants are more accurate than their JC counterparts, although the SAFT-VR Mie[GV] prediction of the 3-heptanone/n-heptane system appears to contradict this observation. This exception is readily explained by considering the parameter set for this system (Table 7.4), and in particular the value of n_p itself: the

regressed value of *0.6449* is notably different to the typical value of *~1.8* seen for the other components and this clearly diminishes the predicted influence of the polar group.
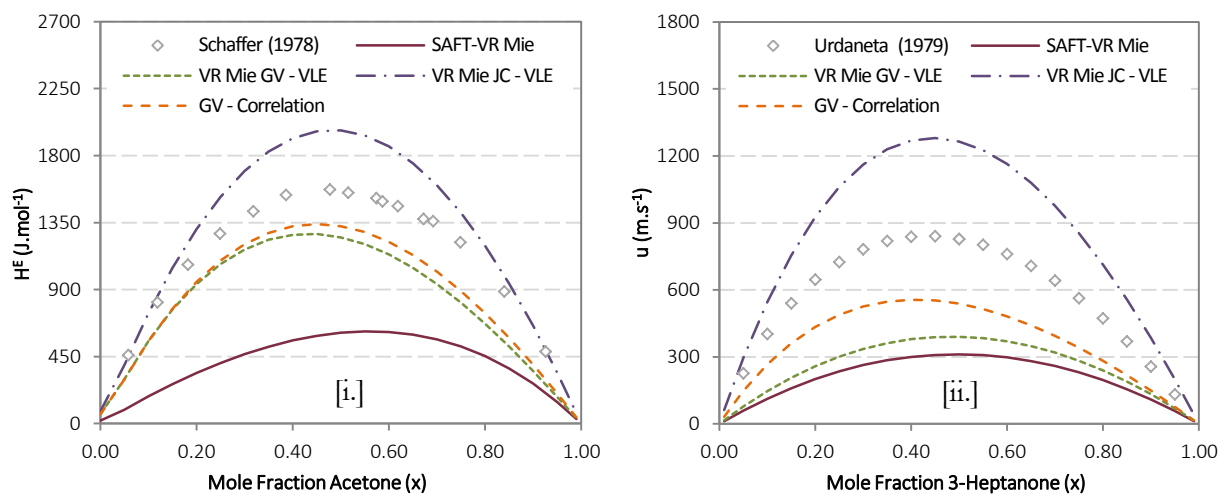
Figure 8.13: Comparison of the "VLE" and "Correlation" parameter set predictions using the SAFT-VR Mie^{GV} and SAFT-VR Mie^{JC} models – application to excess enthalpy of ketone/alkane mixtures: [i.] acetone/n-hexane at 293.15K and [ii.] 3-heptanone/n-heptane at 298.15K.

This explanation is supported by the improved prediction of the *Correlation* parameter set in Figures 8.13 [ii.], where the n_p value was fixed to a more representative value of *1.8486*. This also explains the more marked change in the *Correlation* prediction of this system compared to the acetone/n-hexane system of Figure 8.13 [i.]. It is interesting to note the improvement, albeit small, in the prediction of the n_p *Correlation* parameter sets in both systems, which serves to further validate this regression alternative. Once again, the lack of an x_p *Correlation* set for the ketones means no assessment of the change in prediction accuracy can be made for the SAFT-VR Mie^{JC} model.

The propyl acetate/n-heptane and butyl acetate/n-heptane systems in Figures 8.14 [i.] and [ii.] show that similar trends are in evidence for ester/alkane systems. The nonpolar SAFT-VR Mie prediction is clearly inferior to those of the polar models, while there is still little difference between the sPC-SAFT and SAFT-VR Mie predictions using the same polar term. There is again a marked difference between the predictions of the polar terms themselves, although the JC polar term predictions are now superior to those of the GV polar models.

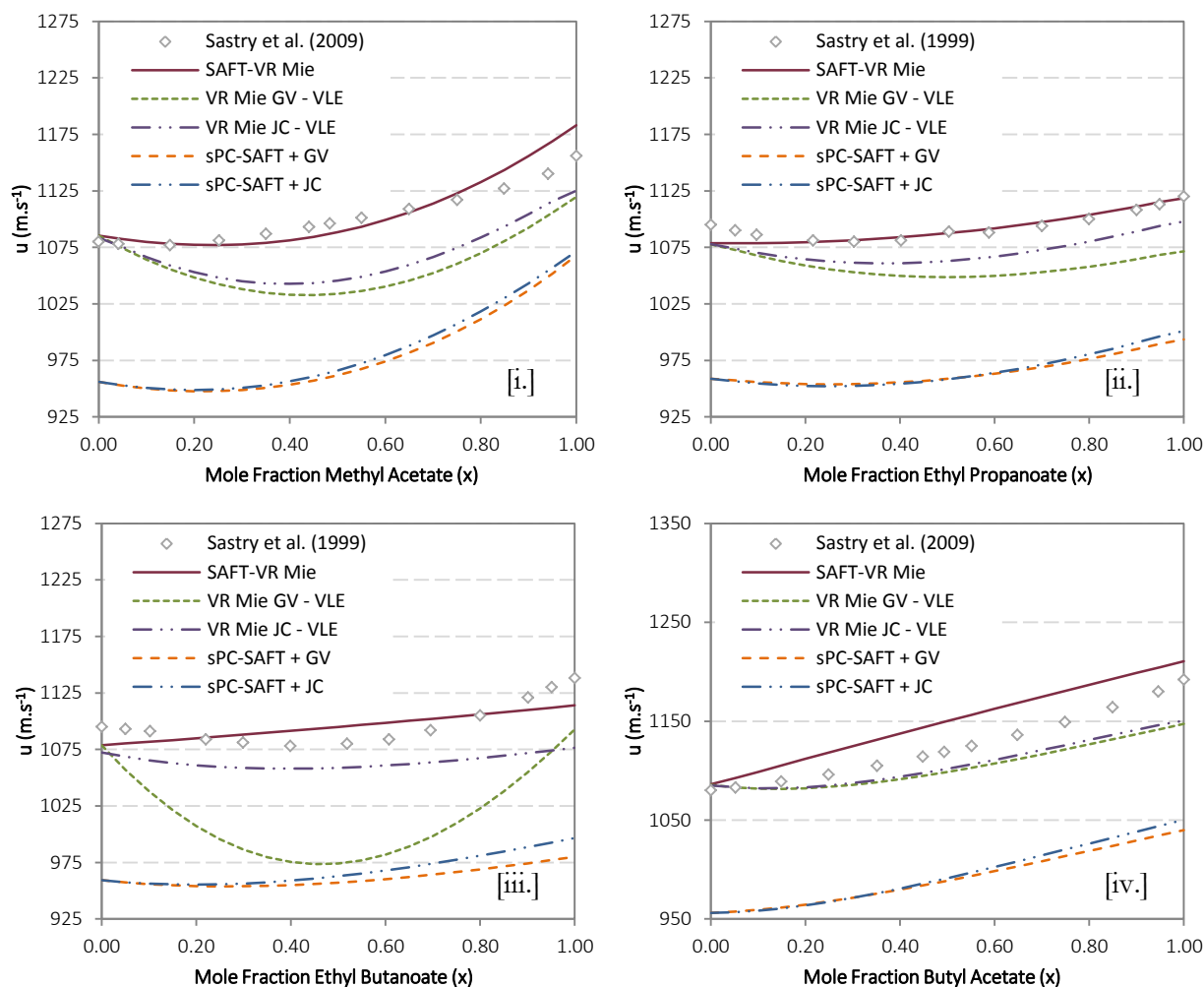*Application of Polar SAFT-VR Mie to Mixture Properties*

Figure 8.14: Predictions of mixture excess enthalpy using polar sPC-SAFT and polar SAFT-VR Mie–application to ester/alkane mixtures: [i.] propyl acetate/n-heptane at 298.15K and [ii.] butyl acetate/n-heptane at 298.15K.

A comparison of the *VLE* and *Correlation* predictions for the esters in Figures 8.15 [i.] and [ii.] yields a similarly contradictory trend; here the *Correlation* predictions are worse than their *VLE* counterparts, where the opposite was true for the ketones. For both SAFT-VR Mie^{GV} and SAFT-VR Mie^{JC}, the *Correlation* regression procedure serves to shift the prediction of mixture H^{ex} to lower values and away from the experimental data.

Figure 8.15: Comparison of the "VLE" and "Correlation" parameter set predictions using the SAFT-VR Mie^{GV} and SAFT-VR Mie^{JC} models – application to excess enthalpy of ester/alkane mixtures: [i.] propyl acetate/n-heptane at 298.15K and [ii.] butyl acetate/n-heptane at 298.15K.

The mixed results presented in this section suggest that, while accurate prediction of mixture H^{ex} is possible using polar SAFT-VR Mie, this result is neither guaranteed nor systematic. The discrepancies in prediction accuracy may simply be a result of using non-optimum parameters for some components and the "true" parameters for others. It should be stressed that improved predictions of these properties could result from explicitly incorporating H^{ex} data in the regression function. **However, this is *not* the case here and so these predictions are merely the by-product of parameter sets that are geared towards accurate representation of phase equilibrium, and give an idea of their holistic application.**

Given that the same trends were evident for the polar sPC-SAFT predictions both here and in similar assessments performed by de Villiers (2011), the mixed results are likely the result of a systematic shortcoming in describing the temperature dependence of *F* within the SAFT framework as a whole. A detailed study, where H^{ex} was the focus of the modelling exercise, would be necessary to confirm or deny these claims, but this is beyond the scope of the preliminary assessment performed here. **In the context of this work, the most significant result is that the predictions of polar SAFT-VR Mie are of the same order of magnitude as their sPC-SAFT counterparts, and that accurate description of mixture speed of sound does not come at the expense of decreased predictive capacity in excess enthalpy.**

8.3.2   Excess Volume

Excess volume accounts for the changes in mixture volume resulting from size asymmetries and differing energetic interactions between the components that constitute the mixture. In a similar fashion to that of H^{ex}, V^{ex} is defined by equation 8.3 (Michelsen & Mollerup, 2007) and is strongly dependent on the first order volume derivative of the system Helmholtz energy.

$$V^{ex} = V_{mix}\left(T, P, \mathbf{n}\right) - \sum_{i=1}^{nc} V_{pure,i}\left(T, P, n_i\right) \qquad\qquad 8.3$$

In the same fashion as the preceding sections, the *VLE* parameter set of SAFT-VR Mie[GV] is used to predict the excess volume data for the 3-pentanone/n-heptane system in Figure 8.16. In the figure, nonpolar SAFT-VR Mie falsely predicts a negative excess volume for this system, which clearly demonstrates the need to explicitly account for dipolar interaction in polar components. The polar SAFT-VR Mie provides a better prediction of the experimental data than the two polar sPC-SAFT variants, suggesting that the volume derivatives are better described in the SAFT-VR Mie framework.
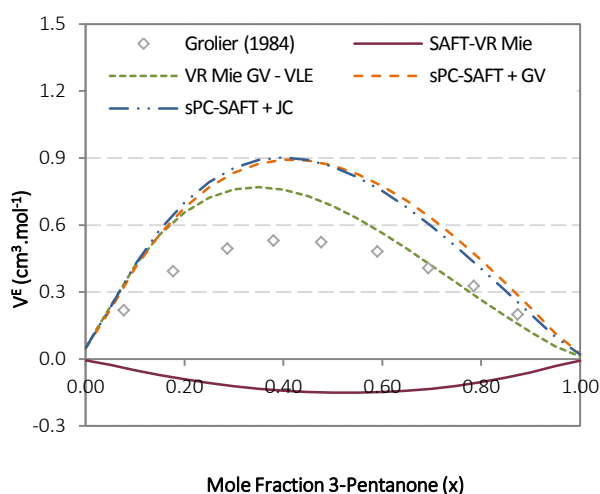
Figure 8.16: Predictions of mixture excess volume using polar sPC-SAFT and polar SAFT-VR Mie–application to 3-pentanone/n-heptane at 298.15K.

The comparison of the *VLE* and *Correlation* predictions for this system is shown in Figure 8.17. The incorporation of u^{liq} data in the *Correlation* regression procedure serves to improve the overall description of the data, better representing the curvature and maximum in the V^{ex} data. This mirrors the trend seen in H^{ex} where the *Correlation* parameter set produced a better prediction than the reference *VLE* parameter set.
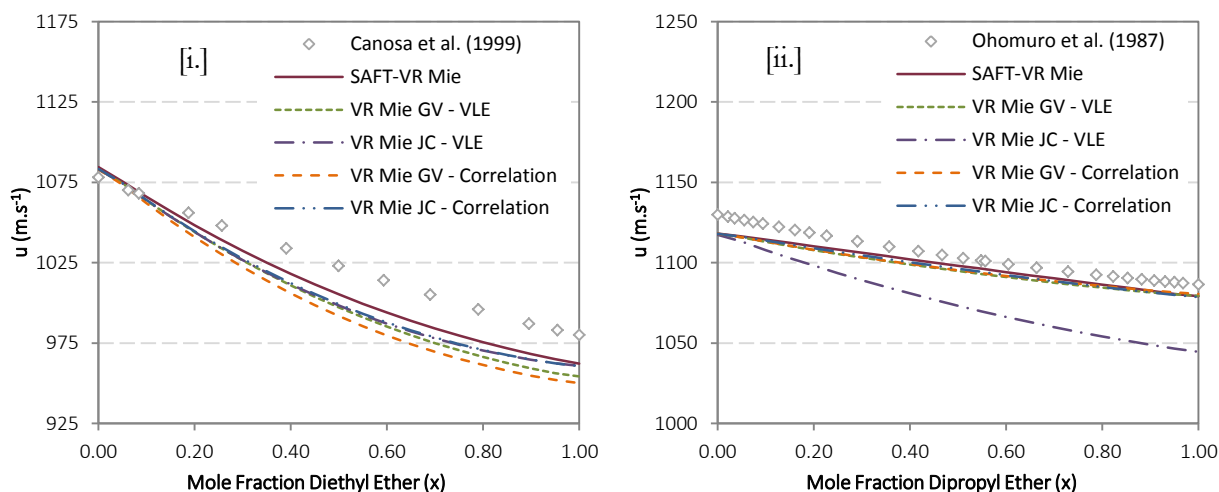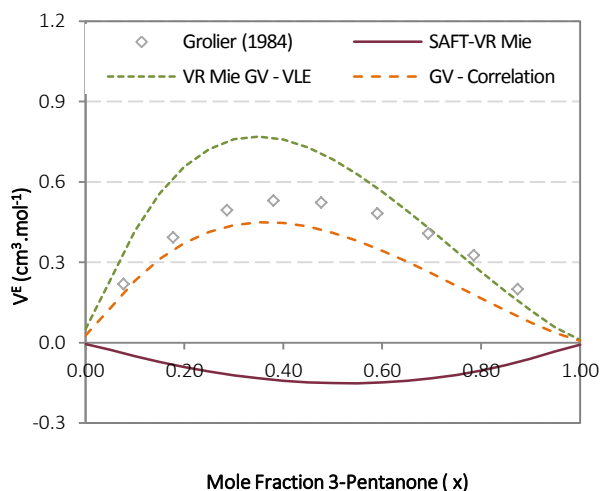

Figure 8.17: Comparison of the "VLE" and "Correlation" parameter set predictions using the SAFT-VR Mie^{GV} model – application to excess volume of 3-pentanone/n-heptane at 298.15K.

The propyl formate/n-heptane and methyl valerate/n-heptane systems are used as representative ester systems in Figures 8.18 [i.] and [ii.]. In the propyl formate system, the nonpolar SAFT-VR Mie prediction is qualitatively correct in predicting positive V^{ex}, but still under predicts the magnitude of the data. This is probably a result of accounting for the effects of size asymmetry, but not the effect of differing energetic interactions. Statistically, the SAFT-VR Mie^{GV} model again provides the best fit of the data, but under predicts the maximum in the data as it did in the 3-pentanone system previously. The SAFT-VR Mie^{JC} prediction is almost identical to the polar sPC-SAFT predictions in over predicting the experimental data.

In Figure 8.18 [ii.], nonpolar SAFT-VR Mie again exhibits a false prediction of a negative V^{ex} for the methyl valerate system. The polar model predictions are somewhat scattered, with the SAFT-VR Mie^{JC} and sPC-SAFT$_{GV}$ predictions exhibiting near identical predictions in excellent agreement with the experimental data, while the SAFT-VR Mie^{GV} prediction is consistent in under-predicting the data. A noteworthy result for the ester systems is consistently accurate V^{ex} predictions in the case of the SAFT-VR Mie^{JC} model, with the propyl formate system of Figures 8.18 [i.] proving the only exception to this trend. The SAFT-VR Mie^{GV} prediction is similarly consistent in its predictions, although here the model regularly under predicts the data as in the example cases here.
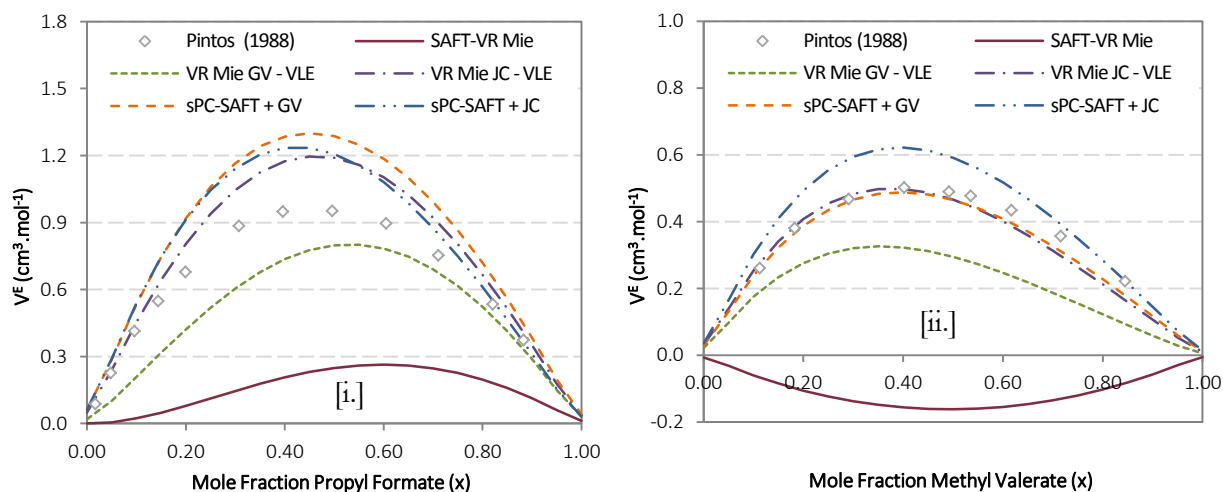
Figure 8.18: Predictions of mixture excess volume using polar sPC-SAFT and polar SAFT-VR Mie– application to ester/alkane mixtures: [i.] propyl formate/n-heptane at 298.15K and [ii.] methyl valerate/n-heptane at 298.15K.

The inclusion of pure component u^{liq} data in the *Correlation* parameter sets for SAFT-VR Mie^{GV} does not result in significant changes to the resulting prediction for either ester/alkane system. As Figures 8.19 [i.] and [ii.] show however, the *Correlation* parameter sets for SAFT-VR Mie^{JC} result in notable decreases in the predicted V^{ex}. In the case of propyl formate, this decrease brings the prediction into better agreement with the experimental data but as already stated, this is the exception. The trend apparent for methyl valerate is true for the majority of ester/alkane mixtures however; predictions of the *Correlation* parameter sets result in notably worse predictions of the experimental data.

Figure 8.19: Comparison of the "VLE" and "Correlation" parameter set predictions using the SAFT-VR Mie^{GV} and SAFT-VR Mie^{JC} models – application to excess isobaric heat capacity of ester/alkane mixtures: [i.] propyl formate/n-heptane at 298.15K and [ii.] methyl valerate/n-heptane at 298.15K.

Considering excess volume predictions in this section yielded interesting results, most notably the consistent accuracy with which the *VLE* parameter sets of SAFT-VR Mie^{JC} predicted experimental V^{ex} mixture data for esters. The inability to test for consistency of this trend in other functional groups due to the already detailed lack of parameters for ketones, and lack of data for ethers is thus a particularly frustrating result. **Of significance to this work however, is that the aim of demonstrating the polar**

SAFT-VR Mie predictions to be qualitatively similar to their polar sPC-SAFT analogues has been achieved. Further, in the case of SAFT-VR Mie^{GV}, these predictions are improved by using the *Correlation* parameter sets for ketones, while the same level of accuracy is maintained for esters.

8.3.3   Excess Isobaric Heat Capacity

The isobaric heat capacity is an extensively used property in industry, and thus accurate description of this property is desirable in a predictive thermodynamic model. The excess isobaric heat capacity is a particularly complex function mathematically, with dependence on both the *dP/dV* and *dP/dT* derivatives, as well as the second temperature derivative of *F*. These former terms are also themselves functions of the second volume and temperature-volume derivatives of the residual Helmholtz energy respectively. These relationships are captured by equations 8.4 to 8.6 (Michelsen & Mollerup, 2007).

$$C_P{}^r\left(T,P,\mathbf{n}\right)=-T\frac{\left(\dfrac{\partial P}{\partial T}\right)^2_{V,\mathbf{n}}}{\left(\dfrac{\partial P}{\partial V}\right)_{T,\mathbf{n}}}-nNk-T^2\left(\frac{\partial^2 F}{\partial T^2}\right)_{V,\mathbf{n}}-2T\left(\frac{\partial F}{\partial T}\right)_{V,\mathbf{n}} \qquad 8.4$$

$$\left(\frac{\partial P}{\partial T}\right)_{V,\mathbf{n}}=-NkT\left(\frac{\partial^2 F}{\partial T\partial V}\right)_{\mathbf{n}}-n \qquad 8.5$$

$$\left(\frac{\partial P}{\partial V}\right)_{T,\mathbf{n}}=-NkT\left(\frac{\partial^2 F}{\partial V^2}\right)_{T,\mathbf{n}}-\frac{nNkT}{V^2} \qquad 8.6$$

Accurate description of $C_P{}^{ex}$ is thus a stringent test of the holistic predictive strength of thermodynamic models, testing three of the six second order derivatives in *F*. Predictions of $C_P{}^{ex}$ for the same 3-pentanone/n-heptane system considered for excess volume are presented in Figure 8.20. It is readily apparent that none of the model predictions accurately account for the trends seen in the experimental data. Indeed, it appears that the nonpolar model provides the best quantitative prediction, but it does not account for the negative $C_P{}^{ex}$ values at low 3-pentanone concentrations. Both sPC-SAFT$_{GV}$ and SAFT-VR Mie^{GV} over predict the positive maximum in $C_P{}^{ex}$, while the sPC-SAFT$_{JC}$ model inaccurately predicts large negative excess heat capacities over the whole composition range.
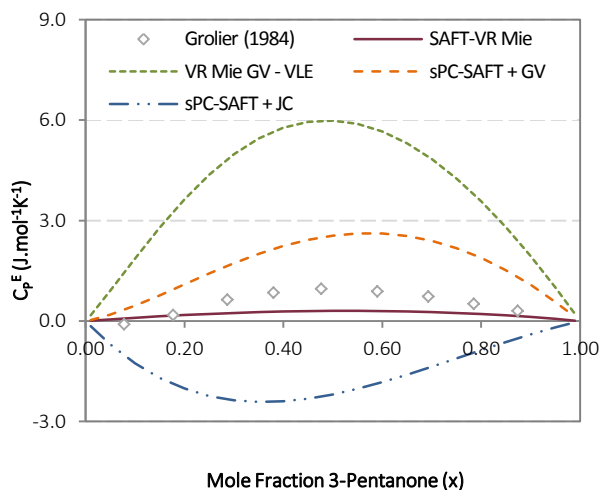
Figure 8.20: Predictions of mixture excess isobaric heat capacity using polar sPC-SAFT and polar SAFT-VR Mie– application to 3 pentanone/n-heptane at 298.15K.

Figure 8.21 shows that the predictions of the *Correlation* parameter set for SAFT-VR Mie^{GV} improve the models prediction. However, the experimental trend of negative C_P^{ex} values in the data is still unaccounted for, and the maximum is still over predicted.
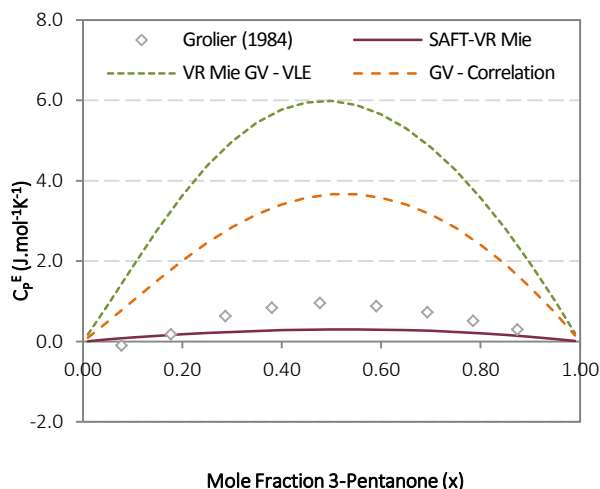
Figure 8.21: Comparison of the "VLE" and "Correlation" parameter set predictions using the SAFT-VR Mie^{GV} model – application to excess isobaric heat capacity of 3 pentanone/n-heptane at 298.15K.

Considering the polar sPC-SAFT vs. polar SAFT-VR Mie comparison for esters in Figures 8.22 [i.] and [ii.], we see that similar trends in the model predictions are apparent. The propyl formate/n-heptane system exhibits qualitatively similar behaviour to the 3-pentanone/n-heptane system, with small negative C_P^{ex} values in the low ester concentration range. The nonpolar SAFT-VR Mie prediction once again provides the best quantitative fit, but the both sPC-SAFT$_{GV}$ and SAFT-VR Mie^{GV} predictions are in much better agreement with the data, qualitatively capturing the shift of the maximum to higher ester concentrations. The SAFT-VR Mie^{JC} model captures the sinusoidal nature of the data, but is inverted and quantitatively incorrect.

Application of Polar SAFT-VR Mie to Mixture Properties
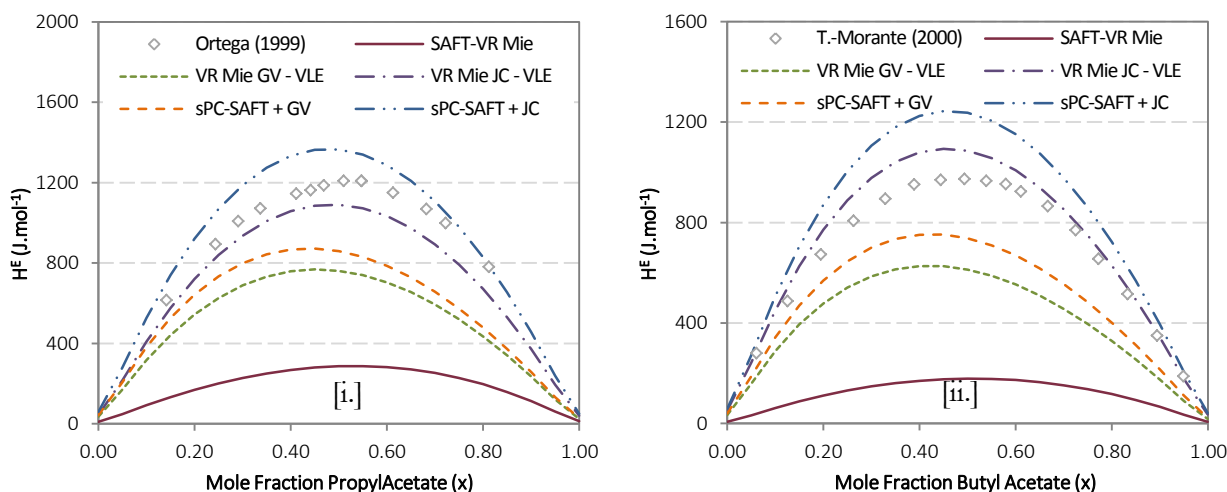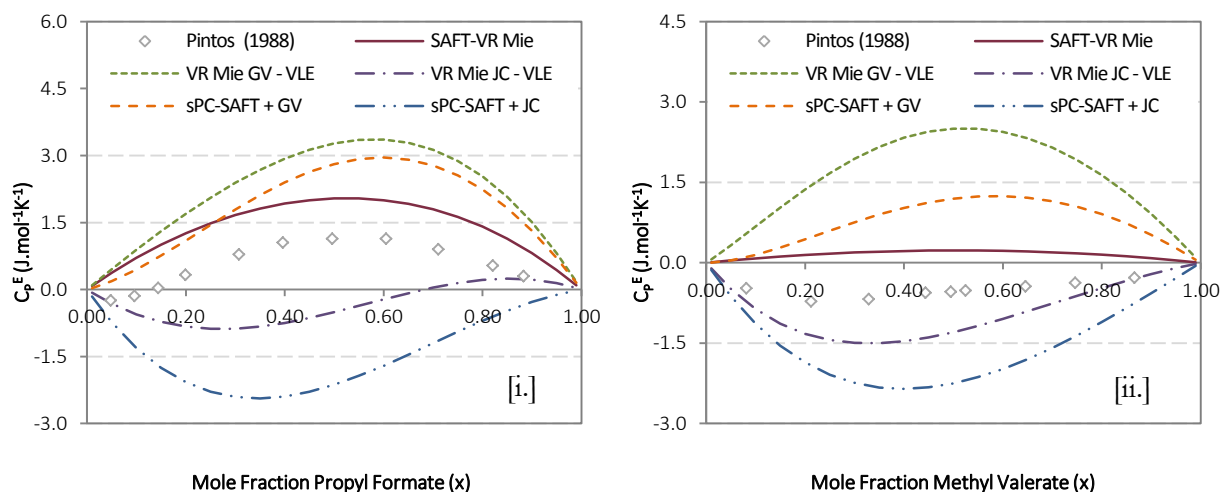

Figure 8.22: Predictions of mixture excess isobaric heat capacity using polar sPC-SAFT and polar SAFT-VR Mie– application to ester/alkane mixtures: [i.] propyl formate/n-heptane at 298.15K and [ii.] methyl valerate/n-heptane at 298.15K.

The methyl valerate/n-heptane system exhibits the highly complex "W-shaped" concentration dependence of the C_P^{ex} curve, with a broad flat maximum in the middle concentration range with local minima in the extrema of the composition space. As Figure 8.22 [ii.] shows, none of the considered models are able to predict the trends in the data with any degree of accuracy. **What is consistent however is the relative performance of the SAFT-VR Mie and sPC-SAFT predictions when the same polar term is used in each case.**
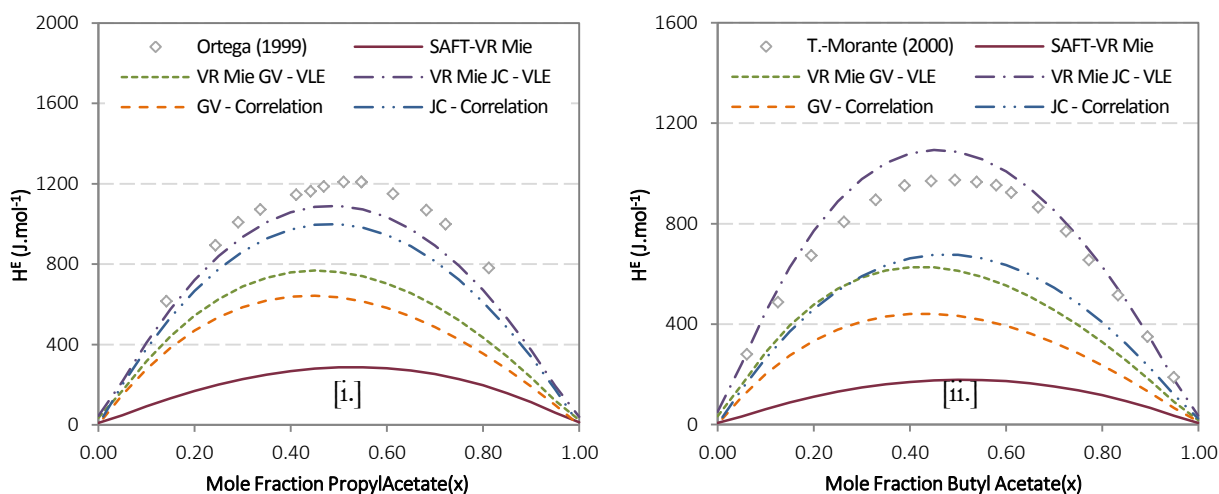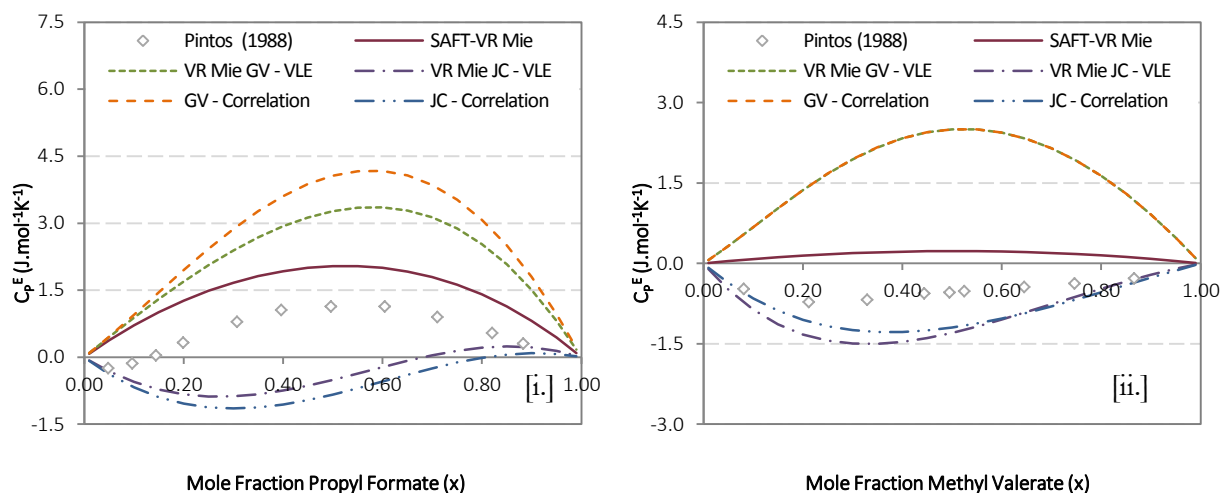

Figure 8.23: Comparison of the "VLE" and "Correlation" parameter set predictions using the SAFT-VR Mie^GV and SAFT-VR Mie^JC models – application to excess isobaric heat capacity of ester/alkane mixtures: [i.] propyl formate/n-heptane at 298.15K and [ii.] methyl valerate/n-heptane at 298.15K.

In Figures 8.23 [i.] and [ii.], we find that the choice of regression procedure using polar SAFT-VR Mie does not significantly affect the prediction of the respective models, with the complex behaviour still not accurately accounted for.

The predictions for mixture excess isobaric heat capacity presented in this section attest to the difficulty of accurately modelling this highly complex property. The results suggest that, in the case of

mixtures containing polar components, the model predictions are dominated by the contribution of the polar term rather than the parent framework - the respective polar sPC-SAFT and SAFT-VR Mie models yield very similar predictions when the same polar term was used. It should again be stressed that these predictions are the by-product of parameter sets geared towards accurate predictions of phase equilibrium. A detailed study of the reason for the models' inability to accurately predict both phase equilibria and C_P^{ex} using a single parameter set is beyond the scope of the work done here. However, a brief analysis of possible causes of deviations is warranted.

Equations 8.4 to 8.6 show that the *dP/dV* derivative is the only element of the C_p^{ex} function which is not itself a direct function of temperature. Speed of sound is also a function of the *dP/dV* derivative (see equation 7.2, reintroduced below) and this property has already been shown to be well predicted by the polar SAFT-VR Mie framework in this work.

$$u^{liq} = \sqrt{-\frac{V^2}{M_w}\frac{C_P}{C_V}\left(\frac{\partial P}{\partial V}\right)_{T,n}}$$

7.2

Thus it would appear that it is the temperature dependence of the state function, *F*, which is not accurately captured by these models. **Poor description of the complex relationship between the temperature derivatives in the description of F results in the overall poor correlation of isobaric heat capacities seen in this section.** This conclusion is supported by the results for the excess enthalpy predictions, where a direct relationship between H^{ex} and the *dF/dT* derivative exists, and smaller discrepancies with the data are in evidence. As further evidence, equation 7.2 shows that speed of sound is a function of the heat capacity ratio. The contribution of C_P^{ex} is small relative to the total C_P, with the same being true of C_V^{ex} defined in equation 8.7. This suggests that errors in model predictions of C_P^{ex} and C_V^{ex}, arising from the incorrect temperature dependence of *F,* would cancel in the heat capacity ratio. This error cancellation would account for the demonstrated accuracy of speed of sound measurements for polar SAFT-VR Mie, despite its poor description of C_p^{ex}, although further study would be required to confirm

$$C_V^{r}(T,V,\mathbf{n}) = -T^2\left(\frac{\partial^2 F}{\partial T^2}\right)_{V,\mathbf{n}} - 2T\left(\frac{\partial F}{\partial T}\right)_{V,\mathbf{n}}$$

8.7

It is significant to note however that similar conclusions regarding erroneous temperature dependence in SAFT-type models have been drawn by de Villiers (2011), Polishuk (2011) and Polishuk & Molero (2011). This suggests that this is a flaw inherent in all the SAFT-type models and is not restricted to the proposed polar SAFT-VR Mie. As with the excess enthalpy and excess volume predictions of the previous sections however, the most significant result in the context of this work is that the model predictions of polar SAFT-VR Mie exhibit similar accuracies to their sPC-SAFT counterparts.

8.4   Holistic Predictions

In the previous sections, the predictions of the proposed polar SAFT-VR Mie models were rigorously tested against an array of important thermodynamic properties. In each section, the aim was to assess the relative performance of the models compared to the renowned sPC-SAFT equivalents for those particular properties. While the models proved robust in these individual applications, it is desirable to assess the holistic predictive capacity before drawing final conclusions. To this end, SAFT-VR Mie[GV] and SAFT-VR Mie[JC] are applied to the full range of considered data for a representative ketone and ester for which such data were available in this section.

Beginning with 2-butanone for the ketone functional group, predictions for nonpolar SAFT-VR Mie and the *VLE* and *Correlation* parameter sets of SAFT-VR Mie[GV] are presented in Figures 8.24 [i.] to [v.]. The need to explicitly account for dipolar interactions by incorporating a polar term is highlighted in the predictions of almost all the considered properties. Considered in this collective fashion, the holistic strength of the SAFT-VR Mie[GV] model in particular is clearly evident. Given that *VLE* parameters could be determined for the SAFT-VR Mie[JC] model for this component, these predictions are also incorporated and exhibit similar accuracy to their GV counterparts.

The discerning factor between the models however is the viability of using the *Correlation* regression procedure to determine equally accurate parameter sets using pure component data alone. In the case of SAFT-VR Mie[GV], this viability has been consistently demonstrated and is maintained throughout Figures 8.24 [i.] to [v.]. However, the inability to generate or test similar x_p *Correlation* parameters for this functional group underpins the weakness of SAFT-VR Mie[JC] when comparing the two polar SAFT-VR Mie variants.
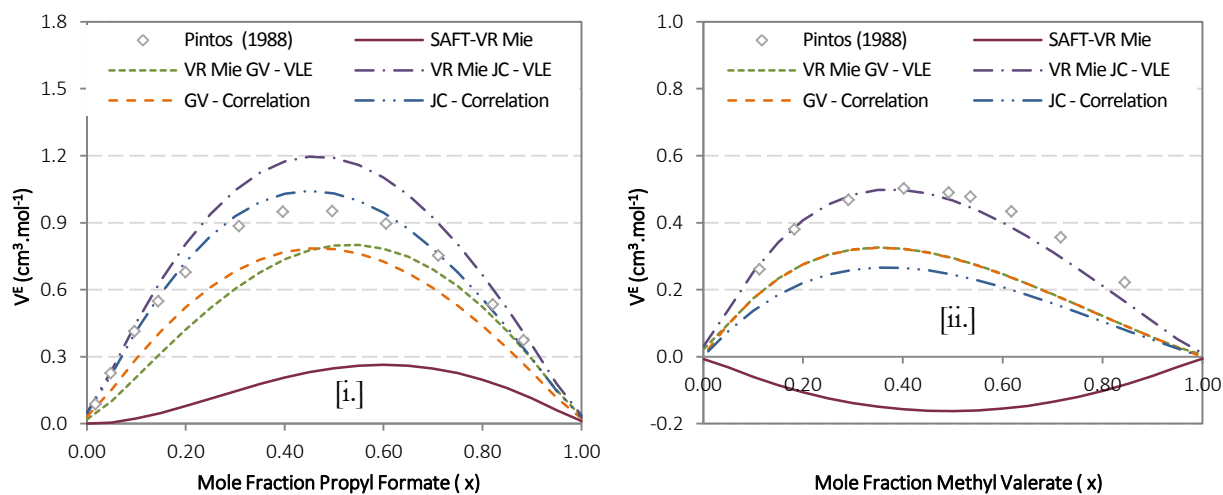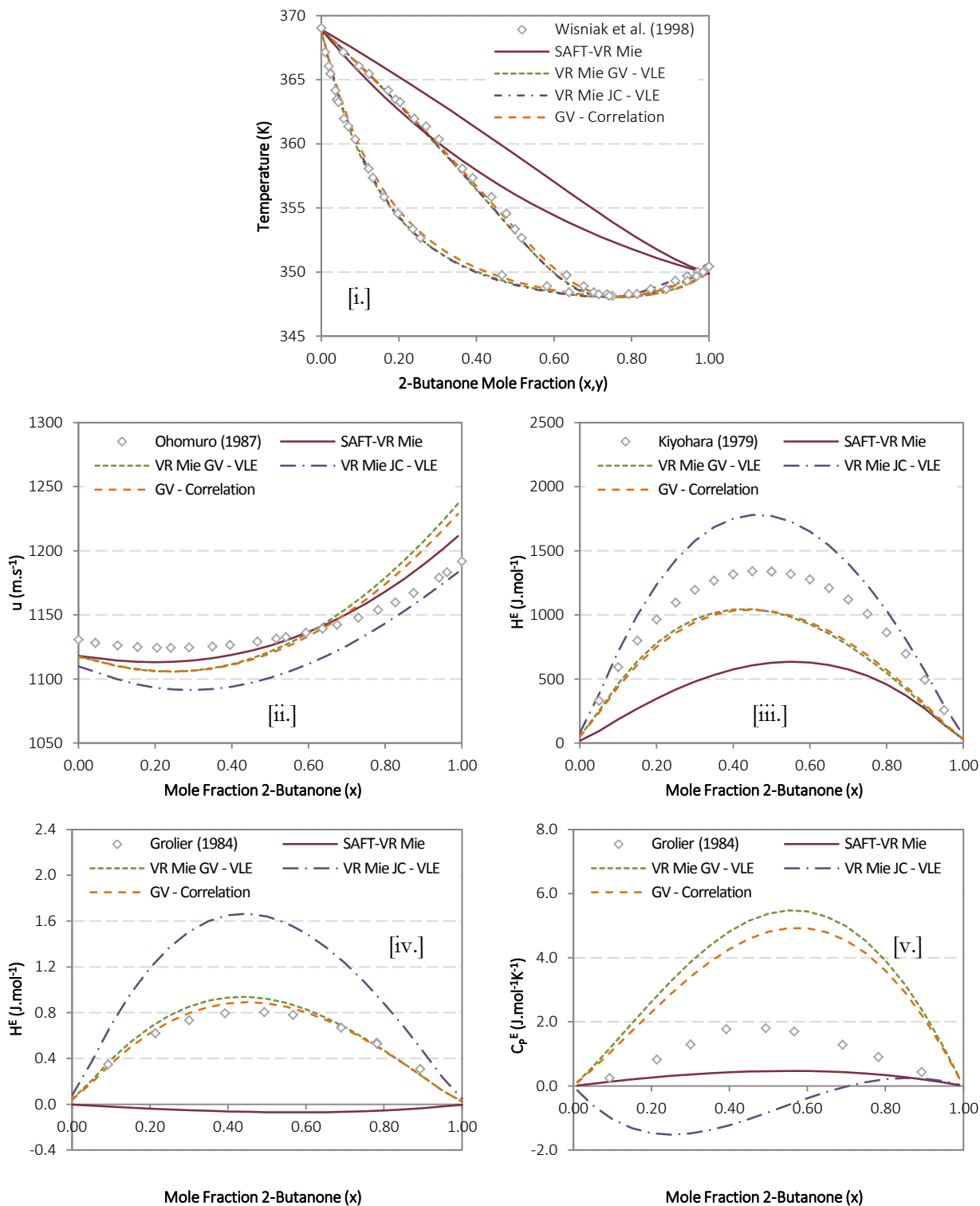
Figure 8.24: Comparison of the "VLE" and "Correlation" parameter set predictions using the SAFT-VR Mie^{GV} and SAFT-VR Mie^{JC} models – application to the full spectrum of considered mixture properties for butanone/n-heptane: [i.] isobaric VLE, [ii.] speed of sound, [iii.] excess enthalpy, [iv.] excess volume and [v.] excess isobaric heat capacity.

The same rounded analysis is performed using ethyl acetate as the representative component for esters in Figures 8.25 [i.] to [v.]. The same conclusions can be drawn regarding the need to explicitly account for dipolar interactions for this more weakly polar functional group, but the distinction between the two polar variants is less clear than for ketones. The consistent improvement in the prediction of H^{ex}

and V^{ex} when using SAFT-VR Mie[JC] as opposed to SAFT-VR Mie[GV] suggests that this is the superior model for the description of ester thermodynamic properties. However, the decrease in SAFT-VR Mie[JC] prediction accuracies noted when employing the *Correlation* parameter is a trade-off that is not apparent for the equivalent SAFT-VR Mie[GV] parameters. This trade-off is seen in all the considered properties, but perhaps most notably for phase equilibrium predictions.
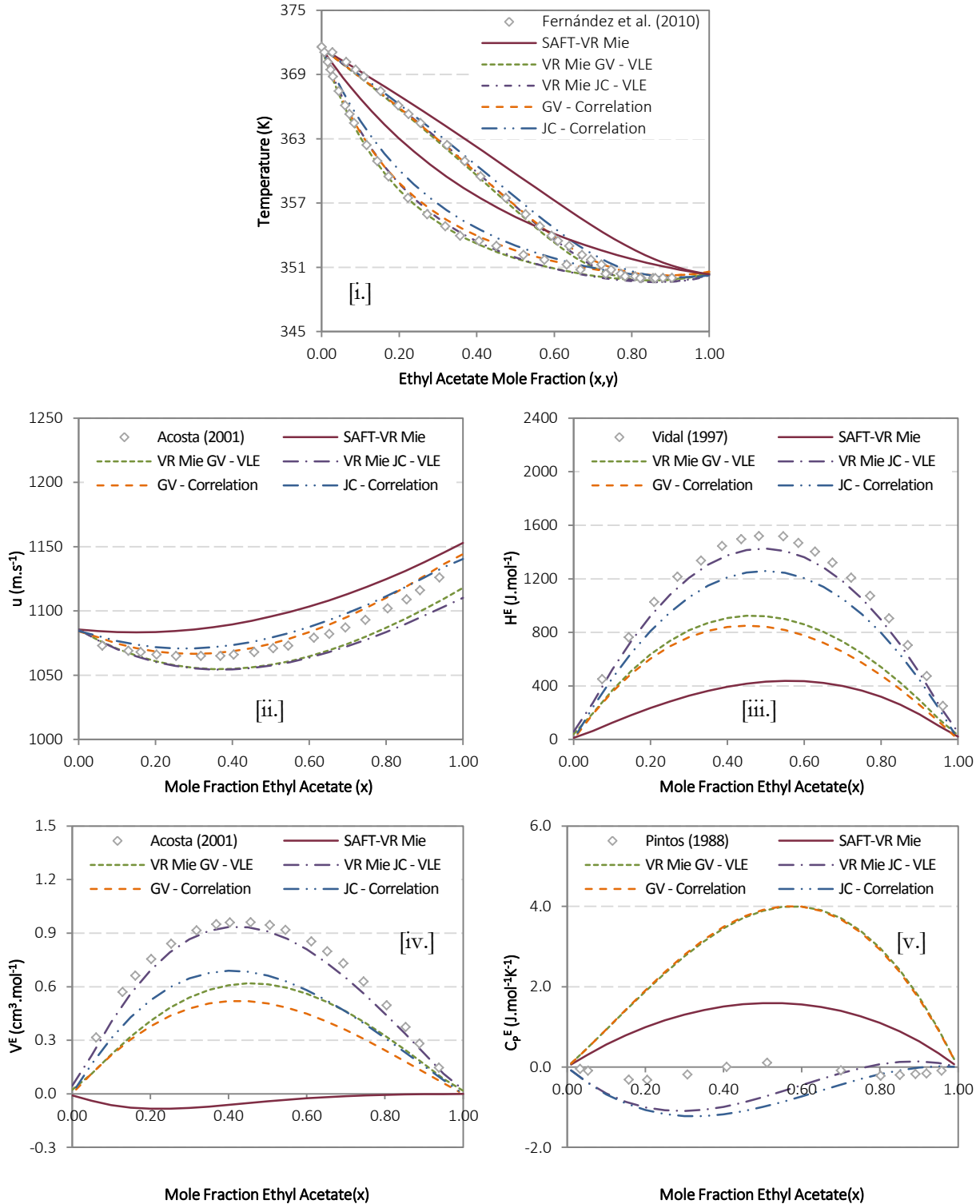
Figure 8.25: Comparison of the "VLE" and "Correlation" parameter set predictions using the SAFT-VR Mie[GV] and SAFT-VR Mie[JC] models − application to the full spectrum of considered mixture properties for ethyl acetate/n-heptane (except u[liq]): [i.] isobaric VLE, [ii.] speed of sound (+n-hexane), [iii.] excess enthalpy, [iv.] excess volume and [v.] excess isobaric heat capacity.

Considering the overall performance of SAFT-VR Mie[GV] and SAFT-VR Mie[JC], prediction results suggest that the former is better suited to describing the behaviour of more strongly polar components, while the latter is better for weaker polar molecules. Such a recommendation is at odds with the goal of espousing a single thermodynamic model capable of accurately predicting the behaviour of polar components and their mixtures as laid out in the aims and objectives of this work.

To this end, the aim of developing a model that yields accurate predictions of equilibrium and thermodynamic properties using parameters regressed from pure component data alone takes precedence. Viewed in this light, the regression difficulties experienced using SAFT-VR Mie[JC] cannot be overlooked, even if notably better results are in evidence for *some* excess properties using this model. Taken as a whole, the modelling results of this chapter clearly point to SAFT-VR Mie[GV] being the superior variant in this new polar framework.

8.5 Chapter Summary

The results of Sections 8.1 and 8.2, considered together, represent the most significant contribution of the proposed polar SAFT-VR Mie models. Polar sPC-SAFT has already been shown to be exceedingly competent in predicting the phase equilibria of polar systems, even the nuanced instances of isomeric systems, if the same *VLE* and *Correlation* regression procedures are considered for their parameter regression. Application of the new SAFT-VR Mie[GV] and SAFT-VR Mie[JC] models to the same mixture equilibria demonstrated that this predictive capacity is maintained when moving to the SAFT-VR Mie framework. This result was an important prerequisite for the proposal of a new model and serves as justification for its development. **The novelty and success of the proposed model is evident however, when these successful equilibrium predictions are considered in conjunction with the vastly improved description of speed of sound in mixtures when using the same parameter sets.**

A primary focus of the work was developing a means of parameter regression that does not necessitate the inclusion of mixture VLE data, yet still provides an accurate description of the range of thermodynamic properties considered. To this end, the success of the *Correlation* regression procedure, adapted from the sPC-SAFT equivalent of Chapter 5, was a notable and important result. The inclusion of u^{liq} data in this regression alternative (or equivalently, isomer u^{liq} data) served to improve the mixture speed of sound predictions, with only a small loss of accuracy in the description of phase equilibrium. **While this constitutes a trade-off for those components where optimum *VLE* data sets were regressed, it is a significant result for those components where no such data set could be determined, as well as for the multitude of components not considered here for which no VLE data have been measured.**

To the author's knowledge, an assessment of the excess properties of real fluids has never been made with SAFT-VR Mie. The rationale behind performing such an analysis was to test whether the increased accuracy in predicting speed of sound came at the expense of significantly reduced predictive

capacity in other thermodynamic properties. To this end, experimental excess enthalpy, excess volume and excess isobaric heat capacity data were used to test the predictions of the new polar SAFT-VR Mie models, as well as those of polar sPC-SAFT. It was stressed that these predictions merely provide a holistic view of the predictive capacity of the *VLE* and *Correlation* parameter sets, given that the focus of these parameters is the accurate description of phase equilibrium. The results illustrated that the choice of polar term is more significant than the parent SAFT framework in defining the model prediction, with both sPC-SAFT$_{GV}$ and SAFT-VR Mie^{GV} yielding similar results. Similarly, the use of the *Correlation* parameter sets was shown to yield predictions at least as good as their *VLE* counterparts. This preliminary analysis also highlighted room for improvement of the model moving forward, while the aims of providing a holistic assessment of the predictive capacity of polar SAFT-VR Mie were met.

The accurate simultaneous prediction of phase equilibria and speed of sound in polar mixtures demonstrates that the new polar SAFT-VR Mie is an improvement over polar sPC-SAFT. **Within this new framework itself, the ability to generate unique parameter sets for *all* considered components, that yield accurate predictions of the range of properties considered, sets SAFT-VR Mie^{GV} apart from its SAFT-VR Mie^{JC} counterpart.**

Chapter 9: CONCLUSIONS

The overarching aim of this work was systematic improvement of the description of thermodynamic properties of polar components and their mixtures, within the SAFT framework. Specifically, the effect of structural isomerism on mixture phase behaviour and non-equilibrium derivative properties were identified as key factors to address in this pursuit.

Objective (i.) Generation of Low Pressure Phase Equilibrium Data

In order to systematically address the former, it was necessary to generate mixture phase equilibrium data for ether and ester components. Chapter 4 presented thermodynamically consistent, isobaric phase equilibrium data that was generated for two C_6 ether isomers with n-heptane as well as five C_6 ester isomers with n-octane at *60*kPa.

This new experimental data demonstrated that distinct phase envelopes are in evidence for respective isomers. These isomeric systems exhibit qualitatively similar phase behaviour; *viz.* narrow, zeotropic phase envelopes for ether/n-heptane systems and minimum boiling azeotropic behaviour for ester/n-octane systems.

Objective (ii.) Polar sPC-SAFT: Structural Isomers & Phase Equilibrium

The experimentally measured phase behaviour data were used to test the predictive capacity of polar sPC-SAFT models in Chapter 5. This modelling exercise was an extension of a previous study (Cripwell, 2014) for ketone isomers, and demonstrated that structural isomerism in polar molecules provides a stringent test of the predictive capacity of thermodynamic models. Specifically, it was concluded that the quality of model predictions decreases as the phase behaviour of the considered isomer approaches that of its nonpolar size equivalent. Furthermore, the prevalence of parameter degeneracy increased following this same trend, most notably for sPC-SAFT$_{JC}$. These results established the trends seen in previous work as a systematic shortcoming of the model framework – the first time such a systematic trend has been established.

Overall, sPC-SAFT$_{GV}$ was found to be a more robust and reliable polar framework than sPC-SAFT$_{JC}$, significantly outperforming its counterpart in their application to the phase behaviour of polar structural isomers. Use of the *VLE* parameter sets brought the predictions of the two terms into agreement with each other and with mixture data, but the requirement of experimental data negates the advantage of model *prediction* over introducing BIPs to correlate the data in more simple semi-empirical models. In this respect, a major finding of the work was the success of employing the *Correlation* regression procedure. This alternative allows for the generation of parameter sets, capable of accurately representing mixture phase behaviour, from pure component data alone while overcoming the mathematical shortcomings of the *Standard pure component regression*.

Objective (iii.) Accounting for Dipolar Interactions in a SAFT-VR Mie Framework

The extensive modelling exercise using polar sPC-SAFT, both here and in the previous work of de Villiers (2011), highlighted strengths as well as inherent shortcomings in the model framework. With the primary aim of *improving* the thermodynamic description of polar components and their mixtures, it was decided to conduct a similar analysis using the recently developed SAFT-VR Mie framework.

It was demonstrated that dipolar interactions need to be explicitly accounted for in the SAFT-VR Mie framework. This was the focus of Chapter 7, where the JC and GV polar terms were incorporated into the SAFT-VR Mie EoS to yield the new polar SAFT-VR Mie^{JC} and SAFT-VR Mie^{GV} variants. These models comprise four regressed nonpolar parameters (σ, m, ε/k & λ_r) as well as a variable polar parameter (x_p or n_p). A range of regression alternatives were considered for determination of these parameters, including the traditional *Standard pure component regression*. Choice of pure component data in the regression procedure was shown to significantly affect the resulting parameters. Specifically, the role of pure component speed of sound, prominent in the development of the base SAFT-VR Mie EoS, was highlighted in producing parameter sets with well-balanced predictive capacity. This demonstrated that the new polar SAFT-VR Mie variants maintain an excellent holistic prediction capacity for pure component properties.

The problems of parameter degeneracy and broad minima in the objective function were found to be more pronounced in the *Standard pure component regression* of polar SAFT-VR Mie, most notably so for SAFT-VR Mie^{JC}. Considered in combination with similar results in Chapter 5, this was linked to the choice of polar term and the dimensionality of the parameter space. The prevalence of this regression hurdle indicates that polar SAFT-VR Mie does not inherently improve the description of phase behaviour of isomeric systems using the same *Standard pure component regression* compared to polar sPC-SAFT. However, the predictions of SAFT-VR Mie^{GV} equal or exceed those of sPC-SAFT$_{GV}$ in these systems. This trend further reinforced the conclusions carried over from Chapter 5 that the GV polar term is a more robust and reliable modelling framework.

Drawing upon the success in sPC-SAFT, it was found that mitigation of regression problems is possible by including the binary *VLE* data in the regression. A more significant result however, was the demonstrated ability to regress parameter sets by fixing the value of the polar parameter in the *Correlation* regression alternative. This alternative reduces the dimensionality of the regression space and removes the dependence on available VLE data, allowing for optimum parameter sets to be determined from pure component data alone.

The optimum parameter sets regressed in Chapter 7 were applied to various thermodynamic properties of polar mixtures in Chapter 8. In this fashion, the all-round predictive capacity was tested, with model results initially compared to their sPC-SAFT analogues, followed by a comparison of the predictions of the *VLE* and *Correlation* parameter predictions. Application to a wide range of phase equilibria demonstrated the robust predictive strength of polar SAFT-VR Mie, particularly

SAFT-VR Mie[GV], displaying excellent agreement with experimental data in all considered systems. The most significant contribution of the new model framework over polar sPC-SAFT was notable and consistent improvement in the description of mixture speed of sound *using the same parameter set*. This was demonstrated for all three functional groups considered and validated the inclusion of the GV and JC polar terms in the SAFT-VR Mie framework.

Novel application of the SAFT-VR Mie framework to excess properties demonstrates that polar SAFT-VR Mie predictions are comparable to those of polar sPC-SAFT. This result is significant as it shows that improved description of mixture speed of sound does not come at the expense of worse predictions for other thermodynamic properties. Results of the excess property analysis highlighted that systematic shortcomings still exist in the SAFT framework, particularly the temperature dependence of A^r, which extends to the polar SAFT-VR Mie model proposed here. However, given that the model parameters were not geared towards accurate description of excess properties, these preliminary results were considered satisfactory.

Addressing the Overarching Aim

Polar SAFT-VR Mie represents a predictive thermodynamic model with the capacity to simultaneously predict both phase equilibrium and derivative properties with a higher degree of accuracy than is achievable with previous thermodynamic models. The systematic regression problems faced by SAFT-VR Mie[JC], resulting in a lack of parameters for many of the components considered here, demonstrate the inferiority of this variant to SAFT-VR Mie[GV]. The latter boasts a full complement of parameter sets for all three polar functional groups considered in this work and exhibits consistently good, holistic predictions for these components.

The most significant outcome of this work however is the results of the *Correlation* regression alternative, which demonstrated that achievability of such accurate results are not limited by the availability of mixture data. The ability to determine accurate parameter sets using pure component data alone is a cornerstone of the ideal of a fundamental, predictive model. The ability to regress such *Correlation* parameter sets is thus a notable step towards this goal. In the context of this work however, the SAFT-VR Mie[GV] EoS addresses the aim of improving the thermodynamic description of polar components and their mixtures.

Chapter 10:   RECOMMENDATIONS

Based on the results and finding of this work, the following are recommended for consideration in future work to further improve the thermodynamic description of polar components and their mixtures:

Generation of Pure Component u^{liq} Data

In Chapter 7, the severe lack of pure component speed of sound data available in the literature was highlighted. This is particularly true for polar components, where "data sets" typically only comprise two to three points. Given the modelling success of the *Correlation* approach in polar SAFT-VR Mie, where speed of sound data are used in the regression procedure, increased access to accurate pure component u^{liq} data is vital. While the use of isomer data as a pseudo property was shown to be a viable short term alternative, true data are required to improve the overall performance of these models.

Systematic Derivative Property Data Generation for Polar Isomers

The experimental aim of this work was the systematic generation of phase equilibrium data for all isomers of a polar molecule with a common second component. Given the difficulty with which these mixtures were accurately modelled, a recommendation is to expand the scope of study of these isomeric components. Specifically, systematic data generation for additional properties such as mixture speed of sound as well as excess properties for these same systems is recommended. This would provide a more holistic picture of the role of polar functional group location on the overall thermodynamic behaviour of these components, which may help in the accurate modelling of these components.

Mapping the Polar SAFT-VR Mie Parameter Space

The primary shortcoming of SAFT-VR Mie[JC] compared to its SAFT-VR Mie[GV] counterpart was the systematic inability of the former to regress unique parameter sets with a nonzero polar contribution. Indeed, this was also true for SAFT-VR Mie[GV] in a select few cases. This was attributed to broad minima in the objective function, which frequently pushed the polar parameter to zero. As highlighted in that section, interesting work has been done by Dufal *et al.* (2015) to map the parameter space of nonpolar SAFT-VR Mie in order to mitigate such regression problems. These mapping procedures help identify what parameter combinations should be specified as initial guesses to yield parameter sets close to the global minimum. These parameter combinations can be assessed based on their physical significance which would systematically improve the overall regression exercise.

Extension of Polar SAFT-VR Mie to Group Contribution Basis

Considering the work of Lafitte and co-workers since the revised SAFT-VR Mie EoS was published, it would appear that the model's development was seen as a stepping stone in the development of a new group contribution approach. The resulting SAFT-γ Mie model has been the focus of subsequent work from that group, with the group contribution approach seen as superior to the component-specific approach of SAFT-VR Mie. Whether these group contribution models are in fact superior is still a subject of debate, especially in the accurate description of isomers which has been a focus of this work. Thus, a recommendation of this work is to incorporate the polar SAFT-VR Mie results presented here into a polar SAFT-γ Mie framework to assess whether the group contribution approach represents a viable alternative.

Systematic Modelling Study of Excess Properties

The modelling of mixture excess properties highlighted predictive shortcomings in both polar sPC-SAFT and polar SAFT-VR Mie. This suggested potential fundamental discrepancies in the SAFT framework as a whole, particularly in the temperature description of A^r, which has already been commented on by a number of authors in the literature. A more thorough investigation of SAFT-type modelling of these excess properties is thus required. Such a study should focus exclusively on the accurate representation of excess properties, without consideration of mixture VLE, to determine whether these complex properties can be accurately represented in the model framework at all. To this end, component parameter could be fit to excess property data, with resulting parameter sets assessed for physical significance in the same fashion as is done when fit to phase equilibria data.

REFERENCES

Acosta, J., Arce, A., Rodil, E. & Soto, A. 2001, "Densities, speeds of sound, refractive indices, and the corresponding changes of mixing at 25 C and atmospheric pressure for systems composed by ethyl acetate, hexane, and acetone", *Journal of Chemical & Engineering Data,* vol. 46, no. 5, pp. 1176-1180.

Acosta, J., Arce, A., Martínez-Ageitos, J., Rodil, E. & Soto, A. 2002, "Vapor−liquid equilibrium of the ternary system ethyl acetate + hexane + acetone at 101.32 kpa", *Journal of Chemical and Engineering Data,* vol. 47, no. 4, pp. 849-854.

Alder, B.J., Young, D.A. & Mark, M.A. 1972, "Studies in molecular dynamics. X. Corrections to the augmented van der Waals theory for the square well fluid", *Journal of Chemical Physics,* vol. 56, no. 6, pp. 3013-3029.

Al-Saifi, N.M., Hamad, E.Z. & Englezos, P. 2008, "Prediction of vapor-liquid equilibrium in water-alcohol-hydrocarbon systems with the dipolar perturbed-chain SAFT equation of state", *Fluid Phase Equilibria,* vol. 271, no. 1-2, pp. 82-93.

Assael, M.J., Trusler, J.P.M. & Tsolakis, T.F. 1998, *Thermophysical properties of fluids: An introduction to their prediction,* Imperial College Press, London.

Azevedo, R.G.d., Szydlowski, J., Pires, P.F., Esperança, J.M.S.S., Guedes, H.J.R. & Rebelo, L.P.N. 2004, "A novel non-intrusive microcell for sound-speed measurements in liquids. Speed of sound and thermodynamic properties of 2-propanone at pressures up to 160 MPa", *The Journal of Chemical Thermodynamics,* vol. 36, no. 3, pp. 211-222.

Barker, J.A. & Henderson, D. 1967, "Perturbation theory and equation of state for fluids. II. A successful theory of liquids", *Journal of Chemical Physics,* vol. 47, no. 11, pp. 4714-4721.

Barker, J.A. & Henderson, D. 1967, "Perturbation theory and equation of state for fluids: The square-well potential", *Journal of Chemical Physics,* vol. 47, no. 8, pp. 2856-2861.

Boublik, T. 1970, "Hard-sphere equation of state", *Journal of Chemical Physics,* vol. 53, pp. 471.

Canosa, J., Rodríguez, A. & Tojo, J. 1999, "Binary mixture properties of diethyl ether with alcohols and alkanes from 288.15 K to 298.15 K", *Fluid Phase Equilibria,* vol. 156, no. 1–2, pp. 57-71.

Chapman, W.G., Gubbins, K.E., Jackson, G. & Radosz, M. 1990, "New reference equation of state for associating liquids", *Industrial and Engineering Chemistry Research,* vol. 29, no. 8, pp. 1709-1721.

Chapman, W.G., Gubbins, K.E., Jackson, G. & Radosz, M. 1989, "SAFT: Equation-of-state solution model for associating fluids", *Fluid Phase Equilibria,* vol. 52, no. C, pp. 31-38.

References

Chen, S.S. & Kreglewski, A. 1977, "Applications of the augmented van der Waals theory of fluids. I. Pure fluids", *Berichte der Bunsengesellschaft für Physikalische Chemie,* vol. 81, no. 10, pp. 1048-1052.

Chen, Z. & Hu, W. 1995, *Chinese Journal of Chemical Engineering,* vol. 3, no. 3, pp. 180.

Cobos, A., Hevia, F., González, J.A., García De La Fuente, I. & Alonso Tristán, C. 2016, "Thermodynamics of amide + ketone mixtures. 1. Volumetric, speed of sound and refractive index data for N,N-dimethylformamide + 2-alkanone systems at several temperatures", *The Journal of Chemical Thermodynamics,* vol. 98, pp. 21-32.

Costas, M. & Patterson, D. 1987, "Order destruction and order creation in binary mixtures of non-electrolytes", *Thermochimica acta,* vol. 120, pp. 161-181.

Cotterman, R.L., Schwarz, B.J. & Prausnitz, J.M. 1986, "Molecular thermodynamics for fluids at low and high densities. Part I: Pure fluids containing small or large molecules", *AIChE Journal,* vol. 32, no. 11, pp. 1787-1798.

Cripwell, J. 2014, *Assessment of the capabilities of two polar sPC-SAFT terms through application to measured ketone-alkane phase equilibria*, Masters edn, Stellenbosch University, Stellenbosch, South Africa.

Cripwell, J.T., Schwarz, C.E. & Burger, A.J. 2016, "Vapor-liquid equilibria measurements for the five linear C6 esters with n-octane", *Journal of Chemical and Engineering Data,* vol. 61, no. 7, pp. 2353-2362.

Cripwell, J.T., Schwarz, C.E. & Burger, A.J. 2015, "Vapor-liquid equilibria measurements for the nine n-alkane/ketone pairs comprising 2-, 3-, and 4-heptanone with n -octane, n -nonane, and n -decane", *Journal of Chemical and Engineering Data,* vol. 60, no. 3, pp. 602-611.

Dahl, S. & Michelsen, M.L. 1990, "High-pressure vapor-liquid equilibrium with a UNIFAC-based equation of state", *AIChE Journal,* vol. 36, no. 12, pp. 1829-1836.

de Villiers, A.J. 2011, *Evaluation and improvement of the sPC-SAFT equation of state for complex mixtures*, Stellenbosch University.

de Villiers, A.J., Schwarz, C.E. & Burger, A.J. 2011a, "Improving vapour-liquid-equilibria predictions for mixtures with non-associating polar components using sPC-SAFT extended with two dipolar terms", *Fluid Phase Equilibria,* vol. 305, no. 2, pp. 174-184.

de Villiers, A.J., Schwarz, C.E. & Burger, A.J. 2011b, "New association scheme for 1-alcohols in alcohol/water mixtures with sPC-SAFT: The 2C association scheme", *Industrial and Engineering Chemistry Research,* vol. 50, no. 14, pp. 8711-8725.

de Villiers, A.J., Schwarz, C.E., Burger, A.J. & Konotgeorgis, G.M. 2013, "Evaluation of the PC-SAFT, SAFT and CPA equations of state in predicting derivative properties of selected nonpolar and hydrogen-bonding compounds", *Fluid Phase Equilibria,* vol. 338, pp. 1-15.

References

DIPPR 801 Database *Design Institute for Physical Properties*, Sponsored by AIChE.

Dominik, A., Chapman, W.G., Kleiner, M. & Sadowski, G. 2005, "Modeling of polar systems with the perturbed-chain SAFT equation of state. Investigation of the performance of two polar terms", *Industrial and Engineering Chemistry Research,* vol. 44, no. 17, pp. 6928-6938.

Dufal, S. 2013, *Development and application of advanced thermodynamic molecular description for complex reservoir fluids containing carbon dioxide and brines* , Doctor of Philosophy edn, Imperial College London, United Kingdom.

Dufal, S., Lafitte, T., Galindo, A., Jackson, G. & Haslam, A.J. 2015, "Developing intermolecular-potential models for use with the SAFT-VR Mie equation of state", *AIChE Journal,* vol. 61, no. 9, pp. 2891-2912.

Economou, I.G. 2002, "Statistical associating fluid theory: A successful model for the calculation of thermodynamic and phase equilibrium properties of complex fluid mixtures", *Industrial and Engineering Chemistry Research,* vol. 41, no. 5, pp. 953-962.

Economou, I.G. & Donohue, M.D. 1991, "Chemical, quasi-chemical and perturbation theories for associating fluids", *AIChE Journal,* vol. 37, no. 12, pp. 1875-1894.

Feng, L.C., Chou, C.H., Tang, M. & Chen, T.P. 1998, "Vapor-liquid equilibria of binary mixtures 2-butanol + butyl acetate, hexane + butyl acetate, and cyclohexane + 2 butanol at 101.3 kPa", *Journal of Chemical and Engineering Data,* vol. 43, pp. 658-661.

Fernández, L., Pérez, E., Ortega, J., Canosa, J. & Wisniak, J. 2013, "Multiproperty modeling for a set of binary systems. Evaluation of a model to correlate simultaneously several mixing properties of methyl ethanoate + alkanes and new experimental data", *Fluid Phase Equilibria,* vol. 341, pp. 105-123.

Fernández, L., Pérez, E., Ortega, J., Canosa, J. & Wisniak, J. 2010, "Measurements of the excess properties and vapor-liquid equilibria at 101.32 kPa for mixtures of ethyl ethanoate + alkanes (from C5 to C10)", *Journal of Chemical and Engineering Data,* vol. 55, pp. 5519-5533.

Freitas, S.V.D., Santos, Â., Moita, M.-.C.J., Follegatti-Romero, L.A., Dias, T.P.V.B., Meirelles, A.J.A., Daridon, J.-., Lima, Á.S. & Coutinho, J.A.P. 2013, "Measurement and prediction of speeds of sound of fatty acid ethyl esters and ethylic biodiesels", *Fuel,* vol. 108, pp. 840-845.

Fuchs, R., Krenzer, L. & Gaube, J. 1984, "Excess properties of binary mixtures composed of a polar component and an alkane", *Berichte der Bunsengesellschaft für Physikalische Chemie,* vol. 88, pp. 642-649.

Galindo, A., Davies, L.A., Gil-Villegas, A. & Jackson, G. 1998, "The thermodynamics of mixtures and the corresponding mixing rules in the SAFT-VR approach for potentials of variable range", *Molecular Physics,* vol. 93, no. 2, pp. 241-252.

Galván, S., Ortega, J., Susial, P. & Pena, J.A. 1994, "Isobaric vapor-liquid-equilibria for propyl methanoate plus (n-alkanes, C-7, C-8, C-9) or n-alkanols (C-2, C-3, C-4)", *Journal of Chemical Engineering of Japan,* vol. 27, no. 4, pp. 529-534.

Garriga, R., Andrés, A.C., Pérez, P. & Gracia, M. 1999, "Vapor pressures at several temperatures and excess functions at 298.15 K of butanone with di-n-propyl ether or diisopropyl ether", *Journal of Chemical and Engineering Data,* vol. 44, no. 2, pp. 296-302.

Geiseler, G. & Köhler, H. 1968, "Thermodynamisches verhalten der mischsysteme methyläthylketoxim/n-heptan, diäthylketon/n-heptan und methyläthylketoxim/diäthylketon", *Berichte der Bunsengesellschaft für Physikalische Chemie,* vol. 72, no. 6, pp. 697-706.

Gil-Villegas, A., Galindo, A., Whitehead, P.J., Mills, S.J., Jackson, G. & Burgess, A.N. 1996, "Statistical associating fluid theory for chain molecules with attractive potentials of variable range", *Journal of Chemical Physics,* vol. 106, no. 10, pp. 4168-4186.

Glukhareva, M., Taravkova, E., Chashchin, A., Kushner, T. & Serafimov, L. 1974, "Liquid-vapor phase equilibriums in the acetone-diethyl ketone, methyl ethyl ketone-diethyl ketone, and diethyl ketone-acetic acid systems at 760 torr", *Tr.Mosk.in-ta tonkoi khim.tekhnol,* vol. 4, pp. 86-89.

Gmehling, J., Onken, U. & Arlt, W. 1979, *Vapour-liquid equilibrium collection. Aldehydes and Ketones. Ethers (Volume 1),* DECHEMA, Frankfurt.

González, J.A., Alonso, I., Mozo, I., García De La Fuente, I. & Cobos, J.C. 2011, "Thermodynamics of (ketone + amine) mixtures. Part VI. Volumetric and speed of sound data at (293.15, 298.15, and 303.15) K for (2-heptanone + dipropylamine, +dibutylamine, or +triethylamine) systems", *Journal of Chemical Thermodynamics,* vol. 43, no. 10, pp. 1506-1514.

Gonzalez-Olmos, R., Iglesias, M., Santos, B.M.R.P. & Mattedi, S. 2008, "Thermodynamics of oxygenate fuel additives as a function of temperature", *Physics and Chemistry of Liquids,* vol. 46, no. 3, pp. 223-237.

Gorbunova, L.V., Lutugina, N.V. & Malenko, Y.I. 1965, *Zhurnal Prikladnoi Khimii,* vol. 38, pp. 374.

Grolier, J.P.E. & Benson, G.C. 1984, "Thermodynamic properties of binary mixtures containing ketones. VIII. Heat capacities and volumes of some n-alkanone + n-alkane mixtures at 298.15 K", *Canadian Journal of Chemistry,* vol. 62, no. 5, pp. 949-953.

Gross, J. 2005, "An equation-of-state contribution for polar components: Quadrupolar molecules", *AIChE Journal,* vol. 51, no. 9, pp. 2556-2568.

Gross, J. & Sadowski, G. 2002, "Application of the perturbed-chain SAFT equation of state to associating systems", *Industrial and Engineering Chemistry Research,* vol. 41, no. 22, pp. 5510-5515.

References

Gross, J. & Sadowski, G. 2001, "Perturbed-chain SAFT: An equation of state based on a perturbation theory for chain molecules", *Industrial and Engineering Chemistry Research,* vol. 40, no. 4, pp. 1244-1260.

Gross, J. & Sadowski, G. 2000, "Application of perturbation theory to a hard-chain reference fluid: An equation of state for square-well chains", *Fluid Phase Equilibria,* vol. 168, no. 2, pp. 183-199.

Gross, J. & Vrabec, J. 2006, "An equation-of-state contribution for polar components: Dipolar molecules", *AIChE Journal,* vol. 52, no. 3, pp. 1194-1204.

Huang, S.H. & Radosz, M. 1991, "Equation of state for small, large, polydisperse, and associating molecules: Extension to fluid mixtures", *Industrial and Engineering Chemistry Research,* vol. 30, no. 8, pp. 1994-2005.

Huang, S.H. & Radosz, M. 1990, "Equation of state for small, large, polydisperse, and associating molecules", *Industrial and Engineering Chemistry Research,* vol. 29, no. 11, pp. 2284-2294.

Jog, P.K. & Chapman, W.G. 1999, "Application of Wertheim's thermodynamic perturbation theory to dipolar hard sphere chains", *Molecular Physics,* vol. 97, no. 3, pp. 307-319.

Jog, P.K., Sauer, S.G., Blaesing, J. & Chapman, W.G. 2001, "Application of dipolar chain theory to the phase behavior of polar fluids and mixtures", *Industrial and Engineering Chemistry Research,* vol. 40, no. 21, pp. 4641-4648.

Kirss, H., Siimer, E., Kuus, M. & Kudryavtseva, L. 2001, "Isobaric vapor-liquid equilibria in the system o-xylene + amyl acetate + nonane", *Journal of Chemical and Engineering Data,* vol. 46, no. 1, pp. 147-150.

Kiyohara, O., Handa, Y.P. & Benson, G.C. 1979, "Thermodynamic properties of binary mixtures containing ketones III. Excess enthalpies of n-alkanes + some aliphatic ketones", *The Journal of Chemical Thermodynamics,* vol. 11, no. 5, pp. 453-460.

Kleiner, M. & Gross, J. 2006, "An equation of state contribution for polar components: Polarizable dipoles", *AIChE Journal,* vol. 52, no. 5, pp. 1951-1961.

Klon-Palczewska, M., Cholinski, J. & Wyrzykowska-Stankiewicz, D. 1980, "Isobaric vapour-liquid equilibrium in binary organic solvent mixtures", *Chem.Stosow.,* vol. 24, pp. 197-209.

Kontogeorgis, G.M. & Folas, G.K. 2010, *Thermodynamics models for industrial applications: From classical and advanced mixing rules to association theories,* John Wiley & Sons, Ltd., Wiltshire, United Kingdom.

Kroenlein, K., Diky, V., Muzny, C.D., Chirico, R.D., Magee, J.W. & Frenkel, M. *, ThermoLit NIST Literature Report Builder for Thermophysical and Thermochemical Property Measurements NIST Standard Reference Database #171*. Available: http://trc.nist.gov/thermolit/main/home.html#home [2016, 02/20].

Lafitte, T., Apostolakou, A., Avendaño, C., Galindo, A., Adjiman, C.S., Müller, E.A. & Jackson, G. 2013, "Accurate statistical associating fluid theory for chain molecules formed from Mie segments", *The Journal of Chemical Physics,* vol. 139, no. 15.

Lafitte, T., Bessieres, D., Piñeiro, M.M. & Daridon, J.-. 2006, "Simultaneous estimation of phase behavior and second-derivative properties using the statistical associating fluid theory with variable range approach", *Journal of Chemical Physics,* vol. 124, no. 2.

Lafitte, T., Piñeiro, M.M., Daridon, J.-. & Bessières, D. 2007, "A comprehensive description of chemical association effects on second derivative properties of alcohols through a SAFT-VR approach", *Journal of Physical Chemistry B,* vol. 111, no. 13, pp. 3447-3461.

Lee, M., Hsiao, C. & Lin, H. 1997, "Isothermal vapor-liquid equilibria for mixtures of methyl tert-butyl ether, methyl acetate, and ethyl acetate", *Fluid Phase Equilibria,* vol. 137, no. 1, pp. 193-207.

Linstrom, P.J. & Mallard, W.G. *, NIST Chemistry WebBook, NIST Standard Reference Database Number 69.* Available: http://webbook.nist.gov [2016, 02/20].

Llovell, F., Peters, C.J. & Vega, L.F. 2006, "Second-order thermodynamic derivative properties of selected mixtures by the soft-SAFT equation of state", *Fluid Phase Equilibria,* vol. 248, no. 2, pp. 115-122.

Macedo, E.A., Mendonca, J.M. & Medina, A.G. 1984, "Vapor-liquid equilibrium for the systems ethyl formate-methyl ethyl ketone, ethyl formate-toluene and ethyl formate-methyl ethyl ketone-toluene: new unifac parameters for interactions between the groups ACH/HCOO, ACCH2/HCOO and CH2Co/HCOO", *Fluid Phase Equilibria,* vol. 18, no. 2, pp. 197-210.

Máchová, I., Linek, J. & Wichterle, I. 1988, "Vapour-liquid equilibria in the heptane - 1-pentanol and heptane - 3-methyl-1-butanol systems at 75, 85 and 95 °C", *Fluid Phase Equilibria,* vol. 41, no. 3, pp. 257-267.

Mansoori, G.A., Carnahan, N.F., Starling, K.E. & Leland, T.W.J. 1971, "Equilibrium thermodynamic properties of the mixture of hard spheres", *Journal of Chemical Physics,* vol. 54, no. 4, pp. 1523-1525.

Marino, G., Piñeiro, M.M., Iglesias, M., Orge, B. & Tojo, J. 2001, "Temperature dependence of binary mixing properties for acetone, methanol, and linear aliphatic alkanes (C6-C8)", *Journal of Chemical & Engineering Data,* vol. 46, no. 3, pp. 728-734.

Maripuri, V.C. & Ratcliff, G.A. 1972, "Isothermal vapour-liquid equilibria in binary mixtures of ketones and alkanes", *Journal of Applied Chemistry and Biotechnology,* vol. 22, no. 8, pp. 899-903.

Marsh, K.N., Niamskul, P., Gmehling, J. & Bölts, R. 1999, "Review of thermophysical property measurements on mixtures containing MTBE, TAME, and other ethers with nonpolar solvents", *Fluid Phase Equilibria,* vol. 156, no. 1–2, pp. 207-227.

References

McDermott, C. & Ellis, S.R.M. 1965, "A multicomponent consistency test", *Chemical Engineering Science,* vol. 20, no. 4, pp. 293-296.

Mejía, A., Segura, H. & Cartes, M. 2011, "Vapor-liquid equilibrium in the binary systems 2-butanol + tert -amyl methyl ether, 2-butanol + heptane, and heptane + tert-amyl methyl ether", *Journal of Chemical and Engineering Data,* vol. 56, no. 5, pp. 2256-2265.

Michelsen, M. L. & Mollerup, J.M. 2007, *Thermodynamic models: Fundamental & computational aspects*, Tie-Line Publications, Holte, Denmark.

Müller, E.A. & Gubbins, K.E. 2001, "Molecular-based equations of state for associating fluids: A review of SAFT and related approaches", *Industrial and Engineering Chemistry Research,* vol. 40, no. 10, pp. 2193-2211.

Ohomuro, K., Tamura, K. & Murakami, S. 1987, "Speeds of sound, excess molar volumes, and isentropic compressibilities of "xCH3COC2H5 + (1 - x)C7H16',...", *The Journal of Chemical Thermodynamics,* vol. 19, no. 2, pp. 163-169.

Ortega, J., Espiau, F., Tojo, J., Canosa, J. & Rodríguez, A. 2003, "Isobaric vapor-liquid equilibria and excess properties for the binary systems of methyl esters + heptane", *Journal of Chemical and Engineering Data,* vol. 48, no. 5, pp. 1183-1190.

Ortega, J., Fernández, L. & Sabater, G. 2015, "Solutions of alkyl methanoates and alkanes: Simultaneous modeling of phase equilibria and mixing properties. Estimation of behavior by UNIFAC with recalculation of parameters", *Fluid Phase Equilibria,* vol. 402, pp. 38-49.

Ortega, J., González, C. & Galván, S. 2001, "Vapor-liquid equilibria for binary systems composed of a propyl ester (ethanoate, propanoate, butanoate) + an n-alkane (C7, C9)", *Journal of Chemical and Engineering Data,* vol. 46, no. 4, pp. 904-912.

Ortega, J., Vidal, M., Toledo-Marante, F.J. & Plácido, J. 1999, "Thermodynamic properties of (a propyl ester+ann-alkane). XII. Excess molar enthalpies and excess molar volumes for {xCH3(CH2)u−1COO(CH2)2CH3+(1−x)CH3(CH2)2v+1CH3} withu=(1to 3), andv=(1to 7)", *The Journal of Chemical Thermodynamics,* vol. 31, no. 8, pp. 1025-1044.

Oswal, S.L., Oswal, P., Modi, P.S., Dave, J.P. & Gardas, R.L. 2004, "Acoustic, volumetric, compressibility and refractivity properties and Flory's reduction parameters of some homologous series of alkyl alkanoates from 298.15 to 333.15 K", *Thermochimica Acta,* vol. 410, no. 1–2, pp. 1-14.

Othmer, D.F., Chudgar, M.M. & Levy, S.L. 1952, "Binary and Ternary Systems of Acetone, Methyl Ethyl Ketone, and Water", *Ind Eng Chem Res,* vol. 44, no. 8, pp. 1872-1881.

Pal, A., Kumar, H., Maan, R. & Sharma, H.K. 2013, "Volumetric and ultrasonic studies of molecular interactions in n -alkoxypropanols + alkyl acetates mixtures at different temperatures", *Journal of Chemical and Engineering Data,* vol. 58, no. 11, pp. 3190-3200.

Park, S.-., Han, K.-. & Gmehling, J. 2002, "Vapor-liquid equilibria and excess properties for methyl tert-butyl ether (MTBE) containing binary systems", *Fluid Phase Equilibria,* vol. 200, no. 2, pp. 399-409.

Patwari, M.K., Bachu, R.K., Boodida, S. & Nallani, S. 2009, "Densities, viscosities, and speeds of sound of binary liquid mixtures of sulfolane with ethyl acetate, n-propyl acetate, and n-butyl acetate at temperature of (303.15, 308.15, and 313.15) K", *Journal of Chemical and Engineering Data,* vol. 54, no. 3, pp. 1069-1072.

Peng, D.-. & Robinson, D.B. 1976, "A new two-constant equation of state", *Industrial and Engineering Chemistry Fundamentals,* vol. 15, no. 1, pp. 59-64.

Pienaar, C. 2011, *Evaluation of entrainers for the dehydration of C2 and C3 alcohols via azeotropic distillation*, Stellenbosch University.

Pintos, M., Bravo, R., Baluja, M.C., Paz-Andrade, M.I., Roux-Desgranges, G. & Grolier, J.P.E. 1988, "Thermodynamics of alkanoate + alkane binary mixtures. Concentration dependence of excess heat capacities and volumes", *Canadian Journal of Chemistry,* vol. 66, no. 5, pp. 1179-1186.

Polishuk, I. & Mulero, A. 2011, "The numerical challenges of SAFT EoS models", *Reviews in Chemical Engineering,* vol. 27, no. 5-6, pp. 241-251.

Polishuk, I. 2011, "Addressing the issue of numerical pitfalls characteristic for SAFT EOS models", *Fluid Phase Equilibria,* vol. 301, no. 1, pp. 123-129.

Rathnam, M.V., Jain, K. & Kumar, M.S.S. 2010, "Physical properties of binary mixtures of ethyl formate with benzene, isopropyl benzene, isobutyl benzene, and butylbenzene at (303.15, 308.15, and 313.15) K", *Journal of Chemical and Engineering Data,* vol. 55, no. 4, pp. 1722-1726.

Reich, R., Cartes, M., Segura, H. & Wisniak, J. 2000, "Isobaric vapor-liquid equilibria in the systems ethyl 1,1-dimethylethyl ether + hexane and + heptane", *Physics and Chemistry of Liquids,* vol. 38, no. 2, pp. 217-232.

Resa, J.M., Betolaza, M.A., González, C. & Ruiz, A. 1995, "13th IUPAC Conference on Chemical Thermodynamics concerning Fluid Phase Equilibria Isobaric vapor-liquid equilibria of acetone-propyl ether and isopropyl ether-propyl ether systems. Corroboration of no reverse volatility", *Fluid Phase Equilibria,* vol. 110, no. 1, pp. 205-217.

References

Resa, J.M., González, C., Betolaza, M.A. & Ruiz, A. 1999, "Behaviour of butyl ether as entrainer for the extractive distillation of the azeotropic mixture propanone+diisopropyl ether. Isobaric VLE data of the azeotropic components with the entrainer", *Fluid Phase Equilibria,* vol. 156, no. 1–2, pp. 89-99.

Ríos, R., Ortega, J. & Fernández, L. 2012, "Measurements and correlations of the isobaric vapor−liquid equilibria of binary mixtures and excess properties for mixtures containing an alkyl (methyl, ethyl) butanoate with an alkane (heptane, nonane) at 101.3 kPa", *Journal of Chemical and Engineering Data,* vol. 57, pp. 3210-3224.

Ríos, R., Ortega, J., Fernández, L., de Nuez, I. & Wisniak, J. 2014, "Improvements in the experimentation and the representation of thermodynamic properties (iso-p VLE and yE) of alkyl propanoate + alkane Binaries", *Journal of Chemical and Engineering Data,* vol. 59, pp. 125-142.

Rushbrooke, G.S., Stell, G. & Høye, J.S. 1973, "Theory of polar liquids I. Dipolar hard spheres", *Molecular Physics,* vol. 26, no. 5, pp. 1199-1215.

Sandler, S. I. (2006). *Chemical, biochemical, and engineering thermodynamics* John Wiley & Sons, Inc.

Sastry, N.V., Jain, N.J., George, A. & Bahadur, P. 1999, "Viscosities, speeds of sound and excess isentropic compressibilities of binary mixtures of alkyl alkanoate–hydrocarbons at 308.15 K and 318.15 K", *Fluid Phase Equilibria,* vol. 163, no. 2, pp. 275-289.

Sastry, N.V., Patel, S.R. & Soni, S.S. 2013, "Excess molar volumes, excess isentropic compressibilities, excess viscosities, relative permittivity and molar polarization deviations for methyl acetate +, ethyl acetate +, butyl acetate +, isoamyl acetate +, methyl propionate +, ethyl propionate +, ethyl butyrate +, methyl methacrylate +, ethyl methacrylate +, and butyl methacrylate + cyclohexane at T = 298.15 and 303.15 K", *Journal of Molecular Liquids,* vol. 183, pp. 102-112.

Sastry, N.V., Thakor, R.R. & Patel, M.C. 2009, "Excess molar volumes, viscosity deviations, excess isentropic compressibilities and deviations in relative permittivities of (alkyl acetates (methyl, ethyl, butyl and isoamyl) + n-hexane, + benzene, + toluene, + (o-, m-, p-) xylenes, + (chloro-, bromo-, nitro-) benzene at temperatures from 298.15 to 313.15 K", *Journal of Molecular Liquids,* vol. 144, no. 1–2, pp. 13-22.

Sauer, S.G. & Chapman, W.G. 2003, "A parametric study of dipolar chain theory with applications to ketone mixtures", *Industrial and Engineering Chemistry Research,* vol. 42, no. 22, pp. 5687-5696.

Schaffer, K. 1978, *Dechema Heats of Mixing Collection, Volume III, Part 1,* Dechema.

Segovia, J.J., Martín, M.C., Chamorro, C.R. & Villamañán, M.A. 1998, "Vapor−liquid equilibrium of ternary mixtures containing methyl tert-butyl ether and/or substitution hydrocarbons. Methyl tert-butyl ether + heptane + cyclohexane and methyl tert-butyl ether + cyclohexane + 1-hexene at 313.15 K", *Journal of Chemical and Engineering Data,* vol. 43, no. 6, pp. 1021-1026.

Shaburov, M.A., Sorokin, V.I., Chaschin, A.M. & Lazareva, N.K. 1971, "Vapor-liquid equilibrium of butyl acetate + butyl formate and butyl propionate + butyl formate two component systems", *Gidroliz. Lesokhim. Prom-st.,* vol. 24, pp. 10.

Shealy, G.S. & Sandler, S.I. 1985, "Vapor-liquid equilibria of {xCH3CH(CH3)CHO+(1-x)C7H16}(l) and {xCH3CO2C2H5+(1-x)C7H16}(l)", *The Journal of Chemical Thermodynamics,* vol. 17, no. 2, pp. 143-150.

Shono, H. & Kanazawa, N. 1969, "Vapor–liquid equilibrium in extractive distillation of ethyl acetate–ethanol system", *Kogyo Kagaku Zasshi,* vol. 72, pp. 815.

Smith, J.M., Van Ness, H.C. & Abbott, M.M. 2005, *Introduction to Chemical Engineering Thermodynamics,* 7th edn, McGraw-Hill, New York.

Soave, G. 1972, "Equilibrium constants from a modified Redlich-Kwong equation of state", *Chemical Engineering Science,* vol. 27, no. 6, pp. 1197-1203.

Tan, S.P., Adidharma, H. & Radosz, M. 2008, "Recent advances and applications of statistical associating fluid theory", *Industrial and Engineering Chemistry Research,* vol. 47, no. 21, pp. 8063-8082.

Toledo-Marante, ,F.J., Ortega, ,J., Chaar, ,M. & Vidal, M. 2000, "Thermodynamic properties of (a butyl ester + ann-alkane). XIII. HmE and VmE for {xCH3(CH2)u−1CO2(CH2)3CH3+(1−x)CH3(CH2)2 v+1CH3}, where u= 1 to 3 and v= 1 to 7", *The Journal of Chemical Thermodynamics,* vol. 32, no. 8, pp. 1013-1036.

Treszczanowicz, T. & Lu, B.C.-. 1986, "Isothermal vapour-liquid equilibria for 11 examples of (an ether + a hydrocarbon)", *The Journal of Chemical Thermodynamics,* vol. 18, no. 3, pp. 213-220.

Tumakaka, F. & Sadowski, G. 2004, "Application of the perturbed-chain SAFT equation of state to polar systems", *Fluid Phase Equilibria,* vol. 217, no. 2, pp. 233-239.

Urdaneta, O., Handa, Y.P. & Benson, G.C. 1979, "Thermodynamic properties of binary mixtures containing ketones V. Excess enthalpies of an isomeric heptanone + n-heptane", *The Journal of Chemical Thermodynamics,* vol. 11, no. 9, pp. 857-860.

Varfolomeev, M.A., Zaitseva, K.V., Rakipov, I.T., Solomonov, B.N. & Marczak, W. 2014, "Speed of sound, density, and related thermodynamic excess properties of binary mixtures of butan-2-one with C1-C4 n-alkanols and chloroform", *Journal of Chemical and Engineering Data,* vol. 59, no. 12, pp. 4118-4132.

Vidal, M., Ortega, J. & Plácido, J. 1997, "Thermodynamic properties of (an ethyl ester + andn-alkane). IX. HmE and VmE for {xCH3(CH2)uCOOCH2CH3+ (1−x)CH3(CH2)2v + 1CH3} with u= 0 to 5, and v= 1 to 7", *The Journal of Chemical Thermodynamics,* vol. 29, no. 1, pp. 47-74.

References

Von Solms, N., Michelsen, M.L. & Kontogeorgis, G.M. 2003, "Computational and physical performance of a modified PC-SAFT equation of state for highly asymmetric and associating mixtures", *Industrial and Engineering Chemistry Research,* vol. 42, no. 5, pp. 1098-1105.

Von Solms, N., Michelsen, M.L. & Kontogeorgis, G.M. 2004, "Applying association theories to polar fluids", *Industrial and Engineering Chemistry Research,* vol. 43, no. 7, pp. 1803-1806.

Wei, Y.S. & Sadus, R.J. 2000, "Equations of state for the calculation of fluid-phase equilibria", *AIChE Journal,* vol. 46, no. 1, pp. 169-196.

Wertheim, M.S. 1986, "Fluids with highly directional attractive forces. III. Multiple attraction sites", *Journal of Statistical Physics,* vol. 42, no. 3-4, pp. 459-476.

Wertheim, M.S. 1986, "Fluids with highly directional attractive forces. IV. Equilibrium polymerization", *Journal of Statistical Physics,* vol. 42, no. 3-4, pp. 477-492.

Wertheim, M.S. 1984, "Fluids with highly directional attractive forces. I. Statistical thermodynamics", *Journal of Statistical Physics,* vol. 35, no. 1-2, pp. 19-34.

Wertheim, M.S. 1984, "Fluids with highly directional attractive forces. II. Thermodynamic perturbation theory and integral equations", *Journal of Statistical Physics,* vol. 35, no. 1-2, pp. 35-47.

Wisniak, J., Fishman, E. & Shaulitch, R. 1998, "Isobaric vapor-liquid equilibria in the systems 2-butanone + heptane and 2-butanone + oxolane", *Journal of Chemical and Engineering Data,* vol. 43, no. 4, pp. 537-540.

Wisniak, J. 1994, "The Herington test for thermodynamic consistency", *Industrial and Engineering Chemistry Research,* vol. 33, no. 1, pp. 177-180.

Wisniak, J. 1993, "A new test for the thermodynamic consistency of vapor-liquid equilibrium", *Industrial and Engineering Chemistry Research,* vol. 32, no. 7, pp. 1531-1533.

Wisniak, J., Embon, G., Shafir, R., Segura, H. & Reich, R. 1997, "Isobaric vapor-liquid equilibria in the systems methyl 1,1-dimethylethyl ether + octane and heptane + octane", *Journal of Chemical and Engineering Data,* vol. 42, no. 6, pp. 1191-1194.

Wisniak, J., Magen, E., Shachar, M., Zeroni, I., Reich, R. & Segura, H. 1997, "Isobaric vapor-liquid equilibria in the systems methyl 1,1-dimethylethyl ether + hexane and + heptane", *Journal of Chemical and Engineering Data,* vol. 42, no. 2, pp. 243-247.

Wolfová, J., Linek, J. & Wichterle, I. 1991, "Vapour-liquid equilibria in the heptane-2-pentanol and heptane-2-methyl-1-butanol systems at 75, 85 and 95°C", *Fluid Phase Equilibria,* vol. 64, no. C, pp. 281-289.

Wolfová, J., Linek, J. & Wichterle, I. 1990, "Vapour-liquid equilibria in the heptane - 3-pentanol and heptane - 2-methyl-2-butanol systems at constant temperature", *Fluid Phase Equilibria,* vol. 54, no. C, pp. 69-79.

Wu, H.S. & Sandler, S.I. 1988, "Vapor-liquid equilibria for binary mixtures of butyl ether with 2-furaldehyde and with 2-, 3-, and 4-heptanone", *Journal of Chemical and Engineering Data,* vol. 33, no. 3, pp. 316-321.

Zhao, H., Ding, Y. & McCabe, C. 2007, "Phase behavior of dipolar associating fluids from the SAFT-VR+D equation of state", *Journal of Chemical Physics,* vol. 127, no. 8.

Zhao, H. & McCabe, C. 2006, "Phase behavior of dipolar fluids from a modified statistical associating fluid theory for potentials of variable range", *Journal of Chemical Physics,* vol. 125, no. 10.

APPENDIX A: GC-MS RESULTS FOR PENTYL FORMATE

Figure A.1: Pre-purification GC-MS chromatograph and report for pentyl

Dept Process Engineering, US   Library Search Report

Data Path : D:\J Cripwell\
Data File : JAMIE AMYL FORMATE 29-07-2015 INJ2.D
Acq On   : 29 Jul 2015 13:19
Operator :
Sample   :
Misc   :
ALS Vial : 1   Sample Multiplier: 1

Search Libraries: C:\Database\NIST11.L   Minimum Quality: 0

Unknown Spectrum: Apex minus start of peak
Integration Events: ChemStation Integrator - autoint1.e

Pk#	RT	Area%	Library/ID	Ref#	CAS#	Qual
1	11.838	0.38	C:\Database\NIST11.L			
			Methyl cis-2-trimethylsilyl-cyclopropane-1-carboxylate	40242	1000144-79-0	53
			Isobutyl 2,5,8,11-tetraoxatridecan-13-yl carbonate	150869	1000378-27-9	50
			1-Propanamine, N,2-dimethyl-N-nitroso-	14186	053951-45-4	45
2	15.055	1.16	C:\Database\NIST11.L			
			1-Pentanol	2091	000071-41-0	80
			1-Pentanol	2088	000071-41-0	72
			1-Pentanol	2093	000071-41-0	64
3	15.595	98.20	C:\Database\NIST11.L			
			Formic acid, pentyl ester	8122	000638-49-3	78
			1,2-Oxaborolane, 2-ethyl-4,5-dimethyl-	11267	074685-45-3	59
			1-Butanol, 3-methyl-	2123	000123-51-3	56
4	15.870	0.27	C:\Database\NIST11.L			
			N-(2-Acetylcyclopentylidene)cyclohexylamine	66949	1000100-48-5	9
			Hexahydropyridine, 1-methyl-4-[4,5-dihydroxyphenyl]-	66899	094427-47-1	9
			trans-2,3-Methylenedioxy-b-methyl-b-nitrostyrene	66654	086029-47-2	9

DESORBER fr...dated 2015.M Mon Aug 03 13:25:31 2015

Figure A.2: Post-purification GC-MS chromatograph and report for pentyl formate

APPENDIX B: CERTIFICATES OF CALIBRATION

ALEXANDER WIEGAND SE & Co. KG

WIKA

zertifiziert nach DIN ISO 9001
certified by DIN ISO 9001
DQS Reg. Nr. 1830-01

UniTrans

Messwertprotokoll für Drucktransmitter
Test certificate for Pressure Transmitter
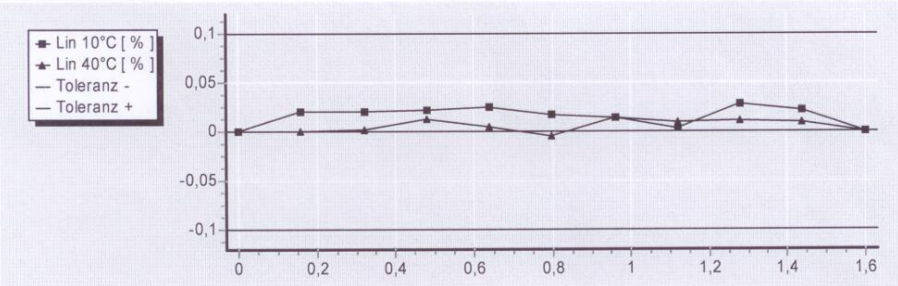
Gerätedaten: Instrument Data:	Kopf-Nr. Head No.	Messbereichsanfang Start of Range	Messbereichsende End of Range	Druckeinheit Unit of Pressure	Genauigkeit [%] Accuracy [%]
	SZ65	0	1,6	bar / abs.	0,1

Ausgang bei 20°C: Output at 20°C:	Nullpunkt Zero		Endwert Full Scale	
	3,99	mA	20,00	mA

Kennlinienwerte: Characteristics:	Referenzdruck Ref Pressure		Linearitätsabweichung [%] Deviation of linearity [%]	
	[%]	[bar]	bei / at 10°C	bei / at 40°C
	0	0,000	0,000	0,000
	10	0,160	0,020	0,001
	20	0,320	0,021	0,002
	30	0,480	0,021	0,013
	40	0,640	0,024	0,005
	50	0,800	0,016	-0,005
	60	0,960	0,014	0,014
	70	1,120	0,003	0,009
	80	1,280	0,028	0,010
	90	1,440	0,022	0,009
	100	1,600	0,000	0,000

Linearitätsabweichung [%]:
Deviation of linearity [%]:

Datum: 10.09.2012   **geprüft von :**   012
Date: testet by:

Die Produktionsabteilung für Druckmessgeräte wird unterstützt und überwacht von dem WIKA DKD-Kalibrationslabor für Druck DKD-K-03701
The pressure department is supported and monitored by the WIKA pressure DKD-Calibration-Laboratory-DKD-K-03701

Druck + Temperatur

WIKA Alexander Wiegand SE & Co. KG   Tel. +49 9372 132-0   Kommanditgesellschaft: Sitz Klingenberg -   Komplementärin:
Alexander-Wiegand-Straße 30   Fax +49 9372 132-406   Amtsgericht Aschaffenburg HRA 1819   WIKA International SE - Sitz Klingenberg -
63911 Klingenberg   E-Mail info@wika.de   Komplementärin: WIKA Verwaltungs SE & Co. KG - Amtsgericht Aschaffenburg HRB 10505
Germany   www.wika.de   Sitz Klingenberg - Amtsgericht Aschaffenburg HRA 4685   Vorstand: Alexander Wiegand
                                                                                                                     Vorsitzender des Aufsichtsrats: Dr. Max Egli

Unique Metrology

Eskom Research & Innovation Centre
Lower Germiston Road • Rosherville
P O Box 145296 • Bracken Gardens • 1452
Tel: 011 626 3808 • Cell: 083 254 3635 • Fax: 086 610 4196
Web: www.unimet.co.za

sanas
Calibration Laboratory
306   205

SANAS ACCREDITED CALIBRATION LABORATORY No 306

TEMPERATURE METROLOGY

CERTIFICATE OF CALIBRATION

Date of issue   :   26/11/2012

Certificate No :   1211T4452-1

Technical Signatory

M Mathieson.

Page 1 of 2 pages.

The results of all measurements are traceable to the national measuring standards.

The values in this certificate are correct at the time of calibration. Subsequently the accuracy will depend on such factors as the care executed in handling and use of the device, and the frequency of use. Recalibration should be performed after the period so chosen to ensure that the instrument's accuracy remains within the desired limits.

This certificate is issued in accordance with the conditions of the accreditation granted by the South African National Accreditation System (SANAS). It is a correct record of the measurements made. This certificate may not be reproduced other than in full except with prior written approval of the issuing laboratory. Legal liability shall be limited to the cost of recalibration and or certification, but the applicant indemnifies Unique Metrology (Pty) Ltd against any consequential or other loss.

The South African National Accreditation System (SANAS) is a member of the International Laboratory Accreditation Cooperation (ILAC) Mutual Recognition Arrangement (MRA). This arrangement allows for the mutual recognition of technical test and calibration data by the member accreditation bodies worldwide. For more information on the Arrangement please contact www.ilac.org.

Appendix B: Certificates of Calibration

Unique Metrology

Eskom Research & Innovation Centre
Lower Germiston Road • Rosherville
P O Box 145296 • Bracken Gardens • 1452
Tel: 011 626 3808 • Cell: 083 254 3635 • Fax: 086 610 4196
Web: www.unimet.co.za

CERTIFICATE OF CALIBRATION

Page 2 of 2 pages.

Certificate Number	: 1211T4452-1
Calibration of a	: PT100 Resistance Thermometer
Manufacturer & Type	: Wika 4 wire
Serial Number	: TE-7855
Calibrated for	: University of Stellenbosch, Process Engineering, Stellenbosch.
Procedure Number	: 53-166-03
Date of Calibration	: 23/11/2012
Date of Issue	: 26/11/2012
Laboratory Environment	: 21.4°C.
Reference Standards	: 306-S-21 Fluke 9144 Block Calibrator S/N B26027
	306-S-07 Hewlett Packard Multimeter S/N 1206L5
	306-S-05 Time Electronics Current Sourse S/N 3146A70688

Reference Temperature °C	Indicated Reading Ohms	Equivalent Temperature °C	Correction °C
40	115.565	40.1	-0.1
80	130.950	80.2	-0.1
140	153.622	140.1	-0.1
200	175.952	200.3	-0.3

The uncertainty of measurement is ± 0.3°C
The reported uncertainty is based on a standard uncertainty multiplied by a coverage factor
of k=2, which unless specifically stated otherwise, provides a confidence level of 95%, in
accordance with the Guide to the Uncertainty in Measurement, first edition, 1993.

Comments: The correction should be added to the indicated temperature to obtain the
actual temperature.
The PT100 was submerged to a constant depth of 150mm in the
block calibrator during the calibration.

Calibrated by :   AJ Mathieson

Technical Signatory

APPENDIX C: GC CALIBRATION & ERROR ANALYSIS

Butyl Ethyl Ether/n-Heptane
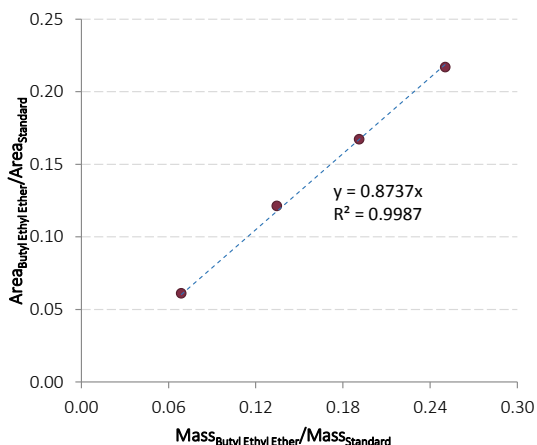
Figure C.1: Butyl ethyl ether calibration curve for butyl ethyl ether/n-heptane system
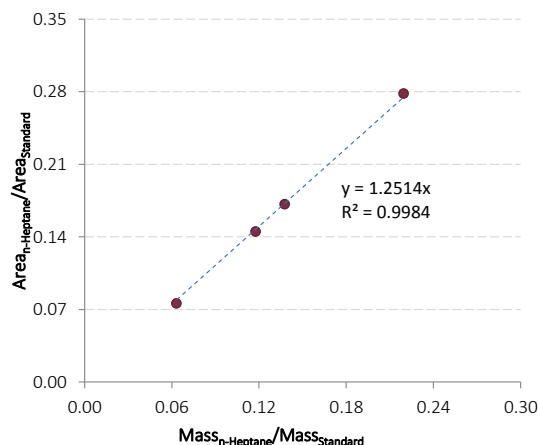
Figure C.2: n-Heptane calibration curve for butyl ethyl ether/n-heptane system

Table C.1: Sample preparation details for GC calibration in the butyl ethyl ether/n-heptane system

BEHGC5	Reference				BEHGC5A		BEHGC5B		BEHGC5C		BEHGC5D	
	Preparation Mass (g)	Individual Mass (g)	Mass Fraction	Sample Mass (g)	Area	A_{comp}/A_{std}	Area	A_{comp}/A_{std}	Area	A_{comp}/A_{std}	Area	A_{comp}/A_{std}
Butyl Ethyl Ether	2.47290	0.03200	0.19070	0.00305125	364274	0.21713	362463	0.21641	363252	0.21653	361907	0.21743
n-Heptane	2.48100	0.00810	0.04827	0.0007723	126842	0.07561	126106	0.07529	126708	0.07553	126253	0.07585
2-Heptanone (I.S.)	2.44090	0.12770	0.76103	0.012176	1677682	1.00000	1674858	1.00000	1677618	1.00000	1664494	1.00000
Vial	2.31320		GC Mass (g)	0.016								

BEHGC6	Reference				BEHGC6A		BEHGC6B		BEHGC6C		BEHGC6D	
	Preparation Mass (g)	Individual Mass (g)	Mass Fraction	Sample Mass (g)	Area	A_{comp}/A_{std}	Area	A_{comp}/A_{std}	Area	A_{comp}/A_{std}	Area	A_{comp}/A_{std}
Butyl Ethyl Ether	2.48860	0.02450	0.14609	0.00268813	304771	0.16542	302002	0.16527	303898	0.16527	325739	0.17213
n-Heptane	2.50370	0.01510	0.09004	0.0016568	263595	0.14307	261394	0.14304	262891	0.14297	284139	0.15015
2-Heptanone (I.S.)	2.46410	0.12810	0.76386	0.014055	1842420	1.00000	1827360	1.00000	1838817	1.00000	1892361	1.00000
Vial	2.33600		GC Mass (g)	0.0184								

BEHGC7	Reference				BEHGC7A		BEHGC7B		BEHGC7C		BEHGC7D	
	Preparation Mass (g)	Individual Mass (g)	Mass Fraction	Sample Mass (g)	Area	A_{comp}/A_{std}	Area	A_{comp}/A_{std}	Area	A_{comp}/A_{std}	Area	A_{comp}/A_{std}
Butyl Ethyl Ether	2.48340	0.01690	0.10582	0.00170376	214728	0.12426	199401	0.11867	198085	0.11852	215002	0.12318
n-Heptane	2.50070	0.01730	0.10833	0.0017441	305158	0.17659	280485	0.16693	278242	0.16648	305024	0.17476
2-Heptanone (I.S.)	2.46650	0.12550	0.78585	0.012652	1728059	1.00000	1680300	1.00000	1671305	1.00000	1745390	1.00000
Vial	2.34100		GC Mass (g)	0.0161								

BEHGC8	Reference				BEHGC8A		BEHGC8B		BEHGC8C		BEHGC8D	
	Preparation Mass (g)	Individual Mass (g)	Mass Fraction	Sample Mass (g)	Area	A_{comp}/A_{std}	Area	A_{comp}/A_{std}	Area	A_{comp}/A_{std}	Area	A_{comp}/A_{std}
Butyl Ethyl Ether	2.45330	0.00850	0.05346	0.00102107	109260	0.06103	109959	0.06064	108951	0.06103	108636	0.06089
n-Heptane	2.48040	0.02710	0.17044	0.0032554	497508	0.27788	503375	0.27758	497422	0.27862	496728	0.27843
2-Heptanone (I.S.)	2.44480	0.12340	0.77610	0.014824	1790366	1.00000	1813420	1.00000	1785332	1.00000	1784027	1.00000
Vial	2.32140		GC Mass (g)	0.0191								

Appendix C: GC Calibration & Error Analysis

Di-n-Propyl Ether/n-Heptane
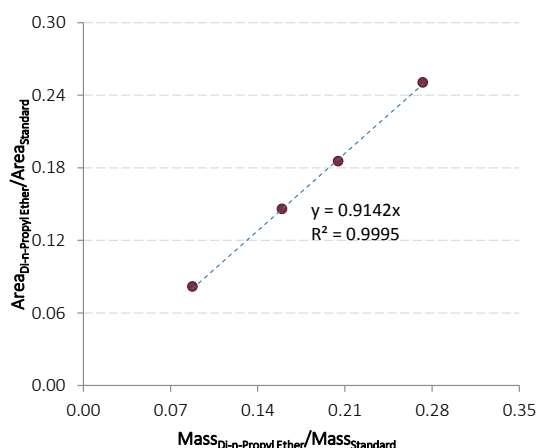
Figure C.3: Di-n-propyl ether calibration curve for di-n-propyl ether/n-heptane system
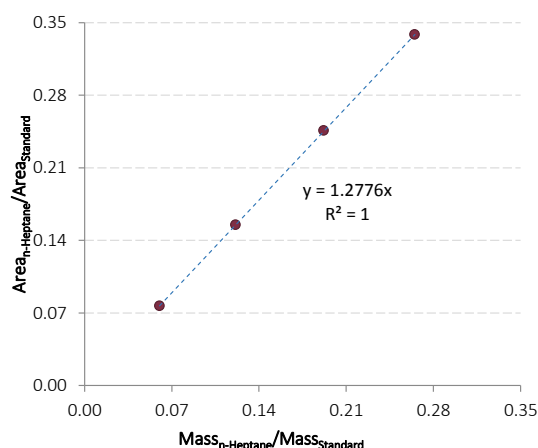
Figure C.4: n-Heptane calibration curve for di-n-propyl ether/n-heptane system

Table C.0.2: Sample preparation details for GC calibration in the di-n-propyl ether/n-heptane system

BEHGC5	Reference				BEHGC5A		BEHGC5B		BEHGC5C		BEHGC5D	
	Preparation Mass (g)	Individual Mass (g)	Mass Fraction	Sample Mass (g)	Area	A_{comp}/A_{std}	Area	A_{comp}/A_{std}	Area	A_{comp}/A_{std}	Area	A_{comp}/A_{std}
Butyl Ethyl Ether	2.47290	0.03200	0.19070	0.00305125	364274	0.21713	362463	0.21641	363252	0.21653	361907	0.21743
n-Heptane	2.48100	0.00810	0.04827	0.0007723	126842	0.07561	126106	0.07529	126708	0.07553	126253	0.07585
2-Heptanone (I.S.)	2.44090	0.12770	0.76103	0.012176	1677682	1.00000	1674858	1.00000	1677618	1.00000	1664494	1.00000
Vial	2.31320		GC Mass (g)	0.016								

BEHGC6	Reference				BEHGC6A		BEHGC6B		BEHGC6C		BEHGC6D	
	Preparation Mass (g)	Individual Mass (g)	Mass Fraction	Sample Mass (g)	Area	A_{comp}/A_{std}	Area	A_{comp}/A_{std}	Area	A_{comp}/A_{std}	Area	A_{comp}/A_{std}
Butyl Ethyl Ether	2.48860	0.02450	0.14609	0.00268813	304771	0.16542	302002	0.16527	303898	0.16527	325739	0.17213
n-Heptane	2.50370	0.01510	0.09004	0.0016568	263595	0.14307	261394	0.14304	262891	0.14297	284139	0.15015
2-Heptanone (I.S.)	2.46410	0.12810	0.76386	0.014055	1842420	1.00000	1827360	1.00000	1838817	1.00000	1892361	1.00000
Vial	2.33600		GC Mass (g)	0.0184								

BEHGC7	Reference				BEHGC7A		BEHGC7B		BEHGC7C		BEHGC7D	
	Preparation Mass (g)	Individual Mass (g)	Mass Fraction	Sample Mass (g)	Area	A_{comp}/A_{std}	Area	A_{comp}/A_{std}	Area	A_{comp}/A_{std}	Area	A_{comp}/A_{std}
Butyl Ethyl Ether	2.48340	0.01690	0.10582	0.00170376	214728	0.12426	199401	0.11867	198085	0.11852	215002	0.12318
n-Heptane	2.50070	0.01730	0.10833	0.0017441	305158	0.17659	280485	0.16693	278242	0.16648	305024	0.17476
2-Heptanone (I.S.)	2.46650	0.12550	0.78585	0.012652	1728059	1.00000	1680300	1.00000	1671305	1.00000	1745390	1.00000
Vial	2.34100		GC Mass (g)	0.0161								

BEHGC8	Reference				BEHGC8A		BEHGC8B		BEHGC8C		BEHGC8D	
	Preparation Mass (g)	Individual Mass (g)	Mass Fraction	Sample Mass (g)	Area	A_{comp}/A_{std}	Area	A_{comp}/A_{std}	Area	A_{comp}/A_{std}	Area	A_{comp}/A_{std}
Butyl Ethyl Ether	2.45330	0.00850	0.05346	0.00102107	109260	0.06103	109959	0.06064	108951	0.06103	108636	0.06089
n-Heptane	2.48040	0.02710	0.17044	0.0032554	497508	0.27788	503375	0.27758	497422	0.27862	496728	0.27843
2-Heptanone (I.S.)	2.44480	0.12340	0.77610	0.014824	1790366	1.00000	1813420	1.00000	1785332	1.00000	1784027	1.00000
Vial	2.32140		GC Mass (g)	0.0191								

Methyl Valerate/n-Octane
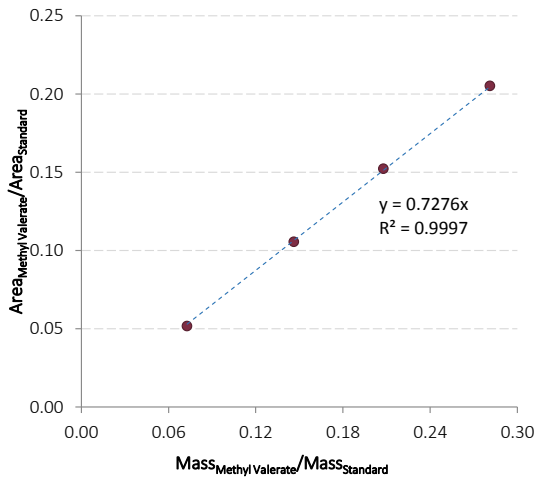
Figure C.5: Methyl valerate calibration curve for methyl valerate/n-octane system
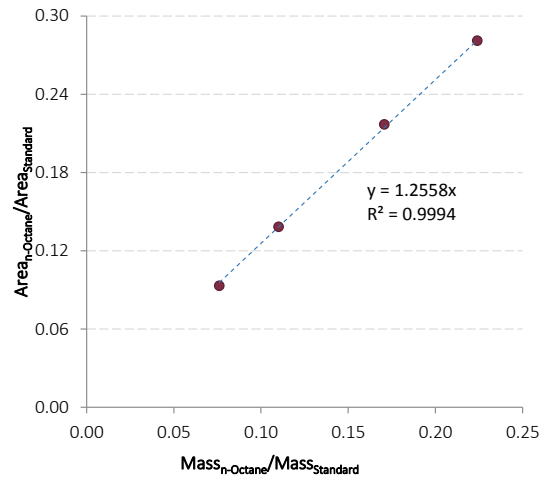
Figure C.6: n-Octane calibration curve for methyl valerate/n-octane system

Table C.3: Sample preparation details for GC calibration in the methyl valerate/n-octane system

MVOGC9	Reference				MVOGC9A		MVOGC9B		MVOGC9C		MVOGC9D	
	Preparation Mass (g)	Individual Mass (g)	Mass Fraction	Sample Mass (g)	Area	A_{comp}/A_{std}	Area	A_{comp}/A_{std}	Area	A_{comp}/A_{std}	Area	A_{comp}/A_{std}
Methyl Valerate	2.48870	0.03360	0.20728	0.00489180	361335	0.20562	355156	0.20469	357413	0.20497	361305	0.20484
n-Octane	2.49780	0.00910	0.05614	0.0013249	164307	0.09350	161052	0.09282	162190	0.09301	163767	0.09284
2-Heptanone (I.S.)	2.45510	0.11940	0.73658	0.017383	1757256	1.00000	1735107	1.00000	1743698	1.00000	1763883	1.00000
Vial	2.33570		GC Mass (g)	0.0236								

MVOGC10	Reference				MVOGC10A		MVOGC10B		MVOGC10C		MVOGC10D	
	Preparation Mass (g)	Individual Mass (g)	Mass Fraction	Sample Mass (g)	Area	A_{comp}/A_{std}	Area	A_{comp}/A_{std}	Area	A_{comp}/A_{std}	Area	A_{comp}/A_{std}
Methyl Valerate	2.45870	0.02510	0.15776	0.00361276	311929	0.15294	285216	0.15154	289160	0.15206	288650	0.15187
n-Octane	2.47200	0.01330	0.08360	0.0019143	285669	0.14007	258662	0.13743	262683	0.13813	261370	0.13752
2-Heptanone (I.S.)	2.43360	0.12070	0.75864	0.017373	2039524	1.00000	1882093	1.00000	1901656	1.00000	1900590	1.00000
Vial	2.31290		GC Mass (g)	0.0229								

MVOGC11	Reference				MVOGC11A		MVOGC11B		MVOGC11C		MVOGC11D	
	Preparation Mass (g)	Individual Mass (g)	Mass Fraction	Sample Mass (g)	Area	A_{comp}/A_{std}	Area	A_{comp}/A_{std}	Area	A_{comp}/A_{std}	Area	A_{comp}/A_{std}
Methyl Valerate	2.45190	0.01730	0.11111	0.00251111	184186	0.10527	184746	0.10531	180423	0.10495	191232	0.10643
n-Octane	2.47210	0.02020	0.12974	0.0029320	377351	0.21567	377880	0.21541	369330	0.21483	397138	0.22103
2-Heptanone (I.S.)	2.43460	0.11820	0.75915	0.017157	1749653	1.00000	1754234	1.00000	1719178	1.00000	1796744	1.00000
Vial	2.31640		GC Mass (g)	0.0226								

MVOGC12	Reference				MVOGC12A		MVOGC12B		MVOGC12C		MVOGC12D	
	Preparation Mass (g)	Individual Mass (g)	Mass Fraction	Sample Mass (g)	Area	A_{comp}/A_{std}	Area	A_{comp}/A_{std}	Area	A_{comp}/A_{std}	Area	A_{comp}/A_{std}
Methyl Valerate	2.46810	0.00870	0.05613	0.00130219	100220	0.05168	101110	0.05155	99526	0.05170	100041	0.05173
n-Octane	2.49490	0.02680	0.17290	0.0040114	545722	0.28139	549420	0.28013	540977	0.28100	543767	0.28115
2-Heptanone (I.S.)	2.45940	0.11950	0.77097	0.017886	1939392	1.00000	1961281	1.00000	1925163	1.00000	1934058	1.00000
Vial	2.33990		GC Mass (g)	0.0232								

Ethyl Butanoate/n-Octane
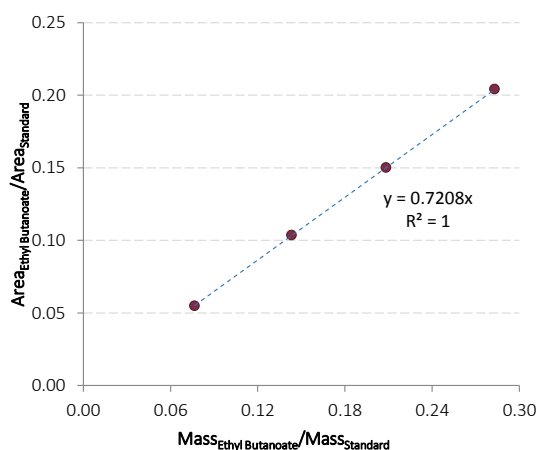
Figure C.7: Ethyl butanoate calibration curve for ethyl butanoate/n-octane system

Figure C.8: n-Octane calibration curve for ethyl butanoate/n-octane system

Table C.4: Sample preparation details for GC calibration in the ethyl butanoate/n-octane system

EBOGC1	Reference				EBOGC1A		EBOGC1B		EBOGC1C		EBOGC1D	
	Preparation Mass (g)	Individual Mass (g)	Mass Fraction	Sample Mass (g)	Area	A_{comp}/A_{std}	Area	A_{comp}/A_{std}	Area	A_{comp}/A_{std}	Area	A_{comp}/A_{std}
Ethyl Butyrate	2.12830	0.03400	0.21092	0.00504094	562673	0.20336	556468	0.20449	561037	0.20418	561084	0.20445
n-Octane	2.13540	0.00710	0.04404	0.0010527	206715	0.07471	202990	0.07459	204471	0.07441	204633	0.07457
2-Heptanone (I.S.)	2.09430	0.12010	0.74504	0.017806	2766937	1.00000	2721234	1.00000	2747815	1.00000	2744348	1.00000
Vial	1.97420		GC Mass (g)	0.0239								

EBOGC2	Reference				EBOGC2A		EBOGC2B		EBOGC2C		EBOGC2D	
	Preparation Mass (g)	Individual Mass (g)	Mass Fraction	Sample Mass (g)	Area	A_{comp}/A_{std}	Area	A_{comp}/A_{std}	Area	A_{comp}/A_{std}	Area	A_{comp}/A_{std}
Ethyl Butyrate	2.47860	0.02560	0.15802	0.00336593	385160	0.15052	384330	0.15025	384824	0.14969	387634	0.15014
n-Octane	2.49210	0.01350	0.08333	0.0017750	354587	0.13857	353416	0.13816	353560	0.13753	355699	0.13777
2-Heptanone (I.S.)	2.45300	0.12290	0.75864	0.016159	2558852	1.00000	2557991	1.00000	2570764	1.00000	2581860	1.00000
Vial	2.33010		GC Mass (g)	0.0213								

EBOGC3	Reference				EBOGC3A		EBOGC3B		EBOGC3C		EBOGC3D	
	Preparation Mass (g)	Individual Mass (g)	Mass Fraction	Sample Mass (g)	Area	A_{comp}/A_{std}	Area	A_{comp}/A_{std}	Area	A_{comp}/A_{std}	Area	A_{comp}/A_{std}
Ethyl Butyrate	2.47570	0.01690	0.10875	0.00246866	301496	0.10364	299462	0.10372	300992	0.10341	305407	0.10321
n-Octane	2.49630	0.02060	0.13256	0.0030091	640421	0.22014	637517	0.22080	639998	0.21987	648307	0.21910
2-Heptanone (I.S.)	2.45880	0.11790	0.75869	0.017222	2909104	1.00000	2887339	1.00000	2910782	1.00000	2958984	1.00000
Vial	2.34090		GC Mass (g)	0.0227								

EBOGC4	Reference				EBOGC4A		EBOGC4B		EBOGC4C		EBOGC4D	
	Preparation Mass (g)	Individual Mass (g)	Mass Fraction	Sample Mass (g)	Area	A_{comp}/A_{std}	Area	A_{comp}/A_{std}	Area	A_{comp}/A_{std}	Area	A_{comp}/A_{std}
Ethyl Butyrate	2.46020	0.00920	0.05913	0.00124165	135430	0.05488	135345	0.05469	134557	0.05479	135658	0.05482
n-Octane	2.48670	0.02650	0.17031	0.0035765	686301	0.27811	686627	0.27743	682115	0.27774	687953	0.27800
2-Heptanone (I.S.)	2.45100	0.11990	0.77057	0.016182	2467764	1.00000	2474992	1.00000	2455922	1.00000	2474616	1.00000
Vial	2.33110		GC Mass (g)	0.021								

Propyl Propanoate/n-Octane
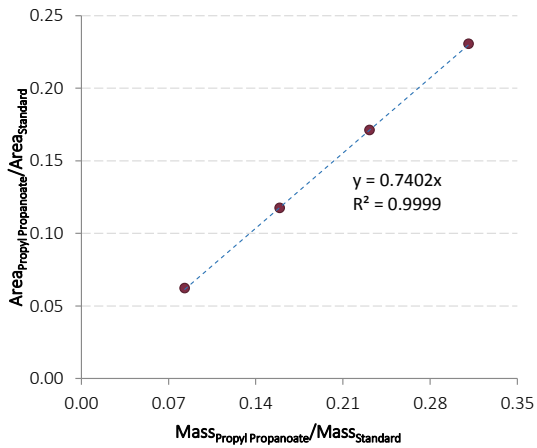
Figure C.9: Propyl propanoate calibration curve for propyl propanoate/n-octane system
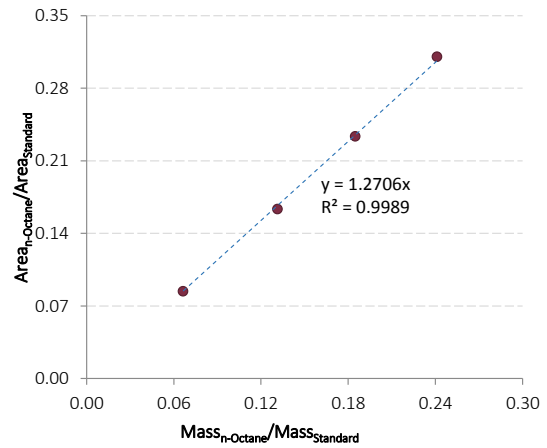
Figure C.10: n-Octane calibration curve for propyl propanoate/n-octane system

Table C.5: Sample preparation details for GC calibration in the propyl propanoate/n-octane system

PPOGC5	Reference				PPOGC5A		PPOGC5B		PPOGC5C		PPOGC5D	
	Preparation Mass (g)	Individual Mass (g)	Mass Fraction	Sample Mass (g)	Area	A_{comp}/A_{std}	Area	A_{comp}/A_{std}	Area	A_{comp}/A_{std}	Area	A_{comp}/A_{std}
Propyl Propionate	2.47090	0.03970	0.22582	0.00499073	481275	0.23122	514878	0.22940	502645	0.23109	500167	0.23064
n-Octane	2.47940	0.00850	0.04835	0.0010685	175795	0.08446	186596	0.08314	182987	0.08413	181752	0.08381
2-Heptanone (I.S.)	2.43120	0.12760	0.72582	0.016041	2081456	1.00000	2244420	1.00000	2175061	1.00000	2168565	1.00000
Vial	2.30360		GC Mass (g)	0.0221								

PPOGC6	Reference				PPOGC6A		PPOGC6B		PPOGC6C		PPOGC6D	
	Preparation Mass (g)	Individual Mass (g)	Mass Fraction	Sample Mass (g)	Area	A_{comp}/A_{std}	Area	A_{comp}/A_{std}	Area	A_{comp}/A_{std}	Area	A_{comp}/A_{std}
Propyl Propionate	2.46910	0.02780	0.16982	0.00371912	358556	0.17177	378638	0.17005	364428	0.17109	356040	0.17179
n-Octane	2.48490	0.01580	0.09652	0.0021137	342029	0.16386	361795	0.16249	347448	0.16312	340290	0.16419
2-Heptanone (I.S.)	2.44130	0.12010	0.73366	0.016067	2087366	1.00000	2226577	1.00000	2130067	1.00000	2072540	1.00000
Vial	2.32120		GC Mass (g)	0.0219								

PPOGC7	Reference				PPOGC7A		PPOGC7B		PPOGC7C		PPOGC7D	
	Preparation Mass (g)	Individual Mass (g)	Mass Fraction	Sample Mass (g)	Area	A_{comp}/A_{std}	Area	A_{comp}/A_{std}	Area	A_{comp}/A_{std}	Area	A_{comp}/A_{std}
Propyl Propionate	2.47260	0.01990	0.11859	0.00247861	253106	0.11681	232055	0.11803	246209	0.11698	233604	0.11788
n-Octane	2.49570	0.02310	0.13766	0.0028772	499777	0.23066	462647	0.23532	490423	0.23301	465618	0.23495
2-Heptanone (I.S.)	2.45270	0.12480	0.74374	0.015544	2166755	1.00000	1966031	1.00000	2104714	1.00000	1981767	1.00000
Vial	2.32790		GC Mass (g)	0.0209								

PPOGC8	Reference				PPOGC8A		PPOGC8B		PPOGC8C		PPOGC8D	
	Preparation Mass (g)	Individual Mass (g)	Mass Fraction	Sample Mass (g)	Area	A_{comp}/A_{std}	Area	A_{comp}/A_{std}	Area	A_{comp}/A_{std}	Area	A_{comp}/A_{std}
Propyl Propionate	2.46740	0.01030	0.06277	0.00135576	135507	0.06196	133325	0.06215	131863	0.06233	130751	0.06221
n-Octane	2.49730	0.02990	0.18221	0.0039356	674846	0.30859	665290	0.31011	657941	0.31101	654516	0.31141
2-Heptanone (I.S.)	2.45710	0.12390	0.75503	0.016309	2186848	1.00000	2145350	1.00000	2115515	1.00000	2101784	1.00000
Vial	2.33320		GC Mass (g)	0.0216								

Butyl Acetate/n-Octane
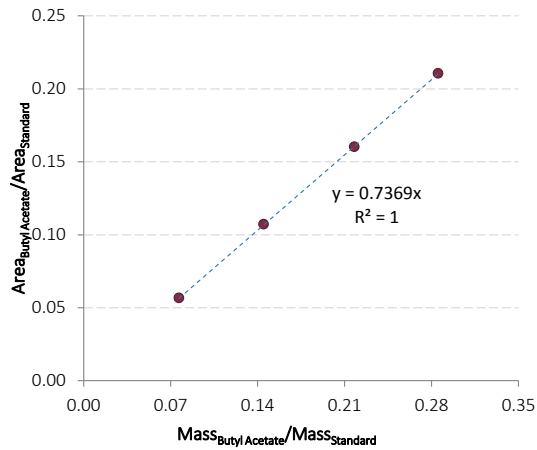
**Figure C.11: Butyl acetate calibration curve for butyl acetate/n-octane system**
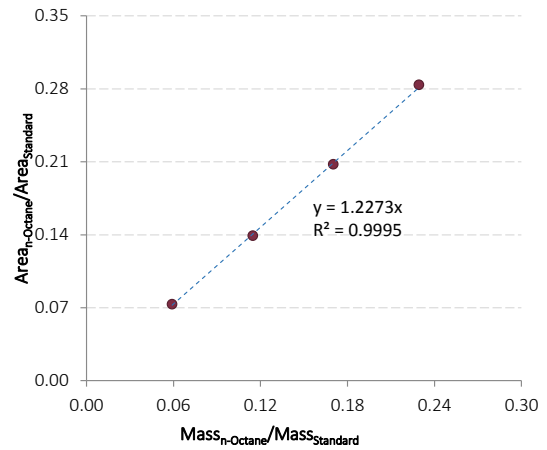
Figure C.12: n-Octane calibration curve for butyl acetate/n-octane system

Table C.0.6: Sample preparation details for GC calibration in the butyl acetate/n-octane system

BAOGC1	Reference				BAOGC1A		BAOGC1B		BAOGC1C		BAOGC1D	
	Preparation Mass (g)	Individual Mass (g)	Mass Fraction	Sample Mass (g)	Area	A_{comp}/A_{std}	Area	A_{comp}/A_{std}	Area	A_{comp}/A_{std}	Area	A_{comp}/A_{std}
Butyl Acetate	2.15200	0.03430	0.21238	0.00501226	568248	0.21382	584493	0.20920	572845	0.21064	568835	0.20866
n-Octane	2.15910	0.00710	0.04396	0.0010375	201924	0.07598	201068	0.07197	198954	0.07316	196016	0.07190
2-Heptanone (I.S.)	2.11770	0.12010	0.74365	0.017550	2657543	1.00000	2793904	1.00000	2719552	1.00000	2726150	1.00000
Vial	1.99760		GC Mass (g)	0.0236								

BAOGC2	Reference				BAOGC2A		BAOGC2B		BAOGC2C		BAOGC2D	
	Preparation Mass (g)	Individual Mass (g)	Mass Fraction	Sample Mass (g)	Area	A_{comp}/A_{std}	Area	A_{comp}/A_{std}	Area	A_{comp}/A_{std}	Area	A_{comp}/A_{std}
Butyl Acetate	2.49660	0.02620	0.16355	0.00384332	411442	0.16055	423254	0.16081	412712	0.15992	418997	0.15973
n-Octane	2.51040	0.01380	0.08614	0.0020243	357329	0.13943	368516	0.14001	357270	0.13844	361992	0.13800
2-Heptanone (I.S.)	2.47040	0.12020	0.75031	0.017632	2562761	1.00000	2631994	1.00000	2580766	1.00000	2623119	1.00000
Vial	2.35020		GC Mass (g)	0.0235								

BAOGC3	Reference				BAOGC3A		BAOGC3B		BAOGC3C		BAOGC3D	
	Preparation Mass (g)	Individual Mass (g)	Mass Fraction	Sample Mass (g)	Area	A_{comp}/A_{std}	Area	A_{comp}/A_{std}	Area	A_{comp}/A_{std}	Area	A_{comp}/A_{std}
Butyl Acetate	2.46150	0.01720	0.11026	0.00252487	247531	0.10767	259985	0.10728	252182	0.10684	250371	0.10702
n-Octane	2.48170	0.02020	0.12949	0.0029653	478493	0.20813	503026	0.20756	487287	0.20645	485160	0.20739
2-Heptanone (I.S.)	2.44430	0.11860	0.76026	0.017410	2299003	1.00000	2423484	1.00000	2360278	1.00000	2339391	1.00000
Vial	2.32570		GC Mass (g)	0.0229								

BAOGC4	Reference				BAOGC4A		BAOGC4B		BAOGC4C		EBOGC4D	
	Preparation Mass (g)	Individual Mass (g)	Mass Fraction	Sample Mass (g)	Area	A_{comp}/A_{std}	Area	A_{comp}/A_{std}	Area	A_{comp}/A_{std}	Area	A_{comp}/A_{std}
Butyl Acetate	2.47300	0.00910	0.05879	0.00125213	115399	0.05642	119556	0.05660	117464	0.05690	118988	0.05668
n-Octane	2.50020	0.02720	0.17571	0.0037426	576817	0.28203	599084	0.28363	589624	0.28562	595515	0.28366
2-Heptanone (I.S.)	2.46390	0.11850	0.76550	0.016305	2045266	1.00000	2112172	1.00000	2064364	1.00000	2099424	1.00000
Vial	2.34540		GC Mass (g)	0.0213								

Pentyl Formate/n-Octane
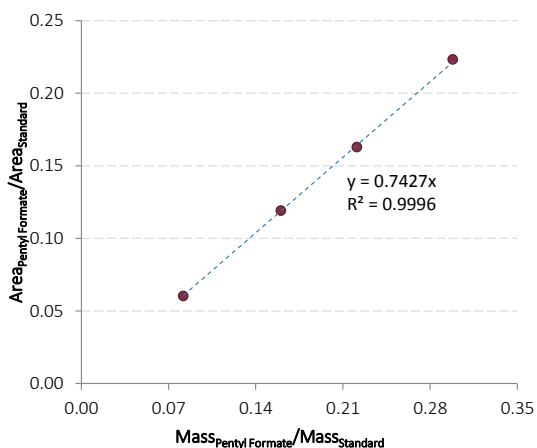
**Figure C.13: Pentyl formate calibration curve for pentyl formate/n-octane system**
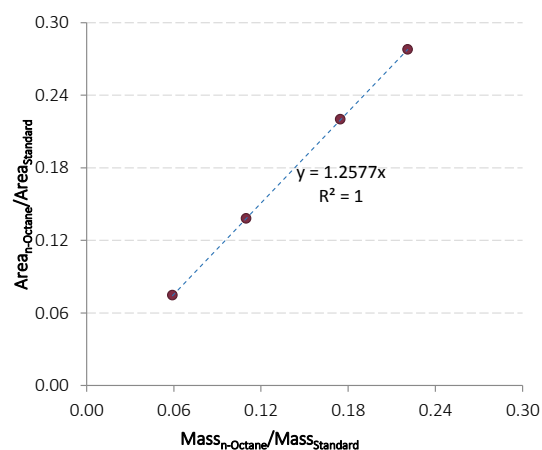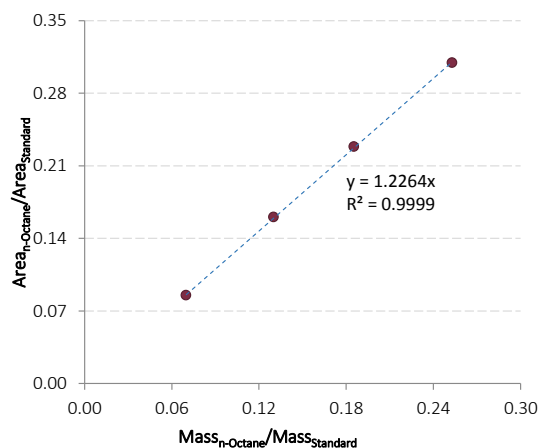

Figure C.14: n-Octane calibration curve for pentyl formate/n-octane system

Table C.7: Sample preparation details for GC calibration in the pentyl formate/n-octane system

AFOGC1	Reference				AFOGC1A		AFOGC1B		AFOGC1C		AFOGC1D	
	Preparation Mass (g)	Individual Mass (g)	Mass Fraction	Sample Mass (g)	Area	A_{comp}/A_{std}	Area	A_{comp}/A_{std}	Area	A_{comp}/A_{std}	Area	A_{comp}/A_{std}
Amyl Formate	2.48970	0.03540	0.21811	0.00447135	281004	0.22350	279861	0.22287	279123	0.22340	278084	0.22313
n-Octane	2.49800	0.00830	0.05114	0.0010484	107096	0.08518	106860	0.08510	106478	0.08522	106291	0.08529
2-Heptanone (I.S.)	2.45430	0.11860	0.73075	0.014980	1257267	1.00000	1255714	1.00000	1249428	1.00000	1246267	1.00000
Vial	2.33570		GC Mass (g)	0.0205								

AFOGC2	Reference				AFOGC2A		AFOGC2B		AFOGC2C		AFOGC2D	
	Preparation Mass (g)	Individual Mass (g)	Mass Fraction	Sample Mass (g)	Area	A_{comp}/A_{std}	Area	A_{comp}/A_{std}	Area	A_{comp}/A_{std}	Area	A_{comp}/A_{std}
Amyl Formate	2.46210	0.02620	0.16385	0.00345729	210617	0.16259	211080	0.16291	210529	0.16233	209031	0.16309
n-Octane	2.47750	0.01540	0.09631	0.0020321	207390	0.16010	207936	0.16049	208281	0.16059	206151	0.16085
2-Heptanone (I.S.)	2.43590	0.11830	0.73984	0.015611	1295409	1.00000	1295670	1.00000	1296950	1.00000	1281664	1.00000
Vial	2.31760		GC Mass (g)	0.0211								

AFOGC3	Reference				AFOGC3A		AFOGC3B		AFOGC3C		AFOGC3D	
	Preparation Mass (g)	Individual Mass (g)	Mass Fraction	Sample Mass (g)	Area	A_{comp}/A_{std}	Area	A_{comp}/A_{std}	Area	A_{comp}/A_{std}	Area	A_{comp}/A_{std}
Amyl Formate	2.46690	0.01860	0.11915	0.00238309	147074	0.11932	146593	0.11889	147581	0.11883	150549	0.11875
n-Octane	2.48840	0.02150	0.13773	0.0027546	281936	0.22873	282666	0.22925	283462	0.22824	287935	0.22711
2-Heptanone (I.S.)	2.44830	0.11600	0.74311	0.014862	1232588	1.00000	1232991	1.00000	1241943	1.00000	1267800	1.00000
Vial	2.33230		GC Mass (g)	0.02								

AFOGC4	Reference				AFOGC4A		AFOGC4B		AFOGC4C		AFOGC4D	
	Preparation Mass (g)	Individual Mass (g)	Mass Fraction	Sample Mass (g)	Area	A_{comp}/A_{std}	Area	A_{comp}/A_{std}	Area	A_{comp}/A_{std}	Area	A_{comp}/A_{std}
Amyl Formate	2.44070	0.00950	0.06145	0.00109994	65892	0.06015	68899	0.06018	72079	0.05991	76172	0.06080
n-Octane	2.47000	0.02930	0.18952	0.0033924	340345	0.31067	353981	0.30917	370371	0.30786	387960	0.30965
2-Heptanone (I.S.)	2.43120	0.11580	0.74903	0.013408	1095515	1.00000	1144937	1.00000	1203036	1.00000	1252900	1.00000
Vial	2.31540		GC Mass (g)	0.0179								

GC Compositional Error Analysis

Table C.8 below is an example of the determination of compositional uncertainty from the analysis procedure. At the conclusion of the experimental sample analysis procedure, four samples of known and variable mass, and thus composition, were prepared and run through the GC four times each. The reported *Absolute GC Error Mole Fraction* illustrates the error induced by a drift in the response factor over the course of the analysis. *WC1* and *WC2* account for potential weighing error which affects the "true" reference composition used to establish calibration curves. For *WC1*, the mass of the ester is increased by *0.0001*g (uncertainty of scale) with the alkane reduced by the same quantity, with the signs opposite in *WC2*. The reported values are thus the difference between the prediction and these worst case scenarios.

Table C.8: Sample repeatability results for GC error analysis using the pentyl formate/n-octane system

	Pentyl Formate Mass	n-Octane Mass	Standard Mass	Pentyl Formate Mole Frac	Octane Mole Frac	Pentyl Formate Area	Octane Area	Standard Area	Predicted Pentyl Formate Mass Frac	Predicted n-Octane Mass Frac	Predicted Pentyl Formate Mole Frac	Predicted n-Octane Mole Frac	Absolute GC Error Mole Fraction	Absolute GC Error Mole Fraction (WC1)*	Absolute GC Error Mole Fraction (WC2)*	Average Absolute GC Error Mole Fraction
KNO1A	0.0469	0.0127	0.0206	0.7841	0.2159	318322	135889	1241392	0.7946	0.2054	0.7918	0.2082	0.0077	0.0061	0.0095	
KNO1B	0.0469	0.0127	0.0206	0.7841	0.2159	328200	145740	1290165	0.7881	0.2119	0.7853	0.2147	0.0012	0.0004	0.0029	
KNO1C	0.0469	0.0127	0.0206	0.7841	0.2159	326864	146053	1283292	0.7870	0.2130	0.7842	0.2158	0.0001	0.0015	0.0019	0.0029
KNO1D	0.0469	0.0127	0.0206	0.7841	0.2159	325931	145724	1275344	0.7869	0.2131	0.7841	0.2159	0.0000	0.0016	0.0018	
KNO2A	0.0369	0.0232	0.0212	0.6100	0.3900	236634	248723	1294805	0.6110	0.3890	0.6071	0.3929	0.0029	0.0045	0.0012	
KNO2B	0.0369	0.0232	0.0212	0.6100	0.3900	240874	251752	1325792	0.6124	0.3876	0.6084	0.3916	0.0016	0.0032	0.0002	
KNO2C	0.0369	0.0232	0.0212	0.6100	0.3900	241436	252947	1327450	0.6118	0.3882	0.6078	0.3922	0.0022	0.0037	0.0004	0.0021
KNO2D	0.0369	0.0232	0.0212	0.6100	0.3900	242611	253549	1334895	0.6124	0.3876	0.6084	0.3916	0.0016	0.0031	0.0002	
KNO3A	0.0242	0.0351	0.0216	0.4041	0.5959	147445	359919	1388876	0.4035	0.5965	0.3995	0.6005	0.0046	0.0061	0.0028	
KNO3B	0.0242	0.0351	0.0216	0.4041	0.5959	148322	362458	1405093	0.4032	0.5968	0.3992	0.6008	0.0048	0.0064	0.0031	
KNO3C	0.0242	0.0351	0.0216	0.4041	0.5959	148689	363799	1400403	0.4029	0.5971	0.3989	0.6011	0.0051	0.0067	0.0033	0.0050
KNO3D	0.0242	0.0351	0.0216	0.4041	0.5959	146735	359778	1381513	0.4024	0.5976	0.3984	0.6016	0.0056	0.0072	0.0039	
KNO4A	0.0144	0.0485	0.0209	0.2260	0.7740	79220	454213	1252013	0.2236	0.7764	0.2207	0.7793	0.0053	0.0068	0.0036	
KNO4B	0.0144	0.0485	0.0209	0.2260	0.7740	81690	465724	1311299	0.2246	0.7754	0.2217	0.7783	0.0043	0.0058	0.0027	
KNO4C	0.0144	0.0485	0.0209	0.2260	0.7740	78632	453959	1242875	0.2224	0.7776	0.2195	0.7805	0.0065	0.0080	0.0048	0.0054
KNO4D	0.0144	0.0485	0.0209	0.2260	0.7740	78551	451596	1238254	0.2231	0.7769	0.2202	0.7798	0.0057	0.0072	0.0041	

APPENDIX D: PURE COMPONENT VAPOUR PRESSURE MEASUREMENTS

Table D.1: Experimentally measured vapour pressures for components of experimental interest to this study

n-Heptane		n-Octane		Di-n-Propyl Ether		Butyl Ethyl Ether		Methyl Valerate		Ethyl Butanoate		Propyl Propanoate		Butyl Acetate		Pentyl Formate	
P (kPa)	T (K)	P (kPa)	T (K)	P (kPa)	T (K)	P (kPa)	T (K)	P (kPa)	T (K)	P (kPa)	T (K)	P (kPa)	T (K)	P (kPa)	T (K)	P (kPa)	T (K)
101.30	371.28	97.58	397.28	101.30	362.87	101.30	365.25	101.3	400.48	101.3	393.78	101.3	395.51	101.3	399.09	101.3	405.12
88.40	366.87	83.70	391.91	96.32	361.18	96.36	363.47	100.4	400.07	100.4	393.63	93.37	392.74	99.03	398.35	93.45	402.19
83.45	364.95	66.74	384.28	89.30	358.73	90.59	361.44	95.08	398.03	90.84	390.23	86.38	390.13	88.69	394.58	86.56	399.55
76.47	362.11	60.05	380.83	84.25	356.85	79.60	357.31	88.17	395.42	84.14	387.65	77.90	386.81	80.09	391.20	80.16	396.89
70.24	359.38	53.65	377.27	78.97	354.82	71.58	354.01	77.71	391.14	77.20	384.82	70.32	383.56	72.71	388.06	73.50	394.01
64.60	356.78	43.33	370.71	72.36	352.11	63.63	350.44	69.02	387.18	65.75	379.65	60.83	379.07	60.15	382.08	68.46	391.65
56.20	352.58	34.91	364.35	62.30	347.55	56.24	346.80	59.35	382.55	58.98	376.28	51.21	373.82	56.43	380.10	60.50	387.67
50.97	349.68	28.95	359.12	57.75	345.34	51.67	344.21	52.83	378.84	54.40	373.83	47.90	371.88	45.02	373.32	55.79	385.08
46.80	347.16			49.98	341.15	44.96	340.35	45.81	374.53	50.00	371.33	40.92	367.30	41.42	370.90	49.42	381.35
38.89	341.94			42.54	336.55	38.60	336.22	40.47	370.86	40.41	365.24	33.58	361.75	32.95	364.47	44.06	377.87
30.59	335.45			36.71	332.57	29.99	331.51	35.06	366.70	35.41	361.56			29.92	361.85	39.15	374.41
26.15	331.39			29.35	326.73			29.41	361.82							33.67	370.04

APPENDIX E: EXPERIMENTAL RESULTS: VLE & CONSISTENCY TESTS

The *PRO-VLE 2.0* software was used to perform the L/W thermodynamic consistency test, which requires inputting a number of component specific properties and correlation constants. The input values for the components used in this study are detailed in Table E.1 below.

Table E.1: Component parameters used for thermodynamic consistency testing

	Butyl Ethyl Ether	Di-n-Propyl Ether	Methyl Valerate	Ethyl Butanoate	Propyl Propanoate	Butyl Acetate	Pentyl Formate	n-Heptane	n-Octane
Antoine A*	6.73327	6.72609	6.77353	6.928582	6.978531	6.864025	6.80815	6.64338	6.94182
Antoine B*	1104.422	1118.741	1220.67	1331.7852	1326.38506	1270.8518	1270.754	1105.257	1365.368
Antoine C*	194.9097	201.1184	186.2061	207.6835	201.4181	193.05968	191.36074	195.5387	210.525
T_c (K)	531	530.6	588.92	571	568.6	575.4	576	540.2	568.7
P_c (atm)	29.509	29.88403	31.609	29.11423	30.19984	30.49592	30.84134	27.04169	24.57438
V_c (cm^3.mol^{-1})	382	382	426.4	403	389	389	389	428	486
T_b (K)	348.84	346.63	383.29	377.21	378.63	381.98	387.69	354.63	380.85
ω	0.385408	0.368756	0.35844	0.401075	0.448676	0.439393	0.515459	0.349469	0.399552
V^L (cm^3.mol^{-1})	147.702 [a]	147.703 [a]	145.276 [a]	147.1255 [a]	146.951 [a]	147.1297 [a]	147.9057 [a]	±158 [a]	±181 [a]
H^{vap} (cal.mol^{-1})	7854	7794	8997	8945	8970	9021	9069	7874	8580
μ (Debye)	1.22019	1.21119	1.62	1.81079	1.78981	1.84077	1.90073	0	0

*Antoine Equation as log$_{10}$P(mmHg) = A − (B/(T(°C) + C))
Listed values taken from DIPPR Database unless otherwise specified
[a] Values of V^L depend on max and min temperatures for mixture of interest – tabulated values are thus averages

In the tables of experimental results that follow, the activity coefficients were generated for each component by the *PRO-VLE 2.0* software. The reported uncertainties in temperature (*0.02*K), pressure (*1.5*mbar) and composition (*0.010* mole fraction) were used to determine *D* and *D$_{max}$* for the McDermott-Ellis consistency test.

Butyl Ethyl Ether/n-Heptane

Table E.2: Experimental data and thermodynamic consistency testing results for butyl ethyl ether/n-heptane system

Sample Name	Experimental Data			L/W Consistency Test					McDermott-Ellis Consistency Test			
	$T\ (K)$	y_{ether}	x_{ether}	L_i	W_i	L_i/W_i	$\Delta x.\ \Sigma L_i$	$\Delta x.\ \Sigma W_i$	γ_{ether}	γ_{hept}	D	D_{max}
Hept.	354.63	0.000	0.000									
Hept.	354.63	0.000	0.000									
BEH11	354.37	0.035	0.026	0.109	0.089	1.220	0.001	0.001	1.127	0.998	0.0035	0.1584
BEH51	354.22	0.049	0.035	0.203	0.185	1.100	0.010	0.009	1.157	0.999	0.0041	0.1658
BEH12	353.87	0.095	0.071	0.341	0.329	1.040	0.004	0.003	1.133	0.998	0.0036	0.1580
BEH52	353.79	0.111	0.081	0.362	0.351	1.030	0.017	0.017	1.162	0.994	0.0050	0.1606
BEH53	353.41	0.160	0.121	0.514	0.510	1.010	0.003	0.003	1.144	0.993	0.0014	0.1587
BEH13	353.34	0.166	0.127	0.549	0.546	1.010	0.027	0.027	1.134	0.995	0.0035	0.1616
BEH14	352.90	0.212	0.169	0.742	0.747	0.990	0.021	0.021	1.102	1.002	0.0049	0.1610
BEH15	352.71	0.245	0.197	0.768	0.777	0.990	0.002	0.002	1.102	0.999	0.0006	0.1612
BEH54	352.68	0.248	0.195	0.810	0.819	0.990	0.034	0.034	1.128	0.993	0.0093	0.1621
BEH55	352.43	0.293	0.236	0.818	0.833	0.980	0.011	0.011	1.108	0.992	0.0010	0.1623
BEH16	352.32	0.305	0.250	0.850	0.866	0.980	0.031	0.032	1.093	0.997	0.0034	0.1630
BEH56	352.06	0.344	0.285	0.903	0.925	0.980	0.004	0.004	1.089	0.996	0.0023	0.1630
BEH17	352.00	0.348	0.289	0.940	0.963	0.980	0.047	0.048	1.088	0.998	0.0013	0.1644
BEH21	351.62	0.395	0.336	1.046	1.077	0.970	0.010	0.010	1.076	1.004	0.0004	0.1647
BEH22	351.59	0.400	0.346	1.019	1.051	0.970	0.011	0.011	1.061	1.011	0.0006	0.1646
BEH57	351.50	0.413	0.356	1.047	1.081	0.970	0.025	0.026	1.066	1.008	0.0032	0.1651
BEH23	351.39	0.436	0.381	1.015	1.051	0.970	0.022	0.023	1.056	1.011	0.0034	0.1654
BEH24	351.29	0.458	0.403	0.988	1.027	0.960	0.008	0.008	1.053	1.010	0.0043	0.1656
BEH58	351.17	0.466	0.410	1.064	1.106	0.960	0.013	0.014	1.054	1.013	0.0070	0.1659
BEH25	351.19	0.479	0.423	0.969	1.010	0.960	0.020	0.021	1.051	1.009	0.0029	0.1664
BEH26	351.05	0.504	0.444	0.989	1.033	0.960	0.011	0.011	1.057	1.002	0.0028	0.1666
BEH48	350.96	0.511	0.455	1.017	1.063	0.960	0.018	0.018	1.050	1.010	0.0018	0.1668
BEH27	350.89	0.525	0.472	0.985	1.033	0.950	0.003	0.003	1.042	1.015	0.0069	0.1668
BEH59	350.77	0.528	0.475	1.090	1.141	0.960	0.016	0.017	1.045	1.019	0.0029	0.1669
BEH47	350.73	0.543	0.490	1.041	1.092	0.950	0.002	0.002	1.043	1.018	0.0057	0.1674
BEH28	350.78	0.546	0.488	1.002	1.052	0.950	0.040	0.042	1.052	1.004	0.0039	0.1680
BEH46	350.51	0.579	0.528	1.045	1.101	0.950	0.038	0.040	1.041	1.019	0.0040	0.1681
BEH45	350.35	0.615	0.565	0.988	1.048	0.940	0.035	0.038	1.038	1.018	0.0037	0.1690
BEH44	350.22	0.644	0.603	0.902	0.965	0.930	0.037	0.040	1.024	1.033	0.0036	0.1690
BEH43	349.98	0.680	0.644	0.905	0.974	0.930	0.034	0.037	1.021	1.043	0.0027	0.1694
BEH42	349.85	0.716	0.684	0.803	0.875	0.920	0.029	0.031	1.016	1.049	0.0005	0.1697
BEH41	349.71	0.749	0.721	0.728	0.802	0.910	0.027	0.030	1.012	1.058	0.0000	0.1699
BEH37	349.55	0.783	0.760	0.666	0.744	0.900	0.021	0.024	1.010	1.064	0.0080	0.1701
BEH36	349.32	0.811	0.790	0.721	0.804	0.900	0.028	0.032	1.013	1.072	0.0059	0.1711
BEH35	349.25	0.851	0.835	0.535	0.620	0.860	0.016	0.019	1.008	1.078	0.0028	0.1708
BEH34	349.12	0.879	0.867	0.483	0.570	0.850	0.021	0.026	1.008	1.088	0.0042	0.1758
BEH33	349.01	0.927	0.921	0.282	0.371	0.760	0.008	0.012	1.004	1.103	0.0007	0.1798
BEH32	348.93	0.963	0.960	0.137	0.226	0.600	0.002	0.004	1.002	1.132	0.0025	0.1885
BEH31	348.89	0.985	0.984	0.010	0.099	0.100	0.000	0.001	1.001	1.121		
BEE	348.84	1.000	1.000									
				L	W	D						
				0.7072	0.7532	3.1521						

Di-n-Propyl Ether/n-Heptane

Table E.3: Experimental data and thermodynamic consistency testing results for di-n-propyl ether/n-heptane system

Sample Name	Experimental Data			L/W Consistency Test					McDermott-Ellis Consistency Test			
	T (K)	y_{ether}	x_{ether}	L_i	W_i	L_i/W_i	$\frac{\Delta x.}{\Sigma L_i}$	$\frac{\Delta x.}{\Sigma W_i}$	γ_{ether}	γ_{hept}	D	D_{max}
Hept.	354.63	0.000	0.000									
DPH31	354.42	0.038	0.027	-0.006	-0.023	0.270	0.002	0.002	1.109	0.994	0.0027	0.1648
DPH32	354.01	0.078	0.055	0.173	0.165	1.050	0.007	0.006	1.120	0.995	0.0009	0.1586
DPH33	353.65	0.115	0.082	0.319	0.319	1.000	0.008	0.008	1.128	0.994	0.0000	0.1575
DPH34	353.33	0.144	0.101	0.480	0.486	0.990	0.032	0.033	1.151	0.992	0.0068	0.1603
DPH35	352.66	0.215	0.154	0.721	0.742	0.970	0.017	0.018	1.152	0.988	0.0039	0.1609
DPH36	352.55	0.232	0.180	0.629	0.655	0.960	0.017	0.018	1.072	1.000	0.0068	0.1607
DPH58	352.34	0.266	0.207	0.615	0.646	0.950	0.001	0.001	1.071	0.996	0.0076	0.1609
DPH37	352.17	0.273	0.209	0.770	0.804	0.960	0.018	0.019	1.095	0.995	0.0090	0.1614
DPH41	351.94	0.307	0.232	0.818	0.857	0.960	0.016	0.016	1.120	0.983	0.0003	0.1615
DPH42	351.75	0.325	0.250	0.858	0.900	0.950	0.005	0.005	1.105	0.987	0.0039	0.1621
DPH43	351.66	0.339	0.256	0.905	0.949	0.950	0.042	0.045	1.130	0.977	0.0024	0.1636
DPH44	351.25	0.381	0.301	0.948	1.000	0.950	0.009	0.010	1.093	0.988	0.0080	0.1636
DPH59	351.07	0.386	0.310	1.055	1.110	0.950	0.022	0.024	1.080	0.999	0.0070	0.1638
DPH45	350.92	0.411	0.332	1.032	1.091	0.950	0.040	0.043	1.082	0.993	0.0079	0.1650
DPH46	350.65	0.450	0.372	0.982	1.046	0.940	0.014	0.015	1.066	0.995	0.0025	0.1653
DPH510	350.46	0.467	0.386	1.058	1.125	0.940	0.032	0.035	1.073	0.993	0.0085	0.1662
DPH47	350.29	0.496	0.418	0.971	1.041	0.930	0.070	0.075	1.057	0.996	0.0076	0.1680
DPH48	349.60	0.558	0.485	1.127	1.207	0.930	0.010	0.011	1.048	1.010	0.0063	0.1679
DPH57	349.60	0.569	0.494	1.054	1.133	0.930	0.053	0.057	1.050	1.002	0.0068	0.1691
DPH28	349.23	0.619	0.545	1.013	1.098	0.920	0.019	0.021	1.046	0.999	0.0028	0.1697
DPH56	349.07	0.632	0.564	1.023	1.109	0.920	0.020	0.021	1.037	1.013	0.0054	0.1698
DPH27	348.96	0.652	0.583	0.978	1.064	0.920	0.034	0.037	1.039	1.004	0.0023	0.1706
DPH26	348.71	0.683	0.618	0.950	1.039	0.910	0.008	0.009	1.035	1.007	0.0038	0.1708
DPH55	348.62	0.688	0.627	0.974	1.064	0.920	0.023	0.025	1.032	1.017	0.0091	0.1712
DPH25	348.54	0.712	0.651	0.857	0.947	0.900	0.026	0.029	1.031	1.006	0.0032	0.1720
DPH24	348.35	0.738	0.683	0.791	0.882	0.900	0.024	0.027	1.024	1.015	0.0045	0.1723
DPH54	348.09	0.762	0.714	0.809	0.901	0.900	0.001	0.001	1.020	1.032	0.0022	0.1721
DPH23	348.09	0.765	0.715	0.798	0.890	0.900	0.024	0.027	1.022	1.023	0.0046	0.1728
DPH22	347.94	0.792	0.747	0.691	0.783	0.880	0.019	0.022	1.017	1.028	0.0023	0.1731
DPH21	347.74	0.813	0.776	0.664	0.756	0.880	0.017	0.020	1.013	1.046	0.0027	0.1730
DPH17	347.60	0.837	0.804	0.586	0.678	0.860	0.013	0.016	1.011	1.047	0.0011	0.1733
DPH16	347.49	0.857	0.828	0.501	0.592	0.850	0.015	0.017	1.009	1.053	0.0012	0.1743
DPH15	347.26	0.883	0.858	0.496	0.587	0.840	0.015	0.018	1.011	1.046	0.0024	0.1758
DPH14	347.11	0.910	0.892	0.371	0.461	0.810	0.009	0.011	1.007	1.065	0.0007	0.1756
DPH13	346.98	0.933	0.920	0.286	0.374	0.760	0.005	0.006	1.006	1.071	0.0109	0.1743
DPH51	346.79	0.938	0.934	0.364	0.453	0.800	0.004	0.005	1.002	1.213	0.0070	0.1751
DPH12	346.82	0.955	0.946	0.235	0.322	0.730	0.005	0.007	1.006	1.075	0.0043	0.1867
DPH11	346.72	0.979	0.974	0.115	0.200	0.580	0.001	0.003	1.004	1.069		
DNPE	346.63	1.000	1.000									
DNPE	346.55	1.000	1.000									
				L	**W**	**D**						
				0.6983	0.7609	4.2874						

Methyl Valerate/n-Octane

Table E.4: Experimental data and thermodynamic consistency results for methyl valerate/n-octane

Sample Name	Experimental Data			L/W Consistency Test					McDermott-Ellis Consistency Test			
	T (K)	y_{ester}	x_{ester}	L_i	W_i	L_i/W_i	$\frac{\Delta x.}{\Sigma L_i}$	$\frac{\Delta x.}{\Sigma W_i}$	γ_{ester}	γ_{oct}	D	D_{max}
Octane	380.82	0.000	0.000									
Octane	380.94	0.000	0.000									
MVO11	379.94	0.082	0.051	1.039	1.178	0.880	0.011	0.011	1.787	0.998	0.010	0.161
MVO12	379.32	0.142	0.095	1.771	1.904	0.930	0.092	0.098	1.692	0.997	0.013	0.162
MVO52	379.05	0.185	0.142	2.158	2.285	0.940	0.023	0.024	1.487	1.007	0.007	0.160
MVO13	378.94	0.186	0.131	2.242	2.371	0.950	0.103	0.108	1.623	0.997	0.003	0.161
MVO53	378.58	0.223	0.173	2.706	2.830	0.960	0.020	0.021	1.494	1.010	0.003	0.160
MVO14	378.56	0.231	0.180	2.744	2.868	0.960	0.133	0.138	1.487	1.009	0.007	0.163
MVO15	378.15	0.267	0.224	3.265	3.383	0.970	0.152	0.157	1.395	1.030	0.005	0.164
MVO54	377.96	0.307	0.269	3.566	3.677	0.970	0.009	0.009	1.349	1.038	0.002	0.164
MVO16	377.95	0.308	0.271	3.582	3.693	0.970	0.222	0.228	1.339	1.042	0.004	0.167
MVO17	377.69	0.350	0.330	3.987	4.090	0.970	0.095	0.097	1.265	1.071	0.005	0.166
MVO55	377.71	0.370	0.353	4.026	4.124	0.980	0.083	0.085	1.245	1.076	0.003	0.166
MVO21	377.64	0.381	0.374	4.146	4.241	0.980	0.149	0.152	1.215	1.094	0.007	0.167
MVO22	377.53	0.406	0.409	4.342	4.431	0.980	0.019	0.020	1.188	1.116	0.007	0.166
MVO56	377.64	0.413	0.413	4.243	4.330	0.980	0.158	0.161	1.190	1.108	0.001	0.168
MVO23	377.65	0.432	0.450	4.324	4.404	0.980	0.104	0.106	1.144	1.143	0.003	0.167
MVO57	377.74	0.453	0.474	4.293	4.367	0.980	0.084	0.085	1.135	1.148	0.005	0.168
MVO24	377.69	0.460	0.494	4.390	4.460	0.980	0.134	0.136	1.108	1.180	0.005	0.167
MVO25	377.73	0.488	0.524	4.424	4.488	0.990	0.168	0.170	1.106	1.188	0.003	0.168
MVO26	377.91	0.509	0.562	4.337	4.391	0.990	0.041	0.041	1.069	1.233	0.008	0.166
MVO58	377.84	0.519	0.572	4.429	4.482	0.990	0.176	0.178	1.075	1.235	0.003	0.166
MVO45	378.05	0.552	0.612	4.317	4.359	0.990	0.039	0.039	1.062	1.261	0.001	0.165
MVO27	378.07	0.558	0.621	4.319	4.358	0.990	0.097	0.098	1.056	1.275	0.000	0.165
MVO44	378.21	0.574	0.644	4.233	4.267	0.990	0.058	0.059	1.044	1.300	0.002	0.165
MVO79	378.34	0.585	0.658	4.137	4.166	0.990	0.055	0.055	1.036	1.315	0.009	0.164
MVO43	378.33	0.600	0.671	4.178	4.204	0.990	0.126	0.127	1.043	1.316	0.002	0.165
MVO42	378.51	0.620	0.701	4.072	4.089	1.000	0.109	0.110	1.025	1.372	0.000	0.164
MVO78	378.70	0.637	0.729	3.947	3.956	1.000	0.041	0.041	1.007	1.435	0.002	0.162
MVO41	378.87	0.653	0.739	3.803	3.807	1.000	0.074	0.074	1.013	1.418	0.005	0.162
MVO77	379.02	0.672	0.759	3.699	3.698	1.000	0.106	0.106	1.011	1.442	0.008	0.161
MVO37	379.53	0.704	0.789	3.262	3.249	1.000	0.046	0.046	1.000	1.472	0.003	0.160
MVO76	379.67	0.717	0.804	3.156	3.138	1.010	0.045	0.045	0.997	1.501	0.008	0.159
MVO36	379.71	0.730	0.818	3.150	3.128	1.010	0.066	0.065	0.996	1.541	0.001	0.158
MVO75	380.05	0.752	0.840	2.862	2.832	1.010	0.049	0.048	0.989	1.592	0.009	0.157
MVO35	380.24	0.775	0.857	2.714	2.677	1.010	0.057	0.056	0.992	1.615	0.001	0.156
MVO74	380.69	0.804	0.880	2.318	2.272	1.020	0.041	0.040	0.988	1.652	0.004	0.154
MVO34	381.08	0.833	0.899	1.973	1.920	1.030	0.044	0.043	0.990	1.654	0.007	0.155
MVO73	381.44	0.864	0.923	1.670	1.608	1.040	0.007	0.007	0.988	1.753	0.004	0.152
MVO33	381.43	0.867	0.928	1.690	1.627	1.040	0.029	0.028	0.987	1.818	0.005	0.152
MVO72	381.90	0.899	0.947	1.266	1.195	1.060	0.011	0.010	0.988	1.868	0.013	0.150
MVO32	381.98	0.916	0.956	1.207	1.133	1.070	0.006	0.006	0.995	1.864	0.001	0.149
MVO71	382.12	0.925	0.962	1.080	1.004	1.080	0.017	0.015	0.995	1.890	0.004	0.159
MVO31	382.78	0.968	0.984	0.472	0.388	1.220	0.004	0.003	0.997	1.890		
Met Val	383.29	1.000	1.000									
Met Val	383.29	1.000	1.000									
				L	W	D						
				3.0973	3.1433	0.7360						

Ethyl Butanoate/n-Octane

Table E.5: Experimental data and thermodynamic consistency results for ethyl butanoate/n-octane

Sample Name	Experimental Data			L/W Consistency Test					McDermott-Ellis Consistency Test			
	T (K)	y_{ester}	x_{ester}	L_i	W_i	L_i/W_i	$\frac{\Delta x.}{\Sigma L_i}$	$\frac{\Delta x.}{\Sigma W_i}$	γ_{ester}	γ_{oct}	D	D_{max}
Octane	380.85	0.000	0.000									
EBO51	380.47	0.029	0.013	0.331	0.477	0.690	0.022	0.027	2.036	0.999	0.009	0.175
EBO31	379.63	0.085	0.045	1.047	1.187	0.880	0.029	0.032	1.732	0.999	0.013	0.153
EBO52	379.14	0.126	0.069	1.447	1.583	0.910	0.030	0.033	1.712	0.993	0.003	0.152
EBO32	378.58	0.155	0.087	1.940	2.070	0.940	0.133	0.140	1.707	0.995	0.016	0.160
EBO53	377.69	0.226	0.145	2.609	2.721	0.960	0.056	0.059	1.530	1.000	0.002	0.158
EBO34	377.40	0.247	0.166	2.820	2.926	0.960	0.003	0.003	1.472	1.006	0.002	0.158
EBO33	377.33	0.253	0.165	2.894	3.000	0.960	0.196	0.202	1.525	0.998	0.006	0.162
EBO54	376.60	0.312	0.227	3.389	3.470	0.980	0.026	0.027	1.390	1.017	0.001	0.161
EBO35	376.43	0.325	0.235	3.531	3.608	0.980	0.197	0.201	1.410	1.013	0.002	0.163
EBO55	375.82	0.375	0.288	3.944	3.997	0.990	0.014	0.014	1.352	1.027	0.000	0.163
EBO36	375.79	0.377	0.284	3.987	4.041	0.990	0.181	0.183	1.378	1.019	0.013	0.165
EBO56	375.66	0.405	0.330	3.948	3.981	0.990	0.016	0.016	1.281	1.043	0.007	0.165
EBO37	375.49	0.412	0.326	4.132	4.166	0.990	0.082	0.082	1.323	1.032	0.006	0.165
EBO41	375.47	0.421	0.346	4.079	4.103	0.990	0.141	0.142	1.275	1.047	0.000	0.166
EBO42	375.26	0.445	0.380	4.163	4.170	1.000	0.019	0.019	1.235	1.066	0.002	0.165
EBO57	375.29	0.447	0.385	4.116	4.121	1.000	0.100	0.100	1.224	1.070	0.003	0.166
EBO43	375.10	0.466	0.409	4.217	4.209	1.000	0.130	0.129	1.208	1.082	0.004	0.167
EBO44	374.87	0.488	0.439	4.336	4.311	1.010	0.045	0.044	1.187	1.100	0.008	0.167
EBO58	374.97	0.492	0.449	4.198	4.169	1.010	0.026	0.025	1.165	1.109	0.004	0.166
EBO45	374.87	0.497	0.455	4.276	4.242	1.010	0.102	0.101	1.165	1.113	0.003	0.167
EBO46	374.83	0.513	0.479	4.228	4.182	1.010	0.103	0.102	1.144	1.128	0.001	0.167
EBO47	374.75	0.534	0.504	4.219	4.160	1.010	0.124	0.122	1.135	1.136	0.002	0.167
EBO48	374.65	0.555	0.533	4.213	4.137	1.020	0.206	0.202	1.119	1.156	0.004	0.168
EBO28	374.66	0.591	0.583	4.022	3.921	1.030	0.207	0.201	1.088	1.192	0.001	0.168
EBO27	374.65	0.627	0.636	3.843	3.714	1.030	0.113	0.109	1.059	1.245	0.004	0.166
EBO26	374.76	0.650	0.666	3.624	3.481	1.040	0.012	0.012	1.045	1.269	0.003	0.166
EBO78	374.70	0.651	0.663	3.696	3.553	1.040	0.117	0.112	1.054	1.254	0.004	0.166
EBO25	374.82	0.672	0.696	3.459	3.302	1.050	0.099	0.094	1.033	1.300	0.005	0.165
EBO24	374.83	0.695	0.725	3.346	3.174	1.050	0.042	0.039	1.025	1.337	0.004	0.164
EBO77	374.81	0.705	0.737	3.321	3.142	1.060	0.030	0.028	1.023	1.354	0.003	0.164
EBO23	374.89	0.712	0.746	3.209	3.027	1.060	0.065	0.061	1.017	1.368	0.009	0.164
EBO22	374.85	0.729	0.767	3.177	2.983	1.060	0.038	0.036	1.015	1.403	0.000	0.163
EBO76	374.92	0.740	0.779	3.063	2.864	1.070	0.102	0.095	1.012	1.416	0.002	0.163
EBO75	375.13	0.773	0.814	2.728	2.517	1.080	0.035	0.033	1.005	1.461	0.001	0.161
EBO21	375.21	0.785	0.827	2.602	2.386	1.090	0.045	0.041	1.002	1.486	0.002	0.161
EBO17	375.32	0.802	0.845	2.429	2.208	1.100	0.020	0.018	0.999	1.518	0.007	0.160
EBO74	375.53	0.814	0.854	2.189	1.969	1.110	0.033	0.030	0.996	1.508	0.011	0.160
EBO16	375.47	0.828	0.869	2.195	1.966	1.120	0.046	0.041	0.997	1.562	0.004	0.159
EBO15	375.64	0.851	0.891	1.948	1.713	1.140	0.003	0.003	0.995	1.612	0.004	0.158
EBO73	375.75	0.855	0.893	1.832	1.600	1.150	0.038	0.033	0.994	1.593	0.002	0.158
EBO14	375.97	0.881	0.916	1.533	1.297	1.180	0.015	0.013	0.992	1.641	0.003	0.156
EBO72	376.18	0.894	0.926	1.285	1.051	1.220	0.016	0.013	0.989	1.667	0.006	0.156
EBO13	376.26	0.911	0.939	1.160	0.923	1.260	0.021	0.016	0.991	1.699	0.001	0.158
EBO12	376.57	0.940	0.961	0.775	0.539	1.440	0.010	0.007	0.990	1.754	0.007	0.158
EBO71	376.75	0.964	0.977	0.540	0.303	1.780	0.002	0.001	0.993	1.778	0.001	0.153
EBO11	376.87	0.971	0.982	0.403	0.169	2.390			0.992	1.806		
Eth But	377.23	1.000	1.000									
Eth But	377.21	1.000	1.000									
				L	W	D						
				3.0917	3.0389	0.8610						

Propyl Propanoate/n-Octane

Table E.6: Experimental data and thermodynamic consistency results for propyl propanoate/n-octane

Sample Name	Experimental Data			L/W Consistency Test					McDermott-Ellis Consistency Test			
	T (K)	y_{ester}	x_{ester}	L_i	W_i	L_i/W_i	$\frac{\Delta x.}{\Sigma L_i}$	$\frac{\Delta x.}{\Sigma W_i}$	γ_{ester}	γ_{oct}	D	D_{max}
Octane	380.76	0.000	0.000									
Octane	380.87	0.000	0.000									
PPO51	380.15	0.062	0.032	0.625	0.762	0.820	0.004	0.004	1.832	0.994	0.0082	0.1501
PPO31	379.92	0.067	0.037	0.844	0.979	0.860	0.056	0.061	1.743	1.000	0.0138	0.1605
PPO32	378.95	0.141	0.080	1.714	1.837	0.930	0.032	0.034	1.734	0.993	0.0076	0.1538
PPO52	378.69	0.164	0.098	1.933	2.051	0.940	0.098	0.103	1.662	0.993	0.0067	0.1590
PPO53	378.07	0.213	0.142	2.450	2.554	0.960	0.203	0.209	1.513	1.002	0.0015	0.1625
PPO54	377.10	0.289	0.214	3.257	3.338	0.980	0.075	0.076	1.413	1.016	0.0002	0.1612
PPO34	376.87	0.309	0.236	3.436	3.510	0.980	0.009	0.009	1.376	1.024	0.0025	0.1611
PPO33	376.85	0.314	0.238	3.450	3.523	0.980	0.097	0.099	1.386	1.020	0.0026	0.1627
PPO55	376.61	0.335	0.266	3.628	3.691	0.980	0.022	0.023	1.334	1.035	0.0047	0.1623
PPO35	376.58	0.344	0.272	3.644	3.705	0.980	0.151	0.153	1.340	1.030	0.0032	0.1639
PPO36	376.18	0.380	0.312	3.954	4.001	0.990	0.171	0.173	1.307	1.043	0.0064	0.1655
PPO37	376.03	0.411	0.355	4.007	4.038	0.990	0.037	0.037	1.251	1.061	0.0025	0.1651
PPO56	376.02	0.415	0.364	3.996	4.023	0.990	0.126	0.126	1.230	1.069	0.0022	0.1657
PPO41	375.90	0.440	0.395	4.046	4.061	1.000	0.176	0.177	1.206	1.080	0.0014	0.1668
PPO57	375.76	0.473	0.438	4.089	4.086	1.000	0.019	0.019	1.172	1.101	0.0026	0.1661
PPO42	375.71	0.474	0.443	4.129	4.124	1.000	0.145	0.144	1.166	1.108	0.0061	0.1669
PPO43	375.53	0.500	0.478	4.232	4.213	1.000	0.078	0.077	1.147	1.130	0.0047	0.1666
PPO44	375.58	0.514	0.496	4.141	4.114	1.010	0.047	0.047	1.132	1.139	0.0026	0.1664
PPO28	375.51	0.523	0.508	4.185	4.154	1.010	0.045	0.045	1.128	1.146	0.0018	0.1667
PPO58	375.53	0.528	0.518	4.141	4.105	1.010	0.034	0.034	1.114	1.159	0.0032	0.1663
PPO45	375.47	0.534	0.527	4.183	4.143	1.010	0.143	0.142	1.113	1.164	0.0005	0.1679
PPO27	375.48	0.548	0.561	4.096	4.042	1.010	0.019	0.019	1.071	1.218	0.0036	0.1667
PPO46	375.44	0.552	0.557	4.147	4.094	1.010	0.101	0.100	1.090	1.196	0.0004	0.1666
PPO47	375.45	0.571	0.581	4.083	4.019	1.020	0.108	0.106	1.078	1.213	0.0057	0.1665
PPO26	375.59	0.590	0.608	3.883	3.808	1.020	0.021	0.021	1.061	1.233	0.0028	0.1664
PPO59	375.55	0.593	0.603	3.935	3.862	1.020	0.083	0.081	1.076	1.211	0.0014	0.1666
PPO48	375.55	0.603	0.624	3.888	3.806	1.020	0.019	0.018	1.057	1.248	0.0042	0.1655
PPO25	375.63	0.609	0.629	3.798	3.713	1.020	0.076	0.074	1.056	1.243	0.0011	0.1657
PPO24	375.69	0.625	0.649	3.693	3.600	1.030	0.131	0.128	1.048	1.258	0.0031	0.1658
PPO23	375.75	0.653	0.686	3.554	3.444	1.030	0.102	0.099	1.035	1.296	0.0006	0.1649
PPO22	375.86	0.677	0.715	3.380	3.257	1.040	0.100	0.096	1.025	1.327	0.0033	0.1643
PPO21	375.97	0.701	0.746	3.204	3.067	1.040	0.066	0.063	1.015	1.371	0.0028	0.1628
PPO17	376.16	0.722	0.767	2.968	2.822	1.050	0.084	0.080	1.011	1.380	0.0053	0.1628
PPO16	376.26	0.748	0.796	2.805	2.646	1.060	0.100	0.094	1.005	1.427	0.0020	0.1618
PPO15	376.57	0.789	0.834	2.413	2.237	1.080	0.086	0.078	1.001	1.460	0.0002	0.1612
PPO14	376.94	0.829	0.873	1.959	1.766	1.110	0.060	0.053	0.993	1.531	0.0024	0.1609
PPO13	377.46	0.881	0.909	1.362	1.155	1.180	0.040	0.032	0.997	1.465	0.0037	0.1627
PPO12	377.87	0.913	0.945	0.877	0.656	1.340	0.020	0.012	0.982	1.732	0.0114	0.1674
PPO11	378.36	0.965	0.978	0.316	0.084	3.770			0.988	1.724		
Prop Prop	378.75	1.000	1.000									
				L 2.9826	W 2.9458	D 0.6198						

Appendix E: Experimental Results: VLE & Consistency Tests

Butyl Acetate/n-Octane

Table E.7: Experimental data and thermodynamic consistency results for butyl acetate/n-octane

Sample Name	Experimental Data			L/W Consistency Test					McDermott-Ellis Consistency Test			
	$T\,(K)$	y_{ester}	x_{ester}	L_i	W_i	L_i/W_i	$\Delta x.\ \Sigma L_i$	$\Delta x.\ \Sigma W_i$	γ_{ester}	γ_{oct}	D	D_{max}
Octane	380.78	0.000	0.000									
BAO61	380.06	0.068	0.037	0.833	0.974	0.860	0.012	0.014	1.974	0.995	0.0065	0.1536
BAO11	379.76	0.081	0.049	1.147	1.287	0.890	0.034	0.038	1.779	1.003	0.0081	0.1551
BAO12	379.32	0.120	0.073	1.617	1.752	0.920	0.066	0.071	1.771	0.999	0.0056	0.1573
BAO62	378.77	0.165	0.108	2.207	2.339	0.940	0.006	0.006	1.683	1.001	0.0032	0.1554
BAO13	378.62	0.172	0.111	2.360	2.492	0.950	0.108	0.114	1.722	1.000	0.0050	0.1589
BAO14	378.08	0.218	0.152	2.948	3.074	0.960	0.131	0.136	1.624	1.006	0.0069	0.1609
BAO63	377.74	0.257	0.193	3.337	3.456	0.970	0.068	0.070	1.518	1.016	0.0005	0.1603
BAO15	377.46	0.284	0.213	3.639	3.756	0.970	0.180	0.185	1.534	1.013	0.0055	0.1638
BAO16	377.19	0.318	0.260	3.964	4.072	0.970	0.027	0.028	1.419	1.034	0.0023	0.1626
BAO64	377.12	0.323	0.267	4.042	4.149	0.970	0.070	0.072	1.410	1.038	0.0047	0.1636
BAO17	377.10	0.334	0.284	4.082	4.185	0.980	0.145	0.149	1.370	1.046	0.0048	0.1646
BAO65	376.83	0.363	0.318	4.391	4.488	0.980	0.017	0.017	1.339	1.060	0.0059	0.1643
BAO21	376.92	0.364	0.322	4.306	4.401	0.980	0.190	0.194	1.324	1.061	0.0060	0.1662
BAO22	376.69	0.394	0.365	4.585	4.672	0.980	0.046	0.047	1.273	1.088	0.0033	0.1654
BAO66	376.76	0.388	0.355	4.503	4.592	0.980	0.219	0.223	1.286	1.079	0.0006	0.1670
BAO23	376.64	0.421	0.402	4.678	4.756	0.980	0.067	0.068	1.234	1.107	0.0047	0.1661
BAO67	376.69	0.431	0.417	4.644	4.719	0.980	0.092	0.093	1.219	1.112	0.0047	0.1666
BAO24	376.60	0.443	0.436	4.756	4.827	0.990	0.135	0.137	1.201	1.129	0.0028	0.1671
BAO25	376.55	0.460	0.464	4.838	4.902	0.990	0.001	0.001	1.173	1.154	0.0006	0.1663
BAO68	376.57	0.462	0.464	4.818	4.882	0.990	0.055	0.056	1.177	1.150	0.0094	0.1664
BAO48	376.72	0.473	0.476	4.681	4.741	0.990	0.102	0.104	1.171	1.145	0.0014	0.1677
BAO26	376.70	0.477	0.498	4.726	4.781	0.990	0.152	0.154	1.130	1.186	0.0077	0.1669
BAO27	376.65	0.501	0.530	4.812	4.859	0.990	0.127	0.128	1.118	1.209	0.0024	0.1666
BAO47	376.77	0.522	0.556	4.722	4.761	0.990	0.090	0.091	1.104	1.224	0.0135	0.1667
BAO28	376.61	0.531	0.575	4.903	4.938	0.990	0.057	0.057	1.092	1.261	0.0084	0.1658
BAO46	376.82	0.545	0.587	4.706	4.737	0.990	0.125	0.126	1.091	1.250	0.0009	0.1661
BAO45	376.94	0.565	0.614	4.616	4.640	0.990	0.069	0.070	1.077	1.273	0.0027	0.1657
BAO59	377.03	0.572	0.629	4.543	4.562	1.000	0.054	0.054	1.061	1.300	0.0040	0.1651
BAO44	377.02	0.580	0.640	4.566	4.582	1.000	0.128	0.128	1.055	1.320	0.0071	0.1650
BAO43	377.09	0.602	0.669	4.527	4.536	1.000	0.025	0.025	1.047	1.353	0.0030	0.1640
BAO58	377.18	0.605	0.674	4.443	4.450	1.000	0.209	0.209	1.042	1.360	0.0006	0.1645
BAO42	377.60	0.648	0.723	4.078	4.069	1.000	0.025	0.025	1.027	1.408	0.0063	0.1623
BAO57	377.56	0.654	0.729	4.124	4.114	1.000	0.113	0.113	1.029	1.417	0.0006	0.1628
BAO41	377.77	0.675	0.757	3.945	3.927	1.000	0.016	0.016	1.015	1.476	0.0008	0.1609
BAO56	377.83	0.680	0.761	3.890	3.870	1.010	0.133	0.132	1.014	1.478	0.0018	0.1612
BAO37	378.27	0.716	0.798	3.490	3.459	1.010	0.078	0.077	1.006	1.526	0.0050	0.1596
BAO55	378.46	0.737	0.820	3.325	3.287	1.010	0.008	0.008	1.001	1.579	0.0105	0.1583
BAO36	378.30	0.738	0.823	3.487	3.449	1.010	0.096	0.095	1.004	1.604	0.0039	0.1584
BAO54	378.82	0.770	0.852	3.000	2.952	1.020	0.077	0.076	0.994	1.669	0.0075	0.1564
BAO53	379.26	0.807	0.880	2.590	2.534	1.020	0.008	0.008	0.996	1.694	0.0014	0.1547
BAO35	379.38	0.813	0.883	2.473	2.417	1.020	0.050	0.049	0.996	1.684	0.0025	0.1551
BAO34	379.75	0.842	0.905	2.127	2.064	1.030	0.033	0.032	0.994	1.733	0.0082	0.1537
BAO52	379.99	0.865	0.921	1.905	1.838	1.040	0.011	0.011	0.996	1.779	0.0021	0.1521
BAO33	380.16	0.873	0.927	1.742	1.673	1.040	0.029	0.028	0.994	1.798	0.0032	0.1526
BAO32	380.58	0.904	0.947	1.342	1.269	1.060	0.028	0.026	0.995	1.817	0.0072	0.1572
BAO31	381.17	0.947	0.973	0.780	0.702	1.110	0.001	0.001	0.996	1.940	0.0067	0.1483
BAO51	381.31	0.949	0.973	0.641	0.563	1.140	0.008	0.007	0.993	1.911		
But Ace	382.01	1.000	1.000									
But Ace	381.99	1.000	1.000									
				L	W	D						
				3.5229	3.5655	0.6016						

Pentyl Formate/n-Octane

Table E.8: Experimental data and thermodynamic consistency results for pentyl formate/n-octane

Sample Name	Experimental Data			L/W Consistency Test					McDermott-Ellis Consistency Test			
	T (K)	y_{ester}	x_{ester}	L_i	W_i	L_i/W_i	$\frac{\Delta x}{\Sigma L_i}$	$\frac{\Delta x}{\Sigma W_i}$	γ_{ester}	γ_{oct}	D	D_{max}
Octane	380.84	0.000	0.000									
Octane	380.82	0.000	0.000									
AFO31	380.39	0.045	0.027	0.651	0.793	0.820	0.032	0.036	2.112	0.999	0.0068	0.1659
AFO32	379.98	0.086	0.060	1.292	1.431	0.900	0.013	0.015	1.828	1.002	0.0003	0.1576
AFO61	379.97	0.088	0.049	1.227	1.368	0.900	0.114	0.122	2.289	0.989	0.0033	0.1702
AFO62	379.21	0.147	0.111	2.427	2.560	0.950	0.028	0.030	1.723	1.012	0.0019	0.1583
AFO33	379.10	0.162	0.123	2.617	2.749	0.950	0.097	0.101	1.722	1.011	0.0017	0.1619
AFO34	378.89	0.192	0.157	3.067	3.195	0.960	0.077	0.080	1.611	1.021	0.0038	0.1627
AFO63	378.82	0.211	0.181	3.306	3.430	0.960	0.052	0.054	1.533	1.029	0.0040	0.1623
AFO35	378.65	0.228	0.196	3.581	3.704	0.970	0.204	0.210	1.543	1.030	0.0017	0.1663
AFO64	378.50	0.266	0.249	4.102	4.216	0.970	0.032	0.032	1.423	1.053	0.0095	0.1647
AFO36	378.32	0.278	0.256	4.334	4.448	0.970	0.148	0.152	1.450	1.053	0.0083	0.1665
AFO37	378.39	0.298	0.290	4.496	4.605	0.980	0.095	0.097	1.372	1.069	0.0022	0.1668
AFO65	378.35	0.310	0.311	4.680	4.785	0.980	0.058	0.059	1.333	1.084	0.0001	0.1667
AFO41	378.37	0.318	0.323	4.745	4.848	0.980	0.178	0.182	1.317	1.090	0.0014	0.1681
AFO42	378.42	0.342	0.360	4.951	5.046	0.980	0.040	0.040	1.269	1.110	0.0024	0.1676
AFO66	378.47	0.345	0.368	4.955	5.049	0.980	0.172	0.175	1.251	1.117	0.0032	0.1685
AFO43	378.51	0.369	0.402	5.150	5.238	0.980	0.159	0.162	1.221	1.137	0.0043	0.1687
AFO44	378.54	0.388	0.432	5.329	5.410	0.980	0.000	0.000	1.192	1.161	0.0071	0.1679
AFO67	378.65	0.388	0.432	5.219	5.299	0.980	0.272	0.276	1.189	1.156	0.0108	0.1699
AFO45	378.69	0.417	0.483	5.527	5.597	0.990	0.109	0.110	1.142	1.208	0.0063	0.1684
AFO68	378.71	0.431	0.502	5.640	5.706	0.990	0.164	0.166	1.132	1.226	0.0055	0.1686
AFO46	378.98	0.448	0.532	5.569	5.628	0.990	0.073	0.074	1.105	1.251	0.0034	0.1675
AFO58	379.05	0.460	0.545	5.589	5.645	0.990	0.093	0.094	1.104	1.257	0.0010	0.1677
AFO47	379.18	0.470	0.561	5.573	5.624	0.990	0.202	0.204	1.089	1.277	0.0055	0.1680
AFO48	379.37	0.493	0.597	5.628	5.670	0.990	0.263	0.265	1.067	1.322	0.0048	0.1671
AFO57	379.83	0.531	0.645	5.489	5.518	0.990	0.044	0.045	1.049	1.368	0.0017	0.1654
AFO28	379.91	0.534	0.653	5.464	5.490	1.000	0.195	0.196	1.039	1.389	0.0141	0.1651
AFO56	380.16	0.565	0.689	5.455	5.472	1.000	0.057	0.057	1.034	1.433	0.0051	0.1635
AFO27	380.41	0.575	0.699	5.276	5.289	1.000	0.110	0.110	1.028	1.440	0.0007	0.1632
AFO26	380.71	0.594	0.720	5.118	5.125	1.000	0.007	0.007	1.021	1.466	0.0149	0.1625
AFO55	380.48	0.594	0.722	5.358	5.365	1.000	0.058	0.058	1.027	1.483	0.0160	0.1623
AFO25	380.90	0.604	0.733	5.014	5.016	1.000	0.099	0.099	1.014	1.490	0.0007	0.1622
AFO24	381.17	0.618	0.753	4.877	4.874	1.000	0.074	0.074	1.002	1.540	0.0116	0.1607
AFO23	381.30	0.635	0.768	4.850	4.842	1.000	0.104	0.104	1.005	1.563	0.0172	0.1600
AFO54	381.49	0.660	0.790	4.805	4.791	1.000	0.036	0.036	1.010	1.597	0.0087	0.1588
AFO22	381.77	0.668	0.798	4.577	4.560	1.000	0.154	0.153	1.003	1.606	0.0006	0.1585
AFO21	382.62	0.712	0.834	3.968	3.940	1.010	0.027	0.027	0.996	1.654	0.0099	0.1564
AFO53	382.53	0.716	0.840	4.102	4.073	1.010	0.059	0.059	0.996	1.705	0.0107	0.1560
AFO17	383.00	0.731	0.856	3.734	3.700	1.010	0.067	0.066	0.984	1.761	0.0106	0.1543
AFO16	383.44	0.761	0.874	3.417	3.379	1.010	0.057	0.057	0.989	1.773	0.0178	0.1531
AFO52	383.79	0.792	0.892	3.183	3.139	1.010	0.033	0.032	0.999	1.773	0.0105	0.1523
AFO15	384.22	0.805	0.903	2.825	2.779	1.020	0.060	0.059	0.990	1.823	0.0109	0.1515
AFO14	384.90	0.848	0.926	2.301	2.250	1.020	0.005	0.005	0.995	1.841	0.0127	0.1498
AFO51	384.69	0.848	0.928	2.526	2.474	1.020	0.054	0.053	0.999	1.909	0.0058	0.1513
AFO13	385.78	0.897	0.955	1.610	1.554	1.040	0.021	0.020	0.994	1.970	0.0083	0.1484
AFO12	386.28	0.927	0.969	1.208	1.149	1.050	0.010	0.009	0.997	2.036	0.0087	0.1463
AFO11	386.51	0.947	0.978	1.036	0.976	1.060	0.011	0.011	1.001	2.072		
Pen For	387.46	1.000	1.000									
Pen For	387.40	1.000	1.000									
				L	W	D						
				4.0200	4.0747	0.6763						

APPENDIX F: sPC-SAFT CORRELATION RESULTS

The correlation results presented in this section are those for the *Standard pure component regression* to demonstrate that such predictions can be brought into agreement with experimental data by introducing small binary interaction parameters.
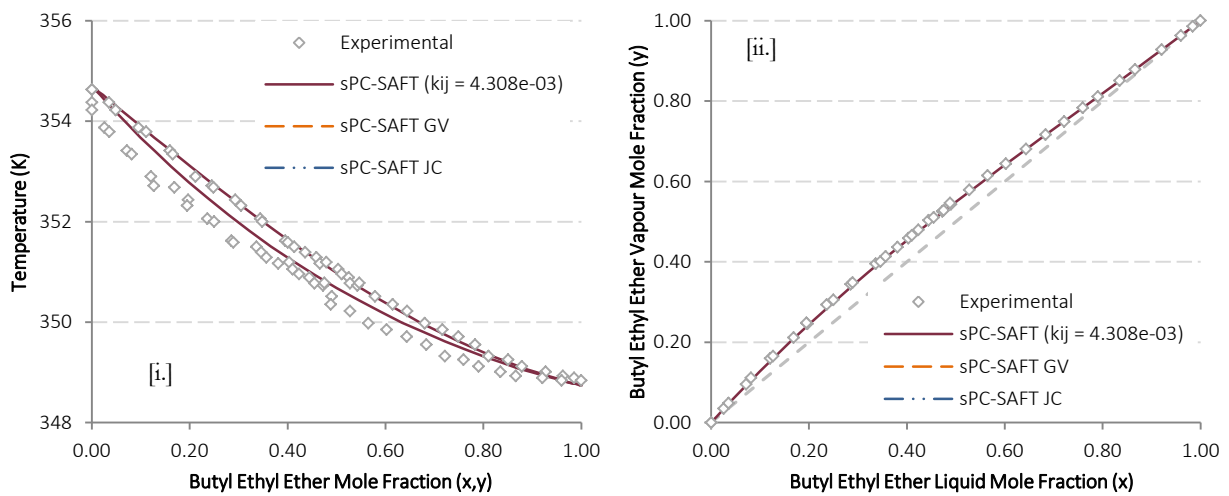
Ether Systems

Figure F.1: [i.] T-xy and [ii.] x-y correlations for the butyl ethyl ether/n-heptane system at 60 kPa using the standard pure component regression procedure. Only correlation of nonpolar sPC-SAFT is possible.
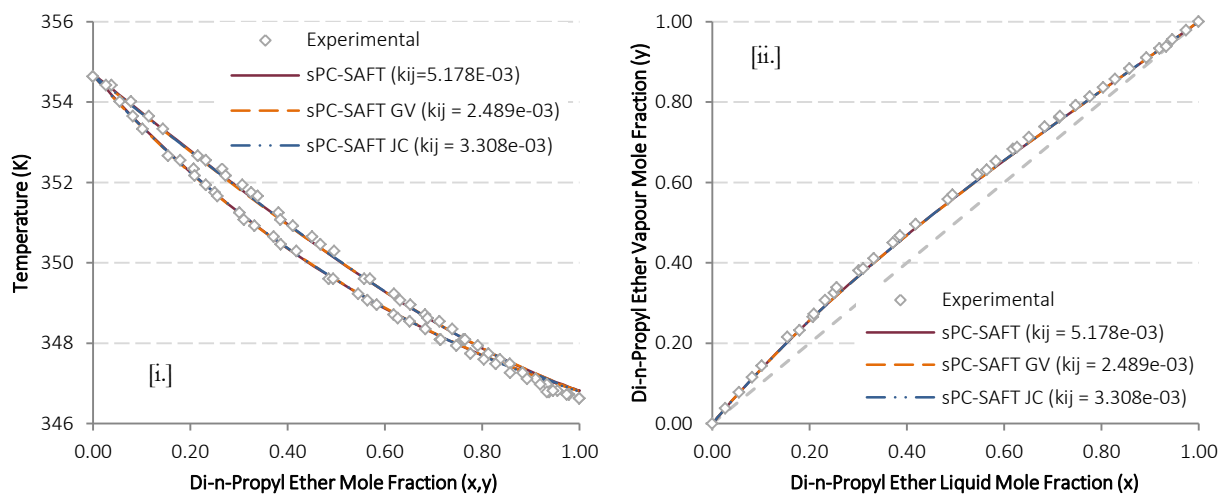

Figure F.2: [i.] T-xy and [ii.] x-y correlations for the di-n-propyl ether/n-heptane system at 60 kPa using the standard pure component regression procedure. The correlation of nonpolar sPC-SAFT is included for comparison.
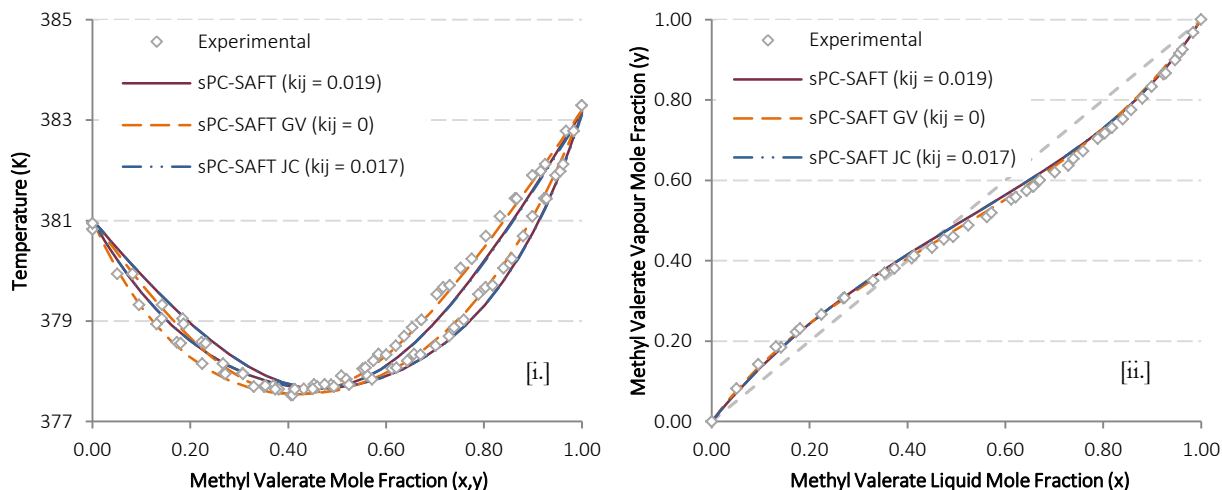
Ester Systems

Figure F.3: [i.] T-xy and [ii.] x-y correlations for the methyl valerate/n-octane system at 60 kPa using the standard pure component regression procedure.
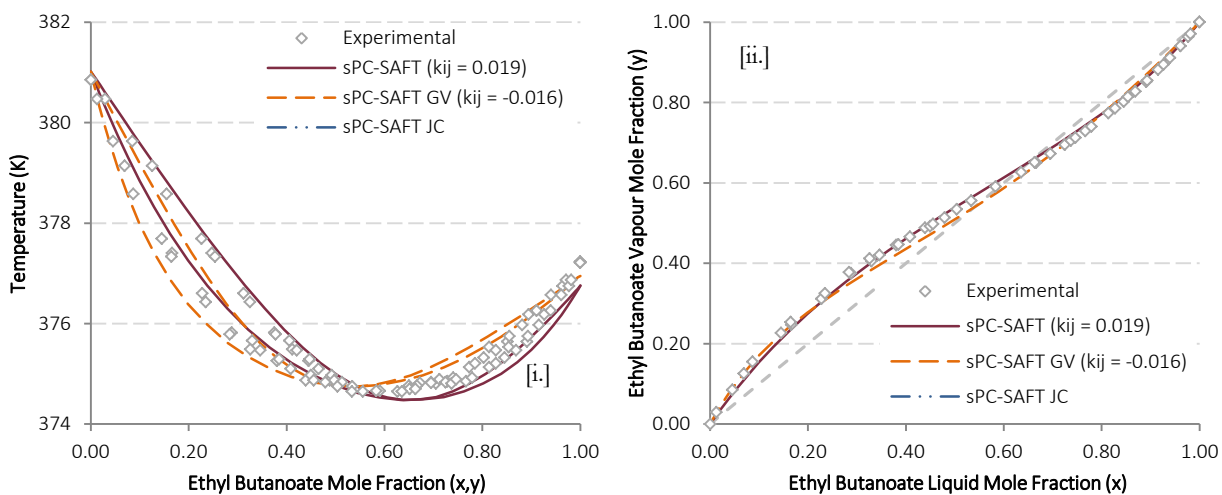

Figure F.4: [i.] T-xy and [ii.] x-y correlations for the ethyl butanoate/n-octane system at 60 kPa using the standard pure component regression procedure.

Figure F.5: [i.] T-xy and [ii.] x-y correlations for the ethyl butanoate/n-octane system at 60 kPa using the standard pure component regression procedure.
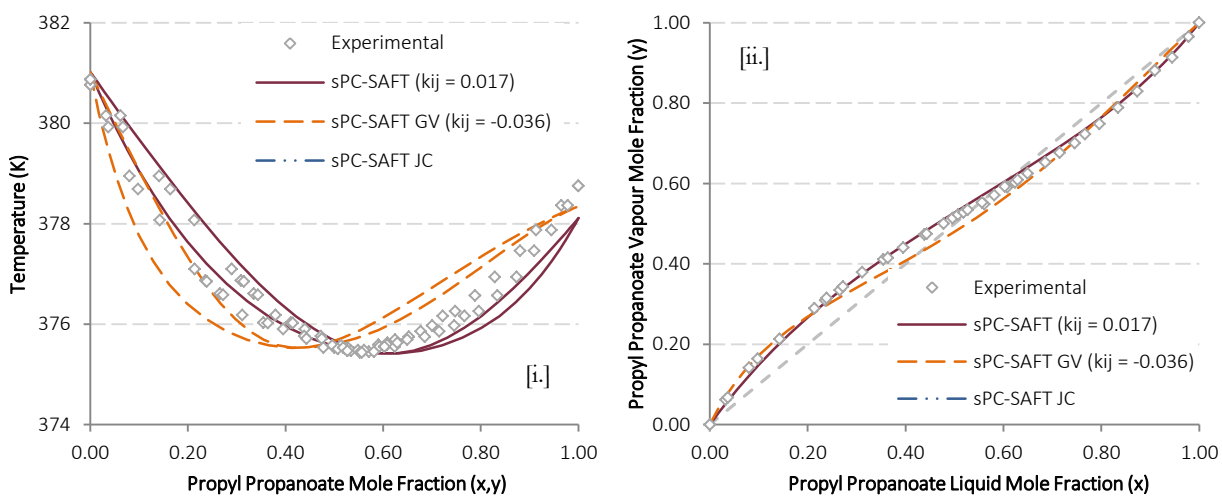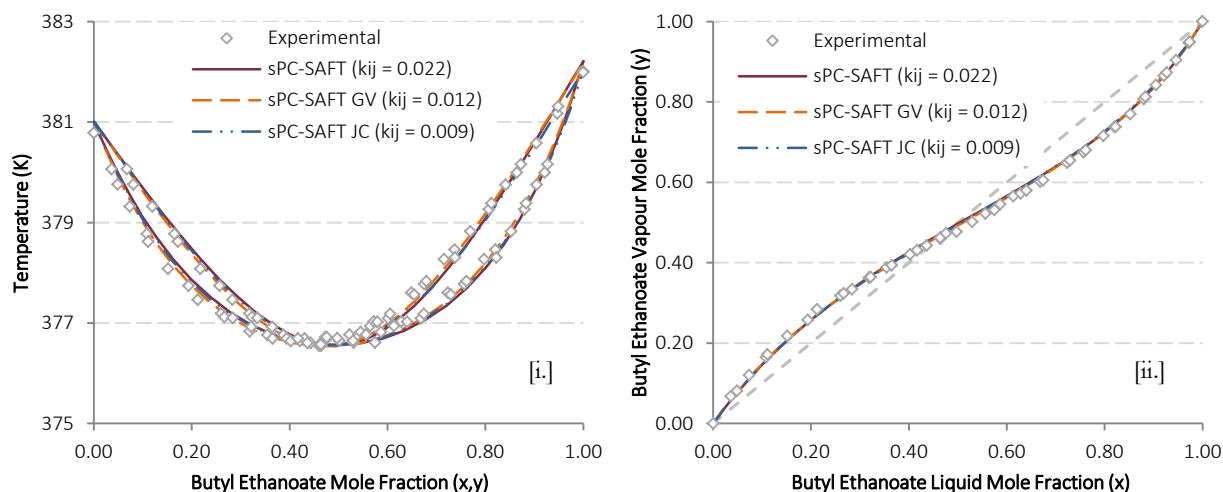
Figure F.6: [i.] T-xy and [ii.] x-y correlations for the butyl acetate/n-octane system at 60 kPa using the standard pure component regression procedure.

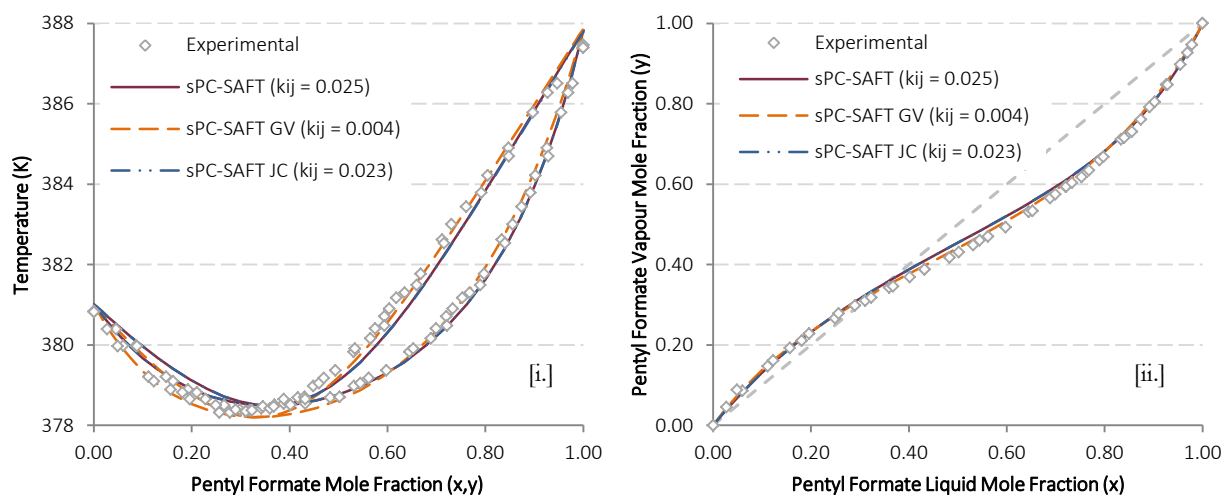**Figure F.7: [i.] T-xy and [ii.] x-y correlations for the pentyl formate/n-octane system at 60 kPa using the standard pure component regression procedure.**

APPENDIX G: POLAR SAFT-VR MIE WORKING EQUATIONS

The working equation for the SAFT-VR Mie EoS comprise *96* pages of equations and are thus not incorporated here for the sake of brevity. These equations can be made available on request.

APPENDIX H: SAFT-VR MIE CODE VALIDATION

The tables presented in this appendix serve to validate the coded working equations of the polar SAFT-VR Mie EoS's. This was achieved by comparing the analytical derivatives of the working equations with those calculated by numerical differentiation using the central differences technique of equation H.1:

$$\frac{\partial f}{\partial x_i} = \frac{f(\mathbf{x}, x_i + \varepsilon) - f(\mathbf{x}, x_i - \varepsilon)}{2\varepsilon} \qquad \text{H.1}$$

where $\mathbf{x} \in \{n_i, \ldots, n_c, T, V\}$.

For the validation considered here, use is made of 2-butanone as a one component reference system with $T = 300$K and $V = 0.091$L.mol^{-1}.

Table H.1: Hard Sphere term code validation results

Function	Analytical Derivative	Numerical Derivative	% Difference
F	7.7521901019	7.7521901019	
$\partial F/\partial n_i$	22.238267552	22.238267552	-2.7631689795e-09
$\partial F/\partial T$	-0.0031236728274	-0.0031236727915	-1.1488186755e-06
$\partial F/\partial V$	-159.95056941	-159.95057477	3.3497458718e-06
$\partial^2 F/\partial n_i \partial n_j$	53.340014737	53.340014736	-1.9514343501e-09
$\partial^2 F/\partial T \partial n_i$	-0.011501854468	-0.011501857244	2.4139341698e-05
$\partial^2 F/\partial V \partial n_i$	-588.9631447	-588.96314504	5.7395196968e-08
$\partial^2 F/\partial T^2$	3.1222034689e-06	3.1222038843e-06	1.3306786763e-05
$\partial^2 F/\partial T \partial V$	0.092509164653	0.092509169515	5.2559470084e-06
$\partial^2 F/\partial V^2$	6503.1400446	6503.1404711	6.5577600577e-06

Table H.2: Dispersion term code validation results

Function	Analytical Derivative	Numerical Derivative	% Difference
F	-12.326263933	-12.326263933	
$\partial F/\partial n_i$	-23.571111032	-23.571111032	-2.1635413435e-09
$\partial F/\partial T$	0.044087590943	0.044087591045	2.2938672881e-07
$\partial F/\partial V$	124.161955	124.16195327	-1.3945991033e-06
$\partial^2 F/\partial n_i\partial n_j$	-8.4396226225	-8.4396226239	1.6665771565e-08
$\partial^2 F/\partial T\partial n_i$	0.084601920044	0.084601920042	-1.937679055e-09
$\partial^2 F/\partial V\partial n_i$	93.18757605	93.18755436	-2.3276118082e-05
$\partial^2 F/\partial T^2$	-0.00030634997067	-0.00030576003188	-0.19257021505
$\partial^2 F/\partial T\partial V$	-0.44734608324	-0.44734607363	-2.1474836516e-06
$\partial^2 F/\partial V^2$	-1028.9469943	-1028.9467165	-2.6992211546e-05

Table H.3: Chain term code validation results

Function	Analytical Derivative	Numerical Derivative	% Difference
F	-0.95502639536	-0.95502639536	
$\partial F/\partial n_i$	-4.1020531806	-4.1020531822	3.8665833056e-08
$\partial F/\partial T$	-0.0021527645815	-0.0021527645788	-1.2498651371e-07
$\partial F/\partial V$	34.74844919	34.748450077	2.5508437266e-06
$\partial^2 F/\partial n_i\partial n_j$	-11.659408048	-11.659408053	4.1113794394e-08
$\partial^2 F/\partial T\partial n_i$	0.0019800565398	0.0019800601159	1.8060413024e-04
$\partial^2 F/\partial V\partial n_i$	128.73940255	128.7394052	2.059346283e-06
$\partial^2 F/\partial T^2$	2.0102043276e-05	1.9255951651e-05	-4.2089832055
$\partial^2 F/\partial T\partial V$	-0.045633270559	-0.045633272766	4.8366237293e-06
$\partial^2 F/\partial V^2$	-1421.4987331	-1421.498782	3.4377290523e-06

Table H.4: Gross & Vrabec polar term code validation results

Function	Analytical Derivative	Numerical Derivative	% Difference
F	-1.1041791612	-1.1041791612	
$\partial F/\partial n_i$	-2.1947518695	-2.1947518695	1.3354533721e-12
$\partial F/\partial T$	0.0042135700211	0.0042135700212	1.0676595779e-09
$\partial F/\partial V$	12.041750175	12.041750176	1.3097517981e-08
$\partial^2 F/\partial n_i\partial n_j$	-2.9635647808	-2.9635647891	-2.800681144e-07
$\partial^2 F/\partial T\partial n_i$	0.0093289890459	0.0093289890462	3.22741879e-09
$\partial^2 F/\partial V\partial n_i$	32.722721235	32.722721236	4.4496426922e-09
$\partial^2 F/\partial T^2$	-1.8734218381e-05	-1.8734218378e-05	-2.0125383973e-08
$\partial^2 F/\partial T\partial V$	-0.056482797954	-0.056482797968	2.527424641e-08
$\partial^2 F/\partial V^2$	-361.31367598	-361.31367604	1.6841188057e-08

Appendix H: SAFT-VR Mie Code Validation

Analysis of the $\partial^2 F/\partial T^2$ results shows fairly large deviations between the numerical and analytical derivatives, particularly when compared to the orders of magnitude of other derivative deviations. Closer inspection shows these instances are confined to the SAFT-VR Mie terms and not the polar contribution. These deviations are thus readily explained by the fact that the temperature dependent diameter in SAFT-VR Mie is calculated by means of 10-point Gauss-Legendre quadrature – thus the numerical derivative of the temperature dependent properties is taking the numerical derivative of a numerical integral. This procedure is inherently error-prone which leads to the larger deviations between analytical and numerical derivatives. Considering the total model deviations in Table H.5, rather than the individual terms, provides a measure of reassurance regarding these deviations however, with a significantly lower overall deviation in evidence.

Table H.5: Total SAFT-VR Mie^{GV} prediction validation results

Function	Analytical Derivative	Numerical Derivative	% Difference
F	-6.6332793876600	-6.6332793876600	
$\partial F/\partial n_i$	-7.6296485301000	-7.6296485317000	2.09708235717E-08
$\partial F/\partial T$	0.0430247235552	0.0430247236959	3.27021276688E-07
$\partial F/\partial V$	11.0015849550	11.0015787530	-5.63736954573E-05
$\partial^2 F/\partial n_i\partial n_j$	30.2774192857	30.2774192700	-5.18537999196E-08
$\partial^2 F/\partial T\partial n_i$	0.0844091111617	0.0844091119601	9.45869454024E-07
$\partial^2 F/\partial V\partial n_i$	-334.313444865	-334.313464244	5.79665586911E-06
$\partial^2 F/\partial T^2$	-3.01859942E-04	-3.02116095E-04	0.0848580353667
$\partial^2 F/\partial T\partial V$	-0.456952987100	-0.456952974849	-2.68101979714E-06
$\partial^2 F/\partial V^2$	3691.38064122	3691.38129656	1.77532490592E-05

The validation of the Jog & Chapman polar term is presented in Table H.6, where a different volume root of $v = 0.104$L.mol^{-1} was solved at the reference temperature of $T = 300$K.

Table H.6: Jog & Chapman polar term code validation results

Function	Analytical Derivative	Numerical Derivative	% Difference
F	-1.4874880008	-1.4874880008	
$\partial F/\partial n_i$	-3.1967520486	-3.1967520485	-2.7766966542e-09
$\partial F/\partial T$	0.0081340854198	0.0081340854209	1.3710292278e-08
$\partial F/\partial V$	16.494002153	16.494002155	1.4934017608e-08
$\partial^2 F/\partial n_i\partial n_j$	-4.198135944	-4.1981359435	-1.191004884E-08
$\partial^2 F/\partial T\partial n_i$	0.016519066644	0.016519066645	9.2171317844e-09
$\partial^2 F/\partial V\partial n_i$	45.054100951	45.054100961	2.1272848624e-08
$\partial^2 F/\partial T^2$	-6.8990402257e-05	-6.8990402274e-05	2.4998304835e-08
$\partial^2 F/\partial T\partial V$	-0.080913126634	-0.080913126646	1.5087819201e-08
$\partial^2 F/\partial V^2$	-390.92214745	-390.92214758	3.4011886423e-08